

---

# Structural performance of steel fibre reinforced concrete

Prepared for the 2<sup>nd</sup> International Conference on

*Fibre Reinforced Concrete*  
– *from research to practice* –

Held at the Budapest University of Technology and Economics,  
Budapest, Hungary  
19 November 2004  
organized by the Hungarian Group of *fib*

by

**Imre Kovács**

Head of Department  
Department of Civil and Structural Engineering  
University of Debrecen, Debrecen, Hungary

**György L. Balázs**

Head of Department  
Department of Construction Materials and Engineering Geology  
Budapest University of Technology and Economics, Budapest, Hungary

---

This Volume was written by Imre Kovács and György L. Balázs.

© Kovács – Balázs, 2004

All right reserved. No part of this publication may be reproduced or transmitted in any form or by any means, electronic or mechanical, including photocopy, recording, or any information storage and retrieval system, without written permission from the publisher.

Although the authors and the publisher did their best to provide accurate and current information, none of them, nor anyone else associated with this publication, shall be liable for any loss, damage or liability directly or indirectly caused or alleged to be caused by this book.

Cover was designed by Salem G. Nehme.

**Published by the Publishing Company of Budapest University of Technology and  
Economics**  
**No.:**

**ISBN**

# Preface

Fibre reinforced concrete is becoming an everyday construction material after several decades of research. Even if use of natural fibres in clay and earth was an ancient idea to improve integrity of bricks and walls, research on mixing fibres to concrete started only in the early 60-ies. It was considered to be as a challenging material to reduce brittleness of concrete and reduce production cost by partially or fully replacing conventional steel bar reinforcement and in some cases reduce the construction time.

Researchers realized that addition of fibres to concrete does not only mean to have a new component in concrete but it considerably influences the technology and behaviour of concrete.

In addition to steel, various other types of fibre materials can be used in concrete as fibre reinforcement like polypropylene, glass, carbon, aramid, ceramics or natural fibres. They all lead to different behaviour. Physical and chemical properties of fibres as well as bond between fibres and matrix may influence all kinds of concrete properties. Fibres are supposed to be randomly oriented in concrete, however, in some practical cases and regions of members it can not be reached.

Extensive research worldwide and many applications resulted an understanding of material behaviour, however, fields of modelling of behaviour and possible applications give further areas for research. Other recent interesting areas are e.g. use of fibre reinforcement in self compacting and in light weight aggregate concrete.

*In present book* we intended to summarize our experimental and theoretical results on steel fibre reinforced concrete obtained during the last ten years. Present results can be classified into three groups:

- material characteristics (compressive strength, splitting strength, shear strength, flexural strength),
- behaviour of elements: beams (non-prestressed or prestressed), slabs, deep beams,
- modelling in tension and modelling of transfer of prestressing force.

These results provided a possibility not only to draw conclusions on a scientific basis, but also to solve practical questions and develop new ideas for applications. Some of our results were integrated into work of RILEM and *fib* committees.

Authors wish to thank for the financial supports during the last ten years by the Hungarian Ministry of Education (Grant MKM 150/94), Hungarian Research Found (OTKA Grants F025 621, T032 525 TEMPUS Project (Nr. S JEP 11236/96) on post-graduate studies).

29 October 2004

Imre Kovács

György L. Balázs

# Content

<b>Preface</b>	3
<b>Content</b>	5
<b>Notations and abbreviations</b>	9
<b>1. Introduction</b>	
1.1 General remarks to fibre reinforced concrete	15
1.2 Behaviour in compression	18
1.3 Tensile strength	22
1.4 Toughness properties	27
1.5 Fibre reinforcement in structural elements	30
1.6 Conclusions	34
<b>2. Material compositions and mechanical properties</b>	
2.1 Material compositions and test specimens	35
2.1.1 Concrete mix proportions and mixing procedures	36
2.1.2 Type of fibres	37
2.1.3 Formworks and test specimens	38
2.2 Behaviour in compression	44
2.2.1 Test specimens and test procedure	44
2.2.2 Compressive behaviour	45
2.2.3 Stress – strain relationship in compression	47
2.2.4 Comparison to results of other researchers	52
2.3 Splitting strength	53
2.3.1 Test specimens and test procedure	53
2.3.2 Test result and test observations	54
2.3.3 Comparison with literature results	56
2.4 Flexural toughness	63
2.4.1 Experimental variables and test procedure	63
2.4.2 Bending stress vs. mid-point deflection relationships	65
2.5 Conclusions	68

---

### **3. Modelling of fibre reinforced materials in tension**

3.1	Modelling of fibre reinforced materials	71
3.2	Modelling of steel fibre reinforced concrete in tension	96
3.3	Conclusions	99

### **4. Behaviour of steel fibre reinforced concrete beams in bending and shear**

4.1	Experimental programme	101
4.1.1	Test specimens and reinforcing details	101
4.1.2	Experimental set-up and test procedure	102
4.2	Experimental results	104
4.2.1	Failure loads and failure modes	104
4.2.2	Load vs. mid-point deflection relationships	110
4.2.3	Cracking behaviour	115
4.3	Modelling of bending behaviour	122
4.4	Conclusions	127

### **5. Behaviour of steel fibre reinforced prestressed pretensioned concrete beams**

5.1	Experimental programme	131
5.1.1	Test specimens and experimental variables	131
5.1.2	Test set-up and experimental procedure	133
5.2	Experimental observation and test results	136
5.2.1	Concrete strains during tension release	136
5.2.2	Draw-in of prestressing strand	139
5.2.2.1	Released prestressing force versus draw-in for series PC-G	139
5.2.2.2	Released prestressing force versus draw-in for series PC-S	145
5.2.3	Camber of PC beams	147
5.2.3.1	Camber of series PC-G	147
5.2.3.2	Camber of series PC-S	149
5.2.4	Determination of transfer length of prestressing strand	150
5.2.4.1	General considerations and governing equations	150
5.2.4.2	Transfer length of prestressing strand for series PC-G	153
5.2.4.3	Proposal	154
5.2.5	Bending test	160
5.2.5.1	Failure loads and failure modes	160
5.2.5.2	Load vs. deflection relationships	162
5.3	Conclusions	163

## **6. Behaviour of steel fibre reinforced concrete deep beams in shear**

6.1	Experimental programme	165
6.1.1	Test specimens and experimental variables	165
6.1.2	Experimental set-up and test procedure	167
6.2	Experimental results	168
6.3	Conclusions	173

## **7. Behaviour of steel fibre reinforced concrete slabs in bending**

7.1	Experimental programme	175
7.1.1	Test specimens and experimental variables	175
7.1.2	Experimental set-up and testing procedure	176
7.2	Experimental results and test observations	177
7.2.1	Failure loads	177
7.2.2	Load – deflection relationships	179
7.2.3	Crack development and failure line	180
7.2.4	Effect of compressive strength	182
7.3	Conclusions	183

<b>References</b>	175
-------------------	-----

<b>Appendix</b>	187
-----------------	-----

<b>Subject Index</b>	231
----------------------	-----

# Notations and Abbreviations

## Upper case letters

$A_p$	cross section area of prestressing tendon	mm <sup>2</sup>
$C_m$	elastic tangential modulus (stiffness) of matrix	MPa
$C_f$	elastic tangential modulus (stiffness) of fibre reinforcement	MPa
$C_m^{ep}$	elastic-plastic tangential modulus of matrix	MPa
$C_f^{ep}$	elastic-plastic tangential modulus of fibre reinforcement	MPa
$E_p$	Young's modulus of prestressing tendon	MPa
$F_u$	failure load	kN
$F_{cr}$	cracking load	kN
$H_m$	hardening/softening modulus of matrix	MPa
$H_f$	hardening/softening modulus of fibre reinforcement	MPa
$K_0$	elastic tangential modulus (stiffness) of fibre reinforced material	MPa
$K_1$	elastic-plastic tangential modulus (stiffness) of fibre reinforced material after yielding of one of the constituents	MPa
$K_2$	elastic-plastic tangential modulus (stiffness) of fibre reinforced material after both constituent yielding	MPa
$L$	transfer length of prestressing tendon	mm
$M$	coupling modulus	MPa
$N_c$	compressive force in the cross-section	kN
$N_t^1$	partial tension force in the cross-section of beam	kN
$N_t^2$	partial tension force in the cross-section of beam	kN
$N_t^3$	partial tension force in the cross-section of beam	kN
$P_0$	initial prestressing force	kN
$P_{eff}$	effective prestressing force	kN
$V$	steel fibre content in volumetric fraction	%
$V_u$	ultimate shear force	kN

### Lower case letters

$a/d$	shear span to depth ratio	
$a_{mid}$	mid-point deflection	mm
$c$	cement content	kg/m <sup>3</sup>
$e$	camber of prestressing tendon	mm
$f_c$	compressive strength	MPa
$f_{c,cube}$	compressive strength measured on standard cube	MPa
$f_{c,cyl}$	compressive strength measured on standard cylinder	MPa
$f_{sp,cyl}$	splitting strength measured on standard cylinder	MPa
$f_{sp}$	splitting strength	MPa
$f_{fy}$	yield strength of steel fibres	MPa
$f_t$	tension strength or yielding strength of matrix	MPa
$f_y$	tension strength or yielding strength of fibre reinforcement	MPa
$f_m$	yield function of matrix	MPa
$f_f$	yield function of fibre reinforcement	MPa
$\bar{f}_t$	residual strength of matrix	MPa
$\bar{f}_y$	residual strength of fibre reinforcement	MPa
$f_{cd}$	design value for the compressive strength of steel fibre reinforced concrete	MPa
$f_{td}$	design value for the tensile strength of steel fibre reinforced concrete	MPa
$f_{fyd}$	design value for the yield strength of steel fibre reinforcement	MPa
$\ell$	length of cylinders	mm
$\ell_f$	length of steel fibres	mm
$s_e$	draw-in of prestressing tendon	mm
w/c	water to cement ratio	
$dx_i^c$	length of concrete portion before deformation due to prestressing	mm
$dx_i^P$	length of tendon portion before deformation due to prestressing	mm
$dx_i^{c*}$	length of concrete portion after deformation due to prestressing	mm
$dx_i^{P*}$	length of tendon portion after deformation due to prestressing	mm
$x_{i-1}^P$	i-1 <sup>th</sup> cross-section of prestressing tendon before deformation	mm
$x_i^P$	i <sup>th</sup> cross-section of prestressing tendon before deformation	mm
$x_{i-1}^c$	i-1 <sup>th</sup> cross-section of concrete before deformation	mm
$x_i^c$	i <sup>th</sup> cross-section of concrete before deformation	mm
$x_{i-1}^{P*}$	i-1 <sup>th</sup> cross-section of prestressing tendon after deformation	mm
$x_i^{P*}$	i <sup>th</sup> cross-section of prestressing tendon after deformation	mm



---

$x_{i-1}^{c*}$	i-1 <sup>th</sup> cross-section of concrete after deformation	mm
$x_i^{c*}$	i <sup>th</sup> cross-section of concrete after deformation	mm
$\Delta x_{i-1}^P$	relative displacement of the i-1 <sup>th</sup> section of prestressing tendon	mm
$\Delta x_i^P$	relative displacement of the i <sup>th</sup> section of prestressing tendon	mm
$\Delta x_{i-1}^c$	relative displacement of the i-1 <sup>th</sup> concrete section	mm
$\Delta x_i^c$	relative displacement of the i <sup>th</sup> concrete section	mm
$\emptyset$	diameter of cylinders	mm
	nominal diameter of reinforcing bar	mm
	nominal diameter of prestressing tendon	mm
$\emptyset_f$	diameter of steel fibres	mm

### Greek letters

$\alpha$	$\bar{f}_t / f_t$	-
$\alpha = \frac{\epsilon_{t0}}{\epsilon_{t2}}$	elastic tension limit strain vs. ultimate tension strain ratio	-
$\beta$	$\bar{f}_y / f_y$	-
$\beta = \frac{\epsilon_{t1}}{\epsilon_{t2}}$	yielding strain vs. ultimate tension strain of fibre reinforced concrete	-
$\ell_{bp}$	transfer length of prestressing tendon in EC2	mm
$\beta_b$	parameter to determine the transfer length in EC2	
$\epsilon$	strain	<sup>0</sup> / <sub>00</sub>
$\epsilon_0$	strain at yielding of one constituent (first yielding)	<sup>0</sup> / <sub>00</sub>
$\epsilon_1$	strain at yielding of other constituent (second yielding)	<sup>0</sup> / <sub>00</sub>
$\epsilon_{c0}$	elastic limit strain of steel fibre reinforced concrete in compression	<sup>0</sup> / <sub>00</sub>
$\epsilon_{c1}$	ultimate limit strain of steel fibre reinforced concrete in compression	<sup>0</sup> / <sub>00</sub>
$\epsilon_{t0}$	elastic limit strain of steel fibre reinforced concrete in tension	<sup>0</sup> / <sub>00</sub>
$\epsilon_{t1}$	strain at yielding of steel fibre reinforcement	<sup>0</sup> / <sub>00</sub>
$\epsilon_{t2}$	ultimate limit strain of steel fibre reinforced concrete in tension	<sup>0</sup> / <sub>00</sub>
$\epsilon^c$	concrete strain developed by prestressing force	<sup>0</sup> / <sub>00</sub>
$\epsilon^P$	strain of prestressing tendon	<sup>0</sup> / <sub>00</sub>
$\epsilon_{i-1}^c$	measured concrete deformations in the i-1 <sup>th</sup> section	<sup>0</sup> / <sub>00</sub>
$\epsilon_i^c$	measured concrete deformations in the i <sup>th</sup> section	<sup>0</sup> / <sub>00</sub>
$\epsilon_{i-1}^P$	deformation of prestressing tendon in the i-1 <sup>th</sup> section	<sup>0</sup> / <sub>00</sub>
$\epsilon_i^P$	deformation of prestressing tendon in the i <sup>th</sup> section	<sup>0</sup> / <sub>00</sub>
$\Sigma$	stress of fibre reinforced material	MPa
$\sigma$	normal stress	MPa
$\sigma_m$	stress of the matrix	MPa

---

$\sigma_f$	stress of the fibre reinforcement	MPa
$\sigma_m^{res}$	residual stress of the matrix after cracking	MPa
$\sigma_f^{res}$	residual stress of the fibre reinforcement after yielding	MPa
$\epsilon_m^p$	plastic strain of the matrix	‰
$\epsilon_f^p$	plastic strain of the fibre reinforcement	‰
$\tau$	shear stress	MPa
$\tau_u$	shear strength	MPa
$\zeta_m$	hardening/softening force of the matrix	MPa
$\zeta_f$	hardening/softening force of the fibre reinforcement	MPa
$\xi = \frac{x}{h}$	position of the neutral axis vs. dept of the cross-section ratio	
$\zeta = \frac{b}{h}$	width of the cross-section vs. dept of the cross-section ratio	
$\chi_m$	hardening/softening variable for the matrix	
$\chi_f$	hardening/softening variable for the fibre reinforcement	
$\lambda_m$	plastic multiplier for the matrix	
$\lambda_f$	plastic multiplier for the fibre reinforcement	
$\kappa$	ratio of $C_m / C_f$	
$\rho$	ratio of $C_f / C_m$	

### Special sub- or superscripts

<i>c</i>	concrete
<i>cr</i>	crack or cracking
<i>cube</i>	the given value is determined on standard cube (150×150×150 mm)
<i>cylinder</i>	the given value is determined on standard cube ( $\ell = 300, \varnothing = 150$ mm)
<i>eff</i>	effective
<i>el</i>	elastic
<i>f</i>	fibre or fibre reinforcement
<i>i</i>	incremental steps in algorithm
<i>m</i>	matrix
<i>max</i>	maximum or ultimate value
<i>min</i>	minimum value
<i>mid</i>	midpoint
<i>pl</i>	plastic
<i>res</i>	residual
<i>sp</i>	splitting

## **Abbreviations**

I and II	characteristic fibre directions
A	notation of slab formwork
ACI	American Concrete Institute
B	notation of slab formwork
B-a	steel fibre reinforced sawn concrete beams
C	notation of slab formwork
C1	prisms of compressive tests
CEB	Comité Euro-international du Béton
D	notation of formwork for steel fibre reinforced concrete beams
DB	deep beam specimens
E	notation of formwork for steel fibre reinforced prestressed pretensioned concrete beams
EC2	Eurocode 2
<i>fib</i>	fédération internationale du béton
FIP	Fédération Internationale de la Précontrainte
FRC	fibre reinforced concrete
JSCE	Japan Society of Civil Engineering
LVDT	linear voltage differential transductor
PC	prestressed concrete
pc	portland cement
RILEM	the International Union of Testing and Research Laboratories for Materials and Structures
R	random steel fibre orientation
REF	reference mix
RC	reinforced concrete
T1	prisms of tension tests

# Chapter 1

## Introduction

*Steel fibre reinforced concrete is extensively used construction material. In the last decades many research studies were directed to determine the material properties of steel fibre reinforced concrete. Chapter 1 gives a concise literature review on behaviour of steel fibre reinforced concrete in compression, in tension and in bending, respectively.*

**Keywords:** *concrete, steel fibre, steel fibre reinforced concrete, compressive strength, behaviour in compression, splitting strength, flexural toughness properties*

### 1.1 General remarks to fibre reinforced concrete

Fibre reinforced concrete is a widely used construction material in civil engineering [Balaguru & Shah (1992)]. Fibre reinforced concrete is composed of plain concrete made of portland cement, with or without silica fume or fly ash, fine and coarse aggregates, water, additives and randomly distributed or oriented short, discrete fibre reinforcement [Hannant (1978), Kausay (1994), Balaguru & Shah (1992)].

Fibres are made of several materials such as steel, polypropylene, glass, natural, etc. with different configurations. However, in civil engineering applications generally steel fibres are used. Fibre shape can be straight, deformed or collocated fibres, hooked, crimped, and paddled, undulated etc. (Table 1.1) [ACI Committee 544 (1986), Kiss (1996), Victor & Ward & Hamza (1992), Balaguru & Shah (1992), Soroushian & Marikunte (1992), Stang & Mobasher & Shah (1990)]. Some fibre types are glued together with water soluble glue in order to get much better fibre distribution and workable concrete mix [Bekaert (1994), ACI Committee 544 (1986)]. Cross-section of fibres can be circular, square, crescent-shaped or irregular [Naaman (1998), Naaman & Reinhardt (1998), Balaguru & Shah (1992)]. The common size is among 10 mm...60 mm (less than 75 mm), diameter 0.1 mm...0.6 mm, fibre content 0.5...2.0 V%, tensile strength 345...1380 N/mm<sup>2</sup>, aspect ratio (fibre length vs. fibre diameter) 30...100 in case of steel fibres [ACI Committee 544 (1986), WAJA (1995)].

Concrete grades used for fibre reinforced concrete may vary from normal strength concrete to high strength, high performance concrete [Goldfein (1965)]. Other

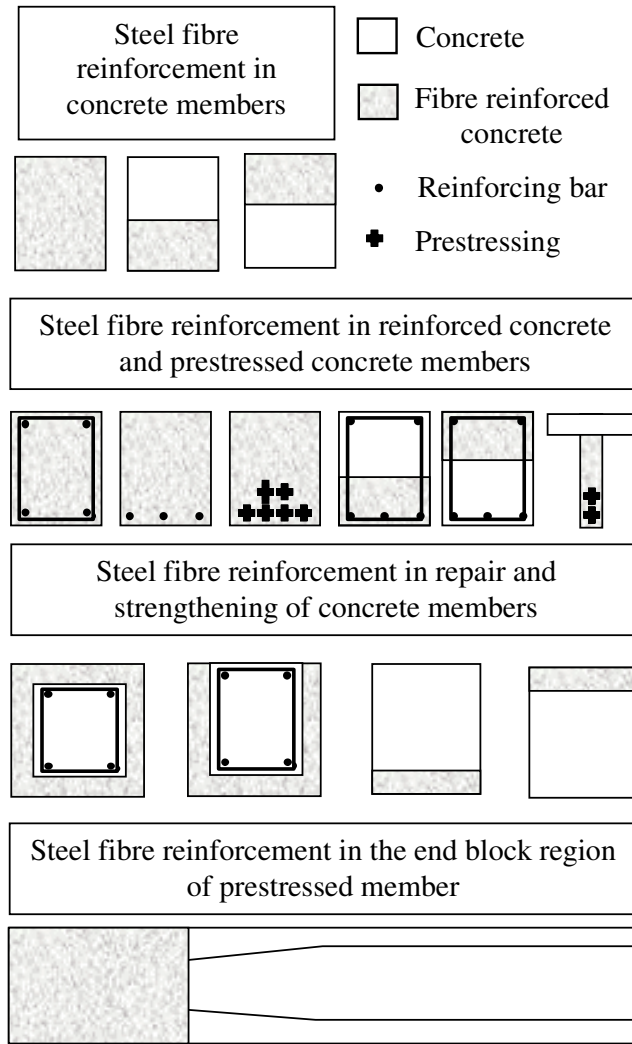
cement based materials such as mortars may also be reinforced by fibres [Gokoz & Naaman (1981), Imam & Vandewalle (1996), Reinhardt (1992)].

Mechanical properties of fibre reinforced concretes are depend on the mechanical properties of concrete mix and the used fibre type [Balaguru & Shah (1992)]. Main purpose of fibre application is to increase energy absorption capacity or ductility as well as fracture toughness of plain concrete [Groth & Noghabai (1996)]. For this reason, many airport runways, tunnels, bridge decks, pipes, industrial floors etc. were built in the last two decades applying also fibre reinforcement [Dombi (1993)].

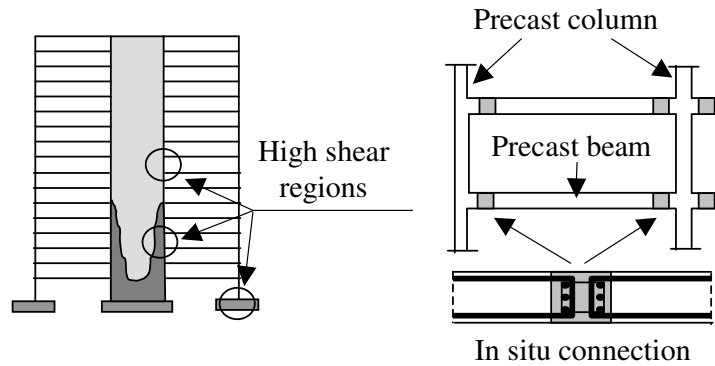
Many previous research and publications cover basic research on fibre reinforced concrete specially applying steel fibres as special construction material with characteristics different from those of conventional concrete.

**Table 1.1: Mechanical properties of different fibres**

Fibre type	Material	Diameter [ $\mu\text{m}$ ]	Length [mm]	Density [ $\text{kN/m}^3$ ]	Young modulus [ $\text{GN/mm}^2$ ]	Poisson ratio	Tensile strength [ $\text{N/mm}^2$ ]	Ultimate strain [%]	Fibre content [V%]
High strength	Steel	100...600	10...60	78.6	200	0.28	700...2000	3.5	0.5...2
Stainless		10...330	10...60	78.6	160	0.28	2100	3	0.5...2
	Asbestos	Krizotil 0.02...30	<40	25.5	164	0.3	200...1800	2...3	10
		Krocidolit 0.1...20	-	33.7	196	-	3500	2...3	-
Very stiff	Carbon	8	10	19	380	0.35	1800	0.5	2...12
High strength		9	10	19	230	0.35	2600	1	2...12
	Glass	A-glass -	-	24.6	64.8	-	3103	4.7	-
		E-glass 8...10	10...50	25.4	72	0.25	3500	4.8	2...8
		NEG AR-glass -	-	27.4	78.6	-	2448	2.5	-
	Polymer	Acrylic 13...104	-	1.17	14.6...19.6	-	207...1000	7.5...5	-
		Aramid I 12	-	1.44	62	-	3620	4.4	-
		Aramid II 10	-	1.44	117	-	3620	2.5	-
		Nylon >4	5...5	1.14	>4	0.4	750...900	13.5	0.1...6
		Polyester -	-	1.34...1.39	17.5	-	896...1100	-	-
		Polyethylene 25...1020	-	0.96	5	-	200...300	3	-
		Polypropylene -	-	0.90...0.91	-	-	310...760	150	-
Individual fibre	Poly propylene	100...200	5...50	9	>5	-	400	18	0.1...6
Bundled fibres		500...4000	20...75	9	>8	0.29...0.46	400	8	0.2...1.2
	Natural	Coconut 0.1...0.4	50...350	11.2...11.5	19...26	-	120...200	10...25	-
		Sisal -	-	-	13...26	-	280...568	3...5	-
		Bamboo 0.05...0.4	-	15	33...40	-	350...500	-	-
		Cellulose -	-	12	10	-	300...500	-	10...20
		Wood 2.5...5.0	15...80	8	-	-	700	-	-
Elephant grass		-	-	-	4.9	-	178	3.6	-



**Figure 1.1:** Application of steel fibre reinforcement in structural engineering after Naaman & Reinhardt (1998)



**Figure 1.2:** Examples of different use of steel fibre reinforcement in seismic resistance and pre cast structures after Naaman & Reinhardt (1998)

Compressive strength, tensile strength [Romualdi & Batson (1963), Stang & Rossi (1999)], tensile splitting strength, shear strength [Siao (1994), Sharma (1986)], punching shear strength [Theodorakopoulos & Swamy (1999)], flexural toughness of concrete [Krstulovic-Opara & Dogan & Uang & Haghayeghi (1997), Erdélyi (1993), Banthia & Trottier (1995)] are the main mechanical properties which are examined and primarily influenced by steel fibre addition [Balaguru & Shah (1992), Naaman & Reinhardt (1998)].

However, few results are available concerning behaviour of steel fibre reinforced concrete in structural reinforced concrete members [Balázs & Kovács (1999), Balázs & Kovács (1999)], partially and axially prestressed members [Balázs & Erdélyi & Kovács (1997), Narayanan & Kareem-Palanjian (1986), Balaguru & Ezeldin (1987)], deep beam specimens [Mansur & Ong (1991)] as well as steel fibre reinforced slabs.

Steel fibre reinforcement may effectively be used strengthening or retrofitting damaged structures such as beams, slabs, columns etc. (Figure 1.1). Other possible structural applications of steel fibre reinforced concrete are summarised in Figure 1.1 and in Figure 1.2.

Steel fibres in concrete are generally considered to be randomly oriented. However, in some special applications fibres may be oriented in the material [Stroeven (1995)] and hence, effect the mechanical properties of concrete.

## 1.2 Behaviour in compression

Since the first publication of Romualdi and Batson [Romualdi & Batson (1963)] a lot of publications dealt with the compressive behaviour of hardened steel fibre reinforced concrete. Many recommendations and standard test methods have been developed characterising the compressive strength and compressive behaviour [JSCE-SF5 (1984), UNE 83-507-86, UNE 83-504-90, RILEM (1978)]. Test methods are generally based on the testing of conventional concrete. Available test results and main conclusions are presented in Table 1.2 and in Figure 1.4.

In the last three decades effect of steel fibre reinforcement on the compressive behaviour of concrete were discussed from many aspects. Summary of the main experimental observations are discussed in this section hereafter.

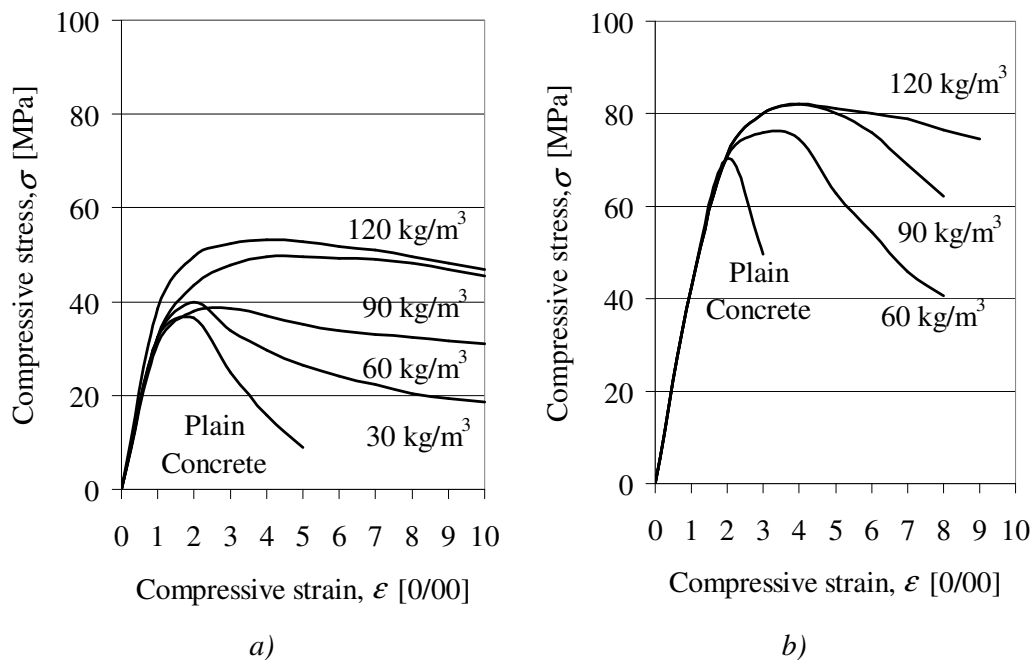
Increment in concrete compressive strength provided by steel fibre reinforcement rarely exceeds 25% [Balaguru & Shah (1992)]. With increased use of the available fibre types, the applied fibre quantity in concrete members is often limited in around 50-60 kg/m<sup>3</sup> [Balaguru & Shah (1992), Bekaert (1994), Kausay (1994)]. At this volume fraction which is less than 0.75 V% the strength increment can be considered negligible for all design purposes [Mansur & Paramasivam (1986), Narayan & Jones & Ciam (1993)]. In some special cases where the steel fibre content is more than 100-120 kg/m<sup>3</sup>, strength increment may be expected [Sanat & Nyogi & Dwarkaranathan (1985), Balaguru & Shah (1992), Naaman & Reinhardt (1998)] as can also be seen in Figure 1.3. However, some researchers reported decrease in concrete strength applying steel fibres which outlines the significance of porosity of concrete, mixing process and appropriate design of concrete mix [Falkner & Kubat & Droese (1994)] (Figure 1.4).

Other main factors to be considered in structural design are the modulus of elasticity, the strain at peak load, the post-peak behaviour and the ultimate compressive strain. Change in modulus of elasticity can be considered negligible from the point of

view of structural design [Balaguru & Shah (1992)]. On the other hand, fibres make a considerable contribution in compressive toughness [Balaguru & Shah (1992), Naaman & Reinhard (1998), Reinhard & Naaman (1999)]. Addition of steel fibres increases the strain at peak load and ultimate strain leading to a less steep and more reproducible descending branch of stress-strain diagram (Figure 1.3). Overall, steel fibre reinforced concrete can absorb more energy before failure in compression compared to plain concrete [Balaguru & Shah (1992), Naaman & Reinhard (1998)].

Increase in compressive toughness or ductility provided by steel fibres depend on many parameters such as fibre volume fraction, fibre geometry and matrix properties [Balaguru & Shah (1992), Naaman & Reinhard (1998), Reinhard & Naaman (1999)]. An increase in fibre content results in an increase in energy absorption capacity. However, the relative magnitude of energy increase in the 0 V% to 0.7 V% fibre volume fraction range is much greater than further energy increase in the 1.0 V% to 2.0 V% volume fraction range [Balaguru & Shah (1992), Naaman & Reinhard (1998)] as can be seen in Figure 1.3.

With respect to the fibre geometry, the fibre length vs. fibre diameter ratio (aspect ratio) is particularly important for the performance of straight steel fibres [Romualdi & Batson (1963)]. As the aspect ratio increases, ductility increases as long as fibres can properly mixed with the concrete [Craig & Parr & Germain & Mosquera & Kamilaes (1986), Erdélyi (1993), El-Niema (1991)]. In the case of deformed steel fibres (hooked, crimped, etc.), fibres provide better energy absorption capacity. However, aspect ratio plays an important role even in the case of deformed steel fibres [Erdélyi (1993)].

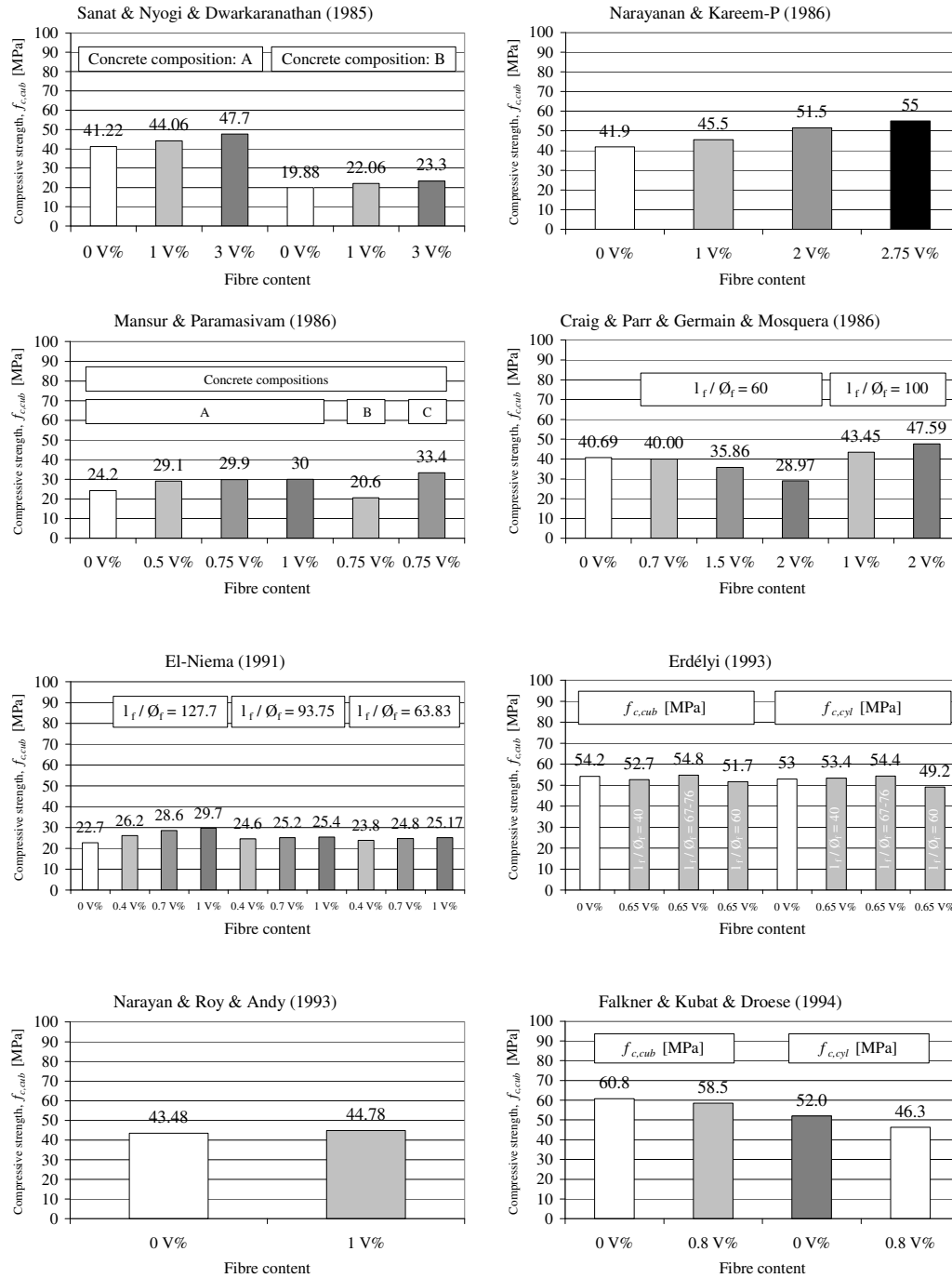


**Figure 1.3:** Compressive stress-strain behaviour of normal (a) and high strength (b) concrete effected by hooked end steel fibre [Balaguru & Shah (1992)]



**Table 1.2:** *Experimental variables and constants for concrete compressive strength experimental results as well as their main conclusions*

<p><b>Sanat &amp; Nyogi &amp; Dwarkaranathan (1985)</b>            Straight steel fibre aspect ratio: <math>l_f / \phi_f = 50 / 1 = 50</math>, Fibre strength: <math>f_f = 326\text{-}360</math> MPa            Fibre contents: 0 V%, 1 V%, 3 V%, Concrete mix proportions:            A: 1 : 1.2 : 2 = cement : fine aggregates : course aggregates, w/c = 0.50            B: 1 : 2.4 : 4 = cement : fine aggregates : course aggregates, w/c = 0.55  <b>Main conclusion:</b> Compressive strength increased by the increase of fibre content independently from the used concrete mix proportion.</p>	Cube test: 150×150×150 mm
<p><b>Mansur &amp; Paramasivam (1986)</b>            Hooked-end steel fibre aspect ratios: <math>l_f / \phi_f = 30 / 0.50 = 60</math>, Concrete mix proportion:            A: 1 : 2.80 : 2.60 = cement : fine aggregates : course aggregates, w/c = 0.62            B: 1 : 3.84 : 3.01 = cement : fine aggregates : course aggregates, w/c = 0.70            C: 1 : 2.32 : 2.06 = cement : fine aggregates : course aggregates, w/c = 0.48            Fibre contents: A: 0 V%, 0.5 V%, 0.75 V%, 1 V%, B: 0.75 V%, C: 0.75 V%  <b>Main conclusion:</b> Slightly increase in compressive strength was observed by the increasing hooked-end steel fibre content.</p>	Cylinder test: $\phi = 150$ mm, $l = 300$ mm
<p><b>Narayanan &amp; Kareem-P. (1986)</b>            Steel fibre aspect ratio: <math>l_f / \phi_f = 38 / 0.38 = 100</math>, Fibre strength: <math>f_f = 1800\text{-}2000</math> MPa            Fibre contents: 0 V%, 1 V%, 2 V%, 2.75 V%, Concrete mix proportions:            1 : 3 = cement : fine aggregate, w/c = 0.50  <b>Main conclusion:</b> Increment in compressive strength measured on standard cube was proportionally to the used steel fibre content.</p>	Cube test: 150×150×150 mm
<p><b>Craig &amp; Parr &amp; Germain &amp; Mosquera &amp; Kamilares (1986)</b>            Hooked- end steel fibres aspect ratios: <math>l_f / \phi_f = 30/0.5 = 60</math>, <math>l_f / \phi_f = 50/0.5 = 100</math>            Fibre contents: 0 V%, 0.70 V%, 1 V%, 1.5 V%, 2 V%  <b>Main conclusion:</b> Concrete strength increased by the use of <math>l_f / \phi_f = 100</math> aspect ratio, while decreased by the use of <math>l_f / \phi_f = 60</math> aspect ratio applying more fibre.</p>	Cylinder test: $\phi = 150$ mm, $l = 300$ mm
<p><b>El-Niema (1991)</b>            Crimped steel fibre aspect ratios: <math>l_f / \phi_f = 127.7</math>, <math>l_f / \phi_f = 95.75</math>, <math>l_f / \phi_f = 63.83</math>            Fibre contents: 0 V%, 0.4 V%, 0.7 V%, 1 V%, Concrete mix proportion:            1 : 2.36 : 2.50 = cement : fine aggregate : course aggregate, w/c = 0.50  <b>Main conclusion:</b> By the increase of steel fibre content higher compressive strength was obtained with higher fibre aspect ratio.</p>	Cylinder test: $\phi = 150$ mm, $l = 300$ mm
<p><b>Narayan &amp; Jones &amp; Andy &amp; Ciam (1993)</b>            Crimped steel fibre aspect ratio: <math>l_f / \phi_f = 50 / 0.50 = 100</math>, Fibre strength: <math>f_f = 1570</math> MPa            Fibre contents: 0 V%, 1 V%  <b>Main conclusion:</b> Increment in compressive strength measured on standard cube was detected by increasing steel fibre content.</p>	Cube test: 150×150×150 mm
<p><b>Erdélyi (1993)</b>            Hooked- end steel fibres aspect ratios: <math>l_f / \phi_f = 40</math>, <math>l_f / \phi_f = 67\text{-}76</math>, <math>l_f / \phi_f = 60</math>            Fibre contents: 0 V%, 0.65 V%, Concrete mix proportion: w/c = 0.38  <b>Main conclusion:</b> Both cube and cylinder strength was effected by the fibre aspect ratio</p>	Cube test: 150×150×150 mm Cylinder test: $\phi = 150$ mm, $l = 300$ mm
<p><b>Falkner &amp; Kubat &amp; Droese (1994)</b>            Hooked-end steel fibre aspect ratios: <math>l_f / \phi_f = 50 / 0.60 = 83.33</math>, Fibre strength: <math>f_f = 1250</math> MPa            Fibre contents: 0 V%, 0.8 V%, Concrete mix proportion:  <b>Main conclusion:</b> Slight decrease in compressive strength was observed by the increasing hooked-end steel fibre content in case of both cube and cylinder tests.</p>	Cube test: 150×150×150 mm Cylinder test: $\phi = 150$ mm, $l = 300$ mm



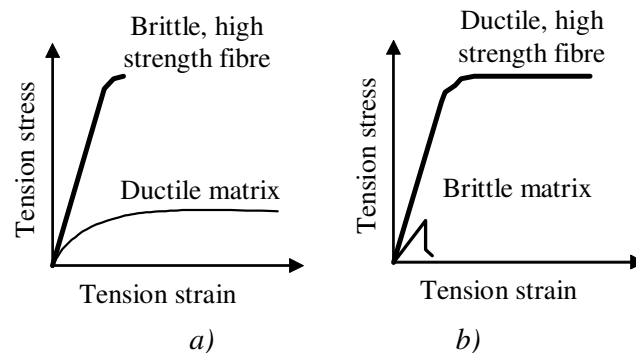
**Figure 1.4:** Summary of literature review on typical test results on compressive strength of steel fibre reinforced concrete. Strengths were determined in 28 days of concrete and measured on standard cube ( $150 \times 150 \times 150$  mm) and standard cylinder ( $\phi = 150$  mm,  $\ell = 300$  mm) specimens.

Brittleness of the matrix itself plays an important role in the behaviour of steel fibre reinforced concrete. High strength concrete tends to be more brittle than normal strength [Balaguru & Shah (1992), Naaman & Reinhard (1998)]. Brittleness is even more pronounced for concrete containing fly ash and silica fume. Application of silica fume in concrete mix tends to provide better bond behaviour between concrete matrix and steel fibres and hence, makes them more effective structural material [Balaguru & Shah (1992), Naaman & Reinhard (1998)].

For this reason, higher fibre volume fraction and higher yielding strength of fibre is needed for high strength concrete to produce ductile failure. Compressive strength seems to govern the brittleness of both plain and steel fibre reinforced concretes. Higher compressive strength always results in a brittle mode of failure for both normal weight and light weight concrete [Balaguru & Shah (1992), Naaman & Reinhard (1998)].

### 1.3 Tensile strength

Development and research of fibre reinforced materials spray largely from the publication of Griffith in 1921. He studied that the strength of glass reinforced composites made with brittle matrix material increased manifold as the diameter of the used high strength but brittle fibre decreased. Further, in 1963, Romualdi and Batson [Romualdi & Batson (1963)] considered steel fibre reinforced cement based composites. In their pioneer research they applied relatively high strength and ductile fibre reinforcement in brittle matrix. In civil engineering applications due to the most applied structural material (concrete and reinforced concrete), generally ductile steel fibre reinforcement are used. Demonstrative stress-strain diagrams for the variation of matrix and fibre behaviours are presented in Figure 1.5. In the last three decades development of fibre reinforced materials have been developing rapidly from the concrete containing relatively low fibre content [Bekaert (1994)] to the high strength high performance cement based composites [Reinhardt & Naaman (1992), Naaman & Reinhardt (1998), Reinhardt & Naaman (1999)].



**Figure 1.5:** Behaviour of fibre reinforced composite constituents in tension  
 a) Brittle fibre and ductile matrix b) Ductile fibre and brittle matrix

Understanding the tensile behaviour of steel fibre reinforced concrete is the bases of any further engineering application or appropriate structural modelling. For this reason proper determination of tensile strength and tensile characteristics of steel fibre reinforced concrete was one of the main objectives in the last decades.

High number of publications, developments, standardised test methods and recommendations have been previously developed on this field. Representative results on tensile splitting strength of steel fibre reinforced concrete are summarised in Figure 1.7. Main conclusions and main experimental parameters of tests and constants are also represented in Table 1.3. Summary of the main experimental observations on the behaviour in direct tension made in the last decades are treated in this section hereafter.

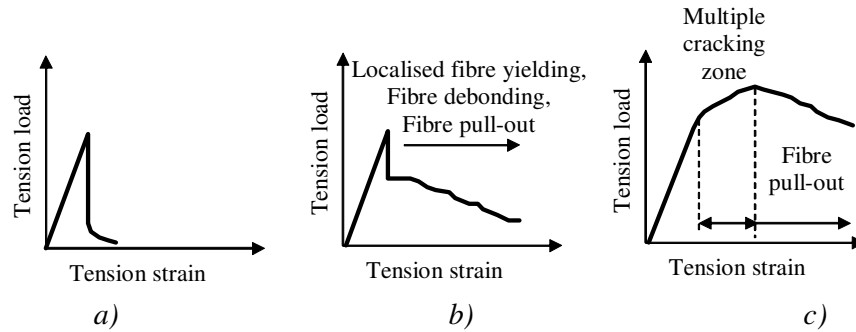
One of the primary reasons for using steel fibres in a relatively brittle tensioned concrete is to improve ductility of plain concrete [Balaguru & Shah (1992), Naaman & Reinhard (1998)]. Though, large dosage of steel fibres gives increase in tensile strength as well [Romualdi & Batson (1963)]. From structural point of view due to the workability problem of the concrete containing high volume fraction of steel fibres it is kept in relatively low level ( $20 \text{ kg/m}^3 - 40 \text{ kg/m}^3$ ) [Bekaert (1994), Kausay (1994), Naaman & Shah (1976)], which resulting in a negligible increase in tension strength. However, in same special application of steel fibre reinforced concretes where the fibre content may be higher than 2.0 V% or more, significant increment in tensile strength can be achieved [Balaguru & Shah (1992), Naaman & Reinhard (1998), Krstulovic-Opara & Malak (1997)]. Tensile response of high performance concretes indicates strain hardening behaviour [Naaman & Reinhard (1998), Krstulovic-Opara & Malak (1997)]. Representative stress-strain curves for steel fibre reinforced concrete in tension are summarised in Figure 1.6.

Due to the different behaviour of concretes in tension caused by increasing fibre content, three different types of concretes can be distinguished [Balaguru & Shah (1992)].

*At low steel fibre contents* fibre reinforced concretes suddenly fracture after cracking. This category of behaviour is very close to the behaviour of plain concrete and hence, does not have any significance on the structural performances (Figure 1.6/a).

*At medium steel fibre contents* the load-carrying capacity could drop but the specimen could continues to resist further loads which are lower than the cracking load after cracking. In this stage of loading the load is transferred from the matrix to the fibres at the cracked interface [Maage & Magne (1978), Naaman & Najm (1991)]. Further load capacity depends on the transfer mechanism of fibres represented by localised fibre yielding, debonding and pull-out of fibres [Naaman & Shah (1976), Balaguru & Shah (1992)]. By increasing load, more and more localised fibre yielding, debonding and pull-out occur, resulting lower and lower load carrying capacities in tension [Gopalaratnam & Abu-Mathkour (1987), Abrishami & Mitchel (1996), Gray & Johnston (1978)]. It is also observed in this range of fibres that steel fibres do not provide an increase in tensile strength but provide significant ductile behaviour which can be represented by the area under the stress-strain diagram (Figure 1.6/b) [Romualid & Batson (1964), Balaguru & Shah (1992)].

*At relatively high steel fibre contents* (Figure 1.6/c), fibres will start carrying increased load [Reinhardt & Naaman (1999)] after cracking. If there is a sufficient amount of fibres in the cracked section they continue to resist higher loads than the cracking load. After cracking the stiffness of the stress-strain diagram will drop because of the loss of concrete contribution [Naaman & Otte & Najm (1991)].



**Figure 1.6:** Steel fibre reinforced concrete behaviour in tension after Balaguru & Shah (1992)

a) Low steel fibre content b) Medium steel fibre content c) High steel fibre content

**Table 1.3:** Experimental variables and constants for experimental results on concrete splitting strength

<i>Hughes &amp; Fattuhi (1977)</i>	Cylinder splitting test: $\varnothing = 150$ mm, $\ell = 300$ mm Hooked-end steel fibre $\ell_f / \varnothing_f = 41 / 0.36 = 113$ , Crimped steel fibre $\ell_f / \varnothing_f = 49 / 0.51 = 96$ , round steel fibre $\ell_f / \varnothing_f = 60 / 0.50 = 120$ and $\ell_f / \varnothing_f = 23 / 0.50 = 46$ , Fibre contents: 0 V%, 1.5 V%.
<b>Main conclusion:</b> Splitting strength of steel fibre reinforced concrete is depend on the aspect ratio of the used steel fibres considering the same fibre volume fraction. Higher aspect ratio result higher splitting strength	
<i>Ghalib &amp; Mudhafar (1980)</i>	Cylinder splitting test: $\varnothing = 150$ mm, $\ell = 300$ mm Flat crimped steel fibres with different aspect ratios: $\ell_f / \varnothing_f = 40 / 0.65 = 62$ , $\ell_f / \varnothing_f = 18 / 0.25 = 72$ , $\ell_f / \varnothing_f = 58 / 0.65 = 89$ , $\ell_f / \varnothing_f = 40 / 0.40 = 100$ , Fibre contents: 0 V%, 1.0 V%, 1.5 V%
<b>Main conclusion:</b> Splitting strength of steel fibre reinforced concrete increased by the use of steel fibre content. Increment in splitting strength was proportionally to the fibre content.	
<i>Sanat &amp; Nyogi &amp; Dwarkaranathan (1985)</i>	Cylinder splitting test: $\varnothing = 150$ mm, $\ell = 300$ mm Straight steel fibre aspect ratio: $\ell_f / \varnothing_f = 50 / 1 = 50$ , Fibre strength: $f_f = 326$ -360 MPa Fibre contents: 0 V%, 1 V%, 3 V%, Concrete mix proportions: A: 1 : 1.2 : 2 = cement : fine aggregates : coarse aggregates, w/c = 0.50 B: 1 : 2.4 : 4 = cement : fine aggregates : coarse aggregates, w/c = 0.55
<b>Main conclusion:</b> Splitting strength increased by the increase of fibre content independently from the used concrete mix proportion.	
<i>Sharma (1986)</i>	Cylinder splitting test: $\varnothing = 150$ mm, $\ell = 300$ mm Hooked-end steel fibre aspect ratio: $\ell_f / \varnothing_f = 50 / 0.6 = 80$ , Fibre contents: 0V%, 0.96 V%, Concrete mix proportions: Plain concrete: 483 : 655 : 980 : 215 = cement : fine aggregates : coarse aggregates : water, w/c = 0.45 Fibre concrete: 483 : 655 : 980 : 235 = cement : fine aggregates : coarse aggregates : water, w/c = 0.49
<b>Main conclusion:</b> Steel fibres was effective to improve the splitting strength of steel fibre reinforced concrete	
<i>Narayanan &amp; Kareem-P (1986)</i>	Cylinder splitting test: $\varnothing = 150$ mm, $\ell = 300$ mm Steel fibre aspect ratio: $\ell_f / \varnothing_f = 38 / 0.38 = 100$ , Fibre strength: $f_f = 1800$ -2000 MPa Fibre contents: 0 V%, 1 V%, 2 V%, 2.75 V%, Concrete mix proportions: 1 : 3 = cement : fine aggregate, w/c = 0.50
<b>Main conclusion:</b> By the increase of steel fibre content higher splitting strength was obtained	
<i>Victor &amp; Ward &amp; Hanza (1992)</i>	Cylinder splitting test on mortar compositions: $\varnothing = 77$ mm, $\ell = 154$ mm Cylinder splitting test on mortar concrete: $\varnothing = 100$ mm, $\ell = 200$ mm Mortar and concrete compositions, Aramid ( $\ell_f = 6.4$ mm), Acrylic ( $\ell_f = 6.4$ mm), Steel ( $\ell_f = 25$ mm and 50 mm) and Polyethylene ( $\ell_f = 12.7$ mm) fibres, Fibre contents: 0 V%, 1.0 V%, 2.0 V%
<b>Main conclusion:</b> Steel fibres are more effective to improve splitting strength than other synthetic fibres	
<i>Wafa &amp; Hasnat &amp; Tarabolsi (1992)</i>	Cylinder splitting test: $\varnothing = 150$ mm, $\ell = 300$ mm Hooked-end steel fibres, Fibre contents: 0 V%, 0.5 V%, 1 V%, 1.5 V%, 2 V%
<b>Main conclusion:</b> significant increment in splitting strength was determined by increasing hooked-end steel fibre content.	

The slope of the post cracking behaviour depends on the steel fibre content and bond properties of fibres. By increasing the load, more cracks will appear along the length of specimens. Finally, when fibres start to pull out from the concrete the load-carrying capacity will start to drop. This type of failure provides for optimum use of the fibre and matrix properties (Figure 1.6/c) even if it usually means workability problem [Balaguru & Shah (1992)].

According to Figure 1.6 three different branches of tensile stress-strain diagram can be distinguished: elastic, inelastic or multiple cracking and post peak. As summarised earlier these three parts of stress-strain diagram may not be always obtained for all fibre reinforced concrete. Existence of the three branches depends on the concrete and steel fibre reinforcement properties such as fibre length, fibre diameter, fibre shape, fibre content and the bond characteristic between fibres and concrete.

First range representing the pre-cracking or elastic behaviour of the material and can be defined by the modulus of elasticity of the concrete by neglecting the effect of steel fibres [Naaman & Otter & Najm (1991)].

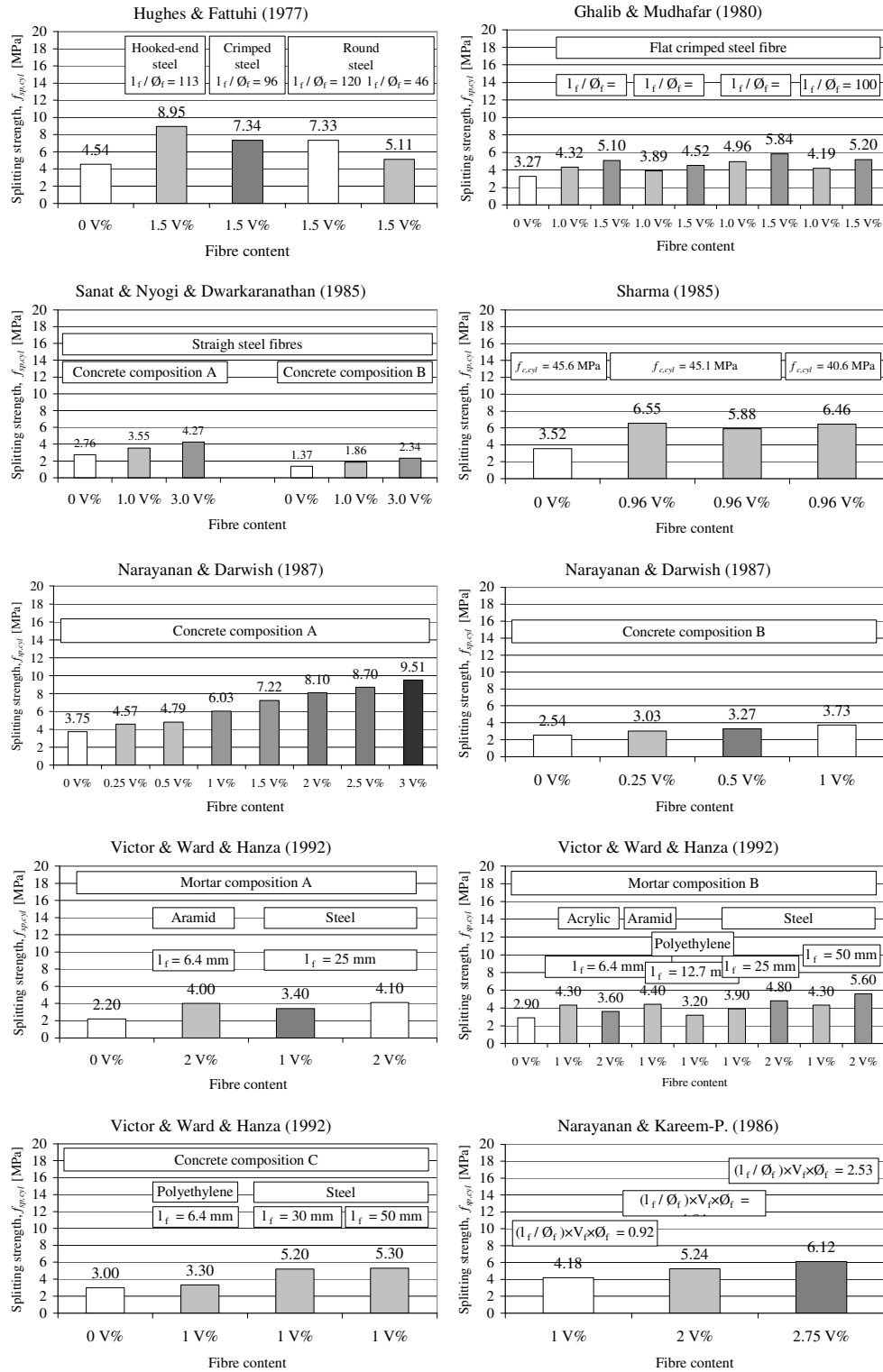
Second segment – if exists – can be considered as a strain region where nonlinear deformations or plastic deformations occur. This region is well identified between the developing of the first crack and the ultimate tensile strength of material [Reinhardt & Naaman (1999)]. This strain hardening type behaviour is often observable for the case of high performance fibre reinforced cement based composites. Third considerable part of the stress-strain diagram represents the post peak behaviour which can be described by the fibre pull-out mechanism depending on the fibre geometry, fibre shape [Naaman (1998)] and fibre volume fraction. The postcracking strength can vary from the negligible (brittle behaviour) to the tensile strength of material (perfectly plastic behaviour) [Balaguru & Shah (1992)].

However, fibres are usually considered to be random in the material which is quite a simplification for thin or 2D structural elements such as slabs, shells or walls [Ward & Li (1990), Mansur & Ong (1991)]. Further, in some special application, structural performances of steel fibre reinforced pre-cast elements are also effect by the fibre orientation due to the casting process or the vibration of concrete. Local or global behaviour of structures are also effect the fibre orientation, particularly in the boundary regions of specimens [Stroeven (1995)]. Steel fibre reinforced concrete started to be a structural material in the last decades but the problems of the fibre orientation is permanently under debate, hence, further experimental and theoretical investigations are needed.

Reliable determination and modelling of stress-strain relationship of steel fibre reinforced concrete in uniaxial tension is important for structural design [Bekaert (1994), Dulácska (1994), Dulácska (1996), Kovács (1998), Kovács (1998), Kovács (1999)].

From the pioneer study of Romualdi and Batson [Romualdi & Batson (1963), Romualdi & Batson (1964)] many experimental and theoretical study were done on the behaviour of different steel fibre reinforced concrete in tension [Bolander & Saito (1992), Krstulovic-Opara & Malak (1997), Lim & Paramasivam & Lee (1987), Naaman & Otter & Najm (1991)].

Analytical and theoretical models for modelling of bending behaviour were developed taking into consideration the effect of fibre and concrete parameters [Dulácska (1994)].



**Figure 1.7:** Summary of literature review on typical test results on cylinder splitting strength of steel fibre reinforced concrete. Strengths were determined in 28 day of concrete and measured on cylinder ( $\phi = 150$  mm,  $\ell = 300$  mm,  $\phi = 100$  mm,  $\ell = 200$  mm,  $\phi = 77$  mm,  $\ell = 154$  mm) specimens.

Due to the experimental complications of the direct tensile test [*Stang (1998), Stang & Rossi (1999)*] stress – strain relationships are indirectly determined based on bending test [*RILEM (1999)*]. Generally, tensile stress – crack opening ( $\sigma - w$  method) [*RILEM (1999)*] relationship is measured. Stress – strain relationships of developed models are generally based on experimental observations (Table 1.4).

In the beyond model proposals steel fibre reinforced concrete is considered to be a material which can be characterised at the level of the material. However, steel fibre reinforced concrete is composed of two phases, the concrete phase (matrix) and the phase of steel fibres (reinforcement) which phases define a fibre reinforced material. The two phases are connected by a third element which couples the plastic deformations of the matrix and the fibres.

## 1.4 Toughness properties

Reinforced concrete members are primarily subjected to bending. In reinforced concrete beams the internal compressive and tensile forces in the cross-section are acting in the compressed portion of the concrete section and in the steel bars, respectively. Application of steel fibre reinforcement in plain concrete may produce residual tension forces in the cracked cross-section after cracking and hence, resulting tougher behaviour [*Naaman & Reinhardt (1998), Naaman & Shah (1976), Reinhardt & Naaman (1992), Reinhard & Naaman (1999)*]. In addition to, primary objectives of steel fibre addition to plain or reinforced concrete is to improve the energy-absorbing capacity [*Balaguru & Shah (1992), Balaguru & Narahari & Patel (1992), Erdélyi (1993), Gopalartnam (1991)*], which can be calculated according to the area under the stress–strain diagram or the load – deflection behaviour [*ASTM C 1018-89 (1990), ASTM C 1018-89 (1990), JSCE-SF3 (1984), JSCE-SF4 (1984)*].

In the case of bending, the area under the load – deflection curve is used to estimate the energy-absorbing capacity or toughness of fibre reinforced concrete.

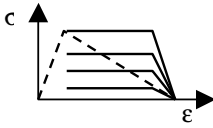
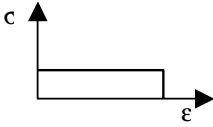
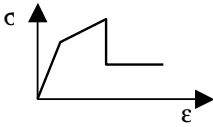
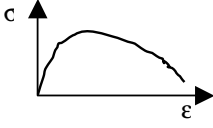
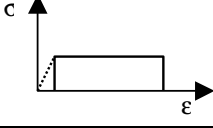
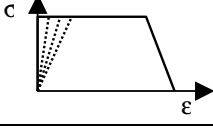
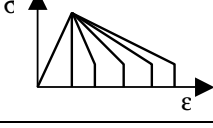
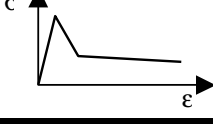
Toughness also means improved performance and resistance in fatigue, impact and explosive loads [*Ramakrishnan & Josifek (1987), Ramakrishnan & Oberling & Tatnall (1987), ACI Committee 215 (1990), Batson (1972), Kormeling & Reinhardt & Shah (1980), Wu & Shivaroj & Ramakrishnan (1989)*]. Toughness mechanism yields to ductile behaviour. Toughness or ductile performances of steel fibre reinforced concrete are often characterized by the use of different toughness indexes [*ASTM C 1018-89 (1990), Banthia & Trottier (1995), JSCE-SF3 (1984)*].

Generally, toughness properties of steel fibre reinforced concrete are determined by the load-deflection relationships. Determination process of toughness are effected by the following main parameters: fibre type, fibre geometry, fibre volume fraction, concrete composition, geometry of specimen, loading configuration, loading rate, deflection measuring system, type of test control (force or displacement controlled) and the stiffness of testing machine compared to stiffness of specimen [*Balaguru & Shah (1992), Erdélyi (1993)*]. However, appropriate determination and accurate expression as well as design purpose of toughness properties are still under discussion [*Balaguru & Shah (1992)*]

Presently available methods for evaluating toughness of steel fibre reinforced concrete on different way are the followings: ASTM C 1018 Standard test method of FRC toughness characterisation [*ASTM C 1018-89 (1990)*], (see Figure 1.8/a),

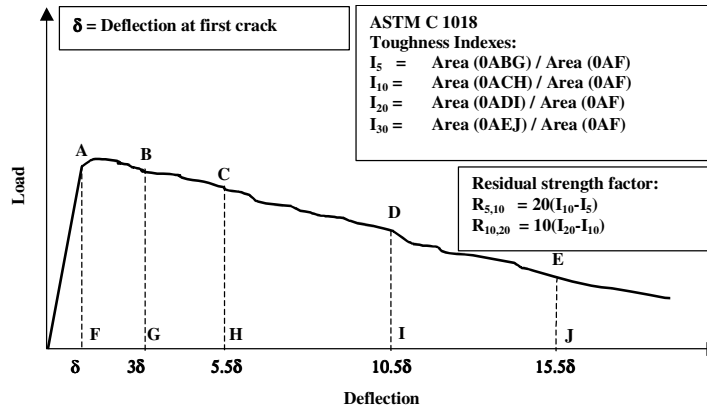


**Table 1.4:** Tensile stress – strain relationships for the tensile stress distributions of cross-sections in bending according to Dulácska (1994)

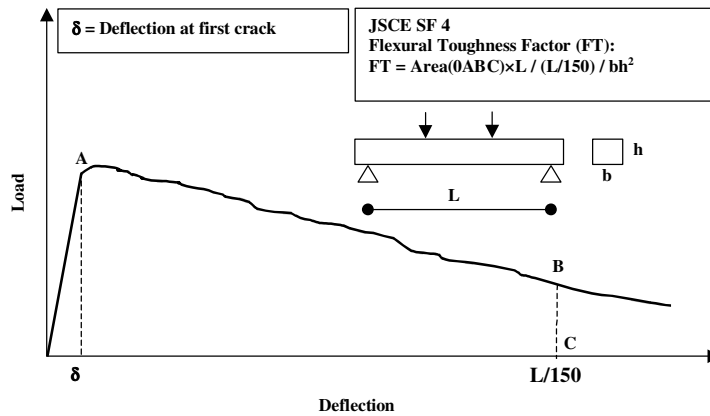
Author(s)	Stress – strain relationship	Main model considerations
Craig (1987)		Proposed model is determined by according to the applied fibre content and the bond properties of fibre and concrete.
Hannant (1978)		Constant residual stress distribution is considered in the tensioned portion of the cross-section.
Kasperkievicz (1978)		Elastic-plastic behaviour of the composite (multiple cracking zone) is represented by elastic stiffness degradation after first cracking.
Laws & Walton (1978)		Model proposal is completely based on the experimental characterisation of the real stress-strain relationships.
Schnütgen (1989)		Constants residual stress distribution is considered acting only in the cracked portion of the cross-section.
Eddington (1973)		Perfectly rigid – perfectly plastic or elastic – perfectly plastic behaviour with different elastic stiffness is considered.
Gretsler & Muni (1991)		Decreasing tensile stress after the elastic branch of the stress-strain diagram which is determined by experiments.
RILEM TC 163-TDF (1999)		Stress-strain relationships are determined by experiments.

JSCE Method of test for flexural strength and flexural toughness of fibre reinforced concrete [(*JSCE-SF3 (1984)*)] (see Figure 1.8/b) and test methods for flexural toughness characterisation of fibre reinforced concrete proposed by Banthia and Trottier [(*Banthia & Trottier (1995)*)], (see Figure 1.8/c).

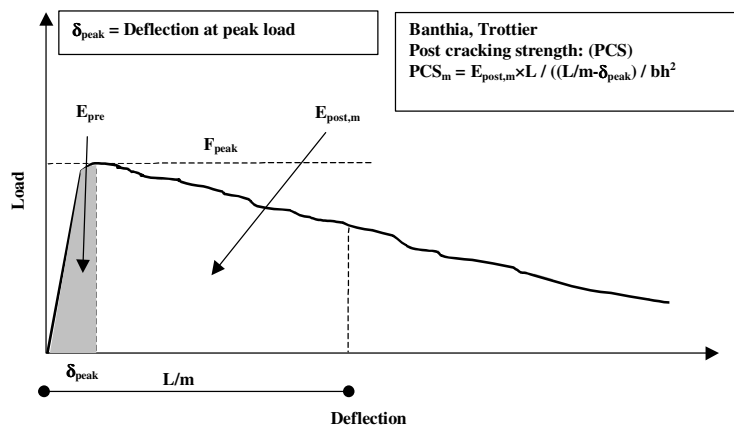
Geometry of specimens as well as the working process influence toughness properties of steel fibre reinforced concrete. Geometry of standardised beam specimens (600×150×150 mm) is not appropriate to investigate real beam behaviour [(*Erdélyi (1993)*)]. In addition to, fibre orientation may also influence the toughness properties [(*Kovács (1998)*)].



a) ASTM C 1018 Standard test method of FRC toughness characterization



b) JSCE SF 4 Method of FRC toughness characterization



c) Proposal of Banthia and Trottier method of post cracking strength

Figure 1.8: Methods for characterizing the toughness properties of steel fibre reinforced concrete

## 1.5 Fibre reinforcement in structural elements

One of the main motivations of applying fibre reinforcement in concrete structures and in reinforced concrete structural elements is to increase the toughness properties of the concrete matrix [Balaguru & Shah (1992), Banthia & Trottier (1995), Dulácska (1994)]. After initiation of cracks, fibres can carry residual forces in the cracked section by bridging the two face of crack providing redistribution of the stresses in the structural elements consequently resulting significant increment in the overall structural toughness [Naaman (1998), Naaman & Reinhardt (1998)]. Therefore steel fibre reinforced concrete is especially applied for concreting industrial floor slabs [Reinhardt & Naaman (1992), Balaguru & Shah (1992)], roads and pavements, airfield runways, tunnel structures, tubes and other concrete products [Reinhardt & Naaman (1999)]. Fibre reinforcement can be effectively used as retrofitting material as well [Krstulovic-Opara & Malak (1997), Krstulovic-Opara & Dogan & Uang & Haghayeghi (1997), Krstulovic-Opara & Al-Shannag (1999)].

On the other hand, application of steel fibre reinforcement – where possible – may reduce the producing cost by partially or fully replacing the conventional steel bar reinforcement by steel fibres and in some case decreasing the building time [Balázs & Kovács (1997), Balázs & Kovács (1999), El-Niema (1991), Imam & Vandewalle (1996)]. The present research aimed to investigate the possible rational application of steel fibre reinforcement in case of load-bearing structures [Kovács (1997), Lim & Paramasivam & Lee (1987), Narayan & Swamy & Jones & Chiam (1993), Swamy & Jones & Chiam (1993), Tan & Murugappan & Paramasivam (1993), Balaguru & Ezelidin (1987), Mansur & Ong & Paramasivam (1986)], apart from the more conventional use of fibres for increasing toughness of slabs etc.

There are two main reasons why fibres were not used earlier in reinforced concrete. One of them is the relatively high fibre cost [Hannant (1978), Balaguru & Shah (1992)]. At the level of material, steel fibre reinforced concrete is more expensive than the conventional reinforced concrete. Secondly, engineers need clear and practical design methods for design structures applying fibre reinforcement. Still, only a few methods are available for design, primarily focusing on some special structural elements or steel fibres [ACI Committee 544 (1988), Bekaert (1994), Craig (1987), DIN (1991), Dulácska (1994), RILEM (1999), Theodorakopoulos & Swamy (1999), DBV-Merkblatt (1991), DBV-Merkblatt (1992), Vorläufige Richtlinien (1995)].

Many publications cover basic research on steel fibre reinforced concrete as special concrete with characteristics different from those of conventional concrete [ACI (1987), Agarwal & Broutman (1980), Balaguru (1994), Balaguru & Ramkrishnan (1986), Di Prisco & Caruso & Piatti (1994), Dubey & Banthis (1998), Mangat & Molloy & Gurusamy (1989)]. However, relatively few results are available concerning the behaviour of steel fibre reinforced concrete in structural members. Previous structural tests generally focused on the bending [Lim & Paramasivam & Lee (1987)], shear [Acharya & Kemp (1965), El-Niema (1991), Mansur & Ong & Paramasivam (1986), Narayanan & Darwish (1987), Tan & Murugappan & Paramasivam (1993), Valle & Buyukozturk (1992)] and torsion [Narayanan & Kareem-P. (1986)] behaviour of beams with or without longitudinal and transversal reinforcement applying also fibre reinforcement.

Many publications cover basic research on steel fibre reinforced concrete as special concrete with characteristics different from those of the conventional concrete [Naaman (1992), Naaman & Reinhardt (1998), Reinhardt & Naaman (1992), Reinhardt & Naaman (1999)]. Few results are available concerning the behaviour of steel fibre reinforced concrete in structural reinforced concrete members [El-Niema (1991), Imam & Vandewalle (1996), Mansur & Ong & Paramasivam (1986), Sharma (1986), Spadea & Bencardio (1997), Swamy & Jones & Chiam (1993), Tan & Murugappan & Paramasivam (1993)], partially prestressed members and axially prestressed members [Balaguru & Ezeldin (1987), Narayanan & Kareem-P. (1986), Wafa & Hasnat & Tarabolsi (1992)]. Tests were carried out to study the punching behaviour of prestressed steel fibre reinforced concrete flat slabs as well [Theodorakopoulos & Swamy (1999)].

In case of prestressed pretensioned structural members the reliable determination of the transfer length of prestressing strands is a very important issue both for the end block design and for the analysis of the structural member under different loads [Erdélyi (1996)]. Short transfer lengths are unfavourable in case of the end block design while long transfer lengths may decrease the moment and shear capacity of the member [Erdélyi (1996)]. End block design needs special care because several cracks may develop during the release of the prestressing force, especially in case of relatively low concrete tensile strength or in absence of proper end-reinforcement. Sudden release of prestressing force often gives an impact to the end block during cutting the strands which also influences the transfer length.

The transfer length of a prestressed pretensioned concrete member is defined as the length required developing the effective prestressing force in the strand by bond. The transfer length is affected by many factors, such as strength of concrete, degree of compaction, transverse reinforcement placed in the end block, size and type of strand, type of strand release etc.

Steel fibres applied for prestressed pretensioned structural members may improve concrete characteristics, may help to resist sudden impact load at release of prestressing force and also may reduce or substitute end block reinforcement while preventing end block cracking [Naaman & Reinhardt (1998)]. Therefore, steel fibre reinforced concrete may play an important role in the design of prestressed pretensioned members as well [Naaman & Reinhardt (1998)].

Promising application of steel fibre reinforcement as we see in Chapter 4 may be the use as shear reinforcement [Balázs & Kovács (1997), Balázs & Kovács (1999), Balázs & Kovács (1999), Di Prisco & Caruso & Piatti (1994)]. Random distribution of fibres offers a close spacing of fine reinforcement in all direction of the material, which can not be replaced by conventional longitudinal and transversal reinforcement [Balaguru & Shah (1992), Balázs & Kovács (1999), Balázs & Kovács (1999)]. Steel fibres control and bridge the micro and macro cracks in three directions, increasing shear capacity and providing substantial post cracking behaviour and ductility [Balaguru & Shah (1992), Craig & Parr & Germain & Mosquera & Kamilaris (1986)].

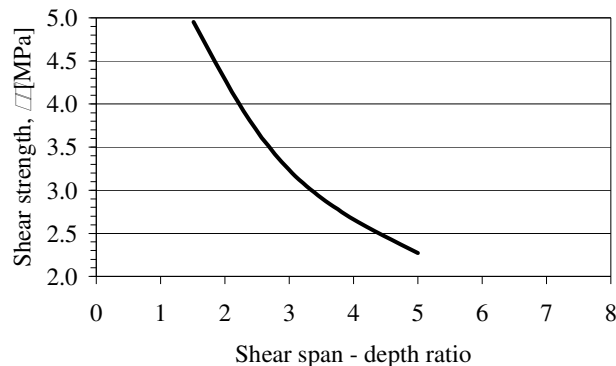
Previous tests on shear strength of steel fibre reinforced concrete included experimental variables such as shear span to depth ratio ( $a/d$ ) (Figure 1.9), steel fibre configuration, steel fibre content, aspect ratio (Figure 1.10), compressive strength of concrete etc [Balaguru & Shah (1992)]. Tests were performed to investigate the shear properties and the shear strength of deep beams effected by steel fibre contents with [Mansur & Ong (1991)] or without web reinforcement [Mau & Hsu (1987), Mansur & Ong & Paramasivam (1986)]. Experimental investigations were developed on the

behaviour of steel fibre reinforced walls, beams, deep beams and corbels [Siao (1994), Sharma (1986)].

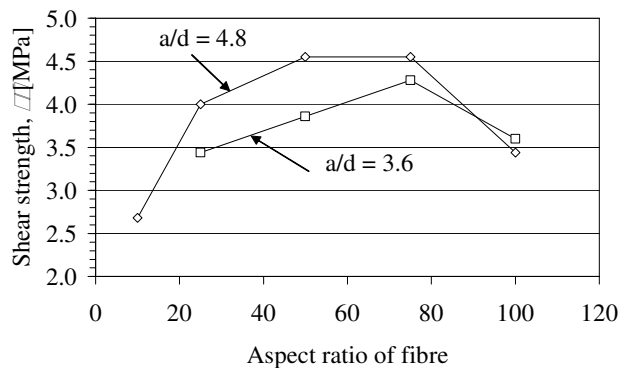
These results indicated that shear strength of concrete can be increased applying steel fibre reinforcement. However, increments were not proportionally to the increase of aspect ratio of steel fibres (Figure 1.10). The increase in aspect ratio of the fibres resulted in an increase of shear strength up to a values of 75 [Balaguru & Shah (1992)]. Higher aspect ratio resulted drastically drop in shear strength due to the balling effect of long steel fibres.

Experimental results shown that shear strength of steel fibre reinforced concrete also effect by the configuration of steel fibres. Hooked-end and crimped steel fibres provide grater contribution both in strength and ductility because of the better anchorage properties of fibres related to straight steel fibres.

Reasonable application of steel fibre reinforcement in concrete and reinforced concrete walls, shear walls and deep beams are strongly constrained by the workability conditions. Generally, structural elements such as deep beams and shear walls to be considered as two dimensional structural elements in design. In the two dimensional case the randomly oriented steel fibre reinforcement may be to strong hypothesis. Characteristic fibre orientation may occur due to the applied casting process (concrete vibrators, wall vibrators, etc.).



**Figure 1.9:** Schematic representation of the shear strength vs. shear span-to depth ratio [Balaguru & Shah (1992)]



**Figure 1.10:** Effect of aspect ratio of fibre on the shear strength of steel fibre reinforced concrete [Balaguru & Shah (1992)]

Oriented fibres result anisotropic features particularly after cracking of concrete resulting different shear strength from that of plain concrete.

Development of new construction materials which are stronger and more durable than conventional materials is one of the most important challenges for building industry [Naaman (1992), Naaman (1998), Naaman & Reinhardt (1998), Reinhardt & Naaman (1992), Reinhard & Naaman (1999)]. Steel fibre reinforced concrete is an example of such materials that has been frequently used by the construction industry primarily for industrial floors [Falkner & Kubat & Droesen (1994), Falkner & Teutsch (1993), Kausay (1994)]. Special applications of steel fibre reinforced composites are the SIFCON type materials [Krstulovic-Opara & Dogan & Uang & Haghayeghi (1997), Krstulovic-Opara & Al-Shannag (1999)]. Due to the high impact resistance of such materials, airfield runways, tunnels, tubes, are commonly made of steel fibre reinforced concrete, SIFCON or other steel fibre reinforced cement based composite materials [Gopalaratnam & Shah (1986), Naaman & Gopalaratnam (1983), Hannant (1989)].

Further developments of cement based fibre reinforced materials represent an economical and durable solution for the restoration or retrofitting of deteriorated, highly stressed structural elements (e.g. reinforced concrete frame joints) or bridge decks and other traffic areas (place of bus stops) subjected to high intensity of traffic load [Naaman (1992), Naaman (1998), Naaman & Reinhardt (1998), Reinhardt & Naaman (1992), Reinhard & Naaman (1999)]. With the rapidly increasing application of steel fibre reinforced concretes different types of fibres has been developed and manufactured in the last decades [Naaman (1998), WAJA (1995), Stang & Rossi (1999)]. Steel fibres are available with different configurations and mechanical properties on the market [Naaman (1992), Naaman (1998), Naaman & Reinhardt (1998), Reinhardt & Naaman (1992), Reinhard & Naaman (1999), WAJA (1995)]. However, the huge number of fibre types also means wide ranging mechanical properties.

Beside the civil engineering applications, the other promising purpose of steel fibre reinforcement in construction is to fully or partially replace the shear reinforcement in flat slabs. By the use of steel fibres shear strength of plain concrete can be increased in high shear region of reinforced concrete slabs [Theodorakopoulos & Swamy (1999)].

In many cases of the two dimensional structural elements (slabs, walls) the homogeneity of the steel fibre reinforced concrete material may be very restrictive assumption. This hypothesis may even more valid in the case of special thin product [Hannant (1989)]. At structural level or in a local portion of slabs steel fibre reinforcement may be oriented in a characteristic direction. Orientation of steel fibres in concrete products may influence the crack development and hence, the overall structural performance as well.

## 1.6 Conclusions

Based on the literature review for the mechanical properties of steel fibre reinforced concrete the following main conclusions can be drawn:

1. There is a wide range of **fibres** to use as fibre reinforcement in concrete such as steel, polymeric, glass, carbon, aramid, natural, etc.
2. Increment in **modulus of elasticity** and in **compressive strength** provided by steel fibres can be considered negligible for design purposes.
3. With respect to fibre geometry, the fibre length vs. fibre diameter ratio (**aspect ratio**) is particularly important for mixing and for the performance.
4. High fibre volume fraction and high yield strength of fibre is needed for high strength concrete to produce ductile failure.
5. **Pre-cracking** behaviour in tension can be defined by neglecting the effect of steel fibres. **Post-cracking** behaviour can be different depending on fibre length, content, shape and diameter.
6. Application of steel fibre reinforcement in concrete may produce **residual tension** forces in the cracked cross-section after cracking resulting tougher behaviour.
7. Due to the experimental complications of the direct tensile test, stress vs strain relationships are generally indirectly determined based on bending test.

# Chapter 2

## Material compositions and mechanical properties

*Chapter 2 deals with experimental characterisation of mechanical properties of steel fibre reinforced concrete for structural elements. An extensive experimental programme has been developed to investigate the effect of steel fibre reinforcement on the mechanical performance.*

*Specimens and test methods were selected to be able to detect realistic behaviour. material compositions, test methods, test set-ups as well as test arrangements will be detailed.*

*Measurements on compressive strength, stress-strain relationship, splitting strength and toughness to various concrete compositions will be presented and compared to those of other researchers.*

**Keywords:** *concrete, steel fibre reinforcement, steel fibre reinforced concrete, compressive strength, behaviour in compression, splitting strength, toughness properties, characterisation of toughness, fibre orientation*

### 2.1 Material compositions and test specimens

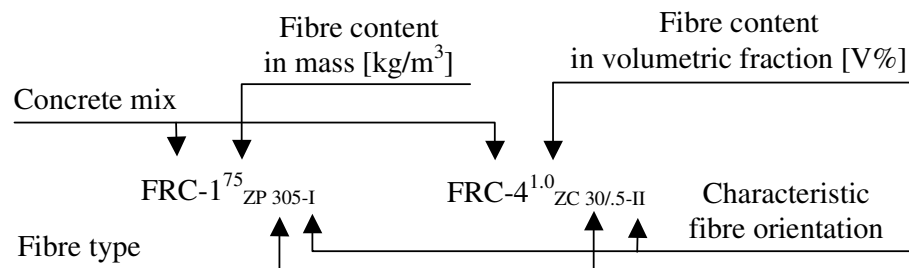
Properties of hardened steel fibre reinforced concrete are influenced by many material parameters. Most important parameters are: fibre content, fibre length, fibre shape, fibre diameter which all may influence workability [ACI (1987), ACI Committee 544 (1984), ACI Committee 544 (1986), ACI Committee 211 (1989), Agarwal (1980), Balaguru (1988), Chern (1989), Chern (1992), Dubey (1998), Gokoz (1981), Gopalaratnam (1986), Groth (1996), Stroeven (1995)]. Fibres are normally considered to be randomly oriented [RILEM (1978), ACI Committee 544 (1988), Bekaert (1994), JSCE SF1-SF7 (1984), DIN (1991), ASTM A 820-90, ASTM C 1018-89 (1990), UNE 83 500-513, DVB-Merkblatt (1991), DVB-Merkblatt (1992)]. However, effect of non-random distribution of fibres in standard specimens may be significant [Stroeven (1995), Torrenti & Djebri (1992, 1995)].

Actual values of experimental parameters were taken to obtain workable concrete mixes which represent realistic behaviour.



### 2.1.1 Concrete mix proportions and mixing procedures

Concrete mix proportions are summarised in Table 2.1. Several types of concrete mixes were designed in order to introduce the influences of various mechanical properties. In the notations of mixes FRC stays for steel fibre reinforced concrete. Concretes made without fibres as reference concrete mixes are denoted by a numerated “REF” notation, where the number refers to different concrete mixes. Superscripts and subscripts denote the fibre content in mass (0 kg/m<sup>3</sup> as reference, 75 kg/m<sup>3</sup>, 150 kg/m<sup>3</sup>) or in volumetric fraction (0 V% as references or 0.5 V%, 1.0 V%) and the type of fibre (Dramix<sup>®</sup> ZP 305, Dramix<sup>®</sup> ZC 30/5 and D&D<sup>®</sup>~30/5), respectively. For example:



Two washed and classified aggregate fractions were used, 0 to 4 mm sandy-gravel and 4 to 8 mm gravel fractions. Maximum aggregate diameter therefore was 8 mm [Balázs & Erdélyi & Kovács (1997), Balázs & Kovács (1999)].

Two types of Hungarian Portland Cements were used. For mixes noted by FRC-1<sup>75</sup><sub>ZP305</sub> to FRC-2<sup>150</sup><sub>ZP305</sub> CEM I. 52.5 (550 pc) was used while for the other mixes from FRC-3<sub>REF</sub> to FRC-4<sup>1.0</sup><sub>D&D 30/5</sub> made of CEM I. 42.5 (450 pc). Proper workability was obtained by the addition of superplasticizer in order to reduce the water to cement ratio in case of mixes FRC-1<sup>75</sup><sub>ZP 305</sub>, FRC-1<sup>150</sup><sub>ZP 305</sub>, FRC-2<sup>75</sup><sub>ZP 305</sub> and FRC-2<sup>150</sup><sub>ZP 305</sub>. The superplasticizer used was SIKAMENT-10 HBR.

Concrete mixes were produced at the Laboratory of the Department of Structural Engineering and at the Department of Construction Materials and Engineering Geology,

**Table 2.1:** Concrete composition in dry material [kg/m<sup>3</sup>] (present tests)

Nr.	Notation of mix	Fine aggregates		c	Super-plasticizer	w/c	Fibre content		Air content [l/m <sup>3</sup> ]	Porosity [%]
		0-4 mm	4-8 mm				V%	kg/m <sup>3</sup>		
1	FRC-1 <sup>75</sup> <sub>ZP 305</sub>	1056	829	330	5,952	0.512	~ 1.0	75	36.7	8.95
2	FRC-1 <sup>150</sup> <sub>ZP 305</sub>	1056	829	330	8,571	0.512	~ 2.0	150	60.8	11.62
3	FRC-2 <sup>75</sup> <sub>ZP 305</sub>	958	752	500	9,048	0.372	~ 1.0	75	28.0	3.80
4	FRC-2 <sup>150</sup> <sub>ZP 305</sub>	958	752	500	10,476	0.372	~ 2.0	150	74.4	8.59
5	REF-3	1035	635	460	-	0.478	0	-	91.88	14.75
6	FRC-3 <sup>0.5</sup> <sub>ZC 30/5</sub>	1035	635	460	-	0.478	0.5	39.2	50.03	10.83
7	FRC-3 <sup>1.0</sup> <sub>ZC 30/5</sub>	1035	635	460	-	0.478	1.0	78.5	31.20	8.95
8	REF-4	919	751	460	-	0.478	0	-	23.66	7.95
9	FRC-4 <sup>0.5</sup> <sub>ZC 30/5</sub>	919	751	460	-	0.478	0.5	39.2	54.25	12.22
10	FRC-4 <sup>1.0</sup> <sub>ZC 30/5</sub>	919	751	460	-	0.478	1.0	78.5	43.73	12.08
11	FRC-4 <sup>0.5</sup> <sub>D&amp;D ~30/5</sub>	919	751	460	-	0.478	0.5	39.2	54.25	12.22
12	FRC-4 <sup>1.0</sup> <sub>D&amp;D ~30/5</sub>	919	751	460	-	0.478	1.0	78.5	43.73	12.08

Budapest University of Technology and Economics. Two types of concrete mixers were used. Mixes noted by FRC-3<sub>REF</sub> to FRC-4<sup>1.0</sup><sub>D&D 30/5</sub> were produced in a mixer with a maximum capacity of 250 ℓ. Mixes noted by FRC-1<sup>75</sup><sub>ZP305</sub> to FRC-2<sup>150</sup><sub>ZP305</sub> were prepared in a concrete mixer with a capacity of 50 ℓ. Specimens with the same fibre content were cast from the same batches.

Possible mixing processes of concretes containing fibres are detailed in the literature [ACI Committee 544 (1984), Balaguru & Ramkrishnan (1988), Balaguru & Shah (1992), Reinhardt & Naaman (1992), Reinhardt & Naaman (1999), ASTM A 820-90, DBV-Merkblatt (1992), Vorläufige Richtlinien (1995), JSCE-SF1 (1984), UNE 83-502-88]. In the present study mixing sequence was the following: dry mixing of the aggregates, addition of cement and dry mixing, addition of water and superplasticizer in small quantities and finally addition of steel fibres in small quantities parallel to the addition of water and superplasticizer. During mixing and casting there was no noticeable workability problem. However, in case of concrete mixes FRC-2 lower energy was needed to mix and cast due to their relatively high superplasticizer content.

### 2.1.2 Type of fibres

Steel fibres were used for all mixtures since many studies showed that polymer or natural fibres do not have significant effects on the structural performance of concrete [Naaman & Reinhardt (1998), Reinhardt & Naaman (1992), Reinhardt & Naaman (1999), Kiss (1996)].

BEKAERT Dramix<sup>®</sup> hooked-end fibres were applied for mixes (see Table 2.1) FRC-1<sup>75</sup><sub>ZP 305</sub>, FRC-1<sup>150</sup><sub>ZP 305</sub>, FRC-2<sup>75</sup><sub>ZP 305</sub>, FRC-2<sup>150</sup><sub>ZP 305</sub>, FRC-3<sup>0.5</sup><sub>ZC 30/5</sub>, FRC-3<sup>1.0</sup><sub>ZC 30/5</sub>, FRC-4<sup>0.5</sup><sub>ZC 30/5</sub> and for FRC-4<sup>1.0</sup><sub>ZC 30/5</sub>, where the subscripts indicate the type of fibre Dramix<sup>®</sup> ZP 305 and Dramix<sup>®</sup> ZC 30/5, respectively [Bekaert (1994)]. To the mixes FRC-4<sup>0.5</sup><sub>D&D ~30/5</sub> and FRC-4<sup>1.0</sup><sub>D&D ~30/5</sub> the Hungarian D&D type crimped steel fibres D&D<sup>®</sup> ~30/5 were applied (see Table 2.1) [Waja (1995)].




In order to distinguish mixes in Table 2.1 the fibres are given by their own notations using subscript indices like ZP 305, ZC 30/5 and D&D 30/5. For instance, a steel fibre of length  $l_f=30$  mm and diameter  $\varnothing_f=0.5$  mm is denoted “ZP 305”. The configurations and other data of the chosen fibres are summarized in Table 2.2.

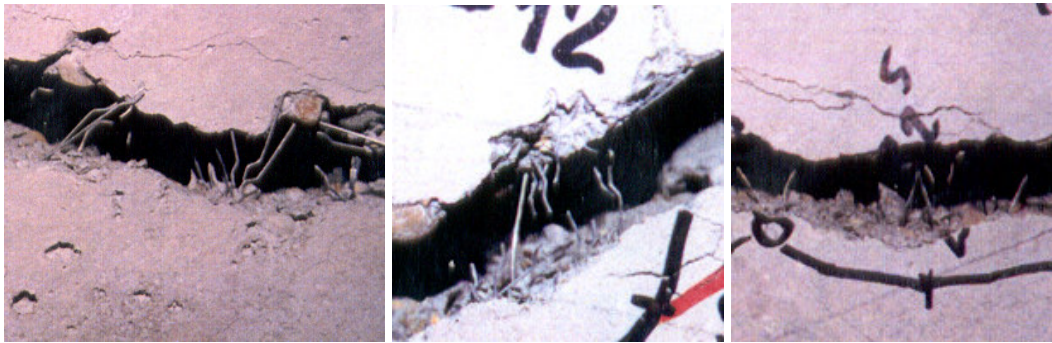
Dramix<sup>®</sup> fibres are made with hooked-ends as can be seen on Photo 2.1 [Bekaert (1994)]. They are delivered as bundles of fibres glued together with water soluble adhesive [Bekaert (1994)]. Since, in this way the fibres form small plates in the mix they behave as a flat aggregate during the mixing process until resolving the glue resulting in homogenous fibre dispersion. It was also observable when fibres was added to the mix of aggregates, cement and water, that the coarser aggregates crashed the plates of glued fibres resulting smaller plates of glued fibres and finally single fibres.

D&D<sup>®</sup> fibres are crimped fibres and delivered as single fibres [Waja (1995)]. Therefore, the fibres were added to the mix by hand in small quantities in order to achieve homogenous fibre dispersion.

Since one of the objectives of present study was to characterise the mechanical properties of steel fibre reinforce concrete as structural material, four relatively high fibre dosages were used: 39,2 kg/m<sup>3</sup> (0.5 V%), 78,5 kg/m<sup>3</sup> (1.0 V%), 75 kg/m<sup>3</sup> (~1.0 V%) and 150 kg/m<sup>3</sup> (~2.0 V%) fibre content were applied. They appeared in the superscripts of the mixes (see Table 2.1).

**Table 2.2:** Types of fibres and their mechanical properties (present tests)

Notation	Material type	Configuration	Aspect ratio $l_f/\varnothing_f$	Density [kg/m <sup>3</sup> ]	Yield strength [MPa]	Elastic modulus [GPa]
Dramix <sup>®</sup> ZP 305	Steel		60	7800	1100	200
Dramix <sup>®</sup> ZC 30/.5	Steel		60	7800	1100	200
D&D <sup>®</sup> ~30/.5	Steel		60	7800	1400	200

**Photo 2.1:** Dramix type steel fibres in the failure surface

### 2.1.3 Formworks and test specimens

Types, sizes and number of formworks to specimens detailed in Table 2.1 are given in Table 2.3 [Kovács (1996), Balázs & Kovács (1999)]. Test specimens and their geometrical parameters are summarised in Figure 2.1.

Slab elements had the following dimensions Slab A: 800×500×100 mm, Slab B: 820×630×80 mm and Slab C: 600×600×50 mm.

Special beam formworks were made for the reinforced concrete beam specimens, as well as for the prestressed pretensioned concrete beam specimens. Each of them contained three beams. They were noted by D and E, respectively. Steel fibre reinforced concrete beams had a geometry of 2000×150×100 mm, while steel fibre reinforced prestressed pretensioned concrete beams had a geometry of 2000×120×80 mm.

**Table 2.3: Type and number of formworks (present tests)**

Nr.	Notation of mix	Type of formworks						
		Cube <sup>1</sup>	Cylinder <sup>2</sup>	A <sup>3</sup>	B <sup>4</sup>	C <sup>5</sup>	D <sup>6</sup>	E <sup>7</sup>
1	FRC-1 <sup>75</sup> <sub>ZP 305 - I</sub>	-	-	1	1	1	-	-
	FRC-1 <sup>75</sup> <sub>ZP 305 - II</sub>	-	-	1	1	-	-	-
2	FRC-1 <sup>150</sup> <sub>ZP 305 - I</sub>	-	-	1	1	1	-	-
	FRC-1 <sup>150</sup> <sub>ZP 305 - II</sub>	-	-	1	1	-	-	-
3	FRC-2 <sup>75</sup> <sub>ZP 305 - I</sub>	-	-	1	1	1	-	-
	FRC-2 <sup>75</sup> <sub>ZP 305 - II</sub>	-	-	1	1	-	-	-
4	FRC-2 <sup>150</sup> <sub>ZP 305 - I</sub>	-	-	1	1	1	-	-
	FRC-2 <sup>150</sup> <sub>ZP 305 - II</sub>	-	-	1	1	-	-	-
5	REF-3	6	-	-	-	-	1	1/3
6	FRC-3 <sup>0.5</sup> <sub>ZC 30/5</sub>	6	-	-	-	-	1	1/3
7	FRC-3 <sup>1.0</sup> <sub>ZC 30/5</sub>	5	-	-	-	-	1	1/3
8	REF-4	5	3	-	-	-	1	1/3
9	FRC-4 <sup>0.5</sup> <sub>ZC 30/5</sub>	5	3	-	-	-	-	1/3
10	FRC-4 <sup>1.0</sup> <sub>ZC 30/5</sub>	3	3	-	-	-	-	1/3
11	FRC-4 <sup>0.5</sup> <sub>D&amp;D ~30/5</sub>	5	3	-	-	-	1	-
12	FRC-4 <sup>1.0</sup> <sub>D&amp;D ~30/5</sub>	3	3	-	-	-	1	-

<sup>1</sup> Cube with a geometry of 150×150×150 mm

<sup>2</sup> Cylinder with geometry of 300 mm length and 150 mm diameter

<sup>3</sup> Slab formwork with a geometry of 800×500×100 mm

<sup>4</sup> Slab formwork with a geometry of 820×630×80 mm

<sup>5</sup> Slab formwork with a geometry of 600×600×50 mm

<sup>6</sup> Formwork for steel fibre reinforced concrete beams with a geometry of 2000×150×100 mm related to one beam, each contain 3 beams

<sup>7</sup> Formwork for steel fibre reinforced prestressed pretensioned concrete beams with a geometry of 2000×100×80 mm related to one beam, each contain 3 beams

**Table 2.4: Characteristic fibre orientation of specimens (present tests)**

	Notation	Type of Formworks						
		Cube	Cylinder	A	B	C	D	E
1	FRC-1 <sup>75</sup> <sub>ZP 305</sub>			I & II <sup>2</sup>	I & II	I	-	-
2	FRC-1 <sup>150</sup> <sub>ZP 305</sub>			I & II	I & II	I	-	-
3	FRC-2 <sup>75</sup> <sub>ZP 305</sub>			I & II	I & II	I	-	-
4	FRC-2 <sup>150</sup> <sub>ZP 305</sub>			I & II	I & II	I	-	-
6	FRC-3 <sup>0.5</sup> <sub>ZC 30/5</sub>	R <sup>1</sup>	-	-	-	-	R	R
7	FRC-3 <sup>1.0</sup> <sub>ZC 30/5</sub>	R	-	-	-	-	R	R
9	FRC-4 <sup>0.5</sup> <sub>ZC 30/5</sub>	R	R	-	-	-	-	R
10	FRC-4 <sup>1.0</sup> <sub>ZC 30/5</sub>	R	R	-	-	-	-	R
11	FRC-4 <sup>0.5</sup> <sub>D&amp;D ~30/5</sub>	R	R	-	-	-	R	-
12	FRC-4 <sup>1.0</sup> <sub>D&amp;D ~30/5</sub>	R	R	-	-	-	R	-

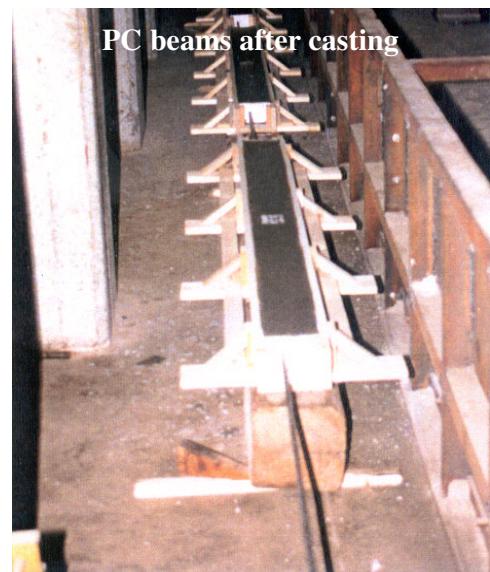
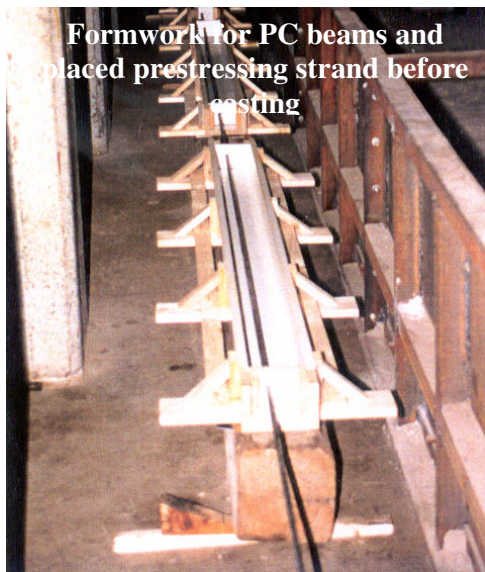
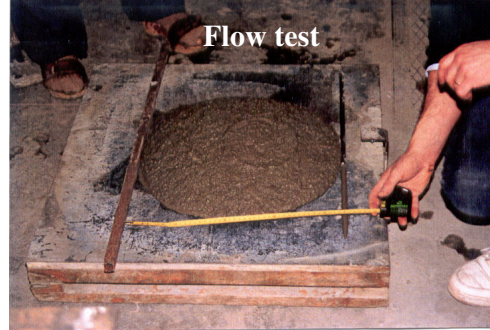
<sup>1</sup> Notations of the introduced characteristic fibre orientations which is parallel to the longer side of the formwork in case of I, and perpendicular to that of side in case of II.

<sup>2</sup> Characteristic fibre orientation was not introduced into the mixtures (R = random)

In addition to the concrete mix proportion and the fibre content, characteristic fibre orientation was the major experimental variable. Series devoted to study the effect of characteristic fibre orientation on the mechanical properties of steel fibre reinforced concretes are noted by roman numbers I and II. Numbers denote the considered two characteristic fibre orientations introduced into the slabs during casting. Fibre orientations were considered to be in the plane of slabs and hence, effect of fibres oriented in the third direction was not taken into consideration. Fibre orientation may play an important role in the anisotropy of material, particularly in the range of post cracking behaviour and hence, it is essential in structural analysis [*Stroeven (1995), Torrenti & Djebri (1992, 1995)*]. Characteristic fibre orientations were systematically introduced in the material by a P14 type handy vibrator of 28 mm diameter. In specimens denoted by I and II, the characteristic fibre orientations were perpendicular to each other. Fibre orientations were formed by moving the vibrator only in one direction in the slabs. On the other hand, fibre orientation was random (R) in test series aimed to study the structural behaviour of RC and PC beams applying also steel fibres.

After a week of casting specimens A, B and C, different specimens were sawn out of them. The sawing plan is summarised in Table 2.6. 6+6 prisms with the size of 240×100×100 mm and a small deep beam with a size of 500×170×100 mm were sawn out of specimen A denoted by T1...T6, C1...C6 and DB-a. T indicates that the prism will be tested in direct tension while C denotes the prisms tested in compression. Notation DB-a indicates the type of deep beam element (see Table 2.6).

Specimens denoted by B were divided into four portions. Three of them are beams with the geometry of 820×85×80 mm noted by B-a, B-b and B-c which indicate three different positions in the formwork, respectively. The fourth is a deep beam specimen denoted by DB-b and has a geometry of 820×340×80 mm. Tests on specimens DB-a as well as on DB-b are detailed in Chapter 6. Geometry of sawn specimens are summarised in Table 2.6.



*Photo 2.2: Casting of specimens in laboratory (present tests)*

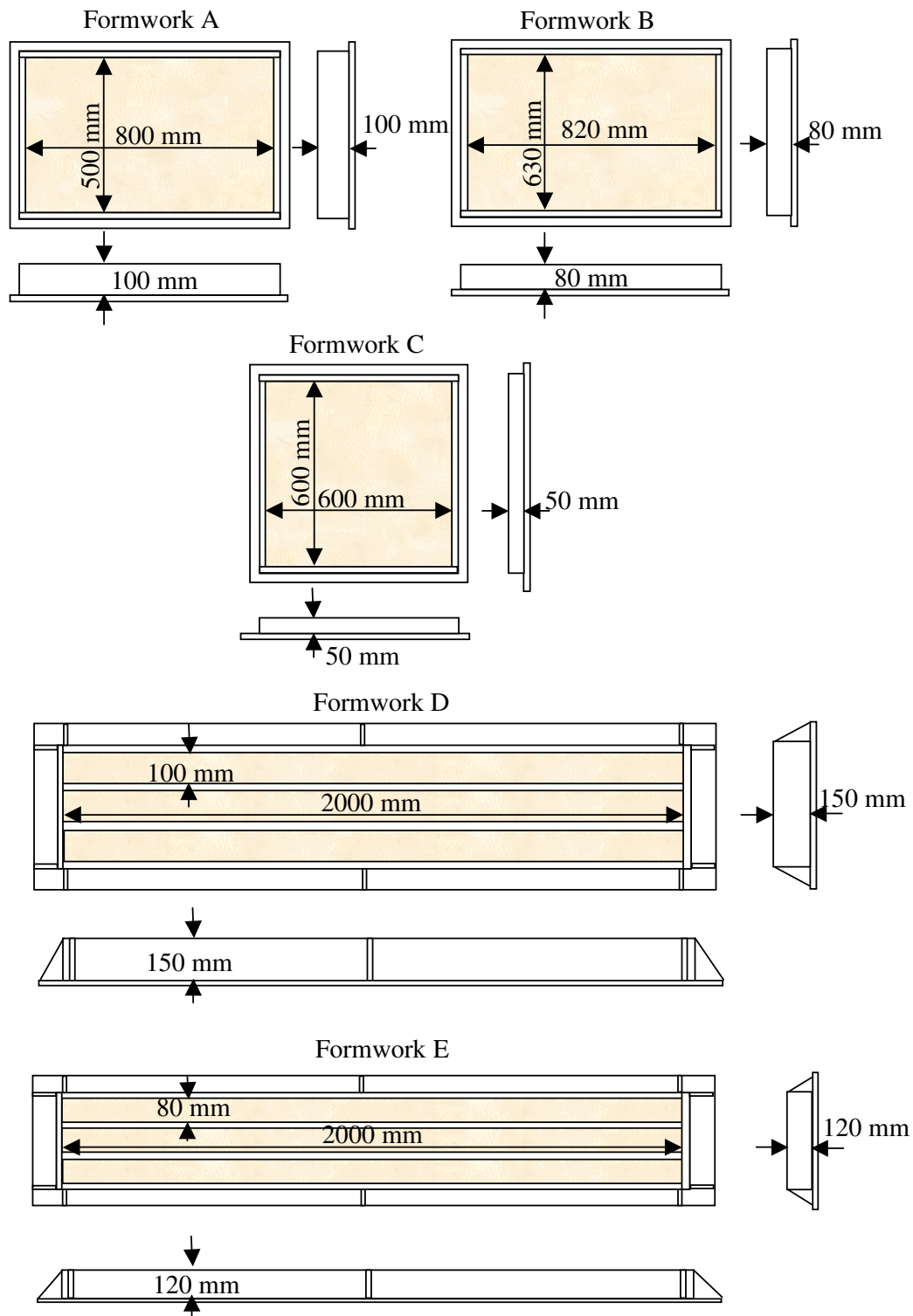
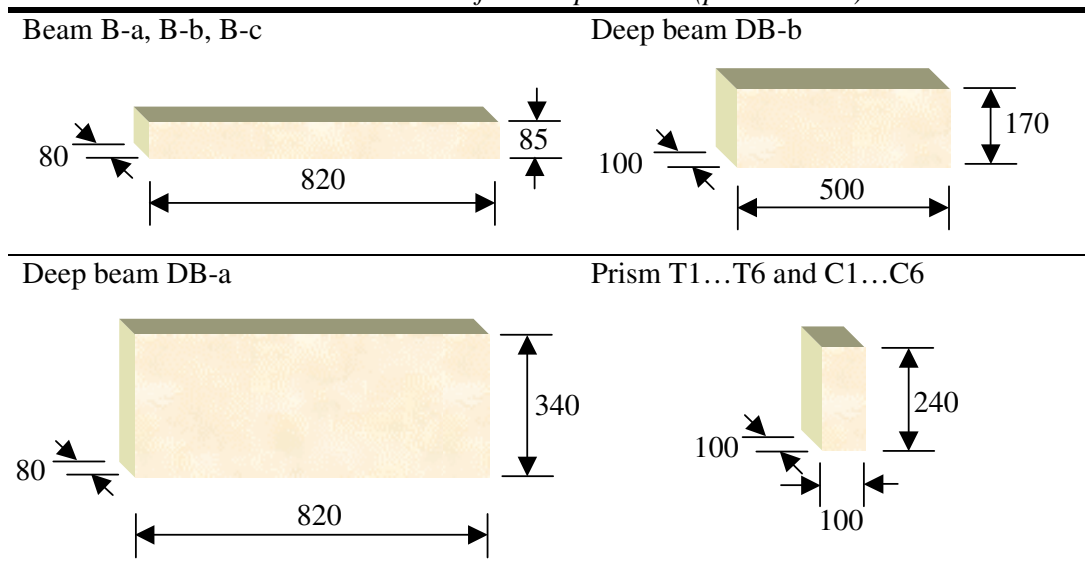

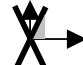
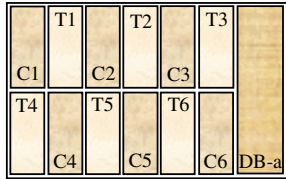
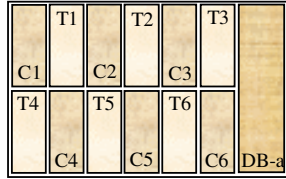
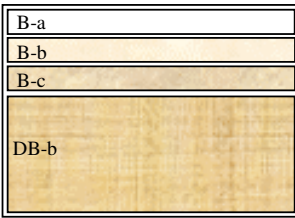
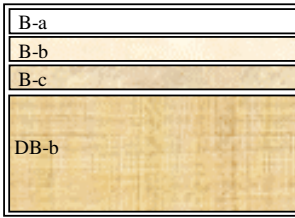



Figure 2.1: Types of formworks and their geometries (present tests)

**Table 2.5: Geometries of sawn specimens (present tests)**



**Table 2.6: Sawing plan of specimens made of FRC-1, FRC-2 (present study)**

Notation of characteristic fibre orientation	I	II
Fibre orientation		
A. Type of specimen		
B. Type of specimen		
C. Type of specimen		



## 2.2 Behaviour in compression

### 2.2.1 Test specimens and test procedure

Concrete classes are given according to their compressive strength. Compressive strength is generally determined on cubes of 150 mm sizes [*DBV-Merkblatt Anhang A (1992)*] or on cylinders of  $\varnothing=150$  mm diameter and  $\ell=300$  mm height [*JSCE-SF2 (1984)*, *JSCE-SF3 (1984)*, *UNE 83-504-90 (1990)*, *UNE 83-505-86 (1986)*, *UNE 83-506-86 (1986)*, *UNE 83-507-86 (1986)*, *UNE 83-507-86 (1986)*].

Due to the aim of present test series and the limited load capacity of the available test machines, four types of specimens were tested in compression as summarised in Table 2.7. Standard cubes and cylinders were cast in steel forms to mixes REF-3, FRC-3 and REF-4, FRC-4 and tested at 63 and 52 days after casting, respectively. Other compressive tests related to concrete compositions FRC-1 and FRC-2 were carried out in different age after casting. Strength values were calculated to 28 days according to Weber [*Weber (1979)*].

To study the effect of fibre orientation on the behaviour of concrete members in compression 6+6 prisms (240×100×100 mm) were sawn out of slab elements noted by A made of mixes FRC-1 and FRC-2, respectively. Cylinder specimens ( $\varnothing=70$  mm,  $\ell=100$  mm) were also drilled out of non-destroyed portions of deep beams noted by DB-b after their testing.

**Table 2.7: Type and piece of specimens in compressive tests (present study)**

	Notation of mixture	Type of specimen			
		Cube <sup>1</sup>	Cylinder <sup>2</sup>	Prism <sup>3</sup>	Cored cylinder <sup>4</sup>
1	FRC-1 <sup>75</sup> <sub>ZP 305 – I</sub>	-	-	6	1
	FRC-1 <sup>75</sup> <sub>ZP 305 – II</sub>	-	-	6	1
2	FRC-1 <sup>150</sup> <sub>ZP 305 – I</sub>	-	-	6	1
	FRC-1 <sup>150</sup> <sub>ZP 305 – II</sub>	-	-	6	1
3	FRC-2 <sup>75</sup> <sub>ZP 305 – I</sub>	-	-	6	1
	FRC-2 <sup>75</sup> <sub>ZP 305 – II</sub>	-	-	6	1
4	FRC-2 <sup>150</sup> <sub>ZP 305 – I</sub>	-	-	6	1
	FRC-2 <sup>150</sup> <sub>ZP 305 – II</sub>	-	-	6	1
5	REF-3	6	-	-	-
6	FRC-3 <sup>0.5</sup> <sub>ZC 30/.5</sub>	6	-	-	-
7	FRC-3 <sup>1.0</sup> <sub>ZC 30/.5</sub>	5	-	-	-
8	FRC-3 <sup>0.5</sup> <sub>D&amp;D ~30/.5</sub>	5	3	-	-
9	FRC-3 <sup>1.0</sup> <sub>D&amp;D ~30/.5</sub>	5	3	-	-
10	REF-4	3	3	-	-
11	FRC-4 <sup>0.5</sup> <sub>ZC 30/.5</sub>	5	3	-	-
12	FRC-4 <sup>1.0</sup> <sub>ZC 30/.5</sub>	3	3	-	-

<sup>1</sup> Cube with geometry of 150×150×150 mm  
<sup>2</sup> Cylinder with geometry of 300 mm length and 150 mm diameter  
<sup>3</sup> Prism with geometry of 240×100×100 mm  
<sup>4</sup> Cylinder with geometry of 100 mm length and 70 mm diameter

Force controlled testing machine was used with the capacity of 6000 kN to determine concrete strength on standard cube and standard cylinder for mixes REF-3, FRC-3, REF-4 and FRC-4.

Displacement controlled Instron type testing machine with the capacity of 500 kN were used to determine compressive strength on sawn prisms (240×100×100 mm) as well as on drilled cylinder specimens ( $\varnothing=70$  mm,  $\ell=100$  mm) made of mixes FRC-1 and FRC-2. In order to fulfil the standard requirements rate of cross-head of test machine was 0.2 mm/min [JSCE-SF2 (1984), JSCE-SF3 (1984), DBV-Merkblatt Anhang A (1992), UNE 83-504-90 (1990), UNE 83-505-86 (1986), UNE 83-506-86 (1986), UNE 83-507-86 (1986), UNE 83-507-86 (1986)].

Failure loads as well as stress – strain relationships were registered in the case of each specimen. Compressive toughness values for standard cube specimens of mixes REF-3, FRC-3, REF-4 and FRC-4 were derived from the stress-strain relationships.

## 2.2.2 Compressive behaviour

Test results of compressive tests are numerically summarised in Table 2.8 to Table 2.11 and graphically represented in Figure 2.2.

Compressive strength of concrete prisms (240×100×100 mm to series FRC-1 and FRC-2) were influenced by fibre orientation. In the case of specimens made of mix FRC-1 <sup>75</sup><sub>ZP 305 – II</sub> the mean (6 prisms) concrete compressive strength was lower with 11.2 % related to specimens made of FRC-1 <sup>75</sup><sub>ZP 305 – I</sub> and with 6.2 % in the case of mix FRC-1 <sup>150</sup><sub>ZP 305 – II</sub> related to mix FRC-1 <sup>150</sup><sub>ZP 305 – I</sub>, respectively. In the case of mix FRC-2 containing 75 kg/m<sup>3</sup> steel fibres compressive strength was not considerably effected by fibre orientation. However, drop off in concrete strength was 6 % considering specimens noted by FRC-2 <sup>150</sup><sub>ZP 305 – II</sub> related to specimens noted by FRC-2 <sup>150</sup><sub>ZP 305 – I</sub>.

Considerable decrease in compressive strength of prism made of FRC-1 and FRC-2 made with 150 kg/m<sup>3</sup> Dramix<sup>®</sup> ZP 305 hooked-end steel fibres was observed in relation to the same concrete composition applying 75 kg/m<sup>3</sup> Dramix<sup>®</sup> ZP 305 hooked-end steel fibre content. This is due to the higher porosity observed in the concrete matrix, concerning larger visible pores appeared on the concrete surface and the drilled concrete surface as well (see Table 2.1).

Fibres perpendicular to the direction of compressive load were more effective to increase compressive strength than fibres which were parallel to that (Table 2.9).

Figure 2.3 summarises the mean test results of measured concrete compressive strengths on different specimens and concrete compositions as a function of cement content (Figure 2.3/a), water to cement ratio (Figure 2.3/b) and fibre content (Figure 2.3/c). Increasing cement content and fibre content as well as decreasing water to cement ratio result in increasing compressive strength of fibre reinforced concrete (Figure 2.3). However, increase of cement content by itself was not suitable to achieve higher strengths of steel fibre reinforced concrete having relatively high fibre contents.

Use of 150 kg/m<sup>3</sup> Dramix ZP 305 hooked-end steel fibre did not result in higher compressive strength for FRC-2 made with 500 kg/m<sup>3</sup> cement content related to mixes (REF-3, REF-4, FRC-3 and FRC-4) made of 460 kg/m<sup>3</sup> cement content. In addition to, considering relatively high steel fibre content (75 kg/m<sup>3</sup> ~1.0 V%, 150 kg/m<sup>3</sup> ~2.0 V%) in concrete composition FRC-1 and FRC-2, compressive strength measured on both prism (240×100×100 mm) and cylinder ( $\varnothing=70$  mm,  $\ell=100$  mm) specimens decreased by the increase of steel fibre content. Higher compressive strength could be achieved in

the case of FRC-3 and FRC-4 even though the increments were not proportional to the applied steel fibre content. Further, as Figure 2.3/c shows, more than 1.0 V% fibre content was not appropriate to improve compressive strength, even if higher cement content were applied.

Fibre contents (0.5 V% and 1.0 V%) and fibre types (Dramix<sup>®</sup> ZC 30/.5 hooked-end and D&D<sup>®</sup> 30/.5 crimped steel fibre) produced slight increments of concrete strength. However, strength increments were not proportional to the increments of fibre contents. Higher concrete strengths were achieved for both FRC-3 and FRC-4 mixes made with 0.5 V% Dramix<sup>®</sup> ZC 30/.5 hooked-end and D&D<sup>®</sup> 30/.5 crimped steel fibres related to the corresponding mix made with 1.0 V% fibre content.

D&D<sup>®</sup> 30/.5 crimped steel fibres were more effective to increase cube strength than Dramix<sup>®</sup> ZC 30/.5 hooked-end steel fibres which may be caused by their higher yield strength (D&D<sup>®</sup> 30/.5 crimped steel fibres:  $f_{fy}=1400$  MPa, Dramix<sup>®</sup> ZC 30/.5 hooked-end steel fibres:  $f_{fy}=1100$  MPa).

Failure mode was also influenced by the fibre content and the fibre orientation as well. In the case of prism specimens (FRC-1 and FRC-2) made with  $150 \text{ kg/m}^3$  Dramix<sup>®</sup> ZP 305 hooked-end steel fibres tougher failure modes were observed than in the case of specimens made with  $75 \text{ kg/m}^3$  Dramix<sup>®</sup> ZP 305 hooked-end steel fibres. Contribution of fibre orientation was also considerable on the failure mode of specimens. When the characteristic fibre orientation was parallel to the axis of load, more rigid failure was observed. Some plastic deformations were detected after the peak load when the characteristic fibre orientation was perpendicular to the axis of the load. However, the failure mode was always rigid in the case of concrete composition FRC-2 applying higher cement content. Typical diagonal failure was observed by the prisms ( $240 \times 100 \times 100$  mm, Photo 2.3) and the cylinders ( $\varnothing=70$  mm,  $\ell=100$  mm, Photo 2.4).

**Table 2.8:** Concrete compressive strength measured on  $240 \times 100 \times 100$  mm prisms

No	Notation of mix	Notation of specimens Concrete strength [MPa]						Mean [MPa]	Mean (I, II) [MPa]	Mean (mix) [MPa]	Age (day)
		C1	C2	C3	C4	C5	C6				
1	FRC-1 <sup>75</sup> <sub>ZP 305-I</sub>	39.78	46.19	45.36	45.00	38.97	33.20	41.42			28
	FRC-1 <sup>75</sup> <sub>ZP 305-II</sub>	36.66	36.38	38.22	44.96	31.04	33.34	36.77	39.10		28
	FRC-1 <sup>150</sup> <sub>ZP 305-I</sub>	35.99	37.39	30.97	32.91	35.49	-	34.55			28
	FRC-1 <sup>150</sup> <sub>ZP 305-II</sub>	31.23	33.30	32.23	31.08	31.89	34.67	32.40	33.48	36.29	28
2	FRC-2 <sup>75</sup> <sub>ZP 305-I</sub>	37.50	50.03	42.73	47.89	43.84	42.14	44.02			28
	FRC-2 <sup>75</sup> <sub>ZP 305-II</sub>	40.12	38.60	47.87	48.40	44.75	44.56	44.05	44.04		28
	FRC-2 <sup>150</sup> <sub>ZP 305-I</sub>	37.70	38.87	36.68	38.00	39.09	37.29	37.94			28
	FRC-2 <sup>150</sup> <sub>ZP 305-II</sub>	38.00	35.36	32.09	35.68	37.10	-	35.65	36.80	40.42	28

**Table 2.9:** Concrete compressive strength measured on  $150 \times 150 \times 150$  mm cubes

No	Notation of mix	Notation of specimen Concrete strength [MPa]						Mean [MPa]	Age (day)
		C1	C2	C3	C4	C5	C6		
3	REF-3	37.80	34.10	36.30	38.40	39.60	39.30	37.58	28
	FRC-3 <sup>0.5</sup> <sub>ZC 30/.5</sub>	38.40	40.00	41.10	38.90	38.00	42.70	39.85	28
	FRC-3 <sup>1.0</sup> <sub>ZC 30/.5</sub>	39.60	37.90	38.70	38.90	37.60	-	38.55	28
4	REF-4	36.00	44.40	48.20	45.10	39.60	-	42.70	63
	FRC-4 <sup>0.5</sup> <sub>ZC 30/.5</sub>	42.40	44.40	43.10	43.10	44.90	-	43.60	63
	FRC-4 <sup>1.0</sup> <sub>ZC 30/.5</sub>	42.70	42.00	44.90	-	-	-	43.20	63
	FRC-4 <sup>0.5</sup> <sub>D&amp;D-30/.5</sub>	47.80	51.60	48.90	48.40	47.60	-	48.80	63
	FRC-4 <sup>1.0</sup> <sub>D&amp;D-30/.5</sub>	43.80	47.30	47.60	-	-	-	47.16	63

**Table 2.10:** Concrete compressive strength measured on  $\varnothing=70$  mm,  $\ell=100$  mm cylinder

No.	Notation of mix	Notation of specimen		Mean (I, II)	Age (day)
		250×100×100 mm prism			
		Concrete strength		[MPa]	[MPa]
		[MPa]			
C1					
1	FRC-1 <sup>75</sup> <sub>ZP 305 - I</sub>	26.99		26.17	28
	FRC-1 <sup>75</sup> <sub>ZP 305 - II</sub>	25.35			28
	FRC-1 <sup>150</sup> <sub>ZP 305 - I</sub>	26.10		25.02	28
	FRC-1 <sup>150</sup> <sub>ZP 305 - II</sub>	23.94			28
2	FRC-2 <sup>75</sup> <sub>ZP 305 - I</sub>	43.74		41.50	28
	FRC-2 <sup>75</sup> <sub>ZP 305 - II</sub>	39.25			28
	FRC-2 <sup>150</sup> <sub>ZP 305 - I</sub>	37.83		34.75	28
FRC-2 <sup>150</sup> <sub>ZP 305 - II</sub>	31.67		28		

**Table 2.11:** Concrete compressive strength measured on  $\varnothing=150$  mm,  $\ell=300$  mm cylinder

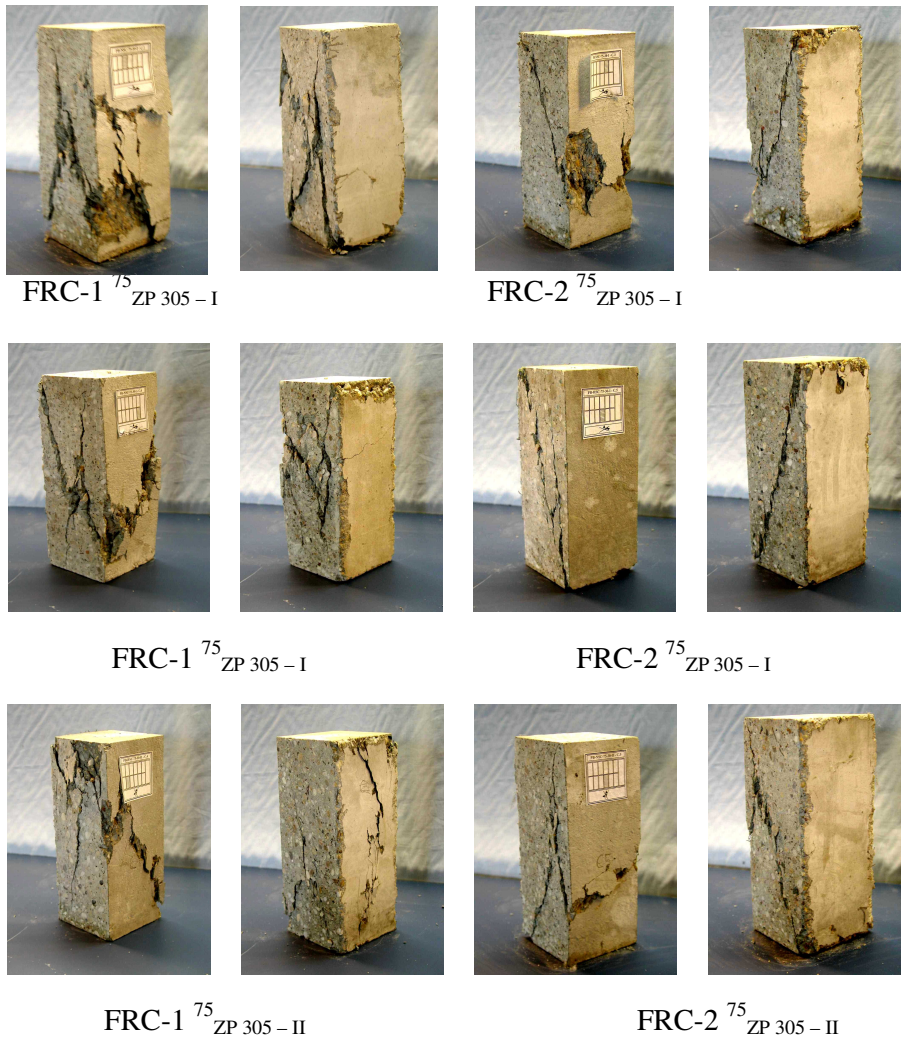
No.	Notation of mix	Notation of specimen			Mean	Age (day)
		$\varnothing=150$ mm, $\ell=300$ mm cylinder				
		Concrete strength				
		[MPa]			[MPa]	
		C1	C2	C3		
	REF-4	36.60	38.50	36.40	37.20	52
4	FRC-4 <sup>0.5</sup> <sub>ZC 30/5</sub>	38.50	36.20	43.00	39.20	52
	FRC-4 <sup>1.0</sup> <sub>ZC 30/5</sub>	36.80	37.10	41.00	38.30	52
	FRC-4 <sup>0.5</sup> <sub>D&amp;D ~30/5</sub>	48.10	46.50	47.00	47.20	52
	FRC-4 <sup>1.0</sup> <sub>D&amp;D ~30/5</sub>	44.70	44.70	45.30	44.90	52

### 2.2.3 Stress – strain relationship in compression

Measured stress – strain relationships to concrete mixes REF-3, FRC-3, REF-4 and FRC-4 measured on 150×150×150 mm cubes are presented in Figure 2.4. Measured stress – strain relationships on  $\varnothing=150$  mm,  $\ell=300$  mm cylinders to concrete mixes REF-4 and FRC-4.

As the stress – strain diagrams in Figure 2.4 indicate both Dramix<sup>®</sup> ZC 30/5 hooked-end steel fibre and D&D<sup>®</sup> 30/5 crimped steel fibre increase ductility or energy absorption capacity of concrete composition REF-3 (FRC-3) and REF-4 (FRC-4) as well. Mixes FRC-3 and FRC-4 absorbed more energy in compression compared to their reference concretes, REF-3 and REF-4. In addition to, compressive toughness was slightly increased by increasing the fibre content. Increment in compressive toughness was not significantly affected by the variation of fibre content. 0.5 V% and 1.0 V% fibre dosages resulted more or less the same toughness properties. However, the relative magnitude of energy increment determined on cube test was greater in case of 0.5 V% fibre content than that of in case 1.0 V% fibre content applying D&D<sup>®</sup> 30/5 crimped steel fibre in concrete composition FRC-4.

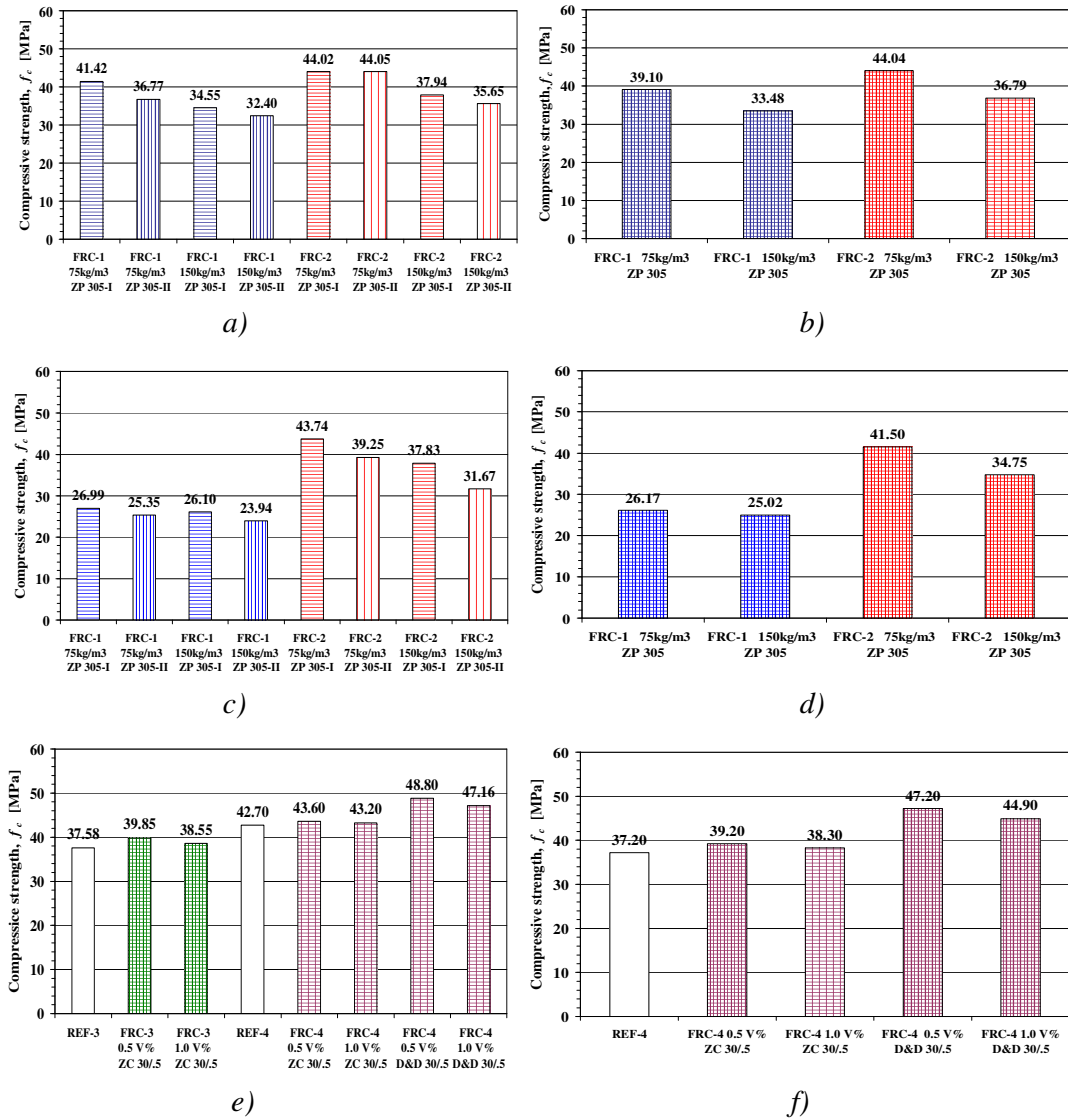
With respect to the fibre type and fibre geometry, both Dramix<sup>®</sup> ZC 30/5 hooked-end steel fibre and D&D<sup>®</sup> 30/5 crimped steel fibre provided similar energy absorption capacities considering concrete composition FRC-4.



*Photo 2.3: Typical failure of 240×100×100 mm prism specimens in compression*

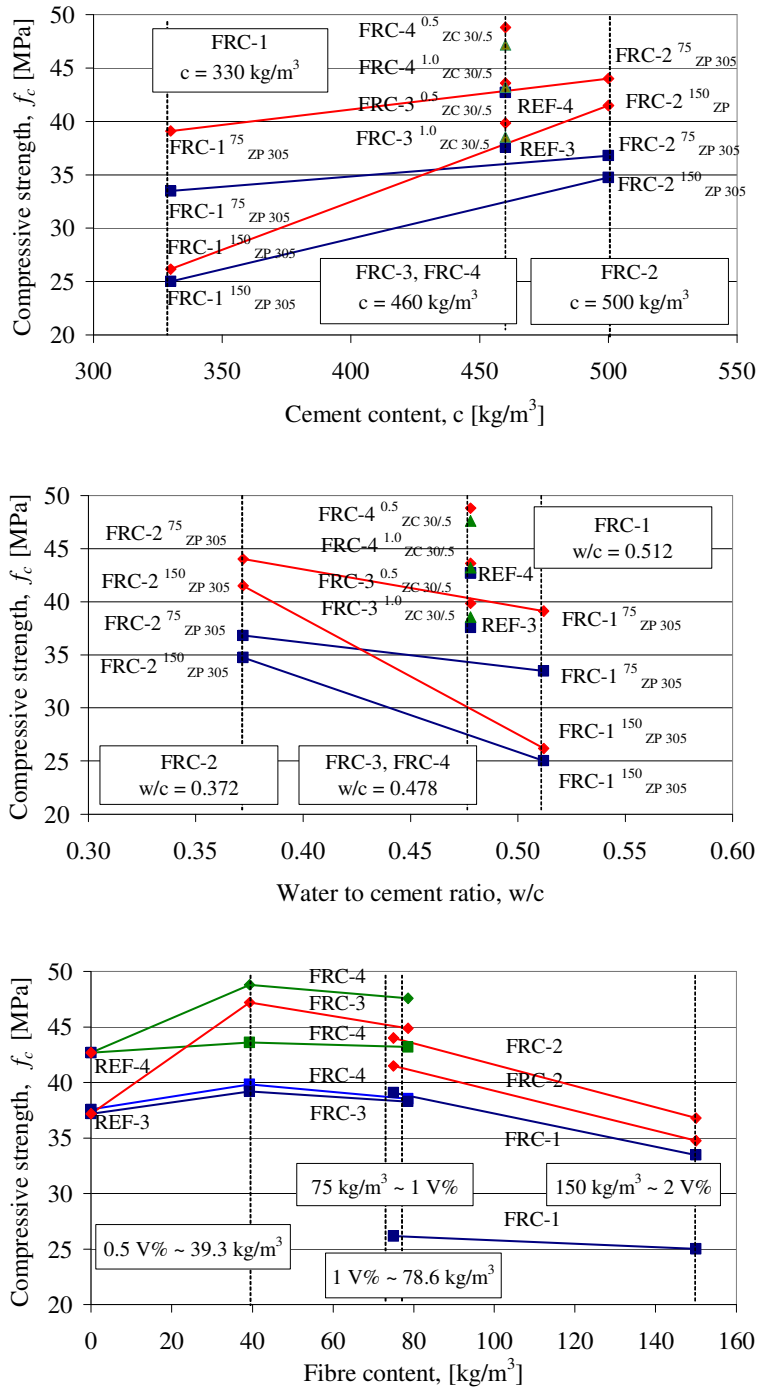


*Photo 2.4: Failure of  $\varnothing=70$  mm,  $\ell=100$  mm cylinders in compression*



**Figure 2.2:** Concrete compressive strength results. Horizontal and vertical strips indicate the characteristic fibre orientations I and II, respectively. In case of horizontal strips the load was perpendicular; however, in case of vertical strips the load was parallel to the characteristic fibre orientation.

- Compressive strength measured on  $240 \times 100 \times 100$  mm prism. Each column represents the mean volume of 6 specimens (Calculated 28 day strength according to Weber (1979)).
- Concrete compressive strength measured on  $240 \times 100 \times 100$  mm prism. Each column represents the mean volume of 12 specimens (Calculated 28 day strength by Weber (1979)).
- Concrete compressive strength measured on  $\varnothing=70$  mm,  $\ell=100$  mm cylinder. Each column represents 1 specimens (Calculated 28 day strength by Weber).
- Concrete compressive strength measured on  $\varnothing=70$  mm,  $\ell=100$  mm cylinder. Each column represents the mean volume of 2 specimens (Calculated 28 day strength by Weber (1979)).
- Concrete compressive strength measured on  $150 \times 150 \times 150$  mm cube. Each column represents the mean volume of 5 specimens (63 day strength).
- Concrete compressive strength measured on  $\varnothing=150$  mm,  $\ell=300$  mm cylinder. Each column represents the mean volume of 3 specimens (52 day strength).



**Figure 2.3:** Compressive strength of concrete mixtures as a function of cement content, water to cement ratio and fibre content

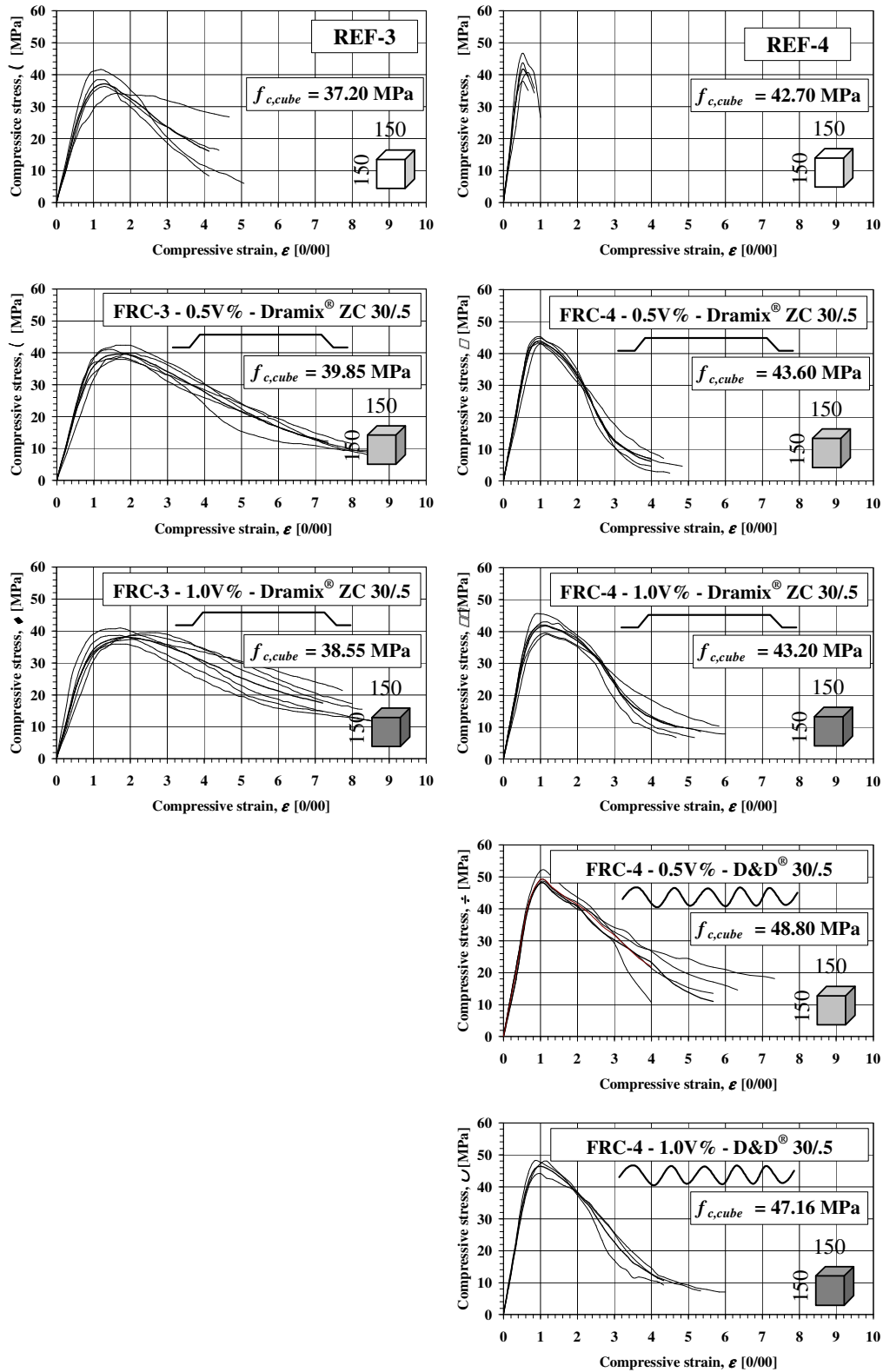


Figure 2.4: Stress – strain relationships for concrete compositions REF-3, FRC-3 and FRC-4 measured on 150×150×150 mm cubes



Due to the fibre addition to REF-3 and REF-4, the compressive strain measured at peak load increased and resulted in a less steep and reasonably flat descending branch as shown in Figure 2.4. Fibre addition to plain concrete significantly increased the ultimate compressive strain. 1.0 V% Dramix® ZC 30/5 hooked-end steel fibre in concrete mix FRC-3 was sufficient to produce a reasonably flat descending branch of stress-strain diagram.

One of the other main parameters in design of concrete structures is the elastic modulus of concrete. Drop of the elastic modulus could be observed applying both by Dramix® ZC 30/5 hooked-end and by D&D® 30/5 crimped steel fibre (Figure 2.4). However, the descending tendency in the elastic modulus was proportional to the applied fibre content.

## 2.2.4 Comparisons to results of other researchers

Available experimental data on compressive tests were summarised in Table 1.2. For comparing the different results steel fibre content seems to be the main governing experimental parameter. Compressive strength increments related to test results of different authors as well as results of the presented study are summarised in Table 2.12 and Table 2.13 as a function of steel fibre content. Increments are also graphically represented in Figure 2.5 where the continuous and dotted lines indicate the tendencies in the variation of compressive strength increments.

Observed compressive strength values given in the literature show a rather wide range to the same fibre content. However, when the concrete compositions, the casting conditions were comparable to the cases of present work, similar tendencies can be found in the changes of compressive strength.

**Table 2.12:** Effect of steel fibre on the increment of concrete compressive strength determined on standard cube specimens and published by different authors in the last three decades

Increments in compressive strength measured on 150×150×150 mm cubes related to the each reference mixes											
Authors	Fibre content in V%										
	0.4	0.5	0.65	0.7	0.75	0.8	1	1.5	2	2.75	3
Sanat & Nyogi & Dwarkaranathan (1985)							+7				+16
							+11				+17
Narayanan & Kareem-P (1986)							+9		+23	+31	
Swamy & Jones & Chiam (1993)							+3				
Erdélyi (1993)			-3		+1						
			-4								
Falkne & Kubat & Droese (1994)							-4				
FRC-3 <sub>ZC 30/5</sub>		+6					+3				
FRC-4 <sub>ZC 30/5</sub>		+2					+1				
FRC-4 <sub>D&amp;D 30/5</sub>		+14					+10				

**Table 2.13:** Effect of steel fibre on the increment of concrete compressive strength determined on standard cylinder specimens and published by different authors in the last three decades

Increment in compressive strength measured on $\varnothing = 150$ mm, $\ell = 300$ mm cylinders cubes related to the each reference mixes												
Authors	Fibre content in V%											
	0.4	0.5	0.65	0.7	0.75	0.8	1	1.5	2	2.75	3	
<i>Mansur &amp; Paramasivam (1986)</i>	+20			+24			+24					
				-15								
				+38								
<i>Craig &amp; Parr &amp; Germain &amp; Mosquera &amp; Kamilaes (1986)</i>				-2					-12		-28	
									+7		+17	
<i>El-Niema (1991)</i>	+15			+26			+31					
	+8			+11			+12					
	+5			+9			+11					
<i>Falkner &amp; Kubat &amp; Droese (1994)</i>							-11					
FRC-4 <sub>ZC 30/5</sub>	+5						+13					
FRC-4 <sub>D&amp;D 30/5</sub>	+27						+21					

## 2.3 Splitting tests

### 2.3.1 Test specimens and test procedure

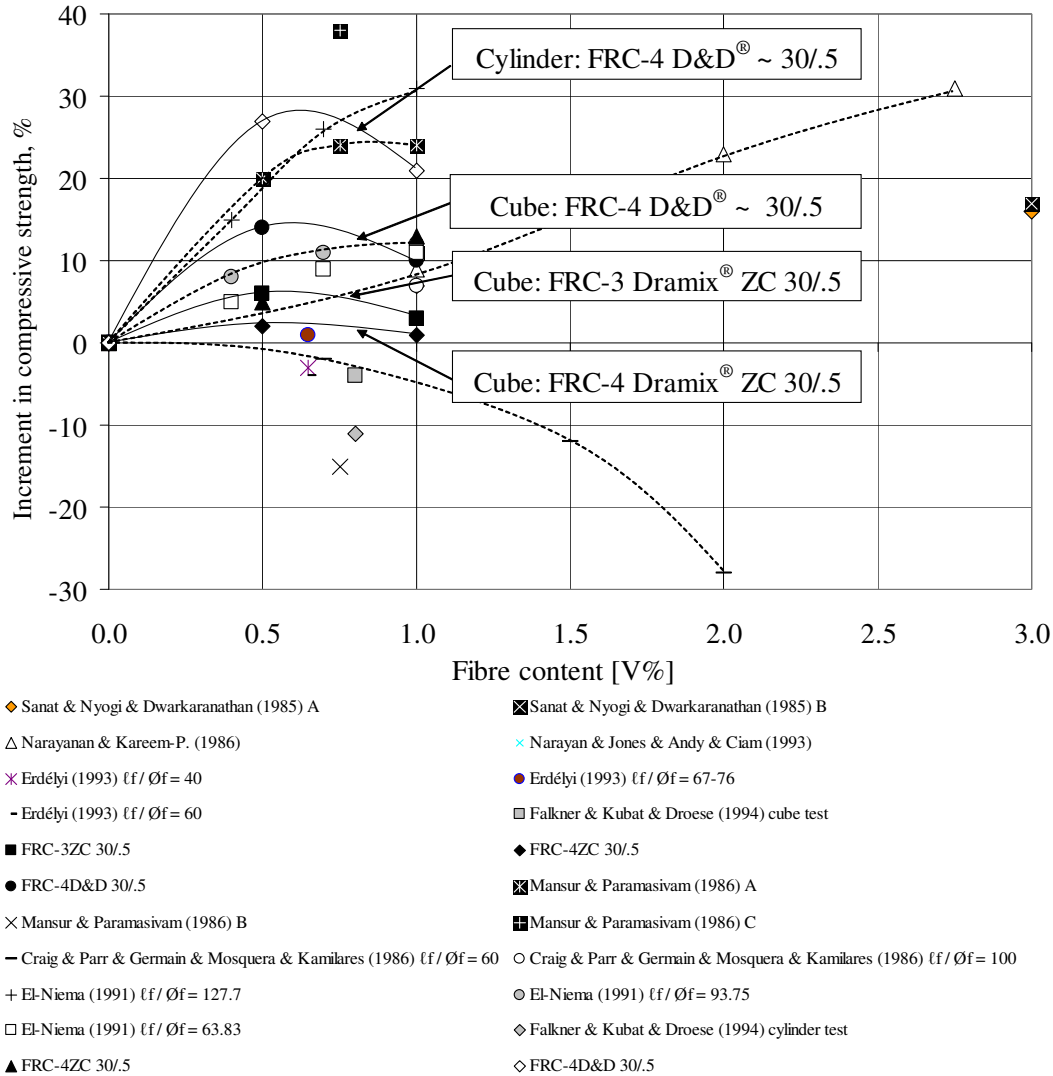
Tensile strength may be indirectly determined from the splitting strength of concrete due to an axial compressive force applied along the length of a cubical or cylindrical specimen. Tensile strength can be obtained by multiplying the splitting strength by a constant, which depends on the test parameters. In case of fibre reinforced concrete indirect methods such as cylinder test seems to considerably overestimate the tensile strength [*Bekaert (1994), Kovács (1996), Krstulovic-Opara & Malak (1997), Krstularovic-Opara & Dogan & Uang & Haghayeghi (1997), Lim (1987), Romualdi & Batson (1963), Romualdi & Batson (1964)*]. However, determination of direct tensile strength experimentally is very sophisticated process therefore indirect method seems to be an appropriate technique for characterising tensile strength properties.

Indirect tensile tests or in other words the so-called Brazilian tests were performed to study the effect of fibre reinforcement on the splitting tensile strength of concrete. Present tests were carried out on standard cylinders ( $\varnothing = 150$  mm,  $\ell = 300$  mm) in the case of concrete mixes REF-3, FRC-3, REF-4 and FRC-4. Force was applied by a force controlled testing machine with the maximum capacity of 6000 kN which was also used for the compression tests.

Effect of fibre orientation on the indirect tensile strength was studied in the case of concrete composition FRC-1 and FRC-2. Consequently, splitting tests were carried out on steel fibre reinforced concrete beams denoted by B-a, B-b and B-c as shown in Table 2.5 and Table 2.6.

Beams were first tested in four-point bending characterizing the toughness properties of fibre reinforced concrete as discussed in the next section. Test specimens after bending failure were subjected to splitting tests in four cross-sections of beams by

the use of a displacement controlled Instron type testing machine. Schematic arrangement of experimental set-up for splitting tests can be seen in Figure 2.11.



**Figure 2.5:** Concrete compressive strength increments as a function of the steel fibre content based on the research work of different authors and the results of the presented study. Continuous lines indicate present, dotted lines and single notations indicate other test results, respectively.

### 2.3.2 Test results and test observations

Results of splitting tests are numerically summarized in Table 2.14 and graphically represented in Figures 2.7 to 2.9. In Figures 2.7 to 2.9 vertical strips indicate parallel and horizontal strips indicate perpendicular directions of splitting tensile stresses to the characteristic fibre orientation for mixes FRC-1 to FRC-4, respectively.

Effect of fibre content, fibre orientation and concrete composition were studied by measuring splitting strengths on steel fibre reinforced concrete specimens.

Higher splitting strengths were obtained by the use of  $75 \text{ kg/m}^3$  Dramix<sup>®</sup> ZP 305 hooked-end steel fibres then applying  $150 \text{ kg/m}^3$  Dramix<sup>®</sup> ZP 305 hooked-end steel fibres considering the same concrete mixes, as shown in Figures 2.7/a and b.

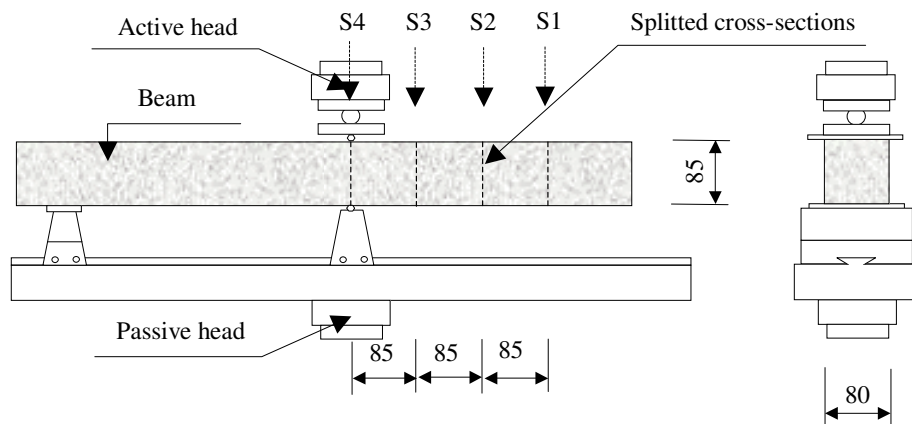
Generally, higher splitting strength was obtained when the characteristic fibre orientation was parallel to the splitting tensile stress, independently from the applied steel fibre contents and the concrete compositions summarised in Figure 2.7/a, b, c and d.

Higher splitting strength was obtained for beams made of concrete mixes FRC-2 related to beams made of mixes FRC-1 including  $75 \text{ kg/m}^3$  Dramix<sup>®</sup> ZP 305 or  $150 \text{ kg/m}^3$  Dramix<sup>®</sup> ZP 305 hooked-end steel fibre as can be seen in Figures 2.8/c and d.

Effect of location of beam specimens (B-a, B-b and B-c) cut out of the original large specimens (B) was also observed on the splitting strength. Splitting strength slightly increased approaching the boundary of original large specimens independently from the experimental parameters (type of mixture, fibre content, characteristic fibre orientation) as shown in Figures 2.8/e, f, g and h.

As discussed in the previous sections, homogenous mixes were obtained after mixing without any balling effect but fibres were oriented during casting. Consequently, even though that the concrete composition was homogenous during mixing, inhomogeneity occurred due to the oriented steel fibres. More fibres situated at the boundary of formworks, and a little higher splitting strength occurred in beams noted by B-a related to beams noted by B-b and B-c.

Significant effect of fibre content was observed on cylinder splitting strength considering concrete mixes FRC-3 and FRC-4 as shown in Figure 2.9 and summarised in Table 2.16. Applying the same fibre content D&D<sup>®</sup> ~ 30/5 crimped steel fibres resulted higher splitting strength than Dramix<sup>®</sup> ZC 30/5 hooked-end steel fibres for concrete mix FRC-3 (Figure 2.9/a). However, application of Dramix<sup>®</sup> ZC 30/5 hooked-end steel fibres in concrete mix FRC-4 caused a slightly higher splitting strength than that of in the concrete mix FRC-3. As diagram in Figure 2.9/d indicates, addition of steel fibres to plain concrete was very effective to improve cylinder splitting strength.



**Figure 2.6:** Test set-up for indirect tensile strength measured on steel fibre reinforced concrete beams made of FRC-1 and FRC-2 mixes

In addition to, the cylinder splitting strength was approximately proportional to steel fibre content. 0.5 V% fibre content resulted 67% and 71% increments of splitting tensile strength in the case of concrete mix FRC-3, applying Dramix<sup>®</sup> ZC 30/.5 hooked-end and D&D<sup>®</sup> ~30/.5 crimped steel fibres, respectively. In the case of mix FRC-4 0.5 V% Dramix<sup>®</sup> ZC 30/.5 fibres resulted 71% increment of splitting strength related to that of the reference mix REF-4. Significant increment of cylinder splitting strength was obtained by the use of Dramix<sup>®</sup> ZC 30/.5 hooked-end and D&D<sup>®</sup> ~30/.5 crimped steel fibres as well. 1.0 V% Dramix<sup>®</sup> ZC 30/.5 hooked-end steel fibres resulted an increment in cylinder splitting strength of 131% for both concrete compositions (FRC-3 and FRC-4) related to the reference mixes. Application of 1.0 V% D&D<sup>®</sup> 30/.5 crimped steel fibres resulted 163% increment in cylinder splitting strength in the concrete composition FRC-4 related to REF-4.

Splitting strength as a function of cement content, water to cement ratio and steel fibre content of mixtures was also studied. Relationships taking into consideration the mean test results determined on different specimens made of concrete mixes FRC-1, FRC-2, REF-3, FRC-3, REF-4 and FRC-4 are presented in Figure 2.10. As Figure 2.10/a implies, higher splitting strength could be obtained by the increase of cement content in steel fibre reinforced concrete mixes FRC-1 and FRC-2. Effect of water to cement ratio as one of the other main characteristics of plain concrete was also considerable on the splitting strength as shown in Figure 2.10/b. By the increase of water to cement ratio lower splitting strength was obtained in the case of steel fibre reinforced concretes.

However, according to Figure 2.10/c, increase of cement content by itself was not appropriate to achieve higher splitting tensile strengths of steel fibre reinforced concrete having relatively high fibre contents. Use of 150 kg/m<sup>3</sup> Dramix<sup>®</sup> ZP 305 hooked-end steel fibres did not result higher splitting strength in FRC-1 (cement content: 330 kg/m<sup>3</sup>, w/c = 0.512) and in FRC-2 (cement content: 500 kg/m<sup>3</sup>, w/c = 0.372) related to mixes FRC-3 and FRC-4 both made with 460 kg/m<sup>3</sup> cement content and w/c = 0.478 as shown in Figure 2.10/c).

### 2.3.3 Comparison with literature results

Splitting tensile strength results of different authors as well as their experimental parameters are summarised in Table 2.11. Comparing them with the results of present study, tensile strength increments are numerically and graphically represented in Table 2.14 and Figure 2.7, respectively. In Figure 2.7 continuous and dotted lines indicate the tendencies in the variation of compressive strength increments for the present results and for the results available in literature.

According to Table 2.11 and Figure 2.12 increments of splitting tensile strength values show considerable differences in the literature due to the different concrete compositions and applied steel fibres. For instance, increment is varying from 10% to 80% applying 0.5 V% fibres and from 20% to 160% applying 1.0 V% fibres taking into consideration the presented results as well. Data indicate that splitting tensile strength is very sensitive to the change of the fibre content and the concrete composition but increasing fibre content always produces significant increment in tensile splitting strength which is approximately proportional to the fibre amount.

**Table 2.14:** Splitting strength results for concrete compositions FRC-1, FRC-2, REF-3, FRC-3, REF-4 and FRC-4. In the case of FRC-1 and FRC-2 four tests were carried out on each specimens noted by S1-S4. In the other cases number of splitting strength results represent the number of cylinder tests in the corresponding line.

No.	Notation of mix	Notation of beam	Splitting strength [MPa]				Mean [MPa]	Mean [MPa]	Mean [MPa]
			S1	S2	S3	S4			
1	FRC-1 <sup>75</sup> <sub>ZP 305-I</sub>	Ba	3.30	4.69	3.74	4.96	4.46	4.21	4.20
		Bb	3.51	3.82	4.75	4.98	4.27		
		Bc	3.92	4.21	4.43	3.04	3.90		
	FRC-1 <sup>75</sup> <sub>ZP 305-II</sub>	Ba	5.17	5.59	3.39	3.68	4.46	4.19	
		Bb	3.82	4.68	3.71	5.04	4.31		
		Bc	3.85	3.20	3.82	4.32	3.80		
2	FRC-1 <sup>150</sup> <sub>ZP 305-I</sub>	Ba	3.83	3.29	3.56	4.05	3.63	2.96	2.56
		Bb	2.44	2.67	2.52	2.69	2.58		
		Bc	2.11	2.77	2.68	3.16	2.68		
	FRC-1 <sup>150</sup> <sub>ZP 305-II</sub>	Ba	2.62	2.45	3.28	-	2.79	2.15	
		Bb	2.57	2.27	1.41	1.80	2.01		
		Bc	2.31	2.37	1.93	-	1.65		
3	FRC-2 <sup>75</sup> <sub>ZP 305-I</sub>	Ba	-	5.42	5.90	4.13	5.15	4.73	4.37
		Bb	3.63	4.36	5.07	5.10	4.54		
		Bc	4.25	5.53	4.37	3.89	4.51		
	FRC-2 <sup>75</sup> <sub>ZP 305-II</sub>	Ba	4.31	4.70	4.57	4.66	4.56	4.01	
		Bb	4.69	3.73	3.32	3.23	3.74		
		Bc	3.85	3.26	3.65	4.12	3.72		
4	FRC-2 <sup>150</sup> <sub>ZP 305-I</sub>	Ba	3.86	3.98	4.79	4.54	4.44	3.54	3.09
		Bb	2.85	3.06	3.34	3.85	3.27		
		Bc	2.73	3.02	2.92	2.98	2.91		
	FRC-2 <sup>150</sup> <sub>ZP 305-II</sub>	Ba	3.39	3.58	2.75	5.04	3.69	2.64	
		Bb	3.74	2.11	2.83	1.88	2.64		
		Bc	2.42	2.36	1.60	-	1.59		
5	REF-3	-	1.47	1.67	-	-	1.57	2.61	
6	FRC-3 <sup>0.5</sup> <sub>ZC 30/5</sub>	-	2.50	2.73	-	-	2.62		
7	FRC-3 <sup>1.0</sup> <sub>ZC 30/5</sub>	-	3.61	3.65	-	-	3.63		
8	REF-4	-	1.57	1.66	1.57	-	1.60	2.67	
9	FRC-4 <sup>0.5</sup> <sub>ZC 30/5</sub>	-	2.97	2.72	2.50	-	2.73		
10	FRC-4 <sup>1.0</sup> <sub>ZC 30/5</sub>	-	3.48	4.03	3.58	-	3.70		
11	FRC-4 <sup>0.5</sup> <sub>D&amp;D ~30/5</sub>	-	2.91	2.62	2.90	-	2.81	2.84	
12	FRC-4 <sup>1.0</sup> <sub>D&amp;D ~30/5</sub>	-	4.92	3.75	3.72	-	4.13		

Splitting tensile strength overestimates the real tensile strength of steel fibre reinforced concrete calculated from the compressive strength of concrete according to many recommendations and standards. However, splitting tensile strength of steel fibre reinforced concrete can be an important parameter in shear design. Based on the experimental results of compressive and splitting tests, splitting tensile strength vs. compressive strength relationships were developed as a function of steel fibre content.

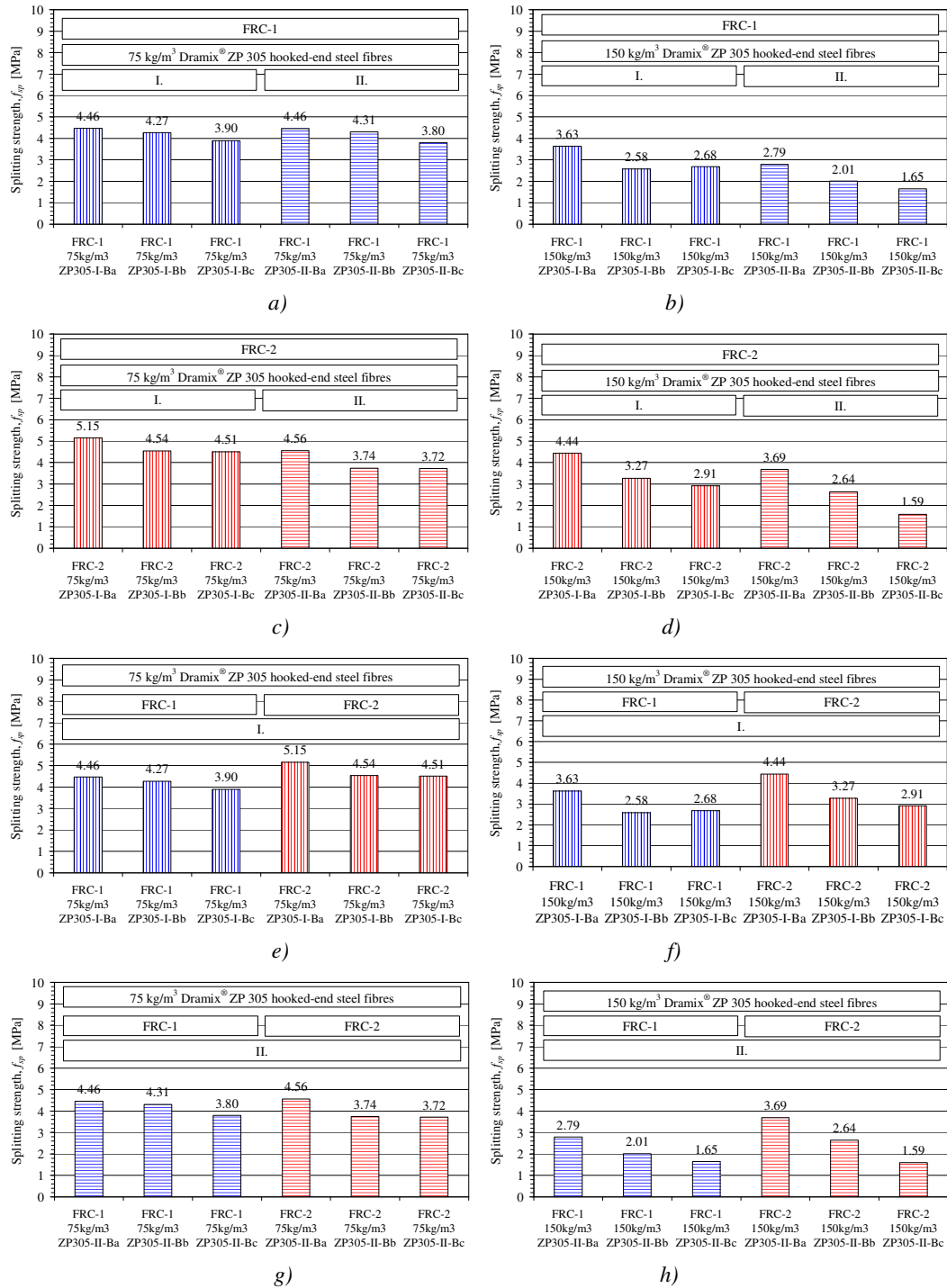
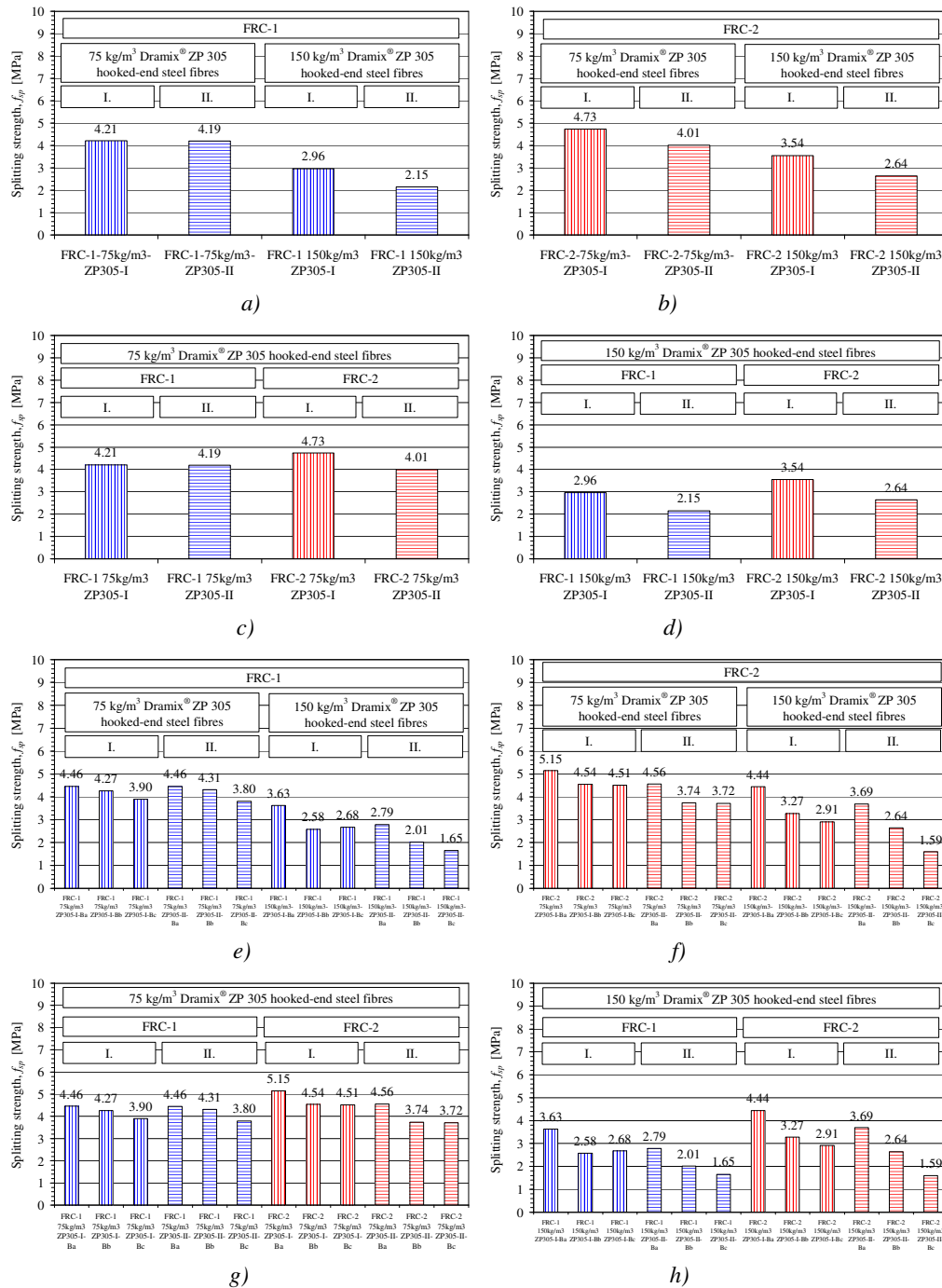


Figure 2.7: Splitting tensile test results for concrete mixes FRC-1 and FRC-2

Each column represents the mean of four results (from S1 to S4)

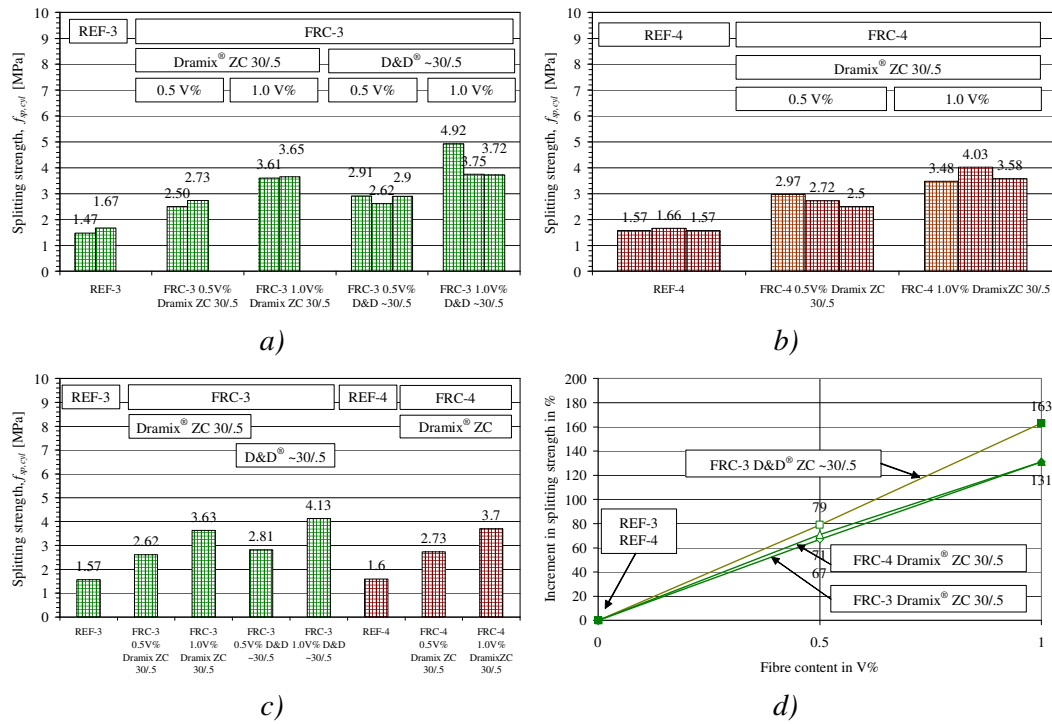
- a) Effect of fibre orientation FRC-1 <sup>75</sup> <sub>ZP 305</sub>
- b) Effect of fibre orientation FRC-1 <sup>150</sup> <sub>ZP 305</sub>
- c) Effect of fibre orientation FRC-II <sup>75</sup> <sub>ZP 305</sub>
- d) Effect of fibre orientation FRC-II <sup>150</sup> <sub>ZP 305</sub>
- e) Effect of concrete type on MIX <sup>75</sup> <sub>ZP 305-I</sub>
- f) Effect of concrete type on MIX <sup>150</sup> <sub>ZP 305-I</sub>
- g) Effect of concrete type on MIX <sup>75</sup> <sub>ZP 305-II</sub>
- h) Effect of concrete type on MIX <sup>150</sup> <sub>ZP 305-II</sub>



**Figure 2.8:** Indirect tensile test results considering FRC-1 and FRC-2

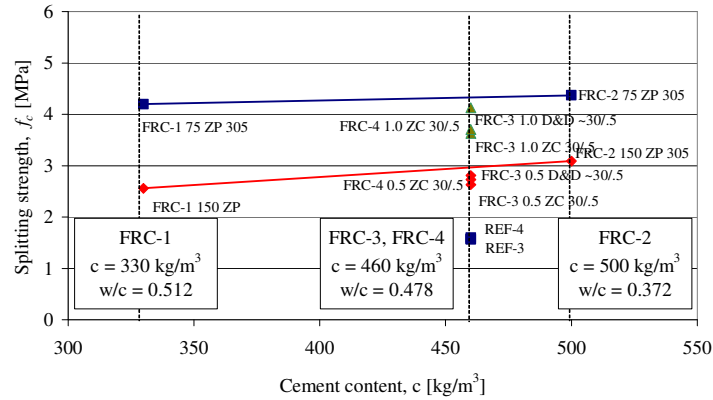
- a) Effect of fibre content and fibre orientation considering concrete type FRC-1 (mean of 12 measures)
- b) Effect of fibre content and fibre orientation considering concrete type FRC-2 (mean of 12 measures)
- c) Effect of concrete type and fibre orientation considering 75 kg/m<sup>3</sup> ZP 305 fibre content
- d) Effect of concrete type and fibre orientation considering 150 kg/m<sup>3</sup> ZP 305 fibre content
- e) Effect of beam position in the formwork considering concrete type FRC-1 (mean of 4 measures)
- f) Effect of beam position in the formwork considering concrete type FRC-2 (mean of 4 measures)
- g) Effect of beam position in the formwork considering 75 kg/m<sup>3</sup> ZP 305 fibre content
- h) Effect of beam position in the formwork considering 150 kg/m<sup>3</sup> ZP 305 fibre content



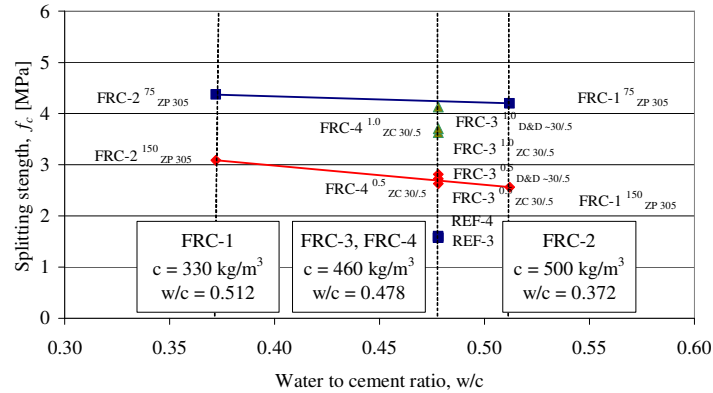


**Figure 2.9:** Cylinder splitting test results for concrete compositions REF-3, FRC-3, REF-4 and FRC-4

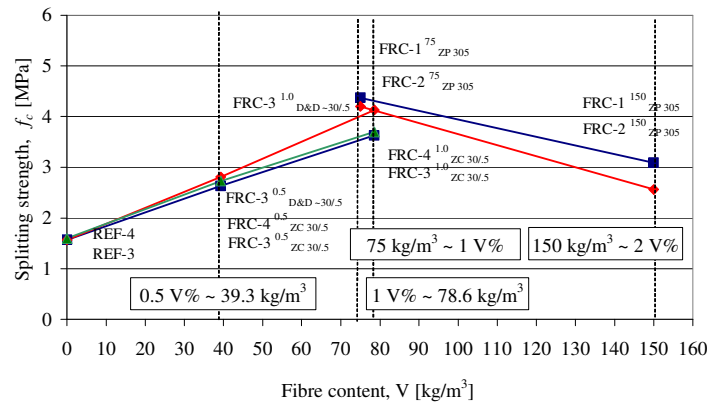
- a) Measured cylinder splitting strength for concrete compositions REF-3 and FRC-3
- b) Measured cylinder splitting strength for concrete compositions REF-4 and FRC-4
- c) Mean cylinder splitting strength for concrete compositions REF-3, FRC-3, REF-4 and FRC-4
- d) Increment in splitting strength in % for concrete compositions REF-3, FRC-3, REF-4 and FRC-4



a) Effect of cement content on the splitting strength (continuous lines indicate the same fibre contents)



b) Effect of water to cement ratio on the splitting strength (continuous lines indicate the same fibre contents)

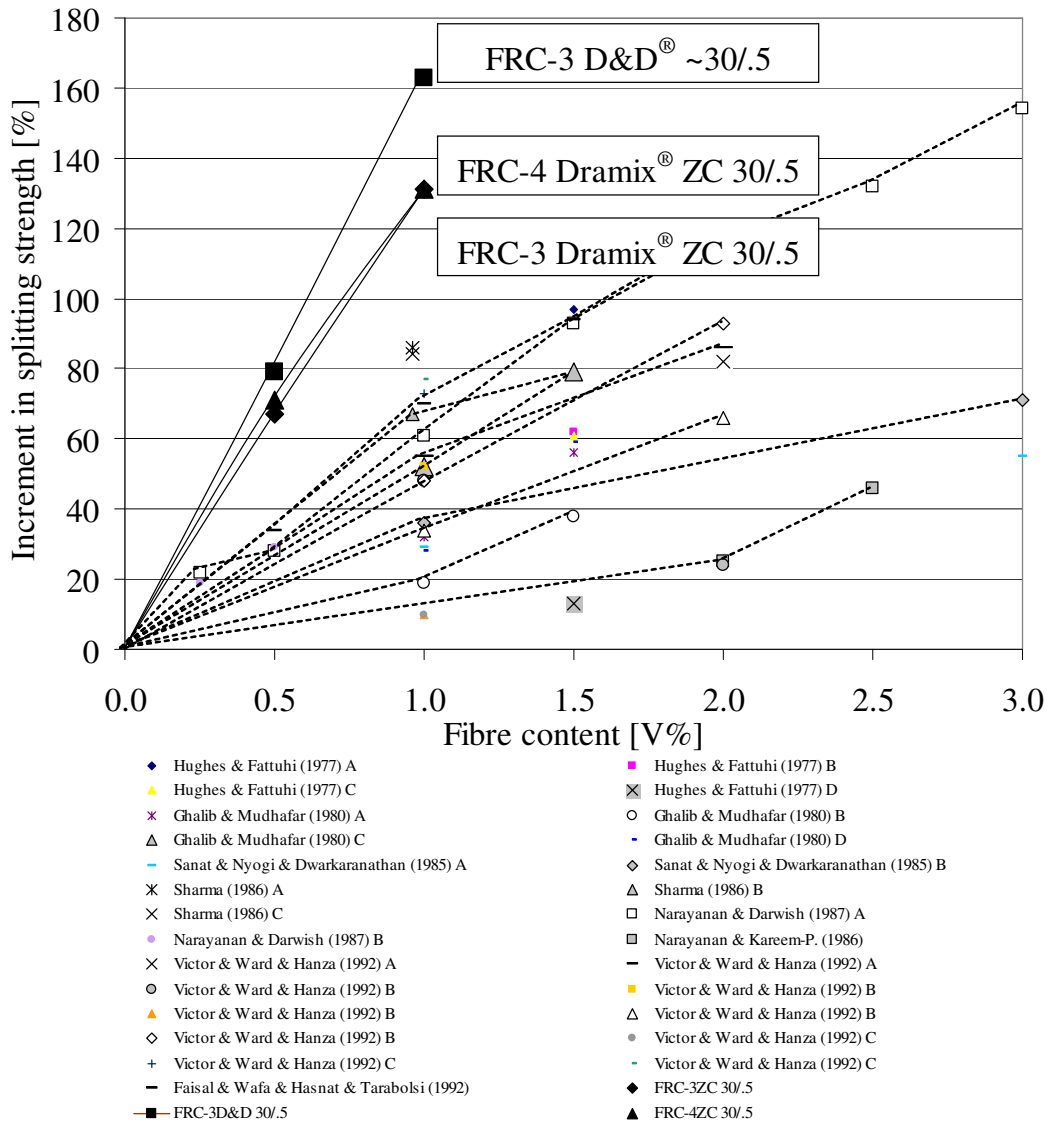


c) Effect of fibre content on the splitting strength, continuous lines indicate the same concrete compositions

**Figure 2.10:** Splitting strength of concrete compositions FRC-1, FRC-2, REF-3, FRC-3, REF-4 and FRC-4 as a function of cement content, water to cement ratio and fibre content

**Table 2.11:** Effect of steel fibres on the increment of concrete splitting strength determined and published by different authors

Authors	Increment in cylinder splitting strength [%]							
	Fibre content, V%							
	0.25	0.5	0.96	1.0	1.5	2.0	2.5	3.0
<i>Hughe &amp; Fattuhi (1977)</i>					+97			
					+62			
					+61			
					+13			
<i>Ghalib &amp; Mudhafar (1980)</i>				+32	+56			
				+19	+38			
				+52	+79			
				+28	+59			
<i>Sanat &amp; Nyogi &amp; Dwarkaranathan (1985)</i>				+29				+55
				+36				+71
<i>Sharma (1986)</i>			+86					
			+67					
			+84					
<i>Narayanan &amp; Darwish (1987)</i>	+22	+28		+61	+93	+116	+132	+154
<i>Narayanan &amp; Darwish (1987)</i>	+19	+29		+47				
<i>Narayanan &amp; Kareem-P. (1986)</i>						+25	+46	
<i>Victor &amp; Ward &amp; Hanza (1992) A</i>						+82		
				+55		+86		
				+48		+24		
<i>Victor &amp; Ward &amp; Hanza (1992) B</i>				+52				
				+10				
				+34		+66		
				+48		+93		
<i>Victor &amp; Ward &amp; Hanza (1992) C</i>				+10				
				+73				
				+77				
<i>Faisal &amp; Wafa &amp; Hasnat &amp; Tarabolsi (1992)</i>		+34		+70	+94	+118		
<i>FRC-3<sub>ZC</sub> 30/5</i>		+67		+131				
<i>FRC-3<sub>D&amp;D</sub> 30/5</i>		+79		+163				
<i>FRC-4<sub>ZC</sub> 30/5</i>		+71		+131				



**Figure 2.12:** Cylinder splitting strength increments as a function of steel fibre content based on research works of different authors and results of the present studies

## 2.4 Flexural toughness

### 2.4.1 Experimental variables and test procedure

Improved toughness is an important characteristic of fibre reinforced concrete. Previously mentioned techniques were used to determine flexural toughness properties of steel fibre reinforced concrete (Chapter 1). Experimental parameters were the fibre content ( $75 \text{ kg/m}^3$  and  $150 \text{ kg/m}^3$ ), the concrete mix proportions (FRC-1 and FRC-2) and the characteristic fibre direction (I and II) as discussed in the previous sections.

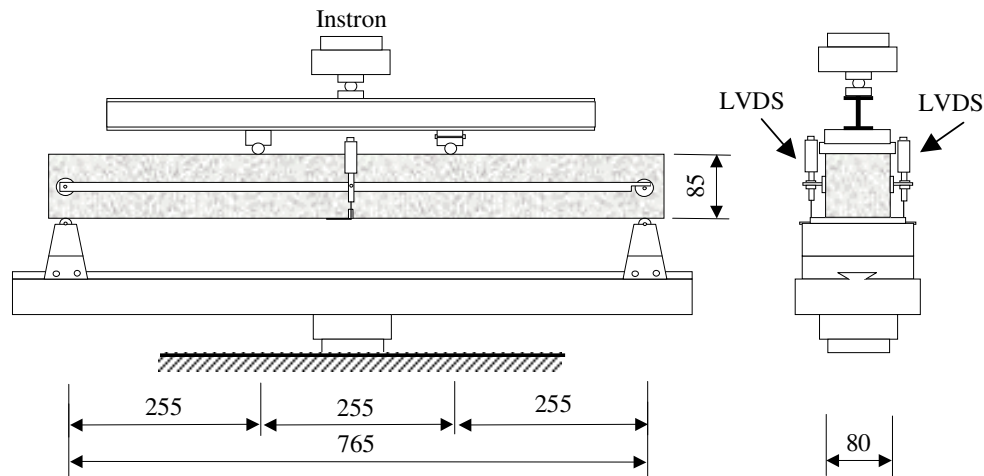
Overall 24 steel fibre reinforced concrete notched beams with the geometry of 820×85×80 mm were tested in four-point bending over a simply supported span of 765 mm. Shear span to depth ratio was 3. Generally, 100×100×350 mm or 150×150×600 mm beams are tested. Beam geometry and testing procedure were developed in order to achieve real beam behaviour in bending despite of standard specimens where the shear span to depth ratio is generally around 1 (350×100×100 mm or 600×150×150 mm) [Balaguru & Shah (1992)].

Beams were sawn out from a concrete slab element (820×630×80 mm, formwork B). Notches were performed after sawing of beams at the mid-section of beam with the geometry of 5×5 mm (5 mm depth and 5 mm width).

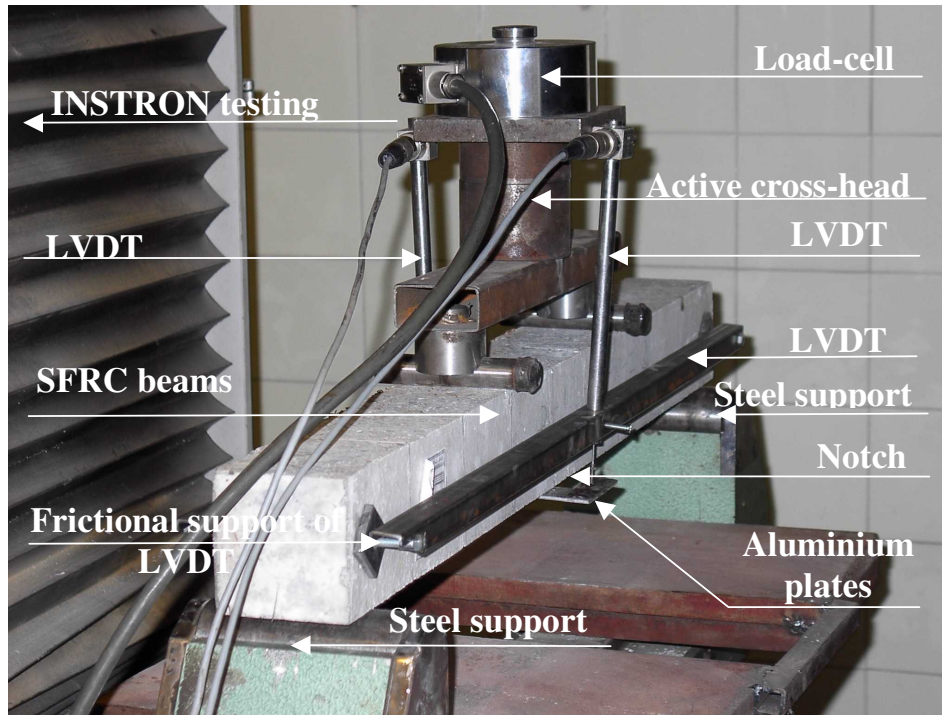
The force was applied by a displacement controlled Instron type testing machine with the capacity of 500 kN. Displacements were controlled by two LVDTs placed on both sides of the beams as shown in Figure 2.13 and in Photo 2.5. Girder elements of LVDSs were placed by two steel plates glued on both side of the beam at the section of the support. One side of measuring system was performed to be a fix; the other was a frictional support as shown in Photo 2.5. Loading rate was 0.2 mm/min. according to the *ASTM* and *JSCE* recommendations.

Due to the inaccuracy of specimen casting and sawing, geometries of beams were slightly different. Effective bending stresses at the mid-section was calculated from the applied load and the measured geometry of the cross section of beams. Bending stress vs. mid-point deflection relationships measured in four point bending summarised in Figure 2.14. First and second columns indicate characteristic fibre directions parallel or perpendicular to the axes of beams, respectively.

Each diagram includes three beams denoted by B-a, B-b and B-c. First character in notation denotes the beam specimens, second character denotes the original position of the beam in the formwork.



**Figure 2.13:** Test set-up and test arrangement for bending test of steel fibre reinforced concrete beams



*Photo 2.5: Bending test on steel fibre reinforced concrete beams*

### 2.4.2 Bending stress vs. mid-point deflection relationships

Calculated bending stress vs. mid-point deflection relationships indicate that significant effect of concrete mix proportions (FRC-1 and FRC-2) and steel fibre content ( $75 \text{ kg/m}^3$  and  $150 \text{ kg/m}^3$ ) as well as characteristic fibre directions (I and II) can be observed on the toughness properties. Based on the load vs. mid-point deflection relationships different toughness indexes were calculated. Flexural toughness indexes [ASTM C 1018-89 (1990)], toughness factors [JSCE-SF3 (1984)] and post cracking strength values [Banthia & Trottier (1995)] summarised in Table 2.16 and Table 2.17.

Generally, better energy absorption capacity or toughness properties were obtained in the case of the mix containing  $75 \text{ g/m}^3$  steel fibres related to specimens made with  $150 \text{ kg/m}^3$ . Reason of the observed phenomena lies in the calculated air content and porosity of concrete (see Table 2.1). Higher air content ( $60.8 \text{ l/m}^3$  for FRC-1 and  $74.4 \text{ l/m}^3$  for FRC-2) and higher porosity ( $116.2 \text{ l/m}^3$  for FRC-1 and  $85.9 \text{ l/m}^3$  for FRC-2) was determined for mixes containing  $150 \text{ kg/m}^3$  steel fibres than for mixes made with  $75 \text{ kg/m}^3$ . In the case of mixes containing  $75 \text{ kg/m}^3$  the air content of mixes were  $36.8 \text{ l/m}^3$  for FRC-1 and  $28.0 \text{ l/m}^3$  for FRC-2 while the porosity were  $89.5 \text{ l/m}^3$  for FRC-1 and  $38.0 \text{ l/m}^3$  for FRC-2 (see Table 2.1).

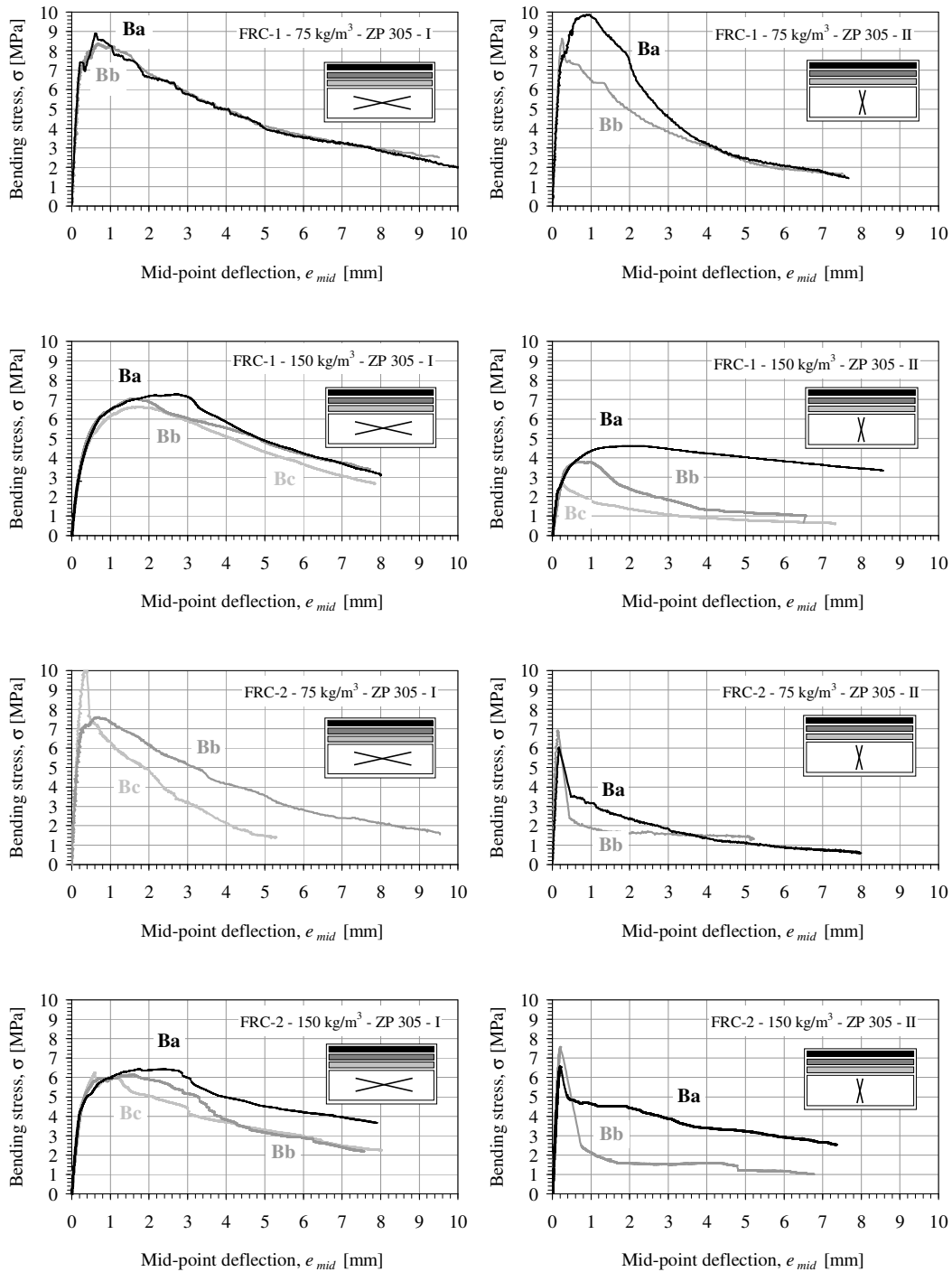


Figure 2.14: Bending stress vs. mid-point deflection relationships for steel fibre reinforced concrete beams

**Table 2.16:** Flexural toughness properties of steel fibre reinforced concrete according to the ASTM C 1018 and JSCE SF4 (Flexural toughness factor)

Concrete mix	Fibre orientation	Beam	Toughness indexes				Residual strength factor		Flexural toughness factor
			I <sub>5</sub>	I <sub>10</sub>	I <sub>20</sub>	I <sub>30</sub>	R <sub>5,10</sub>	R <sub>10,20</sub>	
FRC-1 <sup>75</sup> <sub>ZP 305</sub>	I.	Ba	5.18	10.66	20.25	28.67	109.57	95.93	
		Bb	4.66	9.55	17.86	24.81	97.76	83.14	
		Bc	Beam cracked before testing						
	II.	Ba	5.17	11.30	21.93	28.66	122.52	106.32	
		Bb	2.72	4.82	7.15	9.29	42.12	23.29	
		Bc	Beam cracked before testing						
FRC-1 <sup>150</sup> <sub>ZP 305</sub>	I.	Ba	4.24	8.11					
		Bb	3.95	7.08					
		Bc	4.40	8.61	14.43		84.17	58.17	
	II.	Ba	5.19	12.00	27.60	43.85	136.15	156.03	
		Bb	4.81	9.05	14.53	18.09	84.65	54.86	
		Bc	3.92	6.77	11.23	14.64	57.06	44.62	
FRC-2 <sup>75</sup> <sub>ZP 305</sub>	I.	Ba	Beam cracked before testing						
		Bb	4.32	8.16	14.92	20.17	76.71	67.68	
		Bc	3.58	6.02	9.37	11.21	48.82	33.48	
	II.	Ba	3.99	6.51	10.72	14.26	50.49	42.09	
		Bb	2.82	3.89	5.74	7.43	21.54	18.50	
		Bc	Beam cracked before testing						
FRC-2 <sup>150</sup> <sub>ZP 305</sub>	I.	Ba	4.89	10.63	22.93	34.82	114.79	122.93	
		Bb	5.44	11.60	24.07	35.10	123.23	124.70	
		Bc	5.10	10.57	20.25	28.46	109.46	96.85	
	II.	Ba	3.43	6.17	11.45	16.10	54.71	52.79	
		Bb	3.45	4.40	6.08	7.66	18.90	16.83	
		Bc	Beam cracked before testing						

**Table 2.17:** Flexural toughness properties of steel fibre reinforced concrete (PCS) according to Banthia and Trottier (1995)

Concrete mix	Fibre orientation	Beam	Post Cracking Strength, PCS, [MPa]								
			3000	1500	1000	750	600	400	300	200	150
FRC-1 <sup>75</sup> <sub>ZP 305</sub>	I.	Ba	-	-	-	-	-	-	-	-	-
		Bb	4.63	3.77	3.51	3.26	3.03	2.51	2.09	-	-
		Bc	-	4.20	3.94	3.82	3.64	3.24	2.91	2.39	-
	II.	Ba	12.19	9.64	8.32	7.60	7.04	5.96	5.13	4.04	-
		Bb	3.14	1.99	1.64	1.43	1.33	1.17	1.09	-	-
		Bc	-	-	-	-	-	-	-	-	-
FRC-1 <sup>150</sup> <sub>ZP 305</sub>	I.	Ba	-	-	-	-	-	-	4.24	4.02	3.64
		Bb	-	-	-	-	-	-	3.94	3.67	3.45
		Bc	-	-	-	-	-	3.95	3.85	3.57	3.28
	II.	Ba	-	-	-	-	-	-	2.60	5.98	4.32
		Bb	1.49	1.34	1.27	1.20	1.13	1.02	0.93	0.81	0.72
		Bc	-	-	0.72	0.72	0.71	0.62	0.56	0.47	0.40
FRC-2 <sup>75</sup> <sub>ZP 305</sub>	I.	Ba	-	22.70	20.75	19.70	18.02	14.37	12.00	9.12	-
		Bb	-	4.74	4.30	4.01	3.76	3.53	3.03	2.66	-
		Bc	-	-	-	-	-	-	-	-	-
	II.	Ba	-	21.65	19.62	18.50	17.82	16.09	14.63	12.31	10.60
		Bb	-	5.87	5.76	5.48	5.29	4.75	4.31	3.63	-
		Bc	-	-	-	-	-	-	-	-	-
FRC-2 <sup>150</sup> <sub>ZP 305</sub>	I.	Ba	-	-	-	-	-	3.29	3.20	2.89	2.35
		Bb	-	-	-	-	-	-	3.78	3.41	3.13
		Bc	-	-	3.27	3.31	3.35	3.18	3.05	2.78	2.55
	II.	Ba	1.87	1.53	1.44	1.40	1.37	1.34	1.30	1.21	1.14
		Bb	-	-	1.32	1.09	0.95	0.76	0.67	0.58	0.53
		Bc	-	-	-	-	-	-	-	-	-



Generally, effect of the characteristic fibre direction on the bending behaviour was determined. Characteristic fibre direction parallel to the axis of the beam indicated better energy absorption capacity or toughness properties compared to beams in which the characteristic fibre direction were perpendicular to the beam axis.

In addition to, influence of the original position of beams in the slab element before sawing of the specimens was also observed. Better toughness properties were determined for beams noted by B-a than beams noted by B-b and B-c. Reason of the phenomena may lie in the higher steel fibre concentration at the boundary of the specimens.

## 2.5 Conclusions

### Compressive behaviour

1. Application of steel fibres produced **increase of compressive toughness** of concrete. **Ultimate strain** increased by increasing steel fibre contents resulting in a **less steep** and reasonably **flat descending branch** of the stress-strain diagram. Nevertheless, steel fibre reinforced concrete can absorb more energy in compression than plain concrete resulting **less brittle failure**. Increase of toughness was more considerable from 0 to 0.5 V% than from 0.5 V% to 1.0 V%.
2. **Concrete compressive strength** can be slightly increased by addition of **steel fibres**. Applying 0.5 V% and 1.0 V% (FRC-3 and FRC-4) of steel fibre slight increment of concrete strength was observed. However, the observed strength increments were not proportional to the increments of fibre contents. According to the present and other experimental results maximal increase of compressive strength was observed by applying 0.5 V% ( $\sim 40 \text{ kg/m}^3$ ) to 0.7 V% ( $\sim 55 \text{ kg/m}^3$ ) steel fibres.  
Earlier studies shown that addition of steel fibres to structural concrete can only be effective in higher dosages than 1.0 V%. However, in the presented experimental investigation by the increase of fibre content from 1.0 V% ( $\sim 75 \text{ kg/m}^3$ ) to 2.0 V% ( $\sim 150 \text{ kg/m}^3$ ) decrease in compressive strengths was observed (FRC-1 and FRC-2) which might be caused by the increasing porosity of the concrete matrix.
3. **Compressive strength** was influenced by the **characteristic fibre orientation** applying relatively high steel fibre contents ( $75 \text{ kg/m}^3$  and  $150 \text{ kg/m}^3$ ). Higher compressive strengths were observed when the characteristic fibre orientations were perpendicular to the axis of loads.
4. **Failure mode** of prisms ( $240 \times 100 \times 100 \text{ mm}$ ) in compression was affected by the **characteristic fibre orientation** at relatively high fibre contents ( $75 \text{ kg/m}^3$  and  $150 \text{ kg/m}^3$ ). Tougher failure was observed when the characteristic fibre orientation was perpendicular to the axis of load compared the orientation parallel to the load.

### Splitting tensile strength

5. **Splitting strength increments** were approximately proportional to the applied steel fibre contents up to 1 V% obtained on cylinders. Higher fibre contents were tested

- on beams in our studies. Splitting tests on beams by 2 V% fibre content resulted lower splitting strength than by 1 V %.
6. **Cylinder splitting strength** was not significantly effect by the **configuration of steel fibres** (hooked-end and crimped) made with the **same aspect ratio**.
  7. **Splitting strength** was influenced by the **characteristic fibre orientation** applying relatively high steel fibre contents ( $75 \text{ kg/m}^3$  and  $150 \text{ kg/m}^3$ ) in beam splitting tests. Higher splitting strengths were observed when the characteristic fibre orientations were parallel with the axis of the beams.

### **Toughness properties**

8. **A new experimental set-up** was developed to analyse the toughness properties of steel fibre reinforced concrete. Four point bending tests were performed. Geometry of specimens were determined so that realistic beam behaviour could be obtained ( $a/d = 3$ ).
9. **Bending stress vs. mid-point deflection** relationships as well as different types of **toughness indexes** were derived from the measured load vs. mid-point deflection relationships. Results indicated **considerable influence** of high steel fibre contents ( $75 \text{ kg/m}^3$  and  $150 \text{ kg/m}^3$ ) on the toughness of steel fibre reinforced concrete beams.
11. **Due to the lower** porosity better toughness properties were obtained for mixes containing  $75 \text{ kg/m}^3$  steel fibres, than for mixes containing  $150 \text{ kg/m}^3$  steel fibres.
12. **Generally, toughness indexes** as well as **bending stress vs. mid-point deflection** relationships indicate better toughness properties for specimens having **characteristic fibre direction** parallel to the axis of beam.
13. In addition to, **better toughness properties** were obtained for specimens noted by **B-a** than for specimens noted by B-b and B-c, which may be caused by the **higher steel fibre concentration** at the **boundary** of formwork.

# Chapter 3

## Modelling of fibre reinforced materials in tension

*Mechanical modelling of the uniaxial behaviour of fibre reinforced materials is discussed in this Chapter. A one-dimensional elastic-plastic material model has been developed for fibre reinforced materials taking into consideration plastic matrix-fibre coupling for the irreversible deformations of the matrix and the fibres. Due to the simplicity and clear physical significance of the basic mechanical model which takes into consideration elastic-brittle matrix and elastic-perfectly plastic fibre reinforcement behaviour, the model is extended with residual strength of the constituents and hardening or softening phenomena as well.*

**Keywords:** material model, mechanical model, fibre reinforced material, constituents

### 3.1 Modelling of fibre reinforced materials

Mechanical model is developed for the analysis of one-dimensional behaviour of fibre reinforced material (Figure 3.1).

The model is composed of two parallel sub-devices which represent the behaviour of the constituents (matrix and fibre reinforcement). Elastic-brittle matrix behaviour is composed of an elastic spring (stiffness  $C_m$ ) and a fragile crack element (strength  $f_t$ ) (Figure 3.1-3.2). The behaviour of fibre reinforcement assumed to be governed by an elastic-perfectly plastic material law, described by an elastic spring (stiffness  $C_f$ ) together with a friction element (strength  $f_y$ ) (Figure 3.1-3.2). In addition to, the two parallel sub-devices are coupled by an elastic spring element of stiffness  $M$ , which links the irreversible matrix behaviour (i.e., strain  $\varepsilon_m^p$ ) with the irreversible fibre reinforcement behaviour (i.e., strain  $\varepsilon_f^p$ ).

$\sigma_m$  and  $\sigma_f$  are the resulting stresses of matrix and the fibre reinforcement devices, respectively. The overall stress ( $\Sigma$ ) is provided by the sum of  $\sigma_m$  and  $\sigma_f$  (Figure 3.2):

$$\Sigma = \sigma_m + \sigma_f = (C_m + C_f)\varepsilon - C_m \varepsilon_m^p - C_f \varepsilon_f^p \quad (3.1)$$

$$\sigma_m = C_m(\varepsilon - \varepsilon_m^p) - M(\varepsilon_m^p - \varepsilon_f^p) \quad (3.2)$$

$$\sigma_f = C_f(\varepsilon - \varepsilon_f^p) + M(\varepsilon_m^p - \varepsilon_f^p) \quad (3.3)$$

All quantities are introduced at the macroscopic level of the fibre reinforced material (i.e., typical scale of laboratory test specimen). For instance, the irreversible fibre reinforcement deformation  $\varepsilon_f^p$  is a macroscopic quantity, which accounts for different mechanisms at the microscopic level of the composite, such as debonding, fibre pull-out, localized fibre yielding, etc.

The constituent stresses ( $\sigma_m$  for the matrix and  $\sigma_f$  for the fibre reinforcement) are constrained by the yield function. However,  $\sigma_m$  and  $\sigma_f$  are the partial stresses of the fibre reinforced material that can be calculated from the elastic-plastic solution satisfying the corresponding yield criteria:

$$f_m(\sigma_m) \leq 0 \quad , \quad f_f(\sigma_f) \leq 0 \quad (3.4)$$

where  $f_m(\sigma_m)$  and  $f_f(\sigma_f)$  are defined according to the elastic-brittle matrix and the elastic-perfectly plastic fibre reinforcement behaviour:

$$f_m(\sigma_m) = \sigma_m - f_t \leq 0 \quad , \quad f_f(\sigma_f) = |\sigma_f| - f_y \leq 0 \quad (3.5)$$

According to the relationships in Eq. (3.4) and Eq. (3.5) related to the constituents (matrix and fibre reinforcement), the following yield criterion may be defined at the level of the fibre reinforced material:

$$F(f_m, f_f) = \max\{f_m(\sigma_m), f_f(\sigma_f)\} = \begin{cases} f_m(\sigma_m) = \sigma_m - f_t \leq 0 & \text{if } C_m/C_f > f_t/f_y \\ f_f(\sigma_f) = |\sigma_f| - f_y \leq 0 & \text{if } C_m/C_f < f_t/f_y \end{cases} \quad (3.6)$$

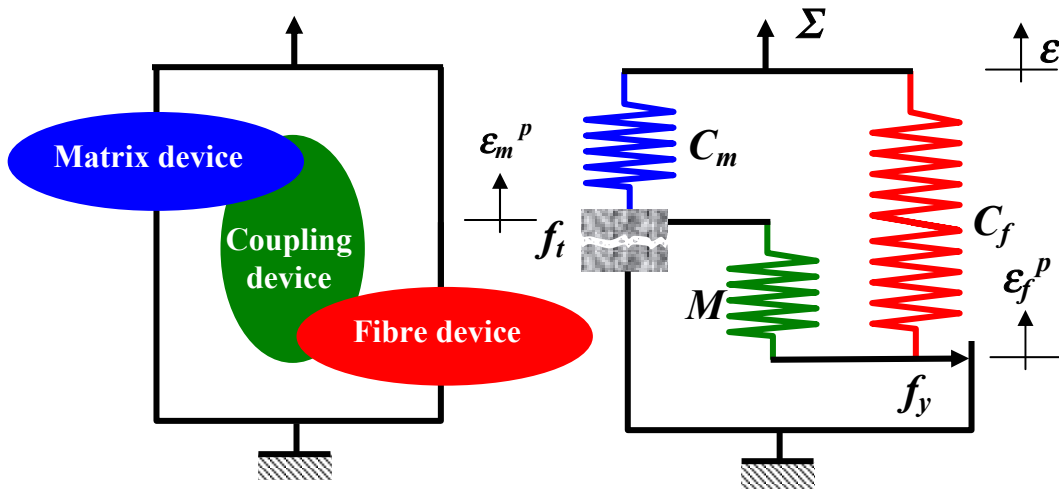
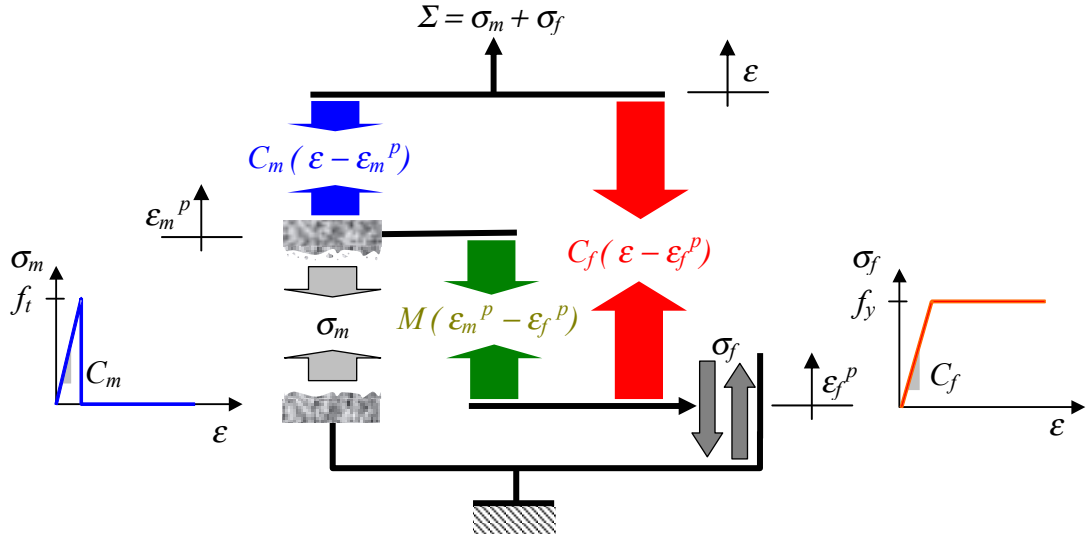


Figure 3.1: 1-D mechanical model for fibre reinforced materials



**Figure 3.2:** Force-flow in the mechanical model and material laws for the constituents

Considering the properties of the constituents, Eq. (3.6) defines the following admissible state of stresses: In case of matrix cracking prior to fibre reinforcement yielding ( $f_t / f_y < C_m / C_f$ ):

- ◀ Elastic state in loading:

$$F(f_m, f_f) := \max\{f_m(\sigma_m), f_f(\sigma_f)\} < 0 \quad , \quad dF(f_m, f_f) > 0$$

- ◀ Elastic state in unloading:

$$F(f_m, f_f) := \max\{f_m(\sigma_m), f_f(\sigma_f)\} \leq 0 \quad , \quad dF(f_m, f_f) < 0$$

- ◀ Matrix yielding and elastic fibre reinforcement:

$$f_m(\sigma_m) = df_m(\sigma_m) = 0 \quad , \quad f_f(\sigma_f) < 0 \quad , \quad df_f(\sigma_f) > 0$$

- ◀ Matrix and fibre reinforcement yielding:

$$f_m(\sigma_m) = df_m(\sigma_m) = 0 \quad , \quad f_f(\sigma_f) = df_f(\sigma_f) = 0$$

and in the case of fibre reinforcement yielding prior to matrix cracking ( $f_t / f_y > C_m / C_f$ ):

- ◀◀ Elastic state in loading:

$$F(f_m, f_f) := \max\{f_m(\sigma_m), f_f(\sigma_f)\} < 0 \quad , \quad dF(f_m, f_f) > 0$$

- ◀◀ Elastic state in unloading:

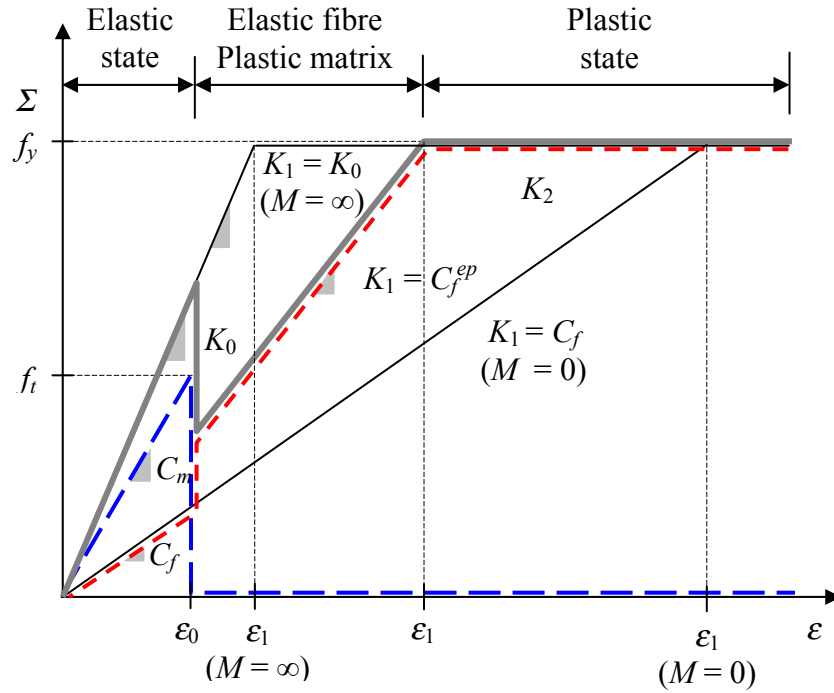
$$F(f_m, f_f) := \max\{f_m(\sigma_m), f_f(\sigma_f)\} \leq 0 \quad , \quad dF(f_m, f_f) < 0$$

- ◀◀ Fibre reinforcement yielding and elastic matrix:

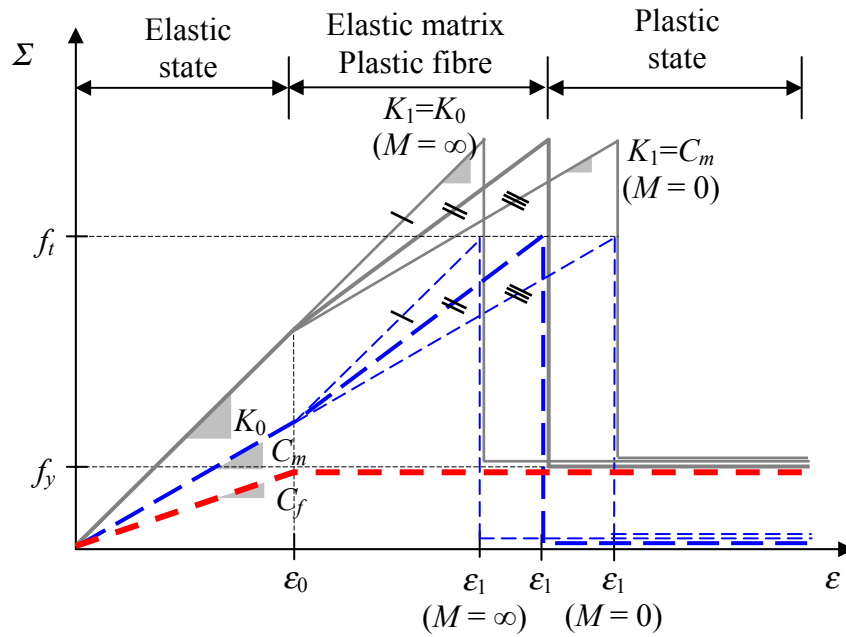
$$f_f(\sigma_f) = df_f(\sigma_f) = 0 \quad , \quad f_m(\sigma_m) < 0 \quad , \quad df_m(\sigma_m) > 0$$

- ◀◀ Fibre reinforcement and matrix yielding:

$$f_f(\sigma_f) = df_f(\sigma_f) = 0 \quad , \quad f_m(\sigma_m) = df_m(\sigma_m) = 0$$



**Figure 3.3:** Stress-strain relationships for fibre reinforced material considering elastic-brittle matrix and elastic-perfectly plastic fibre reinforcement behaviour, matrix cracking prior to fibre reinforcement yielding



**Figure 3.4:** Stress-strain relationships for fibre reinforced material considering elastic-brittle matrix and elastic-perfectly plastic fibre reinforcement behaviour, fibre reinforcement yielding prior to matrix cracking

The yielding function in Eq. (3.4), as well as the strength properties  $f_t$  and  $f_y$  must be defined on the level of the fibre reinforced material. For instance, fibre reinforcement yield strength  $f_y$  is associated with the onset of irreversible fibre deformation at the macroscopic scale of the fibre reinforced material, which comprises debonding, fibre pull-out or localized fibre yielding, etc.

Finally, we should also consider the evolution laws both for the elastic brittle matrix behaviour:

$$\varepsilon_m^p \geq 0 \quad \sigma_m \varepsilon_m^p = 0, \quad (3.7)$$

and for the elastic-perfectly plastic fibre reinforcement (i.e.,  $f_f = df_f = 0$ ):

$$d\varepsilon_f^p = d\lambda_f \frac{\partial f_f}{\partial \sigma_f} = d\lambda_f \text{sign}(\sigma_f), \quad (3.8)$$

where  $d\lambda_f =$  plastic multiplier of the fibre reinforcement, and  $\text{sign}(\sigma_f)$  function defined as:

$$\text{sign}(\sigma_f) = \begin{cases} +1 & \text{if } \sigma_f > 0 \\ -1 & \text{if } \sigma_f < 0 \end{cases} \quad (3.9)$$

Stress-strain relationship for fibre reinforced material considering elastic-brittle matrix and elastic-perfectly plastic fibre reinforcement behaviour with matrix cracking prior to fibre reinforcement yielding is summarised in Figure 3.3.

Stress-strain relationship for fibre reinforced material considering elastic-brittle matrix and elastic-perfectly plastic fibre reinforcement behaviour with fibre reinforcement yielding prior to matrix cracking is summarised in Figure 3.4.

So far, only elastic-brittle matrix and elastic-perfectly plastic fibre reinforcement behaviour were considered, i.e., the residual stress in the matrix was zero after cracking ( $\sigma_m = 0$ ) while the fibre reinforcement stress was equal to the yield strength ( $\sigma_f = f_y$ ).

For the sake of clarity, hardening and/or softening behaviour of the constituents has not been considered here before. However, due to the simplicity of the one-dimensional device element it can easily be expanded for instance by fibre reinforcement softening or hardening and matrix or fibre reinforcement residual strength as well. In this case, yield functions (as detailed before) describe the initial elasticity domain of the fibre reinforced material. Further loading passes the elastic domains. Assume now brittle matrix and brittle fibre behaviour. The admissible stresses are now described by:

$$F(f_m, f_f) = \max\{f_m(\sigma_m, \varsigma_m), f_f(\sigma_f, \varsigma_f)\} = f_m = \sigma_m + \varsigma_m - \bar{f}_t \leq 0 \quad (3.10)$$

$$F(f_m, f_f) = \max\{f_m(\sigma_m, \varsigma_m), f_f(\sigma_f, \varsigma_f)\} = f_f = |\sigma_f + \varsigma_f| - \bar{f}_y \leq 0 \quad (3.11)$$

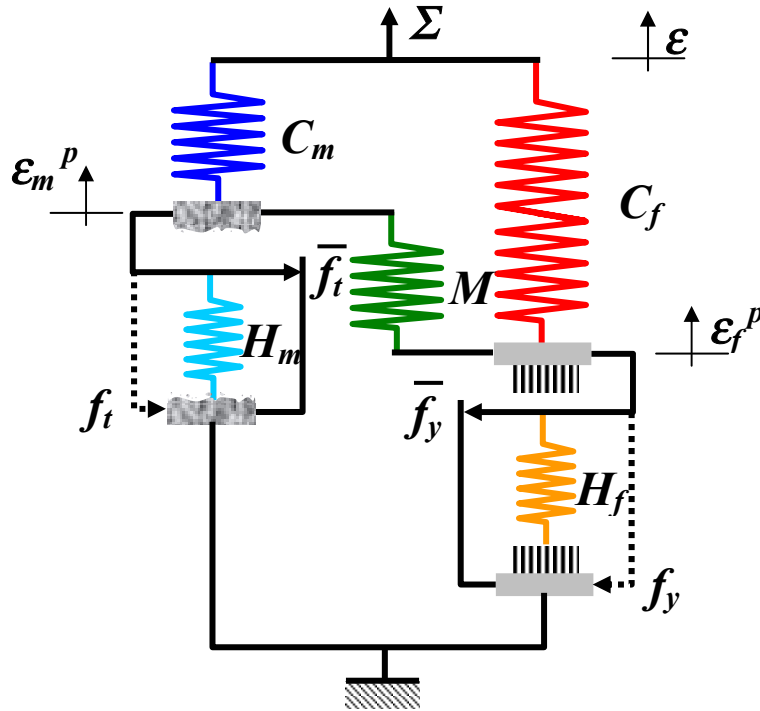
where  $\bar{f}_t$  and  $\bar{f}_y$  denote the residual strength of the matrix and of the fibre reinforcement after matrix cracking and fibre fracture, respectively. Note that

$0 \leq \bar{f}_t \leq f_t$  and  $0 \leq \bar{f}_y \leq f_y$ . Furthermore,  $-\zeta_m$  and  $-\zeta_f$  are the forces (positive in tension) in the hardening spring devices of the matrix and of the fibre reinforcement represented by a spring of rigidity  $H_m$  and  $H_f$ , respectively (Figure 3.3). These forces depend on the hardening variables  $\chi_m$  and  $\chi_f$  (i.e.,  $\zeta_m = \zeta_m(\chi_m)$  and  $\zeta_f = \zeta_f(\chi_f)$ ).

In the uniaxial model  $(\chi_m, \chi_f)$  can be considered to coincide with the plastic constituent strains  $(\varepsilon_m^p, \varepsilon_f^p)$  similarly to the case of linear hardening or softening:

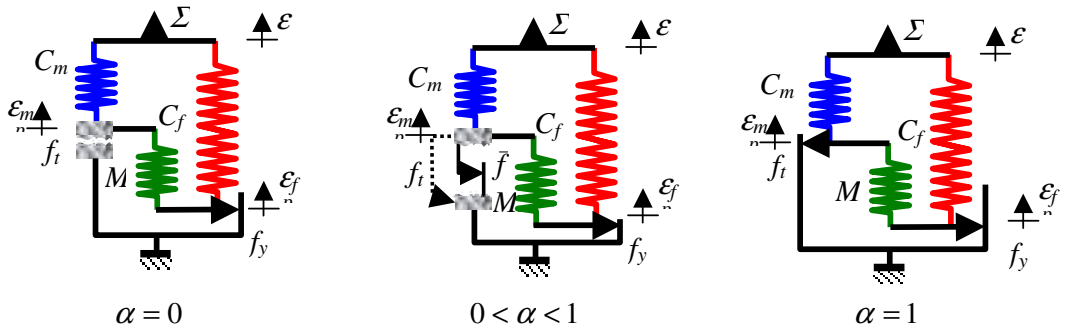
$$\chi_m = \varepsilon_m^p \Leftrightarrow \zeta_m = -H_m \varepsilon_m^p \quad \chi_f = \varepsilon_f^p \Leftrightarrow \zeta_f = -H_f \varepsilon_f^p \quad (3.12)$$

An illustrative 1-D mechanical model for fibre reinforced material has been considered above. Due to the simplicity of the mechanical model, different kinds of matrix and fibre reinforcement behaviours can be considered. Several 1-D models are summarised taking into consideration different constituent behaviours. Their mechanical devices are presented here from Figure 3.6 to Figure 3.17 with the illustration of the matrix and fibre reinforcement behaviour as well as their schematic stress-strain relationships. Characteristic points and tangential relationships of the stress-strain diagram of the fibre reinforced materials are also summarised here from Table 3.2 to Table 3.8 containing the constituent stress-strain relationships. Parametric study on stress-strain relationship related to these different mechanical models taking into consideration their model parameters are also illustrated in Figure 3.7 to Figure 3.15.

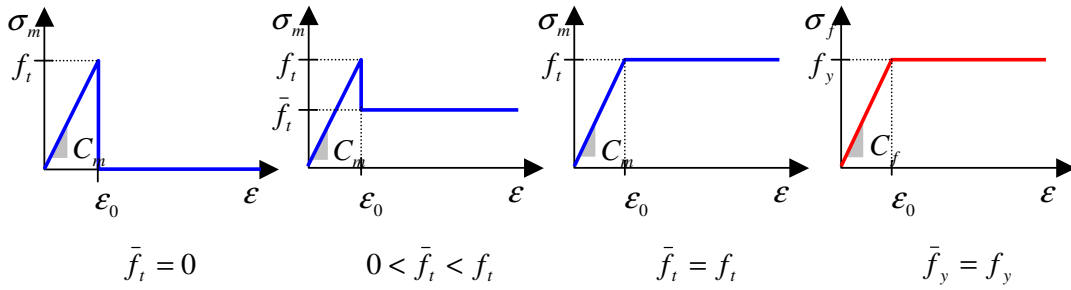


**Figure 3.5:** Mechanical device for fibre reinforced material considering elastic-brittle matrix and fibre reinforcement with hardening or softening behaviour

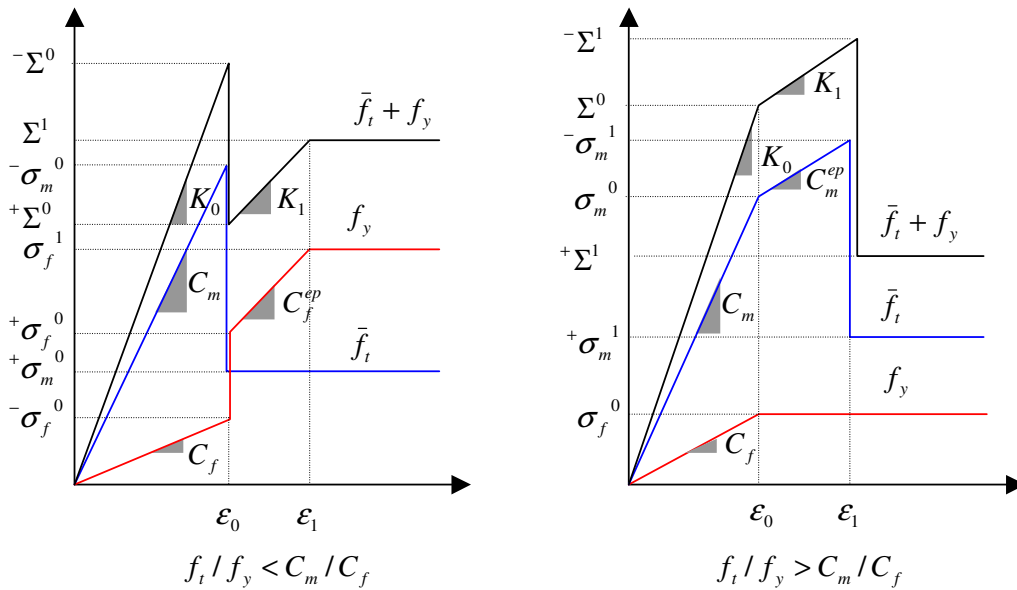




a) Mechanical models



b) Corresponding material laws for the constituents

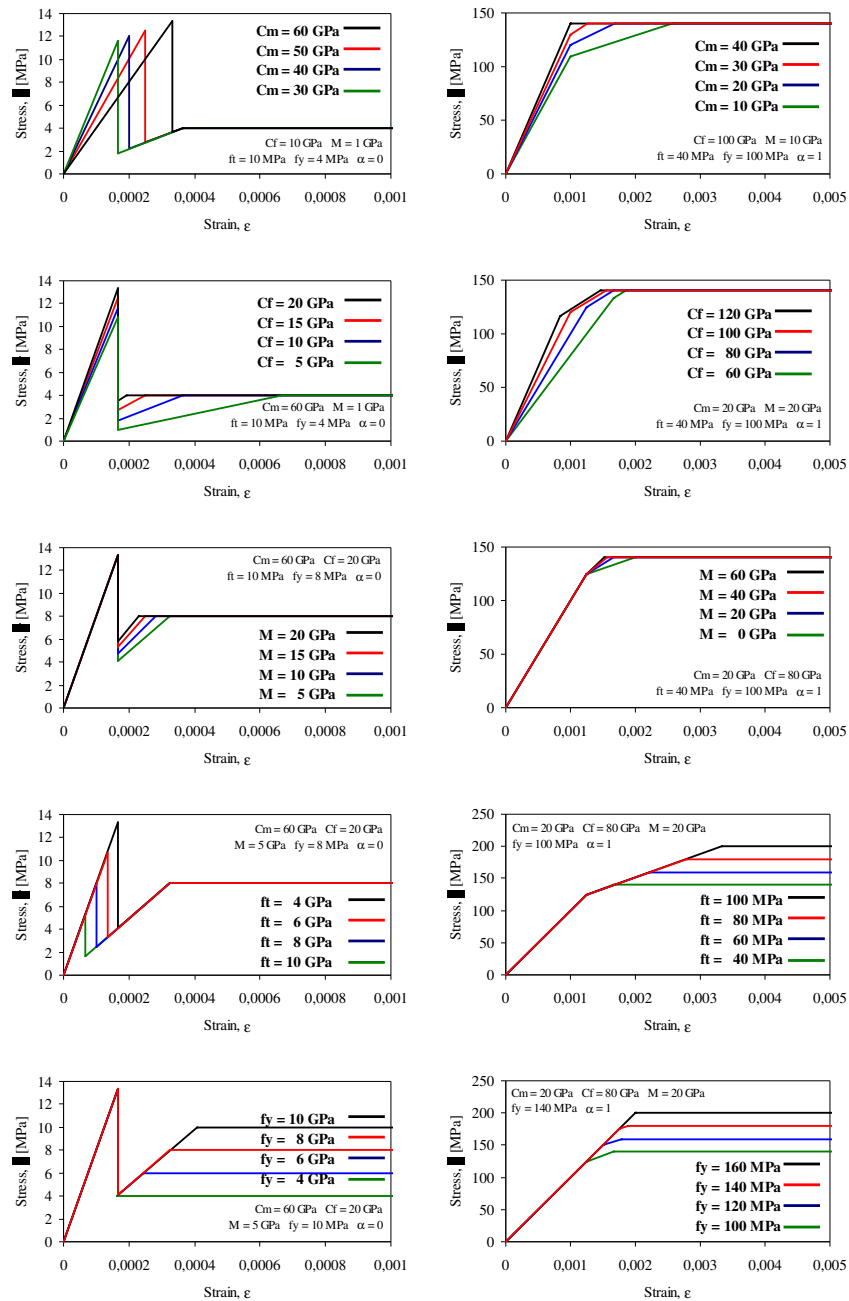


c) Stress-strain relationships for fibre reinforced material and for the constituents

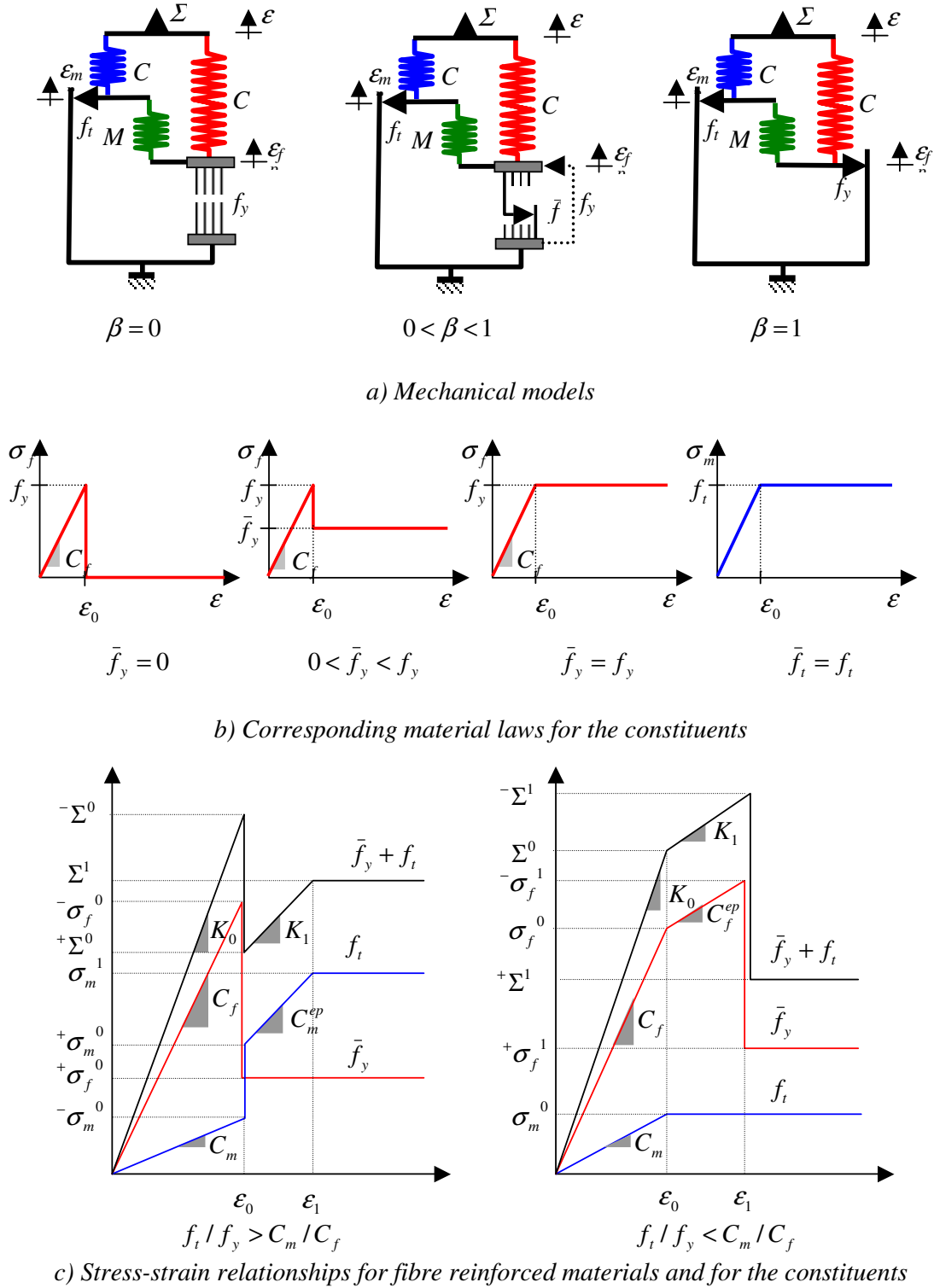
**Figure 3.6:** 1-D material model for fibre reinforced materials considering elastic-brittle matrix behaviour with residual strength ( $0 \leq \bar{f}_t \leq f_t$ ) and elastic-perfectly plastic fibre reinforcement behaviour

**Table 3.1:** 1-D material model for fibre reinforced materials considering elastic-brittle matrix with residual strength and elastic-perfectly plastic fibre reinforcement behaviour

<b>Matrix cracking prior to fibre reinforcement yielding</b>	
<b>Strains</b>	
$\varepsilon_0 = \frac{f_t}{C_m}$	$\varepsilon_1 = \frac{f_y}{C_f^{ep}} + f_t \frac{C_f^{ep} - C_f}{C_f^{ep} C_m} - (1-\alpha) f_t \frac{M}{C_f^{ep} (C_m + M)}$
<b>Matrix stresses</b>	
$^- \sigma_m^0 = f_t$	$\sigma_m^1 = \alpha f_t$
$^+ \sigma_m^0 = \alpha f_t$	
<b>Fibre reinforcement stresses</b>	
$^- \sigma_f^0 = \rho f_t$	$\sigma_f^1 = f_y$
$^+ \sigma_f^0 = f_t \left[ \rho + (1-\alpha) \frac{M}{C_m + M} \right]$	
<b>Fibre reinforced material stresses</b>	
$^- \Sigma^0 = f_t (1 + \rho)$	$\Sigma^1 = \alpha f_t + f_y$
$^+ \Sigma^0 = f_t \left[ 1 + \rho - (1-\alpha) \frac{C_m}{C_m + M} \right]$	
<b>Stiffness</b>	
$K_0 = C_m + C_f$	$K_1 = C_m + C_f - \frac{C_m^2}{C_m + M}$ , $C_f^{ep} = C_f + \frac{C_m M}{C_m + M}$ , $K_1 = C_f^{ep}$ $K_2 = 0$
<b>Fibre reinforcement yielding prior to matrix cracking</b>	
<b>Strains</b>	
$\varepsilon_0 = \frac{f_y}{C_f}$	$\varepsilon_1 = \frac{f_t}{C_m^{ep}} + f_y \frac{C_m^{ep} - C_m}{C_m^{ep} C_f}$
<b>Matrix stresses</b>	
$\sigma_m^0 = \kappa f_y$	$^- \sigma_m^1 = f_t$
	$^+ \sigma_m^1 = \alpha f_t$
<b>Fibre reinforcement stresses</b>	
$\sigma_f^0 = f_y$	$\sigma_f^1 = f_y$
<b>Fibre reinforced material stresses</b>	
$\Sigma^0 = f_y (1 + \kappa)$	$^- \Sigma^1 = f_t + f_y$
	$^+ \Sigma^1 = \alpha f_t + f_y$
<b>Stiffness</b>	
$K_0 = C_m + C_f$	$K_1 = C_m + C_f - \frac{C_f^2}{C_f + M}$ , $C_m^{ep} = C_m + \frac{C_f M}{C_f + M}$ , $K_1 = C_m^{ep}$ $K_2 = 0$
<b>Parameters and ratios</b>	
$C_m$ , $C_f$ , $M$ , $f_t$ , $f_y$ , $\bar{f}_t = \alpha f_t$ , $0 \leq \alpha \leq 1$ , $\rho = \frac{C_f}{C_m}$ , $\kappa = \frac{C_m}{C_f}$	



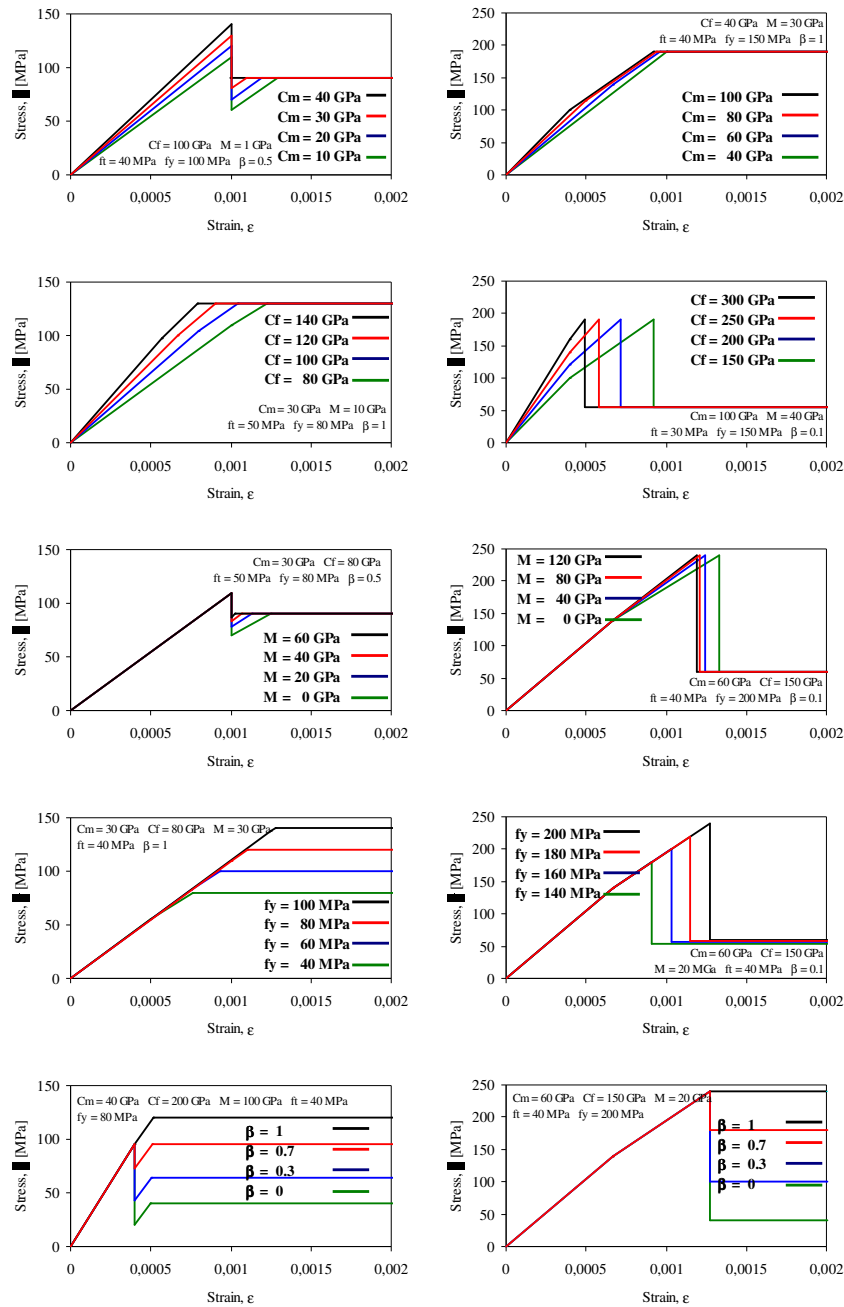
**Figure 3.7:** Effect of model parameters on the stress-strain relationships of fibre reinforced materials considering elastic-brittle matrix behaviour with residual strength ( $0 \leq \bar{f}_t \leq f_t$ ) and elastic-perfectly plastic fibre reinforcement behaviour. First column represents the cases of matrix cracking prior to fibre reinforcement yielding and second column represents the cases of fibre reinforcement yielding prior to matrix cracking.



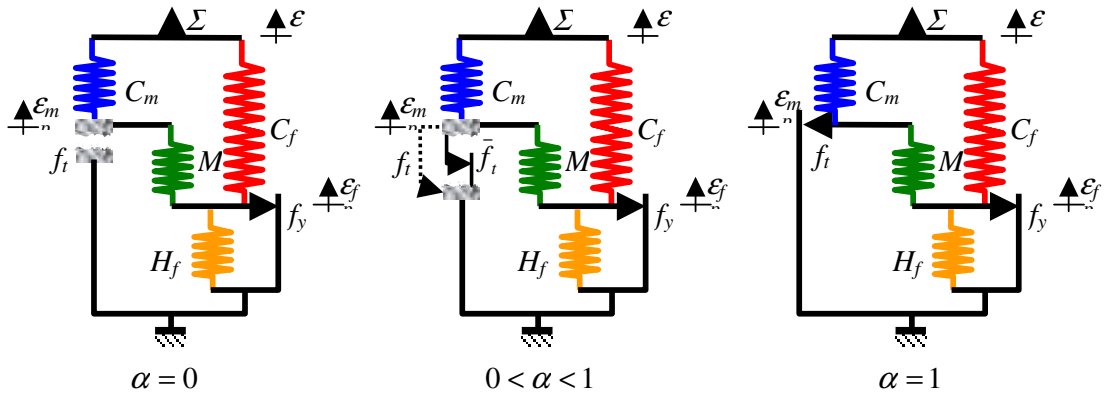
**Figure 3.8:** 1-D material model for fibre reinforced materials considering elastic-brittle fibre reinforcement behaviour with residual strength ( $0 \leq \bar{f}_y \leq f_y$ ) and elastic-perfectly plastic matrix behaviour

**Table 3.2:** 1-D material model for fibre reinforcement materials considering elastic-brittle fibre reinforcement with residual strength and elastic-perfectly plastic matrix behaviour

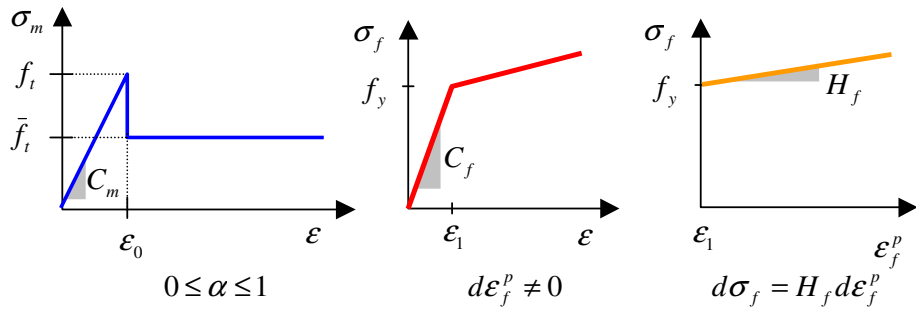
<b>Fibre reinforcement fracture prior to matrix yielding</b>	
<b>Strains</b>	
$\varepsilon_0 = \frac{f_y}{C_f}$	$\varepsilon_1 = \frac{f_t}{C_m^{ep}} + f_y \frac{C_m^{ep} - C_m}{C_m^{ep} C_f} - (1 - \beta) f_y \frac{M}{C_m^{ep} (C_f + M)}$
<b>Matrix stresses</b>	
$\bar{\sigma}_m^0 = \kappa f_y$	$\sigma_m^1 = f_t$
$^+ \sigma_m^0 = f_y \left[ \kappa + (1 - \beta) \frac{M}{C_f + M} \right]$	
<b>Fibre reinforcement stresses</b>	
$\bar{\sigma}_f^0 = f_y$	$\sigma_f^1 = \beta f_y$
$^+ \sigma_f^0 = \beta f_y$	
<b>Fibre reinforced material stresses</b>	
$\bar{\Sigma}^0 = f_y (1 + \kappa)$	$\Sigma^1 = f_t + \beta f_y$
$^+ \Sigma^0 = f_y \left[ 1 + \kappa - (1 - \beta) \frac{C_f}{C_f + M} \right]$	
<b>Stiffness</b>	
$K_0 = C_m + C_f$	$K_1 = C_m + C_f - \frac{C_f^2}{C_f + M}$ , $C_m^{ep} = C_m + \frac{C_f M}{C_f + M}$ , $K_1 = C_m^{ep}$
	$K_2 = 0$
<b>Matrix yielding prior to fibre reinforcement fracture</b>	
<b>Strains</b>	
$\varepsilon_0 = \frac{f_t}{C_m}$	$\varepsilon_1 = \frac{f_y}{C_f^{ep}} + f_t \frac{C_f^{ep} - C_f}{C_f^{ep} C_m}$
<b>Matrix stresses</b>	
$\sigma_m^0 = f_t$	$\sigma_m^1 = f_t$
<b>Fibre reinforcement stresses</b>	
$\sigma_f^0 = \rho f_t$	$\bar{\sigma}_f^1 = f_y$
	$^+ \sigma_f^1 = \beta f_y$
<b>Fibre reinforced material stresses</b>	
$\Sigma^0 = f_t (1 + \rho)$	$\bar{\Sigma}^1 = f_t + f_y$
	$^+ \Sigma^1 = f_t + \beta f_y$
<b>Stiffness</b>	
$K_0 = C_m + C_f$	$K_1 = C_m + C_f - \frac{C_m^2}{C_m + M}$ , $C_f^{ep} = C_f + \frac{C_m M}{C_m + M}$ , $K_1 = C_f^{ep}$
	$K_2 = 0$
<b>Parameters and ratios</b>	
$C_m$ , $C_f$ , $M$ , $f_t$ , $f_y$ , $\bar{f}_y = \beta f_y$ , $0 \leq \beta \leq 1$ , $\kappa = \frac{C_m}{C_f}$ , $\rho = \frac{C_f}{C_m}$	



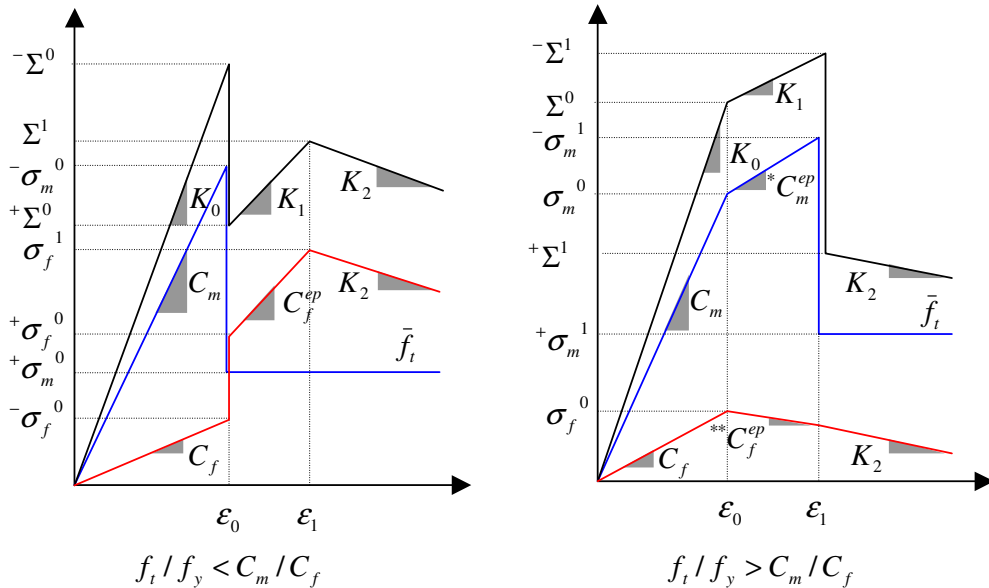
**Figure 3.9:** Effect of model parameters on the stress-strain relationships of fibre reinforced materials considering elastic-brittle fibre reinforcement behaviour with residual strength ( $0 \leq \bar{f}_y \leq f_y$ ) and elastic-perfectly plastic matrix behaviour. First column represents the cases of fibre reinforcement fracture prior to matrix yielding and second column represents the cases of matrix yielding prior to fibre reinforcement fracture.



a) Mechanical models



b) Corresponding material laws for the constituents



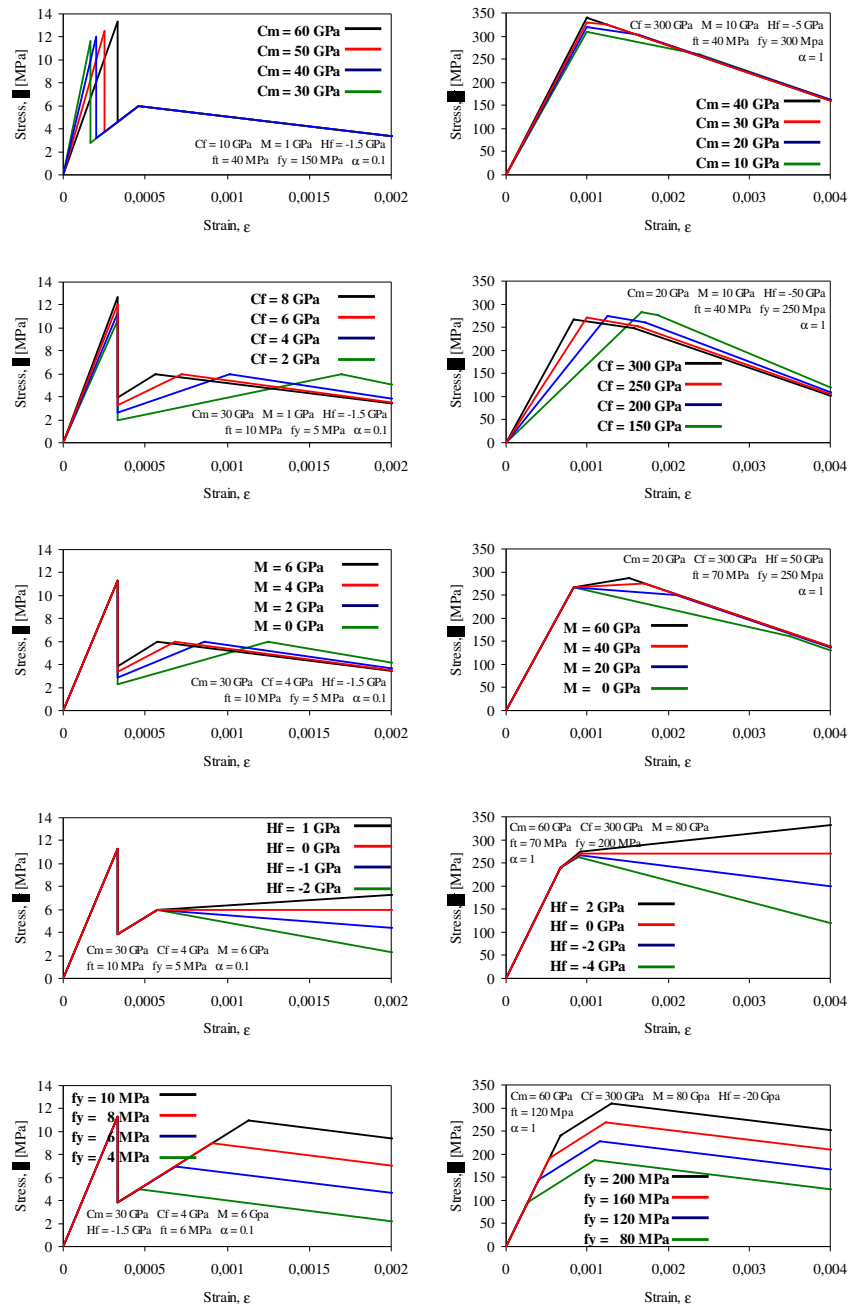
c) Stress-strain relationships fibre reinforced material and for the constituents

**Figure 3.10:** 1-D material model for fibre reinforced materials considering elastic-brittle matrix behaviour with residual strength ( $0 \leq \bar{f}_t \leq f_t$ ) and elastic-perfectly plastic fibre reinforcement behaviour with hardening or softening

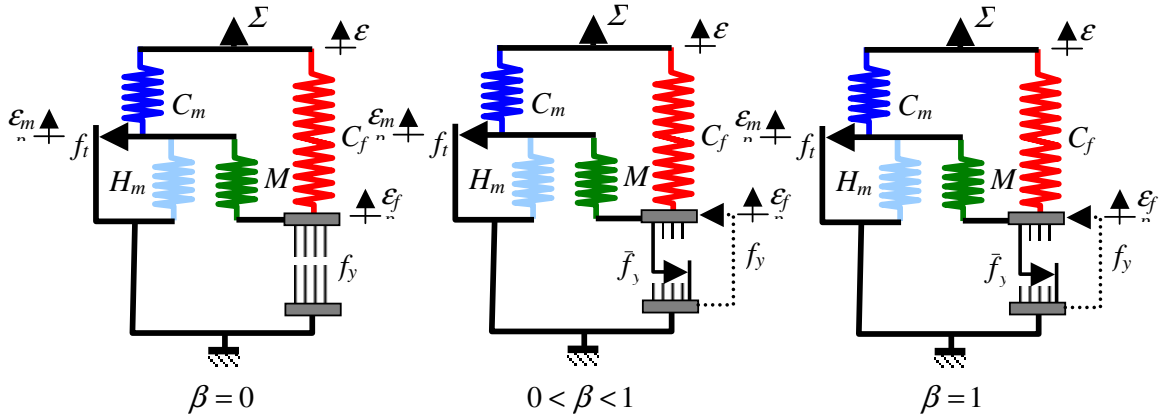
**Table 3.3:** 1-D material model for fibre reinforced materials considering elastic-plastic fibre reinforcement with softening-hardening and elastic-brittle matrix behaviour with residual strength

<b>Matrix cracking prior to fibre reinforcement yielding</b>	
<b>Strains</b>	
$\varepsilon_0 = \frac{f_t}{C_m}$	$\varepsilon_1 = \frac{f_y}{C_f^{ep}} + f_t \frac{C_f^{ep} - C_f}{C_f^{ep} C_m} - (1-\alpha) f_t \frac{M}{C_f^{ep} (C_m + M)}$
<b>Matrix stresses</b>	
$^- \sigma_m^0 = f_t$	$\sigma_m^1 = \alpha f_t$
$^+ \sigma_m^0 = \alpha f_t$	
<b>Fibre reinforcement stresses</b>	
$^- \sigma_f^0 = \rho f_t$	$\sigma_f^1 = f_y$
$^+ \sigma_f^0 = f_t \left[ \rho + (1-\alpha) \frac{M}{C_m + M} \right]$	
<b>Fibre reinforcement stresses</b>	
$^- \Sigma^0 = f_t (1 + \rho)$	$\Sigma^1 = f_y + \alpha f_t$
$^+ \Sigma^0 = f_t \left[ 1 + \rho - (1-\alpha) \frac{C_m}{C_m + M} \right]$	
<b>Stiffness</b>	
$K_0 = C_m + C_f$	$K_1 = C_m + C_f - \frac{C_m^2}{C_m + M}$ , $C_f^{ep} = C_f + \frac{C_m M}{C_m + M}$ , $K_1 = C_f^{ep}$
	$K_2 = \frac{C_f^{ep} H_f}{C_f^{ep} + H_f}$
<b>Fibre reinforcement yielding prior to matrix cracking</b>	
<b>Strains</b>	
$\varepsilon_0 = \frac{f_y}{C_f}$	$\varepsilon_1 = \frac{f_t}{^* C_m^{ep}} + f_y \frac{^* C_m^{ep} - C_m}{^* C_m^{ep} C_f}$
<b>Matrix stresses</b>	
$\sigma_m^0 = \kappa f_y$	$^- \sigma_m^1 = f_t$
	$^+ \sigma_m^1 = \alpha f_t$
<b>Fibre reinforcement stresses</b>	
$\sigma_f^0 = f_y$	$^- \sigma_f^1 = f_y + \frac{^{**} C_f^{ep}}{^* C_m^{ep}} (f_t - \kappa f_y)$
	$^+ \sigma_f^1 = f_y + \frac{^{**} C_f^{ep}}{^* C_m^{ep}} (f_t - \kappa f_y)$
<b>Fibre reinforced material stresses</b>	
$\Sigma^0 = f_y (1 + \kappa)$	$^- \Sigma^1 = f_t + f_y + \frac{^{**} C_f^{ep}}{^* C_m^{ep}} (f_t - \kappa f_y)$
	$^+ \Sigma^1 = \alpha f_t + f_y + \frac{^{**} C_f^{ep}}{^* C_m^{ep}} (f_t - \kappa f_y)$
<b>Stiffness</b>	
$K_0 = C_m + C_f$	$K_1 = ^* C_m^{ep} + ^{**} C_f^{ep}$ , $^* C_m^{ep} = C_m + \frac{C_f M}{C_f + H_f + M}$ , $^{**} C_f^{ep} = \frac{C_f H_f}{C_f + M + H_f}$
	$K_2 = \frac{C_f^{ep} H_f}{C_f^{ep} + H_f}$
	$C_f^{ep} = C_f + \frac{C_m M}{C_m + M}$
<b>Parameters and ratios</b>	
$C_m$ , $C_f$ , $M$ , $H_f$ , $f_t$ , $f_y$ , $\bar{f}_t = \alpha f_t$ , $0 \leq \alpha \leq 1$ , $\kappa = \frac{C_m}{C_f}$ , $\rho = \frac{C_f}{C_m}$	

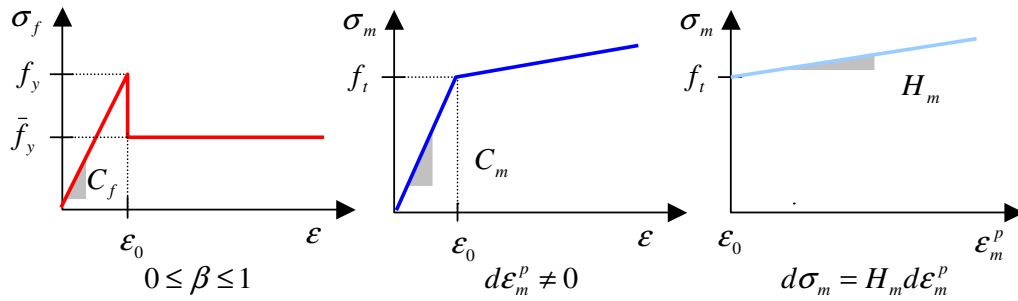




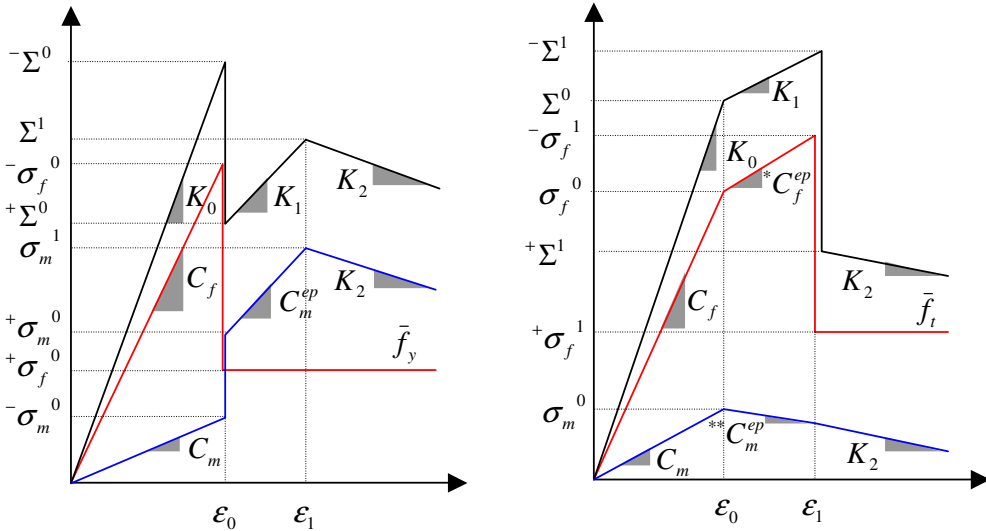
**Figure 3.11:** Effect of model parameters on the stress-strain relationships of fibre reinforced materials considering elastic-brittle matrix behaviour with residual strength ( $0 \leq \bar{f}_t \leq f_t$ ) and elastic-plastic fibre reinforcement behaviour with hardening or softening. First column represents the cases of matrix cracking prior to fibre reinforcement yielding and second column represents the cases of fibre reinforcement yielding prior to matrix cracking.



a) Mechanical models



b) Corresponding material laws for the constituents

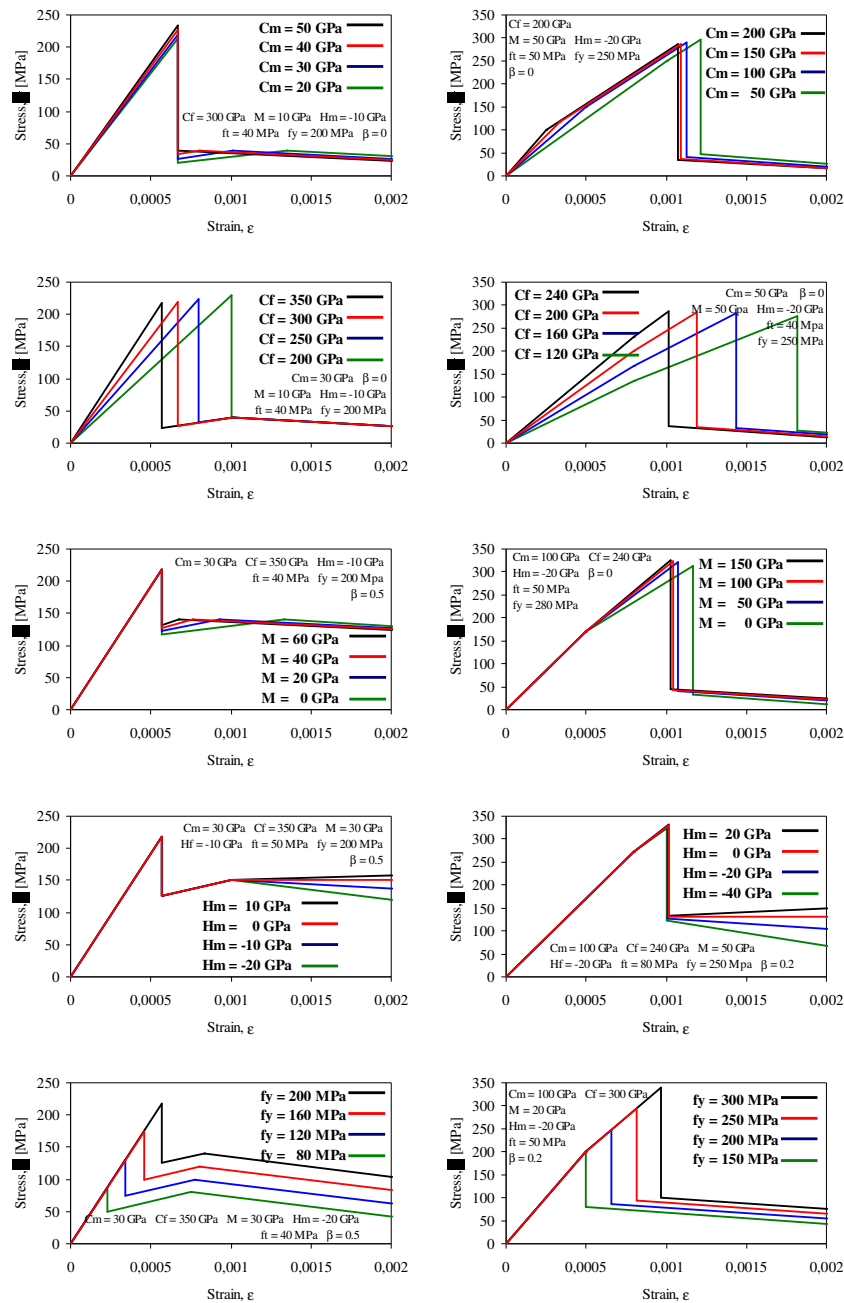


c) Stress-strain relationships for fibre reinforced material and for the constituents

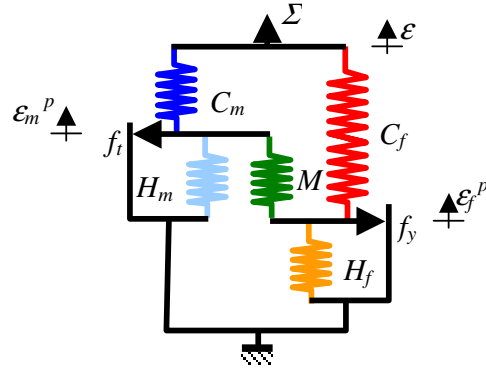
**Figure 3.12:** 1-D material model for fibre reinforced materials considering elastic-brittle fibre reinforcement behaviour with residual strength ( $0 \leq \bar{f}_y \leq f_y$ ) and elastic-perfectly plastic matrix behaviour with hardening or softening

**Table 3.4:** 1-D material model for fibre reinforced materials considering elastic-plastic matrix with softening or hardening and elastic-brittle fibre reinforcement behaviour with residual strength, fibre reinforcement fracture prior to matrix yielding

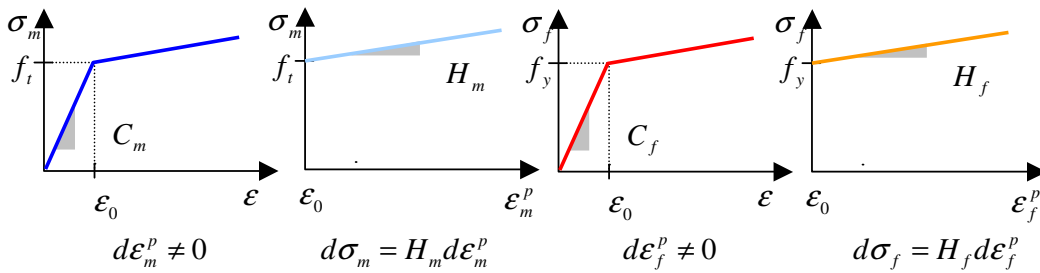
<b>Fibre reinforcement fracture prior to matrix yielding</b>	
<b>Strains</b>	
$\varepsilon_0 = \frac{f_y}{C_f}$	$\varepsilon_1 = \frac{f_t}{C_m^{ep}} + f_y \frac{C_m^{ep} - C_m}{C_m^{ep} C_f} - (1 - \beta) f_y \frac{M}{C_m^{ep} (C_f + M)}$
<b>Matrix stresses</b>	
$^- \sigma_m^0 = \kappa f_y$	$\sigma_m^1 = f_t$
$^+ \sigma_m^0 = f_y \left( \kappa + (1 - \beta) \frac{M}{C_f + M} \right)$	
<b>Fibre reinforcement stresses</b>	
$^- \sigma_f^0 = f_y$	$\sigma_f^1 = \beta f_y$
$^+ \sigma_f^0 = \beta f_y$	
<b>Fibre reinforced material stresses</b>	
$^- \Sigma^0 = f_y (1 + \kappa)$	$\Sigma^1 = f_t + \beta f_y$
$^+ \Sigma^0 = f_y \left( 1 + \kappa - (1 - \beta) \frac{C_f}{C_f + M} \right)$	
<b>Stiffness</b>	
$K_0 = C_m + C_f$	$K_1 = C_m + C_f - \frac{C_f^2}{C_f + M}$ , $C_m^{ep} = C_m + \frac{C_f M}{C_f + M}$ , $K_1 = C_m^{ep}$
	$K_2 = \frac{C_m^{ep} H_m}{C_m^{ep} + H_m}$
<b>Matrix yielding prior to fibre reinforcement yielding</b>	
<b>Strains</b>	
$\varepsilon_0 = \frac{f_t}{C_m}$	$\varepsilon_1 = \frac{f_y}{^* C_f^{ep}} + f_t \frac{^* C_f^{ep} - C_f}{^* C_f^{ep} C_m}$
<b>Matrix stresses</b>	
$\sigma_m^0 = f_t$	$^- \sigma_m^1 = f_t + \frac{^{**} C_m^{ep}}{^* C_f^{ep}} (f_y - \rho f_t)$
	$^+ \sigma_m^1 = f_t + \frac{^{**} C_m^{ep}}{^* C_f^{ep}} (f_y - \rho f_t)$
<b>Fibre reinforcement stresses</b>	
$\sigma_f^0 = \rho f_t$	$^- \sigma_f^1 = f_y$
	$^+ \sigma_f^1 = \beta f_y$
<b>Fibre reinforced material stresses</b>	
$\Sigma^0 = f_t (1 + \rho)$	$^- \Sigma^1 = f_t + f_y + \frac{^{**} C_m^{ep}}{^* C_f^{ep}} (f_y - \rho f_t)$
	$^+ \Sigma^1 = f_t + \beta f_y + \frac{^{**} C_m^{ep}}{^* C_f^{ep}} (f_y - \rho f_t)$
<b>Stiffness</b>	
$K_0 = C_m + C_f$	$K_1 = \frac{^{**} C_m^{ep} + ^* C_f^{ep}}{C_m + H_m + M}$ , $^* C_f^{ep} = C_f + \frac{C_m M}{C_m + H_m + M}$
	$K_2 = \frac{C_m^{ep} H_m}{C_m^{ep} + H_m}$
	$C_m^{ep} = C_m + \frac{C_f M}{C_f + M}$
<b>Parameters and ratios</b>	
$C_m$ , $C_f$ , $M$ , $H_m$ , $f_t$ , $f_y$ , $\bar{f}_y = \beta f_y$ , $0 \leq \beta \leq 1$ , $\rho = \frac{C_f}{C_m}$ , $\kappa = \frac{C_m}{C_f}$	



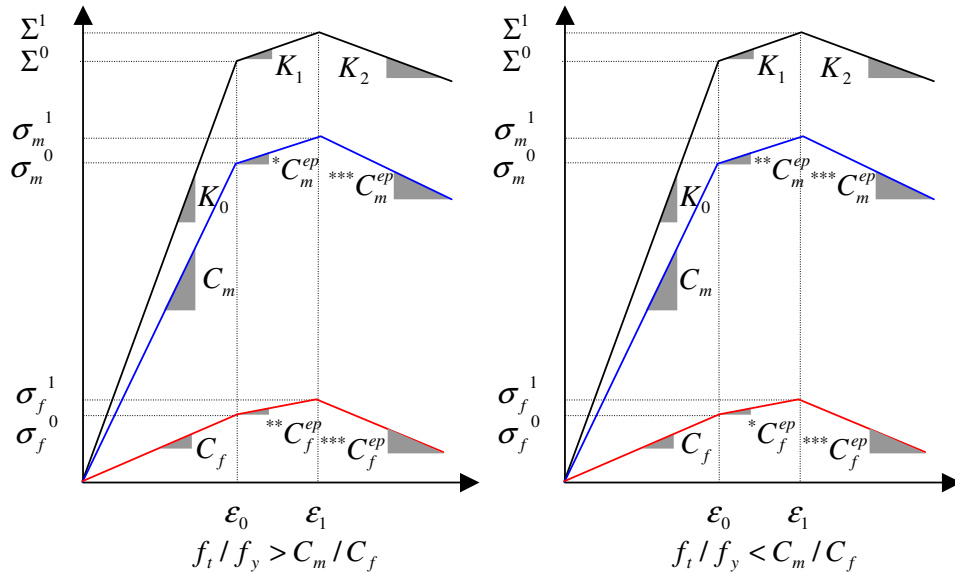
**Figure 3.13:** Effect of model parameters on the stress-strain relationships of fibre reinforced materials considering elastic-brittle fibre reinforcement behaviour with residual strength ( $0 \leq \bar{f}_t \leq f_t$ ) and elastic-plastic matrix behaviour with hardening or softening. First column represents the cases of fibre reinforcement fracture prior to matrix yielding and second column represents the cases of matrix yielding prior to fibre reinforcement fracture.



a) Mechanical model



b) Material laws for the constituents

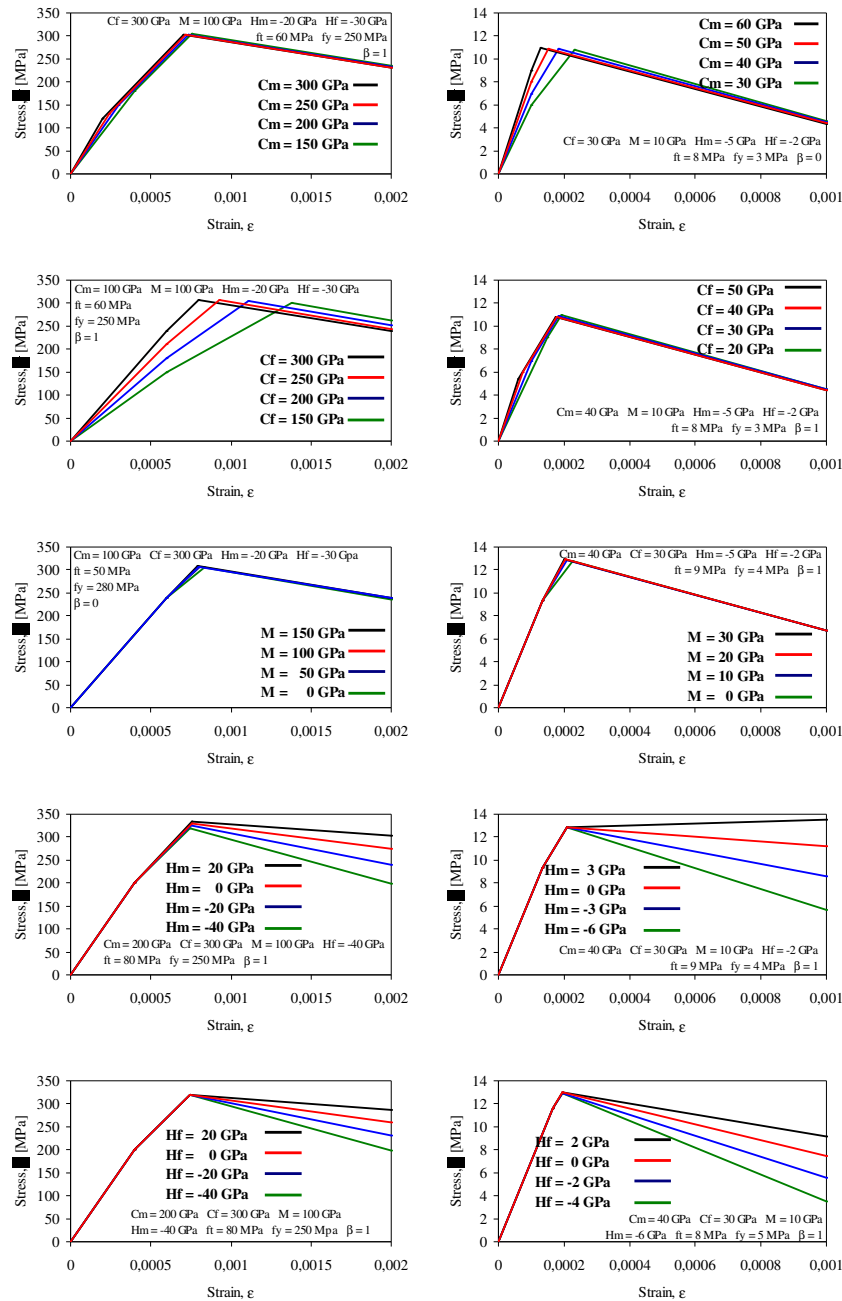


c) Stress-strain relationships for fibre reinforced material and for the constituents

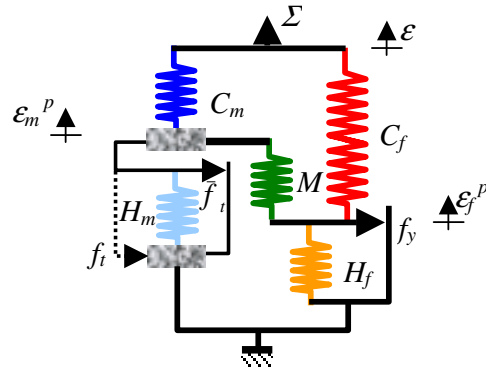
**Figure 3.14:** 1-D material model for fibre reinforced materials considering elastic-plastic matrix and fibre reinforcement behaviour with hardening or softening

**Table 3.5:** 1-D material model for fibre reinforced materials considering elastic-plastic matrix and fibre reinforcement behaviour with softening or hardening

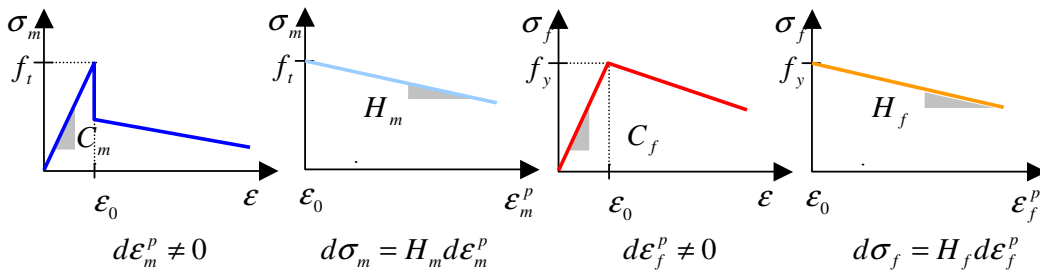
<b>Fibre reinforcement yielding prior to matrix yielding</b>	
<b>Strains</b>	
$\varepsilon_0 = \frac{f_y}{C_f}$	$\varepsilon_1 = \frac{f_t}{^*C_m^{ep}} + f_y \frac{^*C_m^{ep} - C_m}{^*C_m^{ep} C_f}$
<b>Matrix stresses</b>	
$\sigma_m^0 = \kappa f_y$	$\sigma_m^1 = f_t$
<b>Fibre reinforcement stresses</b>	
$\sigma_f^0 = f_y$	$\sigma_f^1 = f_y + \frac{^{**}C_f^{ep}}{^*C_m^{ep}} (f_t + \kappa f_y)$
<b>Fibre reinforced material stresses</b>	
$\Sigma^0 = f_y(1 + \kappa)$	$\Sigma^1 = f_t + f_y + \frac{^{**}C_f^{ep}}{^*C_m^{ep}} (f_t + \kappa f_y)$
<b>Stiffness</b>	
$K_1 = ^*C_m^{ep} + ^{**}C_f^{ep}$	$K_2 = ^{***}C_m^{ep} + ^{***}C_f^{ep}$
$^*C_m^{ep} = C_m + \frac{C_f M}{C_f + H_f + M}$	$^{***}C_m^{ep} = H_m \frac{C_m(C_f + H_f + M) + C_f M}{(C_m + H_m + M)(C_f + H_f + M) - M^2}$
$^{**}C_f^{ep} = \frac{C_f H_f}{C_f + H_f + M}$	$^{***}C_f^{ep} = H_f \frac{C_f(C_m + H_m + M) + C_m M}{(C_m + H_m + M)(C_f + H_f + M) - M^2}$
<b>Matrix yielding prior to fibre reinforcement yielding</b>	
<b>Strains</b>	
$\varepsilon_0 = \frac{f_t}{C_m}$	$\varepsilon_1 = \frac{f_y}{^*C_f^{ep}} + f_t \frac{^*C_f^{ep} - C_f}{^*C_f^{ep} C_m}$
<b>Matrix stresses</b>	
$\sigma_m^0 = f_t$	$\sigma_m^1 = f_t + \frac{^{**}C_m^{ep}}{^*C_f^{ep}} (f_y + \rho f_t)$
<b>Fibre reinforcement stresses</b>	
$\sigma_f^0 = \rho f_t$	$\sigma_f^1 = f_y$
<b>Fibre reinforced material stresses</b>	
$\Sigma^0 = f_t(1 + \rho)$	$\Sigma^1 = f_t + f_y + \frac{^{**}C_m^{ep}}{^*C_f^{ep}} (f_y + \rho f_t)$
<b>Stiffness</b>	
$K_1 = ^{**}C_m^{ep} + ^*C_f^{ep}$	$K_2 = ^{***}C_m^{ep} + ^{***}C_f^{ep}$
$^*C_f^{ep} = C_f + \frac{C_m M}{C_m + H_m + M}$	$^{***}C_m^{ep} = H_m \frac{C_m(C_f + H_f + M) + C_f M}{(C_m + H_m + M)(C_f + H_f + M) - M^2}$
$^{**}C_m^{ep} = \frac{C_m H_m}{C_m + H_m + M}$	$^{***}C_f^{ep} = H_f \frac{C_f(C_m + H_m + M) + C_m M}{(C_m + H_m + M)(C_f + H_f + M) - M^2}$
<b>Parameters and ratios</b>	
$C_m, C_f, M, H_m, H_f, f_t, f_y, \kappa = \frac{C_m}{C_f}$	



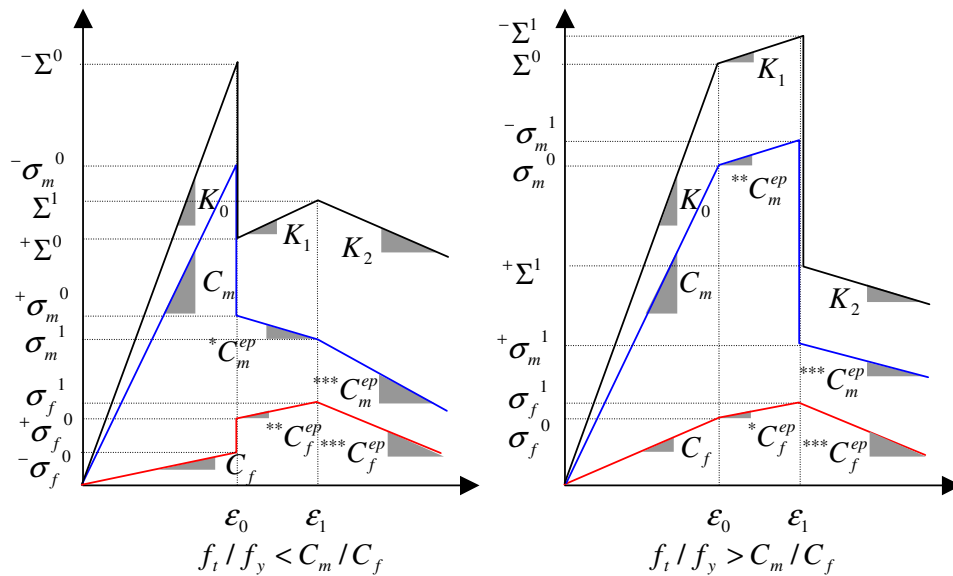
**Figure 3.15:** Effect of model parameters on the stress-strain relationships of fibre reinforced materials considering elastic-plastic fibre reinforcement and matrix behaviour with hardening or softening. First column represents the cases of fibre reinforcement yielding prior to matrix yielding and second column represents the cases of matrix yielding prior to fibre reinforcement yielding.



a) Mechanical model



b) Material laws for the constituents



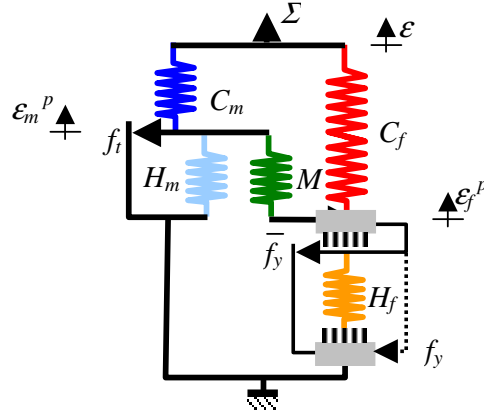
c) Stress-strain relationships for composite and for composite constituents

**Figure 3.16:** 1-D material model for fibre reinforced materials considering elastic-brittle matrix behaviour with residual strength and hardening or softening and elastic-plastic fibre reinforcement behaviour with hardening or softening

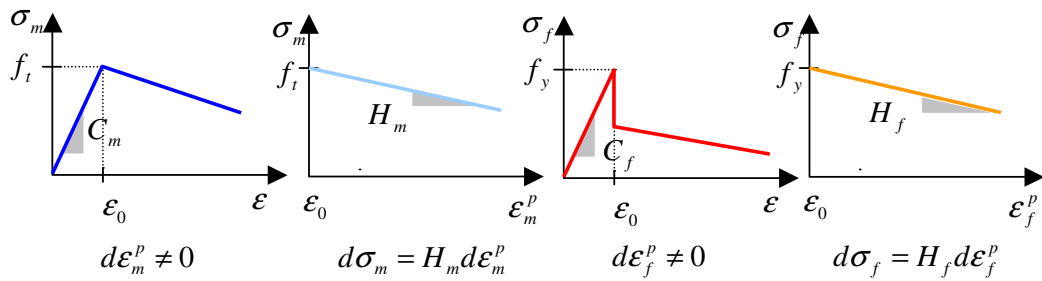


**Table 3.6:** 1-D material model for fibre reinforced materials considering elastic-brittle matrix behaviour with residual strength and hardening or softening and elastic-plastic fibre reinforcement behaviour with hardening or softening

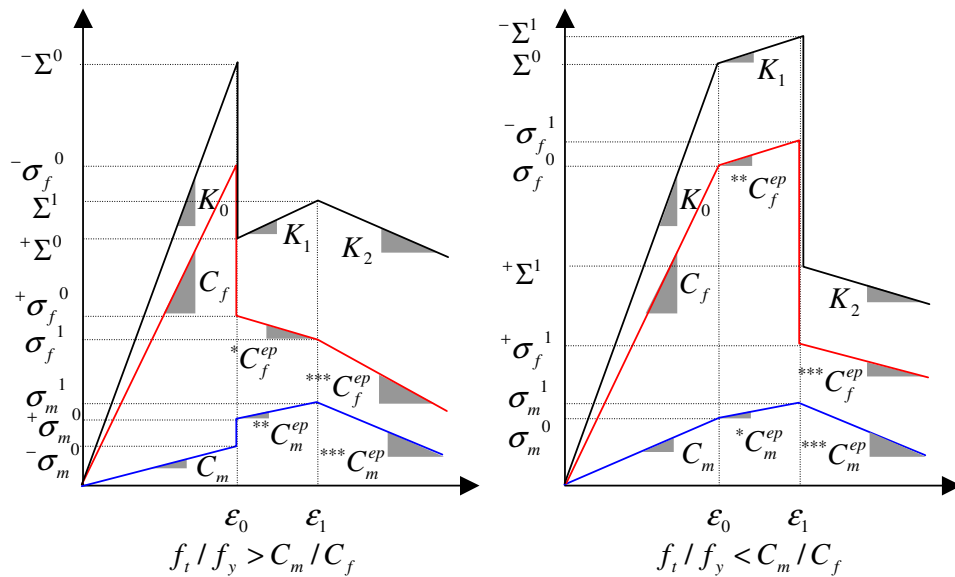
Matrix cracking prior to fibre reinforcement yielding	
<b>Strains</b>	
$\varepsilon_0 = \frac{f_t}{C_m}$	$\varepsilon_1 = \frac{f_y}{{}^*C_f^{ep}} + f_t \frac{{}^*C_f^{ep} - C_f}{{}^*C_f^{ep} C_m} - (1-\alpha) f_t \frac{M}{{}^*C_f^{ep} (C_m + M)}$
<b>Matrix stresses</b>	
${}^- \sigma_m^0 = f_t$	
${}^+ \sigma_m^0 = \alpha f_t$	
<b>Fibre reinforcement stresses</b>	
${}^- \sigma_f^0 = \rho f_t$	
${}^+ \sigma_f^0 = f_t \left[ \rho + (1-\alpha) \frac{M}{C_m + M} \right]$	$\sigma_f^1 = f_y$
<b>Fibre reinforced material stresses</b>	
${}^- \Sigma^0 = f_t (1 + \rho)$	
${}^+ \Sigma^0 = f_t \left[ 1 + \rho - (1-\alpha) \frac{C_m}{C_m + M} \right]$	$\Sigma^1 = \bar{f}_t + f_y + \frac{{}^{**}C_m^{ep}}{{}^*C_f^{ep}} \left( f_y - \rho f_t + (1-\alpha) f_t \frac{M}{C_m + M} \right)$
<b>Stiffness</b>	
$K_1 = {}^{**}C_m^{ep} + {}^*C_f^{ep}$	$K_2 = {}^{***}C_m^{ep} + {}^{***}C_f^{ep}$
${}^*C_f^{ep} = C_f + \frac{C_m M}{C_m + H_m + M}$	${}^{***}C_m^{ep} = H_m \frac{C_m (C_f + H_f + M) + C_f M}{(C_m + H_m + M)(C_f + H_f + M) - M^2}$
${}^{**}C_m^{ep} = \frac{C_m H_m}{C_m + H_m + M}$	${}^{***}C_f^{ep} = H_f \frac{C_f (C_m + H_m + M) + C_m M}{(C_m + H_m + M)(C_f + H_f + M) - M^2}$
Fibre reinforcement yielding prior to matrix cracking	
<b>Strains</b>	
$\varepsilon_0 = \frac{f_y}{C_f}$	$\varepsilon_1 = \frac{f_t}{{}^*C_m^{ep}} + f_y \frac{{}^*C_m^{ep} - C_m}{{}^*C_m^{ep} C_f}$
<b>Matrix stresses</b>	
$\sigma_m^0 = \kappa f_y$	${}^- \sigma_m^1 = f_t$
	${}^+ \sigma_m^1 = \alpha f_t$
<b>Fibre reinforcement stresses</b>	
$\sigma_f^0 = f_y$	$\sigma_f^1 = f_y + \frac{{}^{**}C_f^{ep}}{{}^*C_m^{ep}} (f_t + \kappa f_y)$
<b>Fibre reinforced material stresses</b>	
$\Sigma^0 = f_y (1 + \kappa)$	${}^- \Sigma^1 = f_t + f_y + \frac{{}^{**}C_f^{ep}}{{}^*C_m^{ep}} (f_t + \kappa f_y)$
	${}^+ \Sigma^1 = \bar{f}_t + f_y + \frac{{}^{**}C_f^{ep}}{{}^*C_m^{ep}} (f_t + \kappa f_y)$
<b>Stiffness</b>	
$K_1 = {}^*C_m^{ep} + {}^{**}C_f^{ep}$	$K_2 = {}^{***}C_m^{ep} + {}^{***}C_f^{ep}$
${}^*C_m^{ep} = C_m + \frac{C_f M}{C_f + H_f + M}$	${}^{***}C_m^{ep} = H_m \frac{C_m (C_f + H_f + M) + C_f M}{(C_m + H_m + M)(C_f + H_f + M) - M^2}$
${}^{**}C_f^{ep} = \frac{C_f H_f}{C_f + H_f + M}$	${}^{***}C_f^{ep} = H_f \frac{C_f (C_m + H_m + M) + C_m M}{(C_m + H_m + M)(C_f + H_f + M) - M^2}$
<b>Parameters and ratios</b>	
$C_m$ , $C_f$ , $M$ , $H_m$ , $H_f$ , $f_t$ , $f_y$ , $\kappa = \frac{C_m}{C_f}$	



a) Mechanical model



b) Material laws for the constituents



c) Stress-strain relationships for fibre reinforced material and for the constituents

**Figure 3.17:** 1-D material model for fibre reinforced materials considering elastic-plastic matrix behaviour with hardening or softening and elastic-brittle fibre reinforcement behaviour with residual strength and hardening or softening

**Table 3.7:** 1-D material model for fibre reinforced materials considering elastic-plastic matrix behaviour with hardening or softening and elastic-brittle fibre reinforcement behaviour with residual strength and hardening or softening

<b>Fibre reinforcement fracture prior to matrix yielding</b>	
<b>Strains</b>	
$\varepsilon_0 = \frac{f_y}{C_f}$	$\varepsilon_1 = \frac{f_t}{*C_m^{ep}} + f_y \frac{*C_m^{ep} - C_m}{*C_m^{ep} C_f} - (1 - \beta) f_y \frac{M}{*C_m^{ep} (C_f + M)}$
<b>Matrix stresses</b>	
$\bar{\sigma}_m^0 = \kappa f_y$	$\sigma_m^1 = f_t$
$+\sigma_m^0 = \left( C_m + \frac{C_f M}{C_f + M} \right) \varepsilon_0 - \frac{\bar{f}_y M}{C_f + M} = f_y \left( \kappa + (1 - \beta) \frac{M}{C_f + M} \right)$	
<b>Fibre reinforcement stresses</b>	
$\bar{\sigma}_f^0 = f_y$	$+\sigma_f^0 = \bar{f}_y = \beta f_y$
	$\sigma_f^1 = \bar{f}_y + \frac{*C_f^{ep}}{*C_m^{ep}} \left( f_t - \kappa f_y + (1 - \beta) f_y \frac{M}{(C_f + M)} \right)$
<b>Fibre reinforced material stresses</b>	
$\bar{\Sigma}^0 = f_y (1 + \kappa)$	$+\Sigma^0 = f_y \left( 1 + \kappa - (1 - \beta) \frac{C_f}{C_f + M} \right)$
	$\Sigma^1 = \bar{f}_y + f_t + \frac{*C_f^{ep}}{*C_m^{ep}} \left( f_t - \kappa f_y + (1 - \beta) f_y \frac{M}{C_f + M} \right)$
<b>Stiffness</b>	
$K_1 = *C_m^{ep} + **C_f^{ep}$	$K_2 = ***C_m^{ep} + ****C_f^{ep}$
$*C_m^{ep} = C_m + \frac{C_f M}{C_f + H_f + M}$	$***C_m^{ep} = H_m \frac{C_m (C_f + H_f + M) + C_f M}{(C_m + H_m + M)(C_f + H_f + M) - M^2}$
$**C_f^{ep} = \frac{C_f H_f}{C_f + H_f + M}$	$****C_f^{ep} = H_f \frac{C_f (C_m + H_m + M) + C_m M}{(C_m + H_m + M)(C_f + H_f + M) - M^2}$
<b>Matrix yielding prior to fibre reinforcement fracture</b>	
<b>Strains</b>	
$\varepsilon_0 = \frac{f_t}{C_m}$	$\varepsilon_1 = \frac{f_y}{*C_f^{ep}} + f_t \frac{*C_f^{ep} - C_f}{*C_f^{ep} C_m}$
<b>Matrix stresses</b>	
$\sigma_m^0 = f_t$	$\sigma_m^1 = f_t + \frac{*C_m^{ep}}{*C_f^{ep}} (f_y - \rho f_t)$
<b>Fibre reinforcement stresses</b>	
$\sigma_f^0 = \rho f_t$	$\bar{\sigma}_f^1 = f_y$
	$+\sigma_f^1 = \bar{f}_y$
<b>Fibre reinforced material stresses</b>	
$\Sigma^0 = f_t (1 + \rho)$	$\bar{\Sigma}^1 = f_t + f_y + \frac{*C_m^{ep}}{*C_f^{ep}} (f_y - \rho f_t)$
	$+\Sigma^1 = f_t + \bar{f}_y + \frac{*C_m^{ep}}{*C_f^{ep}} (f_y - \rho f_t)$
<b>Stiffness</b>	
$K_1 = **C_m^{ep} + *C_f^{ep}$	$K_2 = ***C_m^{ep} + ****C_f^{ep}$
$*C_f^{ep} = C_f + \frac{C_m M}{C_m + H_m + M}$	$***C_m^{ep} = H_m \frac{C_m (C_f + H_f + M) + C_f M}{(C_m + H_m + M)(C_f + H_f + M) - M^2}$
$**C_m^{ep} = \frac{C_m H_m}{C_m + H_m + M}$	$****C_f^{ep} = H_f \frac{C_f (C_m + H_m + M) + C_m M}{(C_m + H_m + M)(C_f + H_f + M) - M^2}$
<b>Parameters and ratios</b>	
$C_m, C_f, M, H_m, H_f, f_t, f_y, \kappa = \frac{C_m}{C_f}$	

### 3.2 Modelling of steel fibre reinforced concrete in tension

In this section the developed 1-D mechanical model is adopted for steel fibre reinforced concrete.

In the fibre reinforced materials embedded fibres oriented in one or more directions into the matrix are used to reinforce the matrix. Consequently, steel fibre reinforced concrete can be considered as a fibre reinforced material in which the concrete is the matrix, while the randomly distributed steel fibres are the fibre reinforcements.

In the case of the 1-D model concrete behaviour (matrix constituent) can be considered as an elastic-brittle material (see Figure 3.2) while steel fibre reinforcement behaviour (fibre constituent) can be considered as an elastic-plastic material (see Figure 3.2). Generally, concrete cracking occurs beyond steel fibre reinforcement yielding (pull-out mechanism, concrete-steel fibre debonding, localised fibre yielding). By neglecting the hardening and/or softening behaviour of the concrete and of the steel fibre reinforcement, the detailed simplest one-dimensional mechanical model (see Figure 3.1 -3.2) is used to characterise the behaviour of steel fibre reinforced concrete in uniaxial tension.

According to the assumptions beyond characteristic points of the macroscopic stress-strain relationship (at the level of the steel fibre reinforced concrete which can be understood at laboratory, experimentally scale) reads:

$$\begin{aligned}
 -\Sigma^0 &= (C_m + C_f)\epsilon_0 \\
 +\Sigma^0 &= \left( C_m + C_f - \frac{C_m^2}{C_m + M} \right) \epsilon_0 = -\Sigma^0 - C_m \frac{f_t}{C_m + M} \\
 -\Sigma^1 = +\Sigma^1 &= f_y
 \end{aligned} \tag{3.13}$$

while the tangential stress-strain relationships defines the elastic modulus of the material,  $K_0$  (before matrix cracking) and the elastoplastic modulus of the material,  $K_1$  (after matrix cracking and before fibre reinforcement yielding), respectively:

$$\begin{aligned}
 K_0 &= C_m + C_f = C_m \left( 1 + \frac{1}{\kappa} \right) \\
 K_1 &= C_f + \frac{C_m M}{C_m + M} = C_m \left( \rho + \frac{M}{C_m + M} \right) = C_m \left( \frac{1}{\kappa} + \frac{M}{C_m + M} \right)
 \end{aligned} \tag{3.14}$$

while due to the elastic-perfectly plastic fibre reinforcement behaviour after fibre reinforcement yielding the tangential stress-strain relationships reads:

$$K_2 = 0 \tag{3.15}$$

Eq. (3.13) to Eq. (3.15) define the stress – strain relationships shown in Figure 3.18 together with five model parameters such as  $C_m$  (stiffness of matrix),  $C_f$  (stiffness of

fibre reinforcement),  $M$  (coupling modulus),  $f_t$  (tensile strength of matrix),  $f_y$  (yielding strength of fibre reinforcement). However,  $K_0$  (elastic modulus of the steel fibre reinforced concrete),  $K_1$  (elastoplastic modulus of the steel fibre reinforced concrete after matrix cracking and before fibre reinforcement yielding) are experimentally measurable quantities. The overall composite stress-strain relationships (black line) and its components (black and red lines) together with the five model parameters are summarised in Figure 3.18.

Eq. (3.14) offers a direct way to express the coupling modulus  $M$ , as a function of the measurable elastic stiffness  $K_0$ , the elastoplastic stiffness  $K_1$ , and the elastic fibre reinforcement and elastic matrix stiffness ratio  $\rho = C_f / C_m$  (note  $\rho = 1 / \kappa$ ):

$$M = K_1 \frac{1 + \rho(1 - K_0 / K_1)}{(1 + \rho)^2 (1 - K_1 / K_0)} \quad (3.15)$$

Variation of the modulus of elasticity effected by steel fibre reinforcement can be considered negligible from the point of view of structural design as many earlier studies concluded [Balaguru & Shah (1992)]. For this reason, Figure 3.19 illustrates the variation of the coupling modulus  $M$  as a function of the elastic matrix and fibre reinforcement ratio,  $\kappa$ . Asymptotic behaviour of the coupling modulus  $M$  can be determined as the elastic matrix and fibre stiffness ratio ( $\kappa = C_m / C_f$ ) increases. Hence, Eq. (3.52) reads:

$$\begin{aligned} \lim_{\kappa \rightarrow \infty} K_0 &= \lim_{\kappa \rightarrow \infty} C_m (1 + \rho) = \lim_{\kappa \rightarrow \infty} C_m \left(1 + \frac{1}{\kappa}\right) = C_m \\ \lim_{\kappa \rightarrow \infty} K_1 &= \lim_{\kappa \rightarrow \infty} C_m \left(\rho + \frac{M}{C_m + M}\right) = \lim_{\kappa \rightarrow \infty} C_m \left(\frac{1}{\kappa} + \frac{M}{C_m + M}\right) = \frac{C_m M}{C_m + M} \end{aligned} \quad (3.16)$$

Combining Eq. (3.55), coupling modulus  $M$  can directly be expressed as a function of the two measurable elastic  $K_0$ , and elastoplastic stiffness  $K_1$  at the asymptote for steel fibre reinforced concrete:

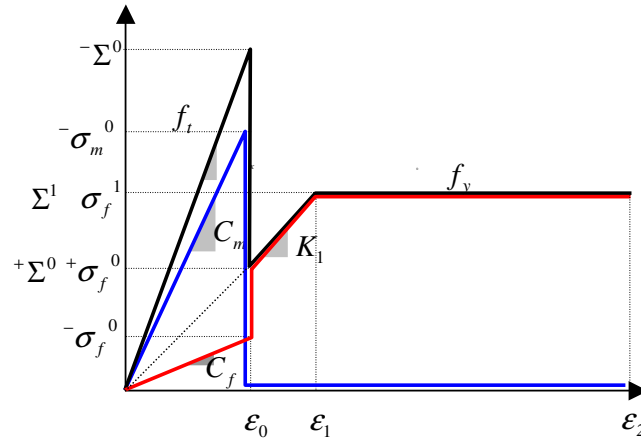
$$\lim_{\kappa \rightarrow \infty} M = \frac{K_0 K_1}{K_0 + K_1} \quad (3.17)$$

Now, the characteristic points of the stress-strain diagram before and after matrix cracking ( $\varepsilon_0 = f_t / C_m$ ) reads:

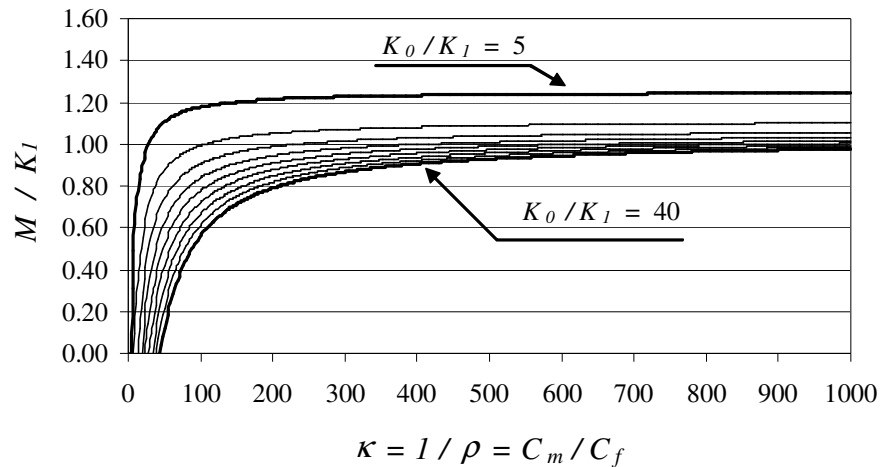
$$\begin{aligned} \lim_{\kappa \rightarrow \infty}^- \Sigma^0 &= \lim_{\kappa \rightarrow \infty} (C_m + \rho) \frac{f_t}{C_m} = \lim_{\kappa \rightarrow \infty} \left(C_m + \frac{1}{\kappa}\right) \frac{f_t}{C_m} = f_t \\ \lim_{\kappa \rightarrow \infty}^+ \Sigma^0 &= \lim_{\kappa \rightarrow \infty} \left(C_m + C_f - \frac{C_m^2}{C_m + M}\right) \frac{f_t}{C_m} = \left(K_0 - \frac{K_0}{K_0 + M}\right) \frac{f_t}{K_0} = f_t \left(1 - \frac{K_0}{K_0 + M}\right) \end{aligned} \quad (3.18)$$

Yielding of the steel fibre reinforcement starts for:

$$-\sigma_f^1 = f_t \left(1 - \frac{K_0}{K_0 + M}\right) + K_1 \left(\varepsilon_1 - \frac{f_t}{K_0}\right) = f_y \quad \Rightarrow \quad \varepsilon_1 = \frac{f_y}{K_1} = f_y \frac{K_0 + M}{K_0 M} \quad (3.19)$$



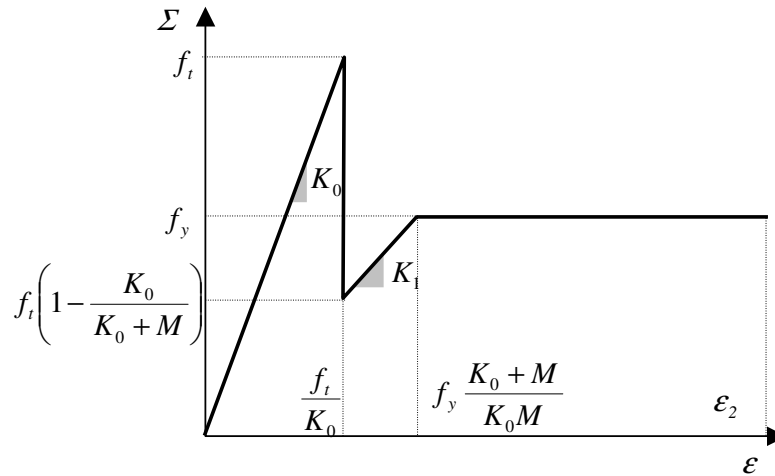
**Figure 3.18:** Overall and partial stress-strain relationships for steel fibre reinforced concrete according to the developed 1-D material model together with the model parameters



**Figure 3.19:** Coupling modulus,  $M$  as a function of the elastic matrix and fibre reinforcement stiffness ratio

Finally, using the assumed asymptotic behaviour of the coupling modulus  $M$ , the five introduced model parameters can be determined:

- stiffness of matrix  $C_m$  is equal to the overall composite stiffness  $K_0$  which can experimentally be determined in uniaxial tensile test.
- stiffness of fibre reinforcement  $C_f$  is negligible
- coupling modulus  $M$  can directly be expressed as a function of the elastic stiffness  $K_0$  and the elastoplastic stiffness  $K_1$  which can experimentally be determined in uniaxial test.
- matrix cracking strength  $f_t$  is equal to the overall composite tensile strength which can experimentally be determined in uniaxial test.



**Figure 3.20:** Derived stress-strain relationships for the uniaxial behaviour of steel fibre reinforced concrete

- allowing for one fibre arrays as before, yielding strength of the steel fibre reinforcement  $f_y$  can be considered as the pull-out strength of the fibre which depends on the bond characteristic of matrix and fibre.

Derived stress-strain relationship for steel fibre reinforced concrete can be seen in Figure 3.20.

### 3.3 Conclusions

Based on the theoretical studies on the modelling of fibre reinforced materials the following conclusions can be made:

1. A **1-D material model** for fibre reinforced **materials** was developed. The model is composed of two devices representing an elastic-brittle material law for the matrix and an elastic-perfectly plastic material law for the fibre reinforcement behaviour, respectively. The two devices are coupled by a third new introduced device which links the irreversible matrix and irreversible fibre reinforcement behaviour and called as coupling modulus.
2. Due to the **simplicity and clear physical significance** of the developed 1-D mechanical model it was **extended by different matrix and fibre reinforcement behaviour** such as residual strength after matrix cracking or fibre fracture, matrix and fibre hardening or softening behaviour.
3. The developed simplest mechanical model considering elastic-brittle matrix and elastic-perfectly plastic fibre behaviours was **adopted for steel fibre reinforced concrete**. Parameters of the developed 1-D model (stress-strain relationship) were derived from experimentally measurable (macroscopic) parameters.

# Chapter 4

## Behaviour of steel fibre reinforced concrete beams in bending and shear

*18 steel fibre reinforced concrete beams in four point bending were tested applying different fibre contents (0 V%, 0.5 V% or 1.0 V%), fibre configurations (hooked-end or crimped), and amounts of conventional shear reinforcement (no stirrup reinforcement,  $\text{Ø}6/240$  and  $\text{Ø}4/240$  mm stirrups or  $\text{Ø}6/120$  and  $\text{Ø}4/120$  mm stirrups), considering the same longitudinal reinforcement ( $2\text{Ø}16$ ).*

*Aim of the tests was to study the structural performance of reinforced concrete beams effected by steel fibre reinforcement. Based on the experimental results and the theoretical investigations presented in the previous Chapter, design procedures has also been developed to determine the moment capacity of steel fibre reinforced concrete beams.*

**Keywords:** *reinforced concrete, steel fibre reinforced concrete, bending behaviour, shear behaviour, failure load, failure mode, bending failure, shear failure, crack propagation, crack pattern, modelling*

### 4.1 Experimental programme

#### 4.1.1 Test specimens and reinforcing details

Experimental program involved 18 steel fibre reinforced concrete beams. Experimental variables were the fibre content (0 V%, 0.5 V% or 1.0 V%), the fibre configuration (hooked-end or crimped), and the amount of conventional shear reinforcement (no stirrup reinforcement,  $\text{Ø}6/240$  and  $\text{Ø}4/240$  mm stirrups or  $\text{Ø}6/120$  and  $\text{Ø}4/120$  mm stirrups) and the concrete mix proportions (REF-3, FRC-3, REF-4, FRC-4). Experimental constants were the geometry of specimens ( $2000\times 150\times 100$  mm) and the amount of longitudinal reinforcement ( $2\text{Ø}16$ ) as well as the test set-up and the test arrangement. Beams manufactured in the laboratory of the Department of Reinforced Concrete Structures, Budapest University of Technology and Economics.

Aim of present tests was to study the effect of fibre reinforcement on the bending and shear behaviour of reinforced concrete beams [Balázs & Kovács (1997),



Balázs & Kovács (1999), Balázs & Kovács (1999)]. Amount of longitudinal reinforcement was determined to reach yielding of longitudinal steel bars earlier than shear failure of beams. Tensioned 2Ø16 longitudinal bars were of Hungarian grades B60.50 (nominal yield strength 500 MPa). Stirrups and the 2Ø6 bars placed at the top of the beam to fix stirrups were of grade B38.24 (nominal yield strength 240 MPa). Reinforcing details of beams are summarised in Figure 4.1.

Stirrups in combination with steel fibres were used as shear reinforcements. Reference beams were made of plain concrete (made of mixes REF-3 and REF-4) with (Ø6/240 and Ø6/120 mm for RC-A, Ø4/240 mm and Ø4/120 mm) for RC-B and without stirrup reinforcement. Two amounts of stirrup reinforcements (spacing 120 mm and 240 mm) were applied. Based on the test results to series of beams REF-3, FRC-3<sup>0.5</sup><sub>ZC 30/5</sub> and FRC-3<sup>1.0</sup><sub>ZC 30/5</sub> stirrup diameter Ø6 mm was changed to Ø4 mm for beams made of mixes REF-4, FRC-4<sup>0.5</sup><sub>D&D ~30/5</sub> and FRC-4<sup>1.0</sup><sub>D&D ~30/5</sub>, in order to underline the effect of fibres on the shear behaviour. Further, for the sake of simplicity beams made of mixes REF-3, FRC-3<sup>0.5</sup><sub>ZC 30/5</sub> and FRC-3<sup>1.0</sup><sub>ZC 30/5</sub> will be referred as series RC-A and beams made of mixes REF-4, FRC-4<sup>0.5</sup><sub>D&D ~30/5</sub> and FRC-4<sup>1.0</sup><sub>D&D ~30/5</sub> as series RC-B, respectively. Series RC-A and series RC-B are numerated according to the applied fibre content and the amount of conventional shear reinforcement (stirrup spacing). They are summarised in Table 4.1.

#### 4.1.2 Experimental set-up and test procedure

Beams were tested in four point bending as illustrated in Figure 4.2. Span was 1800 mm and shear-span was 600 mm for all beams. Since the geometry of beams and the longitudinal reinforcement was constant in tests, the effective depth,  $d$ , was 120 mm and the shear-span to effective depth ratio,  $a/d$ , was 5.

Force was applied by two LUKAS type hydraulic jacks with the capacity of 100 kN. Two jacks worked in one circle. For this reason, jack forces were equal in loading. Since the tests were performed in force control, the force was gradually released. The force steps were 2.0 or 2.5 kN according to the calculated failure loads of the tested beams.

**Table 4.1:** *Experimental variables of steel fibre reinforced concrete beams*

Fibre type	Mixture	Stirrup reinforcement:		
		No	Ø6/240	Ø6/120
Dramix® ZC 30/5	REF-3	RC-A1	RC-A4	RC-A7
	FRC-3 <sup>0.5</sup> <sub>ZC 30/5</sub>	RC-A2	RC-A5	RC-A8
	FRC-3 <sup>1.0</sup> <sub>ZC 30/5</sub>	RC-A3	RC-A6	RC-A9
Fibre type	Mixture	Stirrup reinforcement:		
		No	Ø4/240	Ø4/120
D&D® ~ 30/5	REF-4	RC-B1	RC-B4	RC-B7
	FRC-4 <sup>0.5</sup> <sub>D&amp;D ~30/5</sub>	RC-B2	RC-B5	RC-B8
	FRC-4 <sup>1.0</sup> <sub>D&amp;D ~30/5</sub>	RC-B3	RC-B6	RC-B9

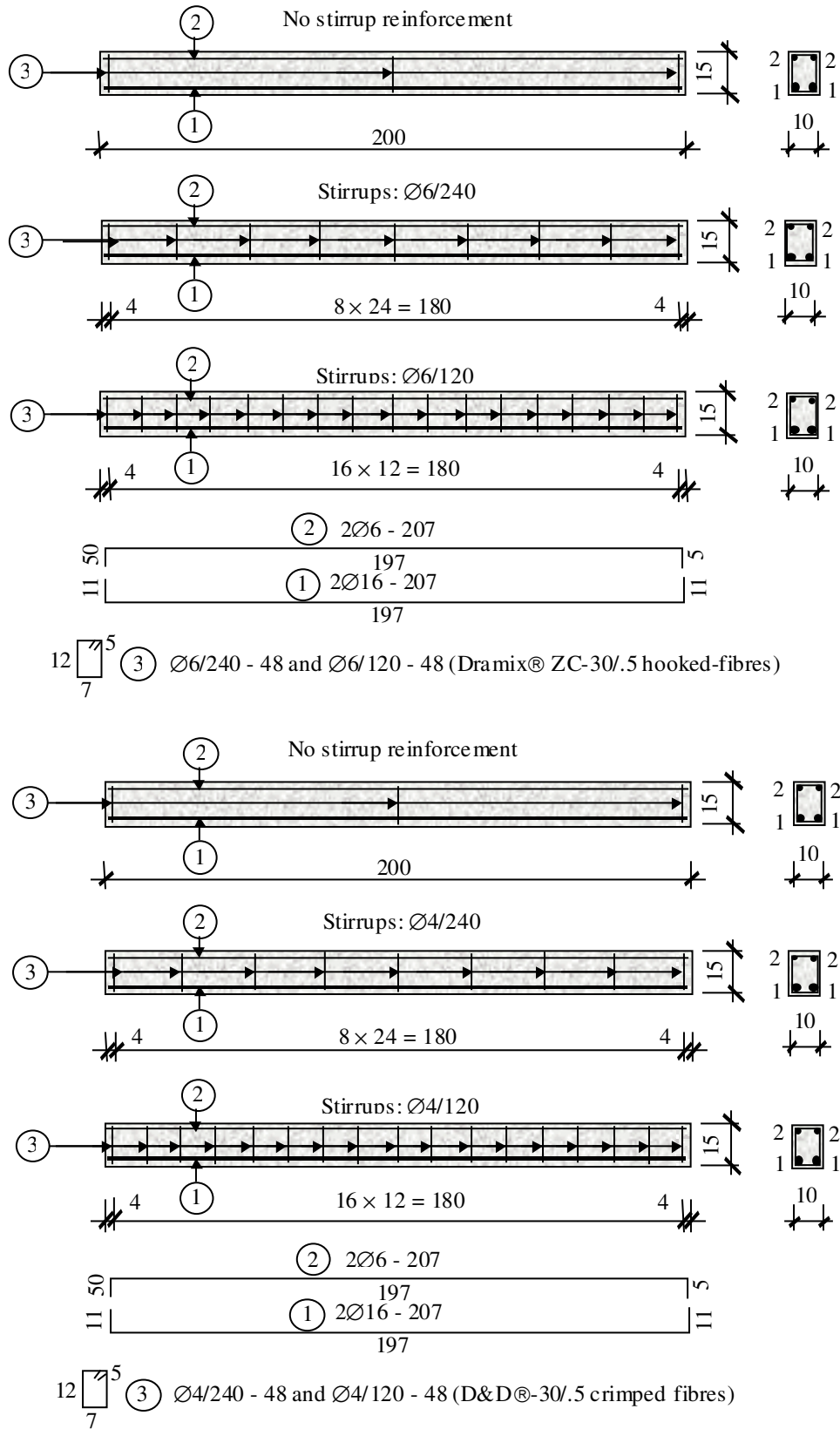
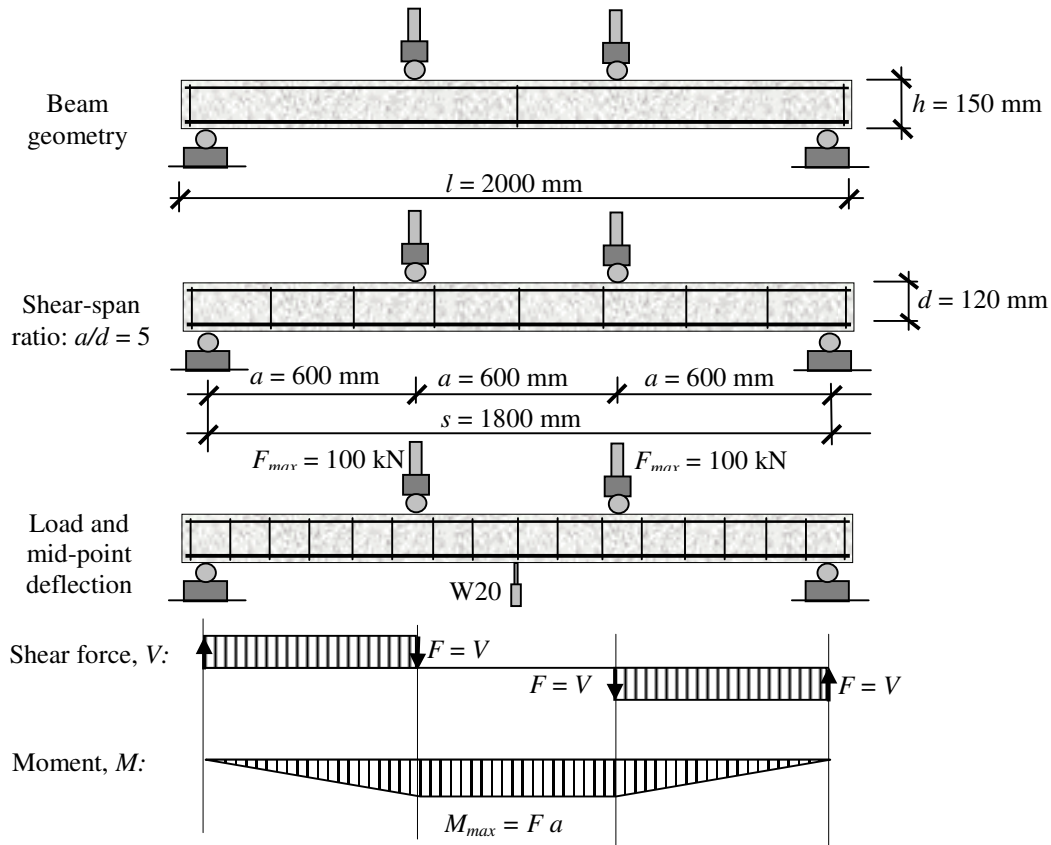


Figure 4.1: Detail of conventional reinforcements for steel fibre reinforced concrete beam series RC-A and RC-B



**Figure 4.2:** Experimental set-up and test arrangement for bending test of steel fibre reinforced RC beams

Mid-span deflections of beams were registered by a W20 measuring device. Force (one jack force) – mid-span deflection relationships were registered graphically. In each load steps positions, formations and developments of cracks were visually monitored and graphically signed on one side of the beam. Crack widths and developments were measured and registered in all load steps.

## 4.2 Experimental results

### 4.2.1 Failure loads and failure modes

Failure loads and failure modes of steel fibre reinforced concrete beams are summarised in Figure 4.3 for series RC-A and in Figure 4.4 for series RC-B. Beams of series RC-A and series RC-B are numerated according to the applied steel fibre content and the amount of stirrup reinforcement. Parameters of reinforcements are also represented for each beam. Shear failure is indicated by failure line, flexural failure is indicated by shaded area. Corresponding concrete cube strengths are summarised in Table 4.2 with the nominal shear strength of beams calculated after Balaguru and Shah [Balaguru & Shah (1992)]. Failure loads and failure modes are also presented in Figure 4.5 and in Figure 4.6 representing the increment of failure load by columns.

Significant effect of steel fibre reinforcement was obtained on shear resistance of steel fibre reinforced concrete beams. Due to increasing fibre content, a considerable improvement in failure load was observed for both series of beams independently from the fibre type. However, increment in failure loads were more significant for beams made without stirrup reinforcement (RC-A1...RC-A3 and RC-B1...RC-B3, see Tab. 3.2).

Shear failure was brittle for beams made without any shear reinforcement (RC-A1 and RC-B1). Failure lines formed suddenly at a load close to the peak load. Due to the force transfer by the steel fibres crossing cracks, rigid shear failure changed to tougher shear failure for both series of beams made with fibres. However, at higher load levels when the flexural capacity was reached, failure mode changed from shear failure (RC-B1 and RC-B2) to simultaneous shear and bending failure for the beam containing 1.0 V% crimped fibres and no stirrup (RC-B3).

Both fibre types produced increase of shear strength as shown in Figure 4.7 [Balaguru & Shah (1995)]. Crimped fibres were more effective to improve shear resistance in series RC-B compared to that of hooked-end fibres in series RC-A. This difference may be caused by the different bond capacities and yield strengths of fibres (see Table 2.2) and different compressive strengths of concrete mixes (Figure 4.8).

In details, for series RC-A lower shear capacity was observed by increasing steel fibre content due to the higher conventional shear reinforcement ratio ( $\varnothing 6/240$  mm was used for beam RC-A4...RC-A6) and lower compressive strength of concrete. However, bending failure was obtained applying 1.0 V% of hooked-end steel fibres related to beams containing lower amount of steel fibres. For beams series RC-A, containing higher amount of conventional shear reinforcement ( $\varnothing 6/120$  mm was used for beam RC-A7...RC-A9) bending failure was detected independently from the fibre content. Ultimate flexural capacity was not influenced by the addition of hooked-end steel fibres, but corresponded to tougher bending failure.

$\varnothing 4$  mm stirrup diameter was applied for beams series RC-B made with crimped steel fibres. Shear capacity improved applying crimped steel fibres considering relatively low amount of stirrup reinforcement,  $\varnothing 4/240$  mm for beams RC-B4...RC-B6. Similarly to the case of beams RC-B1, RC-B2 and RC-B3, failure mode of beams changed from shear failure to bending failure by increasing crimped steel fibre content. Significant increment in shear capacity was obtained with the changing of failure mode from shear (RC-B7 and RC-B8) to bending failure (RC-B9) for beams having  $\varnothing 4/120$  mm stirrup reinforcement and applying also crimped steel fibres. Beam made with 0.5 V% crimped steel fibres showed higher shear capacity (RC-B8: 46.6 kN) than the beam made with only stirrup reinforcement (RC-B7: 35.2 kN) and no fibres. 1.0 V% crimped steel fibres resulted bending failure since the increasing fibre content was able to carry the increasing shear forces in the member (RC-B9).

For series RC-B higher shear strength was obtained by applying 0.5 V% crimped steel fibres related to beams made with no steel fibres for all configuration of stirrup reinforcements. However, combined shear and bending (RC-B3) or bending failure

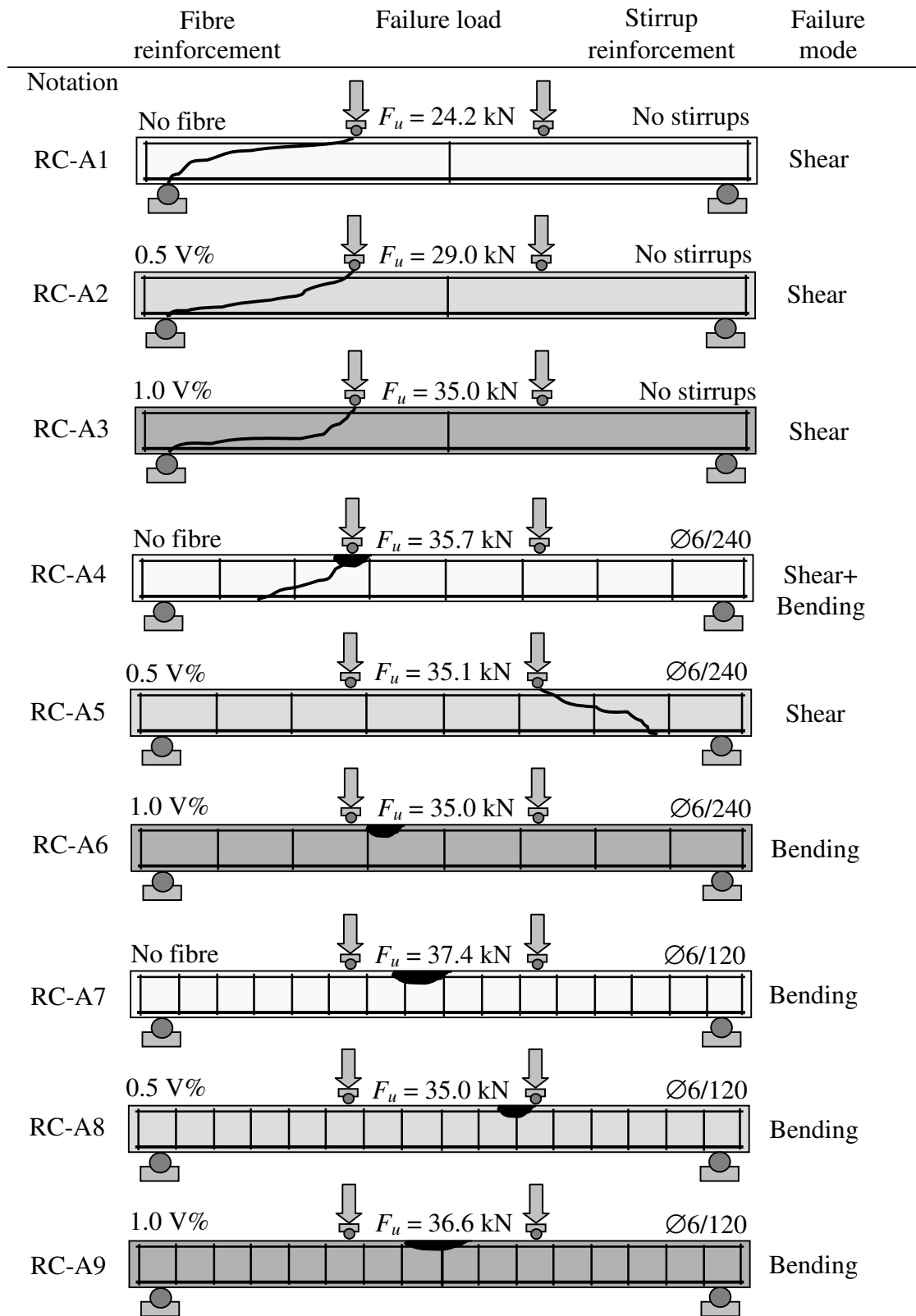
(RC-B6 and RC-B9) were developed applying 1.0 V% crimped steel fibres for all configuration of stirrup reinforcement.

After failure of beams failure surface was visually checked. Pull out of fibres from the concrete was observed without fibre yielding. Anchors of hooked-end steel fibres and the waves of crimped steel fibres were deformed.

Since the applied fibre types (Dramix<sup>®</sup> hooked-end fibres and D&D<sup>®</sup> crimped fibres) as well as the stirrup diameters (Ø6 for series A and Ø4 for series B) were different, amount of shear reinforcements were also different for beam series RC-A and RC-B. Shear reinforcement ratios were defined to make the results comparable: longitudinal reinforcement ratio ( $A_{sl}/bd$ ), conventional stirrup reinforcement ratio ( $A_{sw}/bs$ ) and steel fibre reinforcement ratio ( $A_{sw,eff}/bs_{eff}$ ) (Table 4.4). In the following comparisons of shear capacities are made based on the amount of shear reinforcements (combination of fibres and stirrups).

**Table 4.2: Results of bending tests for steel fibre reinforced concrete beams**

Beam type	Stirrups	Fibre content	Concrete mix	$f_{c,cube}$	$F_u$	Increment in failure load	$\frac{V_u}{bd} \sqrt{f_c^{cube}}$	Increment in shear strength	Failure mode
				[MPa]	[kN]	[%]		[%]	
RC-A1	No stirrups	No fibres	REF-3	37.58	24.2	REF	12.40	REF	Shear
RC-A2		0.5 V%	FRC-3 <sup>0.5</sup> <sub>ZC 30/5</sub>	39.85	29.0	19.8	15.14	22	Shear
RC-A3		1.0 V%	FRC-3 <sup>1.0</sup> <sub>ZC 30/5</sub>	38.55	35.0	44.6	18.12	46	Shear
RC-A4	Ø6/240	No fibres	REF-3	37.58	35.7	REF	18.04	REF	Combined
RC-A5		0.5 V%	FRC-3 <sup>0.5</sup> <sub>ZC 30/5</sub>	39.85	35.1	-1.7	18.33	-1	Shear
RC-A6		1.0 V%	FRC-3 <sup>1.0</sup> <sub>ZC 30/5</sub>	38.55	35.0	-2.0	-	-	Bending
RC-A7	Ø6/120	No fibres	REF-3	37.58	37.4	REF	-	-	Bending
RC-A8		0.5 V%	FRC-3 <sup>0.5</sup> <sub>ZC 30/5</sub>	39.85	35.0	-6.4	-	-	Bending
RC-A9		1.0 V%	FRC-3 <sup>1.0</sup> <sub>ZC 30/5</sub>	38.55	36.6	-2.14	-	-	Bending
RC-B1	No stirrups	No fibres	REF-4	42.70	21.6	REF	11.96	REF	Shear
RC-B2		0.5 V%	FRC-4 <sup>0.5</sup> <sub>D&amp;D -30/5</sub>	48.80	33.6	55.5	19.52	63	Shear
RC-B3		1.0 V%	FRC-4 <sup>1.0</sup> <sub>D&amp;D -30/5</sub>	47.16	44.7	106.9	25.47	113	Combined
RC-B4	Ø6/240	No fibres	REF-4	42.70	27.5	REF	14.95	REF	Shear
RC-B5		0.5 V%	FRC-4 <sup>0.5</sup> <sub>D&amp;D -30/5</sub>	48.80	44.3	61.1	25.86	73	Shear
RC-B6		1.0 V%	FRC-4 <sup>1.0</sup> <sub>D&amp;D -30/5</sub>	47.16	45.7	66.2	-	-	Bending
RC-B7	Ø6/120	No fibres	REF-4	42.70	35.2	REF	19.22	REF	Shear
RC-B8		0.5 V%	FRC-4 <sup>0.5</sup> <sub>D&amp;D -30/5</sub>	48.80	46.6	32.4	27.33	42	Shear
RC-B9		1.0 V%	FRC-4 <sup>1.0</sup> <sub>D&amp;D -30/5</sub>	47.16	45.0	27.8	-	-	Bending



**Figure 4.3:** Failure loads and failure modes of steel fibre reinforced concrete beams applying Dramix® ZC 30/5 hooked-end fibres (series A)

Notation	Fibre reinforcement	Failure load	Stirrup reinforcement	Failure mode
RC-B1	No fibre	$F_u = 21.6$ kN	No stirrups	Shear
RC-B2	0.5 V%	$F_u = 33.6$ kN	No stirrups	Shear
RC-B3	1.0 V%	$F_u = 44.7$ kN	No stirrups	Shear+ Bending
RC-B4	No fibre	$F_u = 27.5$ kN	$\text{Ø}4/240$	Shear
RC-B5	0.5 V%	$F_u = 44.3$ kN	$\text{Ø}4/240$	Shear
RC-B6	1.0 V%	$F_u = 45.7$ kN	$\text{Ø}4/240$	Bending
RC-B7	No fibre	$F_u = 35.2$ kN	$\text{Ø}4/120$	Shear
RC-B8	0.5 V%	$F_u = 46.6$ kN	$\text{Ø}4/120$	Shear
RC-B9	1.0 V%	$F_u = 45.0$ kN	$\text{Ø}4/120$	Bending

**Figure 4.4:** Failure loads and failure modes of steel fibre reinforced concrete beams applying D&D 30/5 crimped fibres (series B)

Shear reinforcement ratios (stirrup reinforcement ratio  $A_{sw}/bs$ , effective steel fibre reinforcement ratio  $A_{sw,eff}/bs_{eff}$ ) vs. failure load relationships were developed and summarised in Figure 4.9/a-b.

Comparing beams RC-A2 and RC-B2 both made with the same steel fibre content, failure load was significantly higher for RC-B2, which may be caused by the higher concrete compressive strength and higher yield strength of crimped steel fibres. Figure 4.9/a indicates that failure load was not significantly effected by the shear reinforcement ratio ( $A_{sw}/bs$ ) in case of beams applying stirrup reinforcement. However, failure mode of beams changed from shear failure to combined or bending failure by increasing steel fibre content.

Due to the lower stirrup reinforcement ratio of series RC-B and the higher compressive strength of concrete, significant effect of steel fibre reinforcement on the shear capacity was obtained applying only crimped steel fibres for RC-B2 (No stirrups,  $\rho_s = 0.00370$ ,  $F_u = 33.6$  kN) and RC-B3 (No stirrups,  $\rho_s = 0.00739$ ,  $F_u = 44.7$  kN) related to reference beam Rc-B1.

Significant improvement in failure load was observed combining stirrup reinforcement with steel fibres for beams series RC-B. Higher failure load was detected for RC-B5 by addition of 0.5 V% steel fibres ( $\text{Ø}4/240$ ,  $\rho_s = 0.00475$ ,  $F_u = 44.3$  kN) related to beam RC-B4 containing only stirrup reinforcement ( $\text{Ø}4/240$ ,  $\rho_s = 0.00105$ ,  $F_u = 27.5$  kN). Addition of 0.5 V% crimped steel fibres resulted 16.8 kN increment in shear failure which increment is very close to the failure load of beam RC-B1,  $F_u = 21.6$  kN.

Effect of steel fibres as shear reinforcement on the shear capacity was also significant for beams having stronger ( $\text{Ø}4/120$ ) stirrup reinforcement of series RC-B. For RC-B8 ( $\text{Ø}4/120$ ,  $\rho_s = 0.00579$ ,  $F_u = 46.6$  kN), 11.4 kN increment in shear failure load was observed related to RC-B7 ( $\text{Ø}4/120$ ,  $\rho_s = 0.00209$ ,  $F_u = 35.2$  kN). Further increase of steel fibres (1.0 V% crimped steel fibre content) indicated bending failure for beam RC-B9.

Amount of shear reinforcement vs. shear strength presented in the form proposed Balaguru and Shah [*Balaguru & Shah (1995)*] in Figure 4.9/c for series A and in Figure 3.9/d for series B. Diagrams also indicate that steel fibres can be effectively used to improve shear strength of concrete. Applying 1 V% hooked-end steel fibres (RC-A3,  $\rho_s = 0.00707$ )  $\tau_u = 18.12 \text{ MPa}^{3/2}$  shear strength was obtained similarly to beam made with only stirrups (RC-A4, 0 V%,  $\text{Ø}6/240$ ,  $\rho_s = 0.00233$ )  $\tau_u = 18.04 \text{ MPa}^{3/2}$ . Power 3/2 of MPa comes from the proposed form by Balaguru and Shah (1995). Higher shear reinforcement ratios resulted combined or clear bending failure. Very characteristic effect of crimped steel fibres on shear strength was obtained in case of series RC-B when the stirrup reinforcement ratio was lower than that of for series RC-A.

Representation of failure loads and shear strengths as a function of steel fibre reinforcement vs. total shear reinforcements ratio ( $\rho_{sf,eff} / \rho_s$ ) was suitable to study the role of fibres in shear behaviour of concrete as shown in Figures 4.9/e to h. As Figure 4.9/e indicates failure load increased significantly when only steel fibres were used as shear reinforcement (RC-A2 and RC-A3). In the other cases, failure load was not effected by the  $\rho_{sf,eff} / \rho_s$  ratio. Consequently, shear strength of concrete was not effect by the  $\rho_{sf,eff} / \rho_s$  ratio. Considering series RC-B, increasing  $\rho_{sf,eff} / \rho_s$  ratio resulted higher failure load together with the changing of failure mode from shear to bending.



**Table 4.3:** Developed reinforcement ratios for analysing the effect of steel fibre reinforcement on the structural performances of RC beams

Serie RC-A									
	RC-A1	RC-A2	RC-A3	RC-A4	RC-A5	RC-A6	RC-A7	RC-A8	RC-A9
$A_s$	2Ø16								
$\rho_{sl}$	0.03350								
Stirrups	No stirrups			Ø6/240			Ø6/120		
$\rho_{sw}$	0			0.00233			0.00467		
fibre content	No fibre	0.5 V%	1.0 V%	No fibre	0.5 V%	1.0 V%	No fibre	0.5 V%	1.0 V%
$\rho_{sf,eff.}$	0	0.00353	0.00707	0	0.00353	0.00707	0	0.00353	0.00707
$\rho_s = \rho_{sf,eff.} + \rho_{sw}$	0	0.00353	0.00707	0.00233	0.00586	0.00940	0.00467	0.00820	0.01174
$\rho_{sf,eff.}/\rho_{sw}$	-	-	-	0	1.50	3.00	0	0.75	1.50
$\rho_{sf,eff.}/\rho_s$	-	1	1	0	0.60	0.75	0	0.43	0.47
Serie RC-B									
	RC-B1	RC-B2	RC-B3	RC-B4	RC-B5	RC-B6	RC-B7	RC-B8	RC-B9
$A_s$	2Ø16								
$\rho_{sl}$	0.0335								
Stirrups	No stirrups			Ø4/240			Ø4/120		
$\rho_{sw}$	0			0.00105			0.00209		
fibre content	No fibre	0.5 V%	1.0 V%	No fibre	0.5 V%	1.0 V%	No fibre	0.5 V%	1.0 V%
$\rho_{sf,eff.}$	0	0.00370	0.00739	0	0.00370	0.00739	0	0.00370	0.00739
$\rho_s = \rho_{sf,eff.} + \rho_{sw}$	0	0.00370	0.00739	0.00105	0.00475	0.00844	0.00209	0.00579	0.00948
$\rho_{sf,eff.}/\rho_{sw}$	-	-	-	0	3.54	7.08	0	1.77	3.54
$\rho_{sf,eff.}/\rho_s$	-	1	1	0	0.78	0.88	0	0.64	0.78

## 4.2.2 Load vs. mid-point deflection relationships

Load vs. mid-point deflection relationships of steel fibre reinforced concrete beams are summarised in Figure 4.7. First and second columns indicate series RC-A and RC-B, respectively. Failure modes and failure loads as well as reinforcing details of beams are represented on the diagrams. Experimental parameters of the beams, mid-point deflections measured at the failure load and the ultimate mid-point deflections are summarised in Table 4.4.

Load vs. mid-point deflection relationships indicate decreasing stiffness of beam applying hooked-end steel fibres for series RC-A, which is believed to be caused by higher porosity of concrete mix FRC-3<sup>0.5</sup><sub>ZC 30/5</sub> and FRC-3<sup>1.0</sup><sub>ZC 30/5</sub> compared to REF-3 due to the workability conditions in the Laboratory at time of casting (see Table 2.2). However, diagrams for beams made of mixes FRC-4<sup>0.5</sup><sub>D&D ~30/5</sub> and FRC-4<sup>0.5</sup><sub>D&D ~30/5</sub> and casting 30.03.1995, indicate stiffer behaviour by increasing steel fibre content related to the reference beam made of mix REF-4 and casting 03.04.1995.

Significant increment of ultimate mid-point deflection was observed applying steel fibres compared to reference beams for both series of beams (Table 4.4).

Considering beams RC-A1...RC-A3, RC-A4 and RC-A5, a short post-peak behaviour was observed even if the beams failed in shear. It might be the result of the

more effective anchorage and bond behaviour of the hooked-end fibres compared to the crimped steel fibres. In addition to, beam RC-A6 failed in bending with significant post-peak resistance.

For beams having higher amount of conventional shear reinforcement ( $\text{Ø}6/120$  mm was used for beam RC-A7...RC-A9) addition of hooked-end steel fibres resulted significant post-peak behaviour.

In case of series RC-B, post-peak response was only observed when flexural failure occurred (RC-B6 and RC-B9).

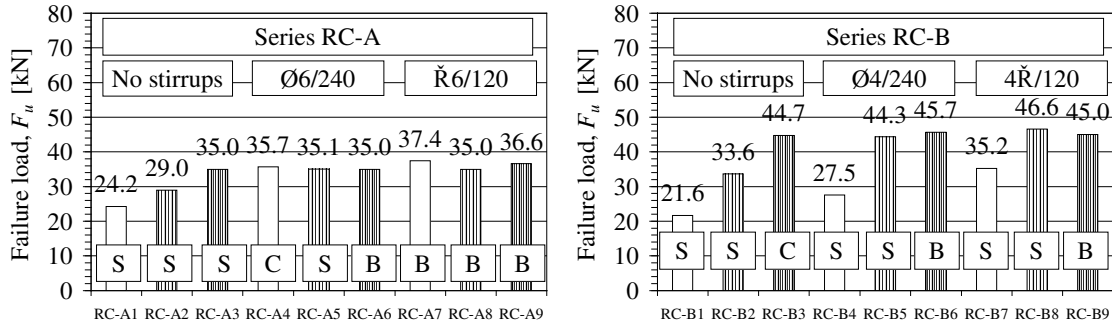


Figure 4.5: Failure loads and failure modes of steel fibre reinforced concrete beams applying Dramix<sup>®</sup> ZC 30/.5 hooked-end steel fibres for series A and D&D<sup>®</sup> 30/.5 crimped steel fibres for series B

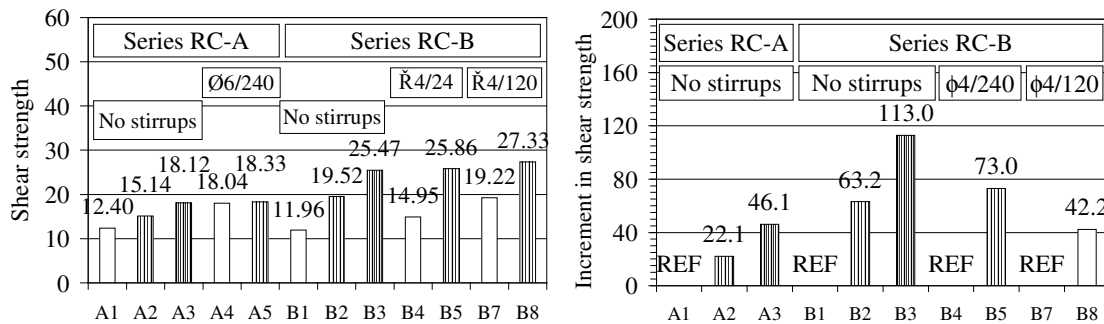
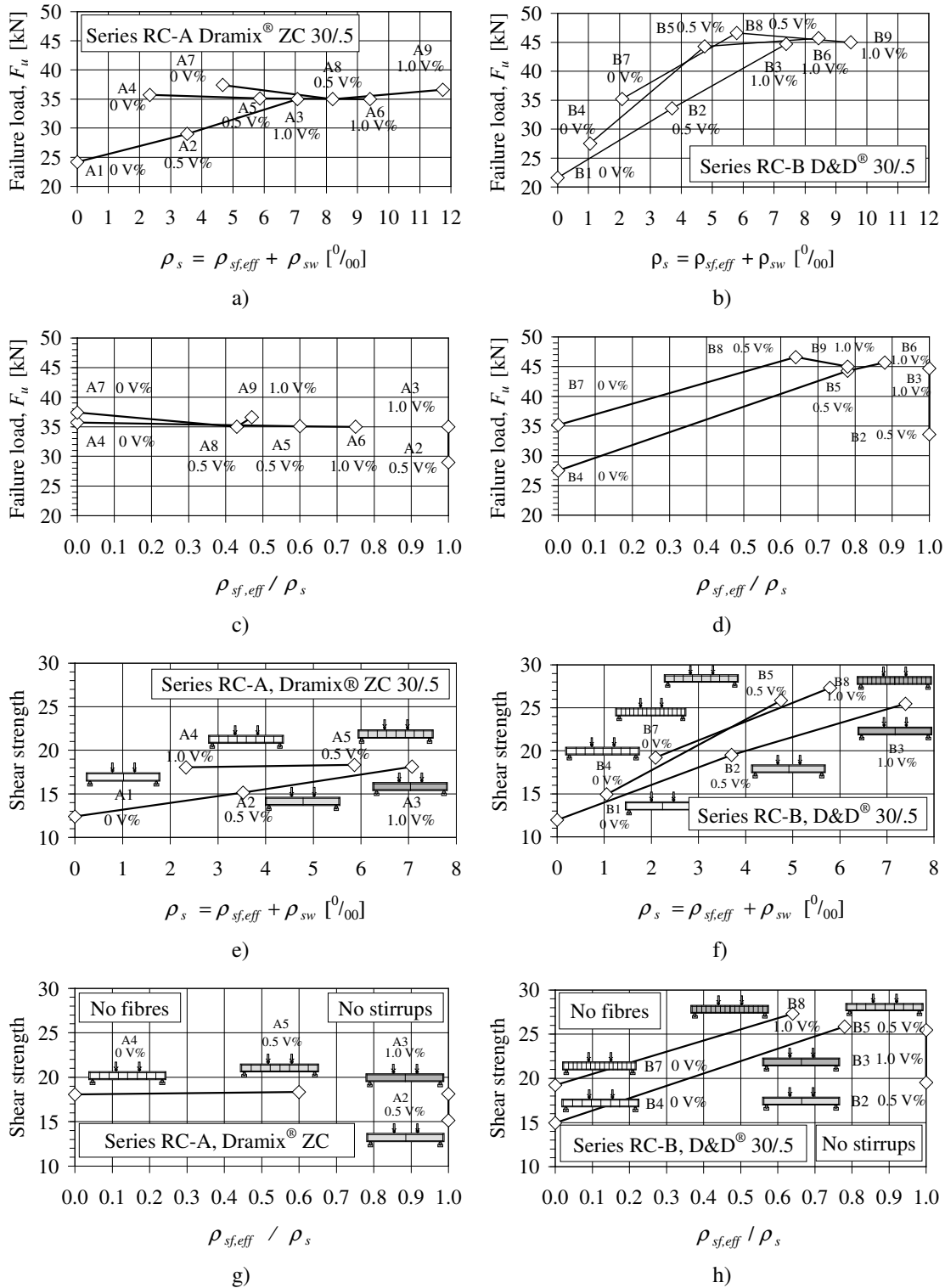


Figure 4.6: Shear strength of reinforced concrete beams calculated after Balaguru & Shah (1995)



**Figure 4.7:** Reinforcement ratios vs. failure loads and shear strengths

a)  $\rho_s - F_u$  for Series A

b)  $\rho_s - F_u$  for Series B

c)  $\rho_{sf,eff} / \rho_s - F_u$  for Series A

d)  $\rho_{sf,eff} / \rho_s - F_u$  for Series B

e)  $\rho_s - \tau$  for Series A

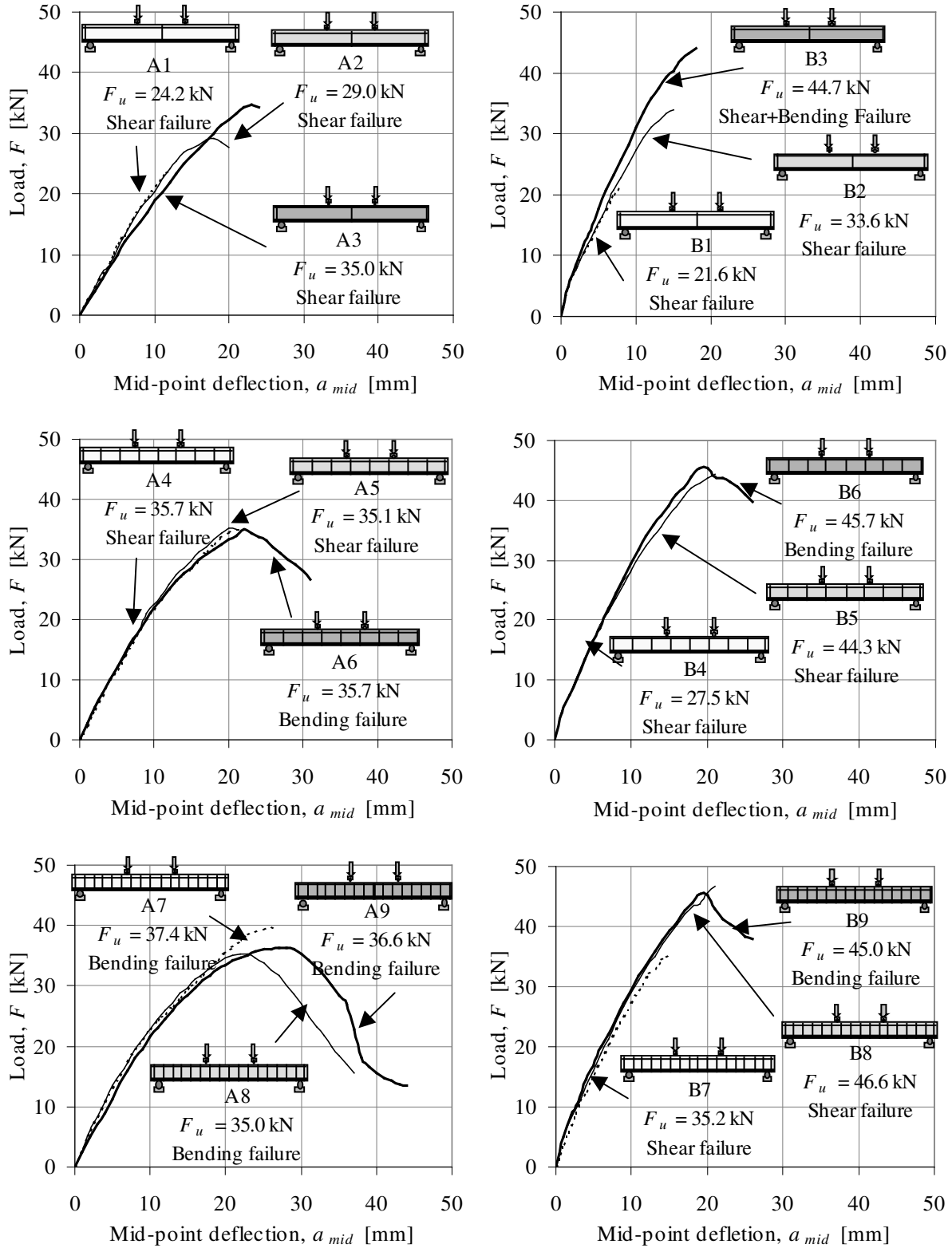
f)  $\rho_s - \tau$  for Series B

g)  $\rho_{sf,eff} / \rho_s - \tau$  for Series A

h)  $\rho_{sf,eff} / \rho_s - \tau$  for Series B

**Table 4.4:** Some characteristic data of the Load vs. Mid-point deflection relationship of steel fibre reinforced concrete beams

Beam type	Stirrups	Fibre content	Concrete mix	$F_u$ [kN]	$a_{mid}^{F_u}$ [mm]	$a_{mid}^{\max}$ [mm]	Increment in $a_{mid}^{\max}$ [%]	Failure mode
RC-A1	No stirrups	No fibres	REF-3	24.2	12	12	REF	Shear
RC-A2		0.5 V%	FRC-3 <sup>0.5</sup> <sub>ZC 30/5</sub>	29.0	18	20	66.7	Shear
RC-A3		1.0 V%	FRC-3 <sup>1.0</sup> <sub>ZC 30/5</sub>	35.0	23	24	100.0	Shear
RC-A4	Ø6/240	No fibres	REF-3	35.7	22	22	REF	Shear
RC-A5		0.5 V%	FRC-3 <sup>0.5</sup> <sub>ZC 30/5</sub>	35.1	20	21	-4.5	Shear
RC-A6		1.0 V%	FRC-3 <sup>1.0</sup> <sub>ZC 30/5</sub>	35.0	22	31	40.9	Bending
RC-A7	Ø6/120	No fibres	REF-3	37.4	26	27	REF	Bending
RC-A8		0.5 V%	FRC-3 <sup>0.5</sup> <sub>ZC 30/5</sub>	35.0	22	37	37.0	Bending
RC-A9		1.0 V%	FRC-3 <sup>1.0</sup> <sub>ZC 30/5</sub>	36.6	28	44	63.0	bending
RC-B1	No stirrups	No fibres	REF-4	21.6	8	8	REF	Sear
RC-B2		0.5 V%	FRC-4 <sup>0.5</sup> <sub>D&amp;D -30/5</sub>	33.6	15	15	87.5	Shear
RC-B3		1.0 V%	FRC-4 <sup>1.0</sup> <sub>D&amp;D -30/5</sub>	44.7	18	18	125.0	Shear+Bending
RC-B4	Ø6/240	No fibres	REF-4	27.5	10	10	REF	Shear
RC-B5		0.5 V%	FRC-4 <sup>0.5</sup> <sub>D&amp;D -30/5</sub>	44.3	21	21	110.0	Shear
RC-B6		1.0 V%	FRC-4 <sup>1.0</sup> <sub>D&amp;D -30/5</sub>	45.7	20	26	160.0	Bending
RC-B7	Ø6/120	No fibres	REF-4	35.2	15	15	REF	Shear
RC-B8		0.5 V%	FRC-4 <sup>0.5</sup> <sub>D&amp;D -30/5</sub>	46.6	21	21	40.0	Shear
RC-B9		1.0 V%	FRC-4 <sup>1.0</sup> <sub>D&amp;D -30/5</sub>	45.0	19	26	73.3	Bending



**Figure 4.8:** Load vs. Mid-point deflection relationships for steel fibre reinforced concrete beams  
(The first column represents series A, the second column represents series B)

### 4.2.3 Cracking behaviour

Increase in energy-absorption capacity yields to remarkable improvement in cracking characteristics. Cracks may be more uniformly distributed resulting reduction in the maximum crack width. Cracking behaviour is effected by the amount of longitudinal and transversal reinforcement as well. Design codes and recommendations generally control the minimum amount of longitudinal and transversal reinforcement. Combining conventional reinforcements with steel fibres may result an economic solution not only to increase shear capacity but also to control crack width and to obtain better crack distribution.

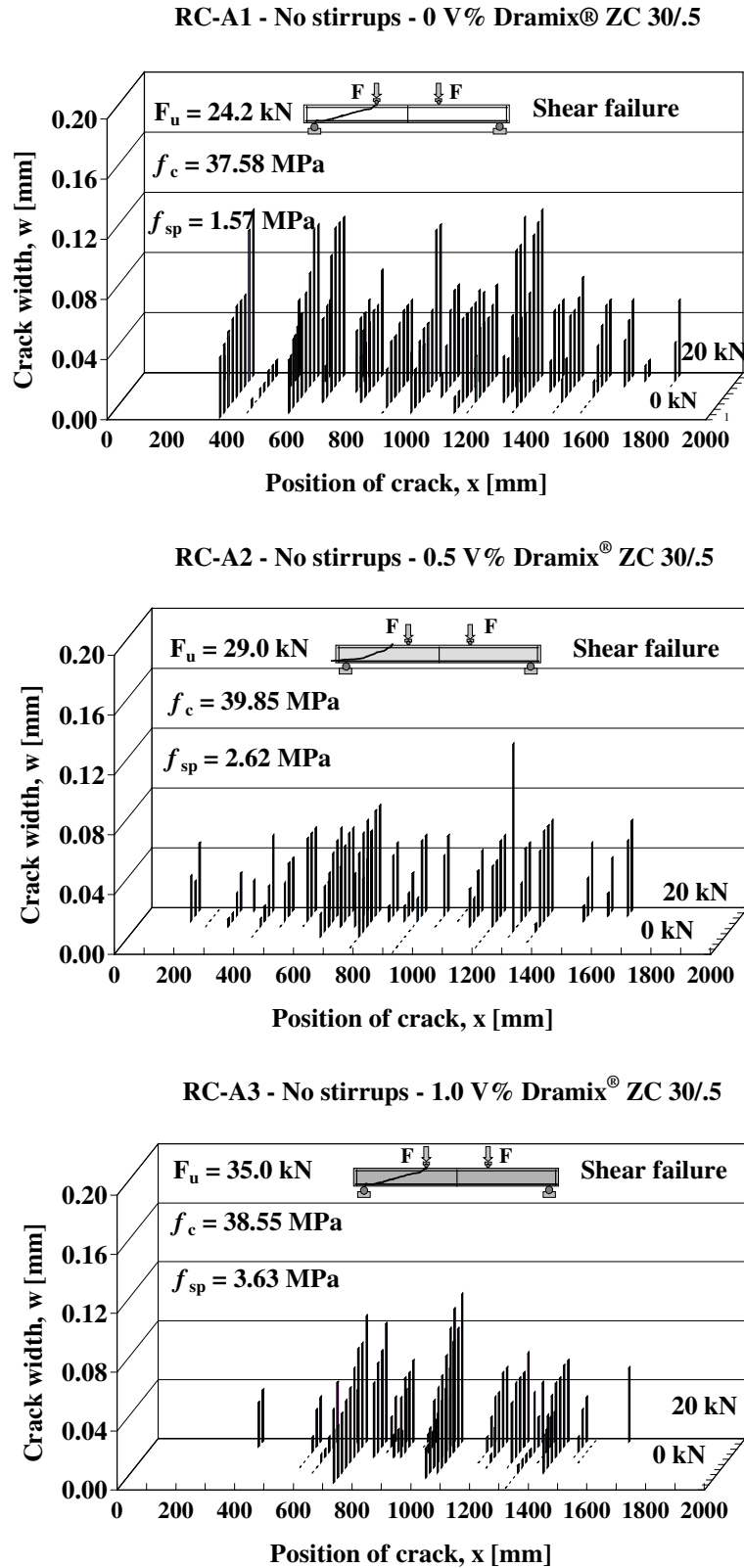
Cracking behaviour of steel fibre reinforced concrete beams measured crack widths values and development of cracks were analyzed on different ways.

Propagation of cracks as a function of the applied loads are presented on 3D diagrams for both series of beams. Beams denoted RC-A1...RC-A3 with no stirrup reinforcement and different fibre contents (0 V%, 0.5 V% and 1.0 V%) of Dramix<sup>®</sup> ZC 30/5 hooked-end steel fibres are given in Figure 4.9. Horizontal, vertical and inclined axis of the diagrams indicates the position of crack on the beam, the crack width measured at the level of the tensioned longitudinal reinforcement, and the applied load, respectively. Failure loads, failure modes, failure lines as well as cube strengths and splitting strengths are also presented. Generally, diagrams indicate more cracks in a portion of beam where failure appeared. These cracks formed at relatively low load levels and their continuous propagation indicates the final failure lines. For bending failure more homogenous crack pattern was developed. It was visually confirmed that crack propagation was favourably influenced by the increase of both hooked-end and crimped steel fibre contents.

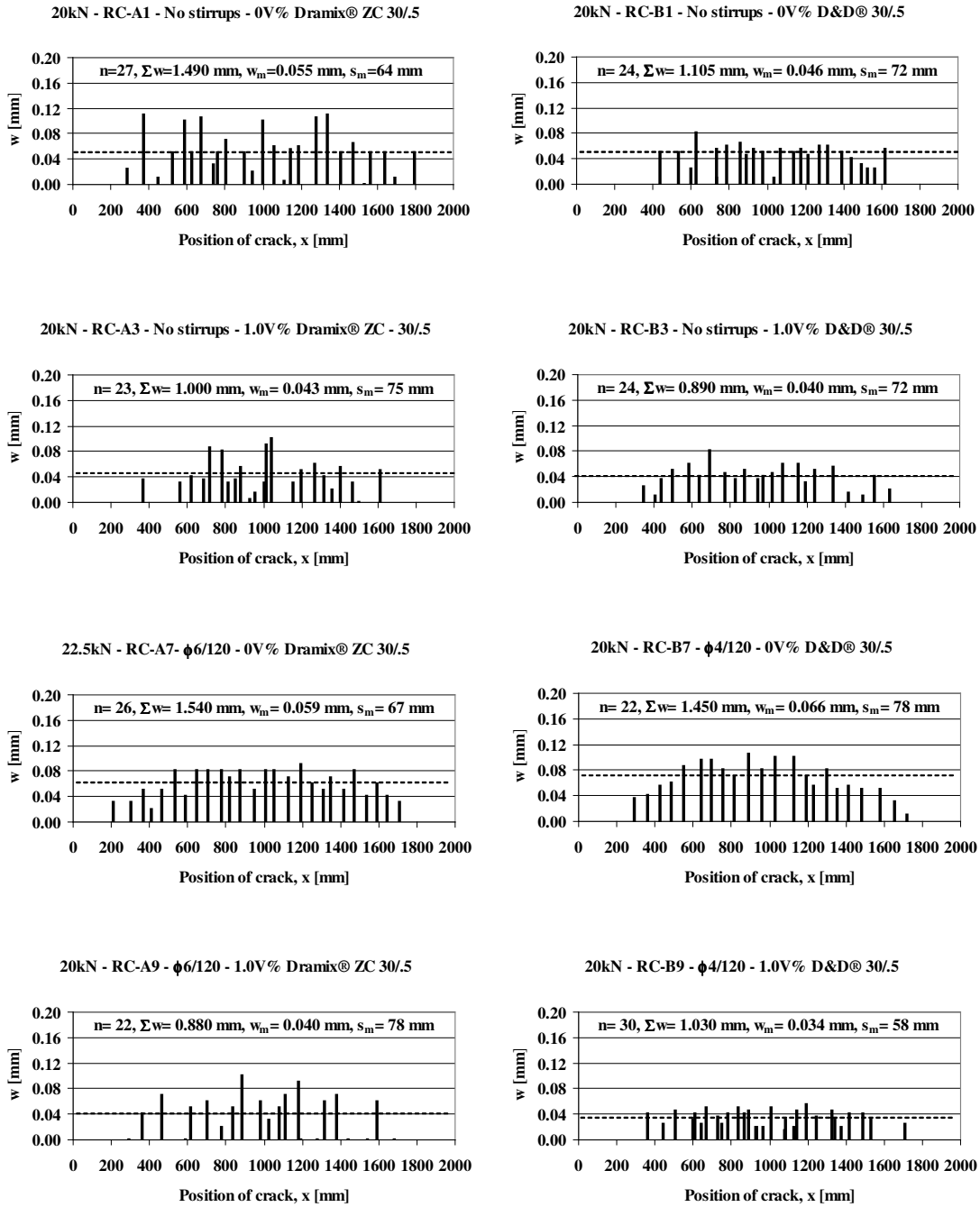
For further analysis, crack patterns to different load levels are separately represented. In this section beams made with 0 V% and 1.0 V% fibre contents are summarised for beams with no stirrup reinforcement and for beams having Ø6/120 and Ø4/120 stirrup reinforcements at 20 kN. The vertical axis of the diagram in Figure 4.10 indicates the measured crack width, the horizontal axis indicates the position of the crack formed on the beam. Position and height of the columns indicate the position of the crack and the measured crack width, respectively. Number of cracks, sum of crack widths, mean crack width and mean crack spacing are also given on the diagrams. Horizontal lines indicate the mean crack width at the given load.

Load vs. number of cracks, load vs. sum of crack widths, load vs. mean crack width and load vs. mean crack spacing relationships were developed for beams (Figure 4.11). Diagrams indicate that all relationships were influenced by the amount of steel fibres. Sum of crack widths and calculated mean crack width at a given load decreased applying 1.0 V% fibres independently from the amount of conventional shear reinforcement and the fibre type used related to beams containing no steel fibres. On the other hand, applying 1.0 V% D&D 30/5 crimped steel fibres, more cracks were developed, hence, smaller crack spacing was observed.

Further details on crack measurements are given in the Appendix in Figs. A1 to A32 and in Tables A1 to A18.

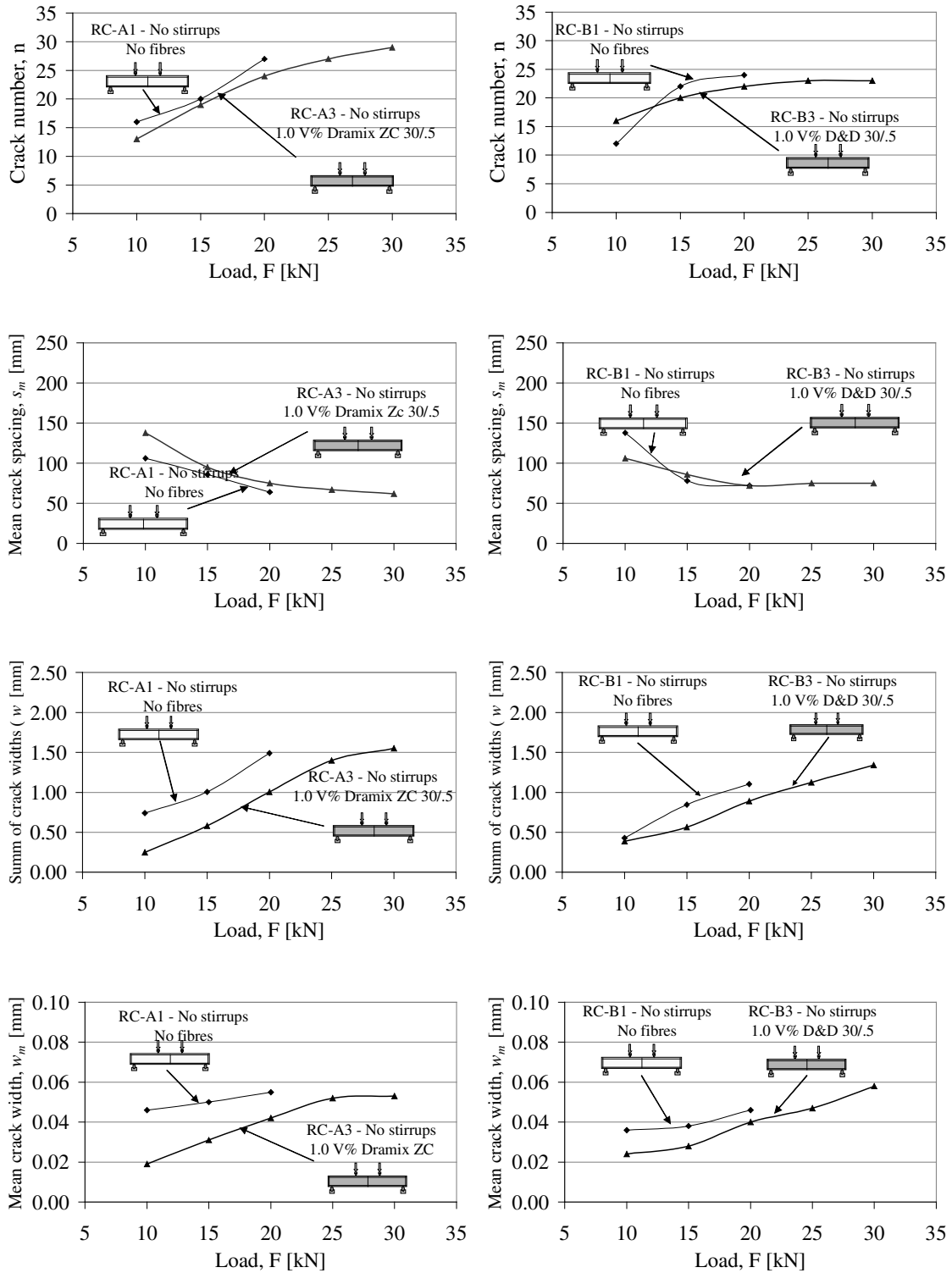


**Figure 4.9:** Development of cracks for beams RC-A1...RC-A3. Horizontal, vertical and inclined axis indicates the position of crack, measured crack width and the applied load, respectively.

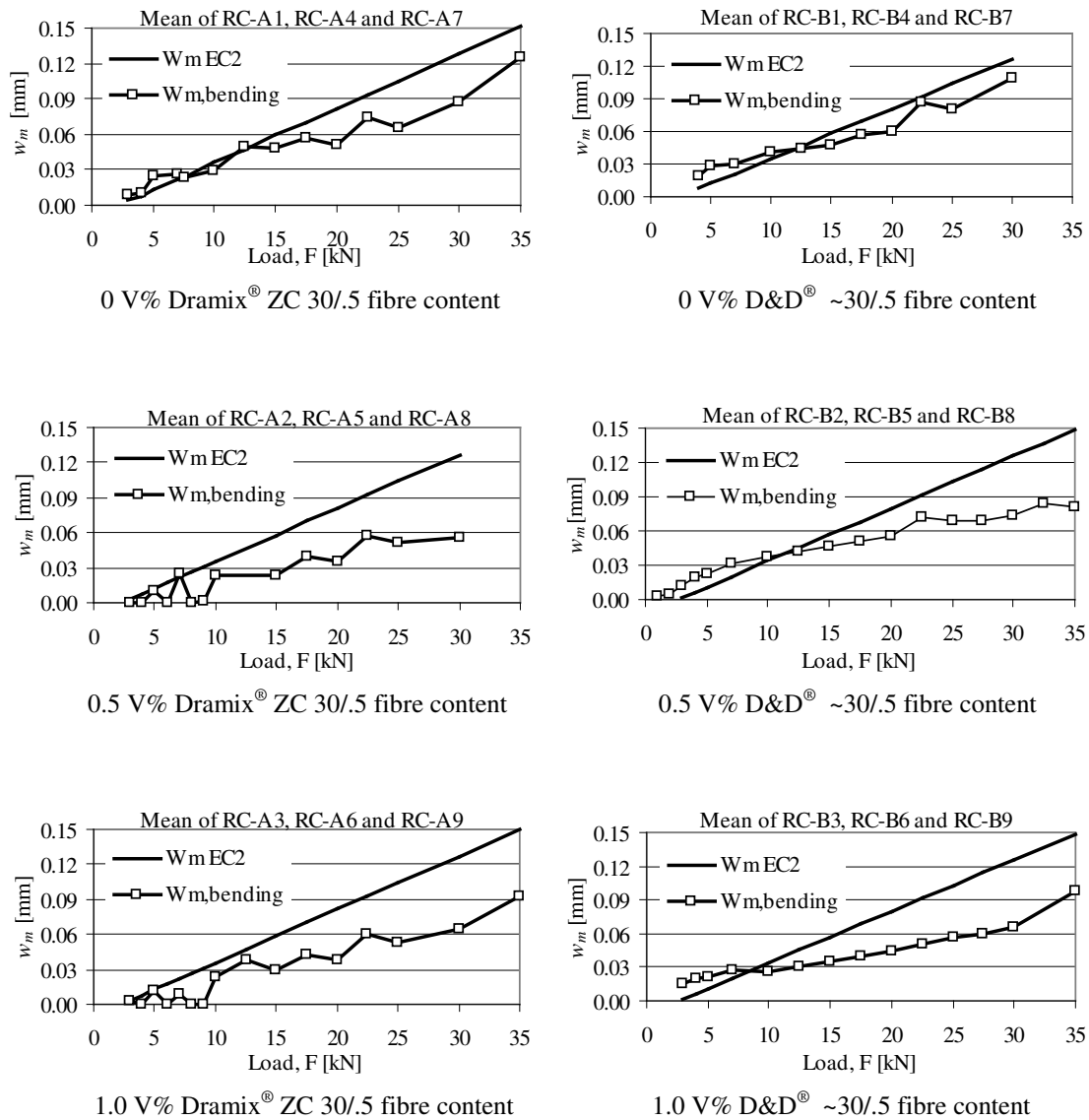


**Figure 4.10:** Crack pattern of beams RC-A1, RC-A3, RC-B1 and RC-B3 measured at 20 kN jack force. Horizontal and vertical axis respectively indicates the position of the crack formed on the beam and the measured crack width at the level of the tensioned reinforcing bars. Horizontal dotted line indicates the mean crack width at the given load.





**Figure 4.11:** Load vs. crack number, load vs. mean crack spacing, load vs. summa of crack width and load vs. mean crack width relationships for beams RC-A1... RC-A3 and for beams RC-B1...RC-B3 made with 0 V% and 1.0 V% Dramix® ZC 30/5 hooked-end and D&D® ~30/5 crimped steel fibres, respectively



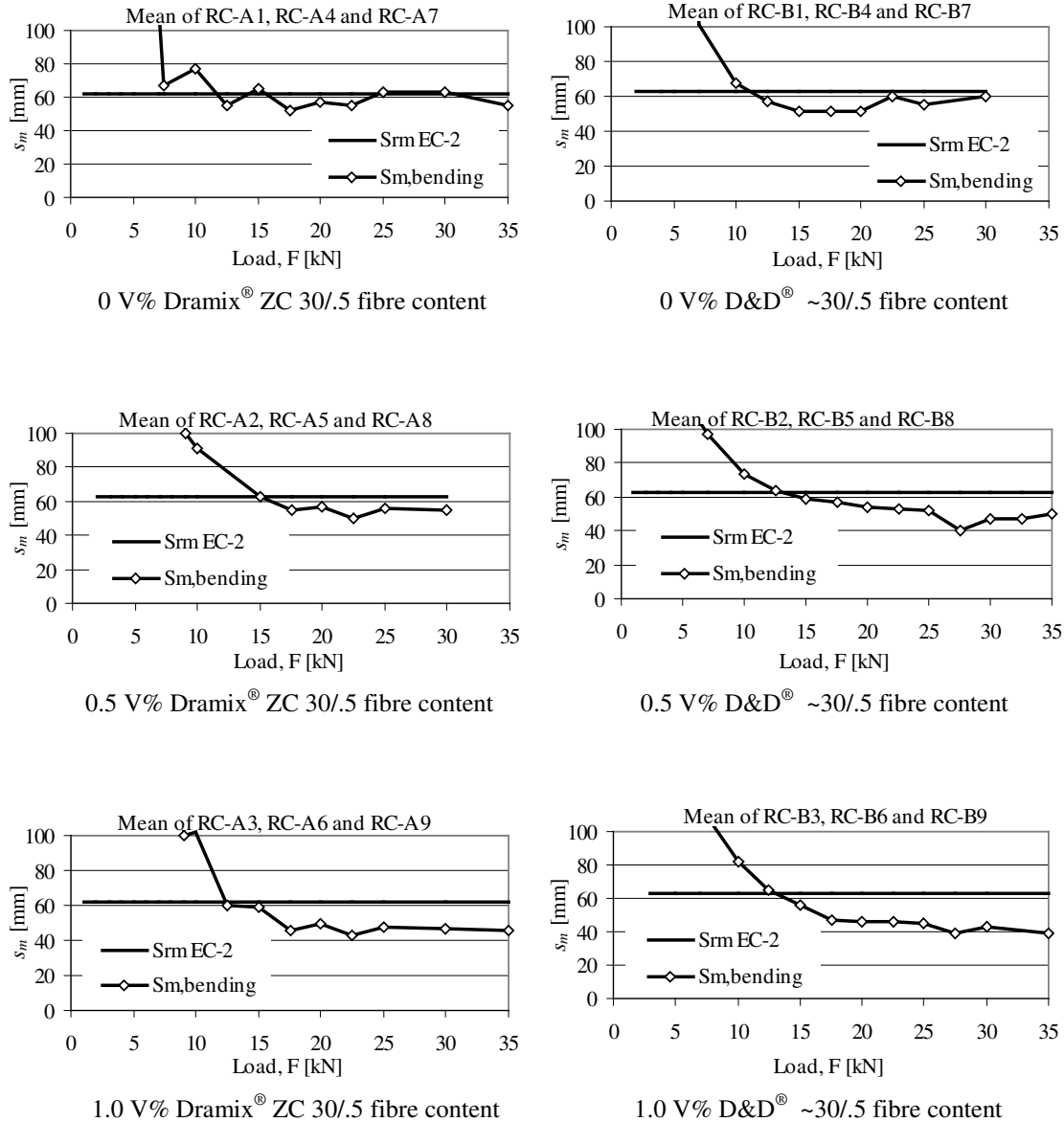
**Figure 4.12:** Crack widths as a function of the applied load. Diagrams represent the mean crack spacing of three beams containing the same steel fibre content.  $w_{m,EC2}$  and  $w_{m,bending}$  indicate the calculated crack width according to the EC-2 and the mean measured crack width considering only the bending portion of beams, respectively. First and second column indicates series RC-A (Dramix<sup>®</sup> ZC 30/.5 hooked-end fibres) and RC-B (D&D<sup>®</sup> ~ 30/.5 crimped fibres), respectively.

Based on the observed crack distributions, mean crack spacings were calculated for the bending portion of beams for the combined bending and shear portion of beams and for the whole beams in each load steps. The mean of the measured crack widths and the derived crack spacing as a function of the applied loads are summarised in Figure 4.12 and in Figure 4.13 considering only the bending portion of beams, respectively. Calculated crack widths and crack spacings according to the EC2 are represented with continuous lines. For the calculation according to EC2 measured crack widths and crack spacings for 0 V% steel fibre content were not considered at all.

For conventional reinforced concrete structures the following formula is used to determine the design value of crack width according to EC2:

$$w_k = \beta s_{rm} \varepsilon_{sm} \tag{4.1}$$

where  $\beta$  is a coefficient relating the average crack width to the characteristic value,  $s_{rm}$  is the average final crack spacing can be calculated as follows:



**Figure 4.13:** Crack spacing as a function of applied load. Diagrams represent the mean crack spacing of beams containing the same steel fibre content considering only the bending portions. Mean values of measured crack spacings  $s_{m,bending}$ , and the mean crack spacing determined according to the EC-2  $s_{m,EC2}$  are presented. First and second column indicates series RC-A (Dramix<sup>®</sup> ZC 30/.5 hooked-end fibres) and RC-B (D&D<sup>®</sup> ~ 30/.5 crimped fibres), respectively.

$$s_{rm} = 50 + 0.25k_1k_2 \frac{\varnothing}{\rho_r} \quad (4.2)$$

and  $\varepsilon_{sm}$  may be calculated from the relation:

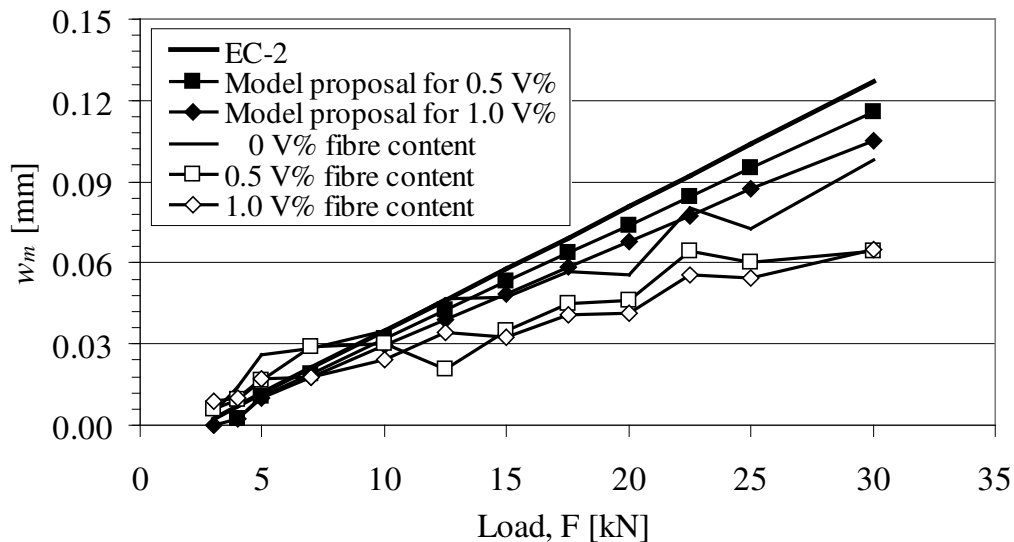
$$\varepsilon_{sm} = \frac{\sigma_s}{E_s} \left[ 1 - \beta_1\beta_2 \left( \frac{\sigma_{sr}}{\sigma_s} \right)^2 \right] \quad (4.3)$$

where the parameters of Eq. (4.1) to Eq. (4.3) are well discussed in EC2. Based on the experimental results a simple method for determine the average final crack width is developed taking into consideration the effect of steel fibres by only modifying the equation. Since the developed crack patterns were not significantly effect by the fibre characteristics, fibre type and other fibre parameters were not taking into consideration in the proposed model. Contribution of steel fibre content could be given by the following terms:

$$s_{rm} = 45 + 0.25k_1k_2 \frac{\varnothing}{\rho_r} \quad (4.4)$$

$$s_{rm} = 40 + 0.25k_1k_2 \frac{\varnothing}{\rho_r} \quad (4.5)$$

where Eq. (4.4) and Eq. (4.5) indicate the average crack spacings by applying 0.5 V% and 1.0 V% steel fibre contents, respectively. Measured crack widths and the proposed model as a function of the applied load are summarised in Figure 4.14.

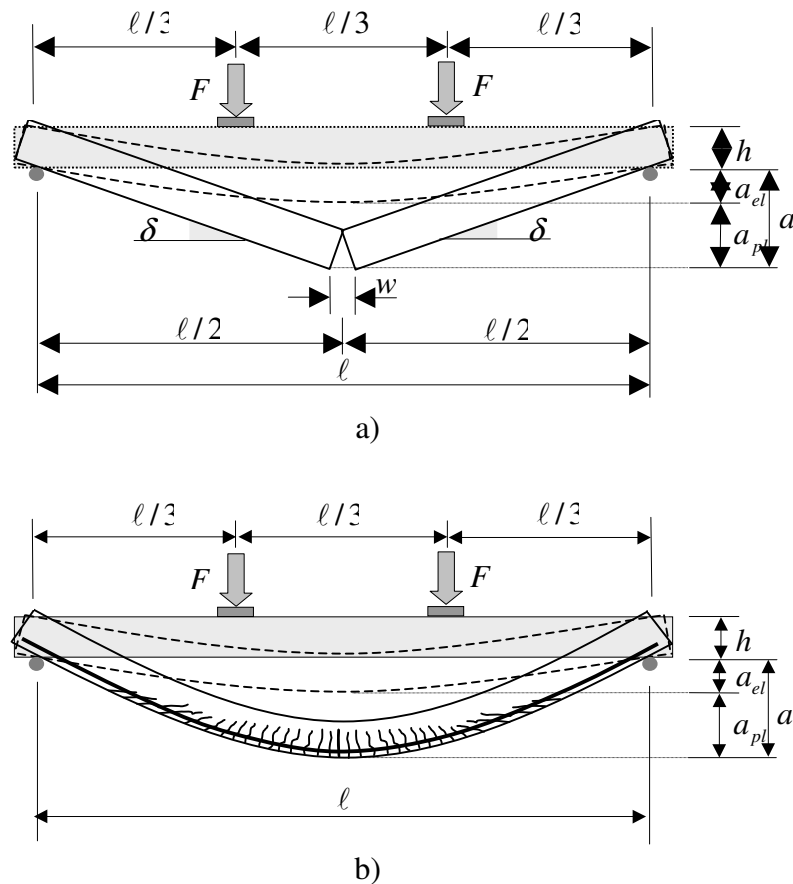


**Figure 4.14:** Load vs. crack width relationships for steel fibre reinforced concrete beams. Each curves noted by 0 V%, 0.5 V% and 1.0 V% fibre content represent mean curve of six beams.

### 4.3 Modelling of bending behaviour

Based on the developed one dimensional material model for fibre reinforced composite materials in Chapter 3, a simple design tool is worked out for steel fibre reinforced concrete beams in bending with or without longitudinal steel bars (Figure 4.15). Presented approach lies close to the conventional engineering calculation method for reinforced concrete members. Method of the equilibrium of internal forces in the cracked section is used. Materials are considered to be linear-elastic before cracking. Using the classical beam theory, plain sections before loading are assumed to remain plain even after cracking, which leads to linear strain distribution in the cross-section.

Beam is in an elastic state before cracking. When elastic limit strain is reached and exceeded, macro-cracks appear at the mid-section of the beam. After cracking, due to the plastic matrix-fibre interaction fibres are activated.



**Figure 4.15:** Behaviour of steel fibre reinforced concrete beams  
 a) steel fibre reinforced concrete beams with no longitudinal steel bars  
 b) steel fibre reinforced concrete beams with longitudinal steel bars

Since the increasing crack length modifies the stress field in the cross-section, fibre activation starts with a plastic matrix-fibre interaction, which yields fibre yielding and/or softening/hardening under increasing load. Furthermore, secondary macro-cracks will not be appeared in the close vicinity as observed in the case of conventional reinforced concrete beams. Such behaviour can be considered as a rigid hinge mechanism for beams made with no longitudinal steel bars (Figure 4.15).

Moment capacity of the cross-section can be calculated when the ultimate tension strain of steel fibre reinforced concrete. The ultimate tension strain depends on the material parameters such as concrete composition, fibre content, fibre type, fibre orientation.

Some characteristic steps of stress - strain distributions can be seen in Figure 4.16 under increasing load considering the simplified one-dimensional model for steel fibre reinforced concrete developed in Chapter 3. Applying also steel bars in the section the classical design process of reinforced concrete section can be used as shown in Figure 4.17.

Characteristic stress – strain relationships for steel fibre reinforced concretes offers a possibility to compute not only the ultimate limit state, but also the serviceability state.

From the given data base which contains the stress – strain relationships for tension and compression, and the material parameters, ultimate limit state can be determined with a simple iteration process. In order to reduce the iteration steps, first we consider the ultimate tension strain,  $\epsilon_{t3}$ , of steel fibre reinforced concrete as tension strain developed at the most tensioned fibre of the section. Then we consider a curvature,  $\kappa$ , or a compressive strain,  $\epsilon_c$  value as the strain of the most compressed fibre of the section. Now, neutral axis of the section can be determined. Using the applied strain distribution and the given stress-strain relationships, the internal forces of the section can be computed. The equilibrium state is governed by the following condition:

$$0 = N_c + N_t \quad (4.6)$$

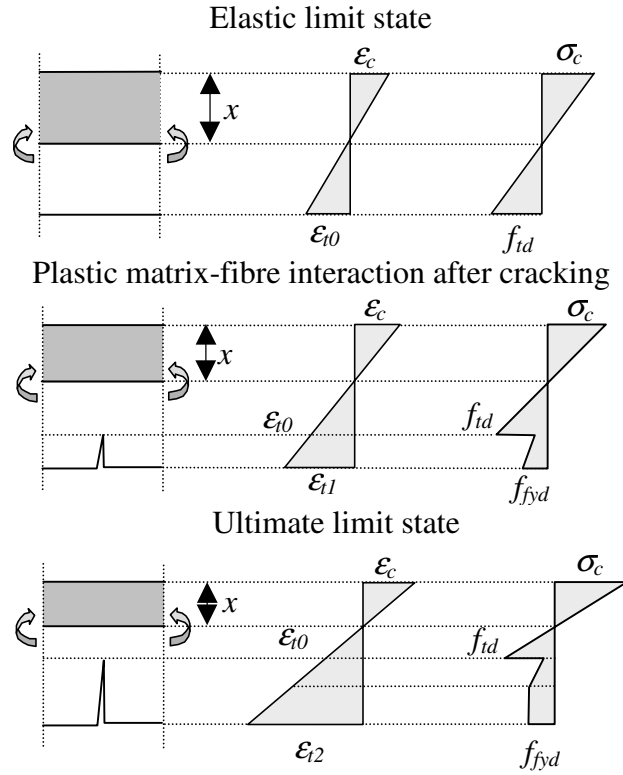
where:

$$N_c = \int_0^x \sigma_c(x) dx \quad \text{and} \quad N_t = \int_x^h \sigma_t(x) dx + N_s \quad (4.7)$$

$N_s$  represents the force in the steel bars. If the condition in Eq. (4.6) is false, we should apply a curvature or compressive strain value again to get a new position of neutral axis. We have to use this procedure until the condition in Eq. (4.6) is fulfilled. When we find the neutral axis, the moment capacity of the section is given by:

$$M_u = N_c z = N_t z \quad (4.8)$$

where  $z$  is the lever arm of the internal forces. Stress and strain distribution of the cross-section with the model parameters can be seen in Figure 4.18. Calculation process with or without steel bars are summarised in algorithms. Block diagrams of the algorithms are summarised in Figure 4.19 and Figure 4.20.



**Figure 4.16:** Stress and strain distributions of steel fibre reinforced concrete beam with no longitudinal steel bars in pure bending

An example to calculate the ultimate moment capacity of steel fibre reinforced concrete cross-section based on the characterised stress-strain relationship considering the simplified one-dimensional material model (elastic-brittle matrix and elastic-perfectly plastic fibre) developed in Chapter 3 is presented here. The equilibrium of internal forces can be expressed as a sum of the internal force components:

$$N_c + N_t^1 + N_t^2 + N_t^3 = 0 \quad (4.9)$$

where  $N_c$  represents the force in the compressive zone while  $N_t^1$ ,  $N_t^2$  and  $N_t^3$  denote the forces acting in the tensioned zone of the cross-section, as defined in Figure 4.19:

$$N_c = \frac{1}{2} K_0 \varepsilon_{t2} \zeta h^2 \cdot \frac{\xi^2}{1-\xi} = A \cdot \frac{\xi^2}{1-\xi} \quad (4.10)$$

$$N_t^1 = \frac{1}{2} (K_0 - K_1) \alpha \varepsilon_{t2} \zeta h^2 \cdot (1-\xi) = B \cdot (1-\xi) \quad (4.11)$$

$$N_t^2 = \frac{1}{2} K_1 \beta^2 \varepsilon_{t2} \zeta h^2 \cdot (1-\xi) = C \cdot (1-\xi) \quad (4.12)$$

$$N_t^3 = K_1 \beta (1-\beta) \varepsilon_{t2} \zeta h^2 \cdot (1-\xi) = D \cdot (1-\xi) \quad (4.13)$$

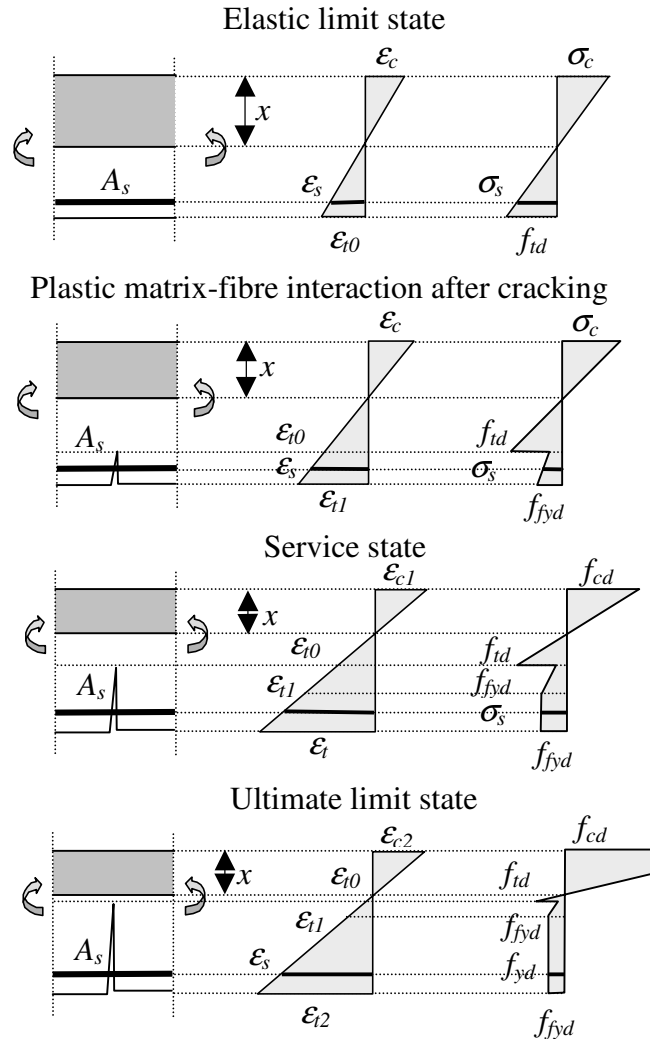


Figure 4.17: Stress and strain distribution of FRC cross-section applying also steel bars for bending

where  $\xi = \frac{x}{h}$  denotes the position of the neutral axis vs. dept of the cross-section ratio;

$\zeta = \frac{b}{h}$  denotes the width of the cross-section vs. dept of the cross-section ratio,

considering rectangular cross-section;  $\alpha = \frac{\epsilon_{i0}}{\epsilon_{i2}}$  represents the elastic tension limit strain

vs. ultimate tension strain ratio of the fibre reinforced concrete; and  $\beta = \frac{\epsilon_{i1}}{\epsilon_{i2}}$  indicates

the yielding strain of fibre reinforced concrete vs. ultimate tension strain of fibre reinforced concrete. Using Eq. (4.10) to Eq. (4.13) in Eq. (4.9) and after the simplification we obtain:



$$(A - B - C - D)\xi^2 + 2(B + C + D)\xi - (B + C + D) = 0 \quad (4.14)$$

From which the neutral axis can be determined and the moment capacity reads:

$$M_u = M_c + M_t^1 + M_t^2 + M_t^3 \quad (4.16)$$

where the components are the following:

$$M_c = \frac{2}{3} A \frac{\xi^3}{1 - \xi} h \quad (4.17)$$

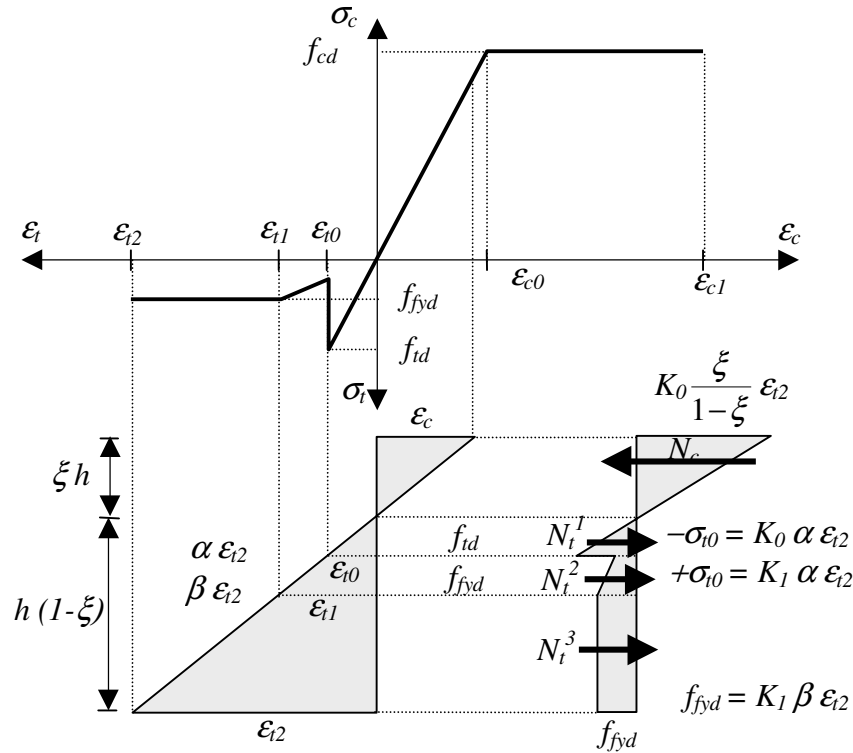
$$M_t^1 = \frac{2}{3} B \alpha (1 - \xi)^2 h \quad (4.18)$$

$$M_t^2 = \frac{2}{3} C \beta (1 - \xi)^2 h \quad (4.19)$$

$$M_t^3 = \frac{1}{2} D (1 - \beta) (1 - \xi)^2 h \quad (4.20)$$

Model parameters of the presented approach are the following:

- $f_{cd}$ : design value for the compressive strength of steel fibre reinforced concrete
- $f_{td}$ : design value for the tensile strength of steel fibre reinforced concrete
- $f_{fyd}$ : design value for the yield strength of steel fibre reinforcement
- $\varepsilon_{c0}$ : elastic limit strain of steel fibre reinforced concrete in compression can be determined as  $\varepsilon_{c0} = f_{cd} / K_0$
- $\varepsilon_{c1}$ : ultimate limit strain of steel fibre reinforced concrete in compression can be considered as  $\varepsilon_{c1} = 3.5^0 / 00$ )
- $\varepsilon_{i0}$ : elastic limit strain of steel fibre reinforced concrete in tension can be determined as  $\varepsilon_{i0} = f_{td} / K_0$
- $\varepsilon_{i1}$ : strain for yielding of steel fibre reinforcement can be determined for the simplest material model as  $\varepsilon_{i2} = f_{fyd} / K_1$
- $\varepsilon_{i2}$ : ultimate limit strain of steel fibre reinforced concrete in tension can be determined according to the material and structural parameters of the member:
  - a) crack width control for rigid hinge mechanism:  $\varepsilon_{i2} = \frac{w_{max}}{\ell} = \frac{4a_{max}h}{\ell^2}$
  - c) strain control for RC member:  $\varepsilon_{i2} = \varepsilon_{uk}$
- $K_0$ : elastic modulus of steel fibre reinforced concrete can be considered to be equal to the elastic modulus of plain concrete
- $K_1$ : elastoplastic modulus of steel fibre reinforced concrete can be determined experimentally for different concrete mix proportions



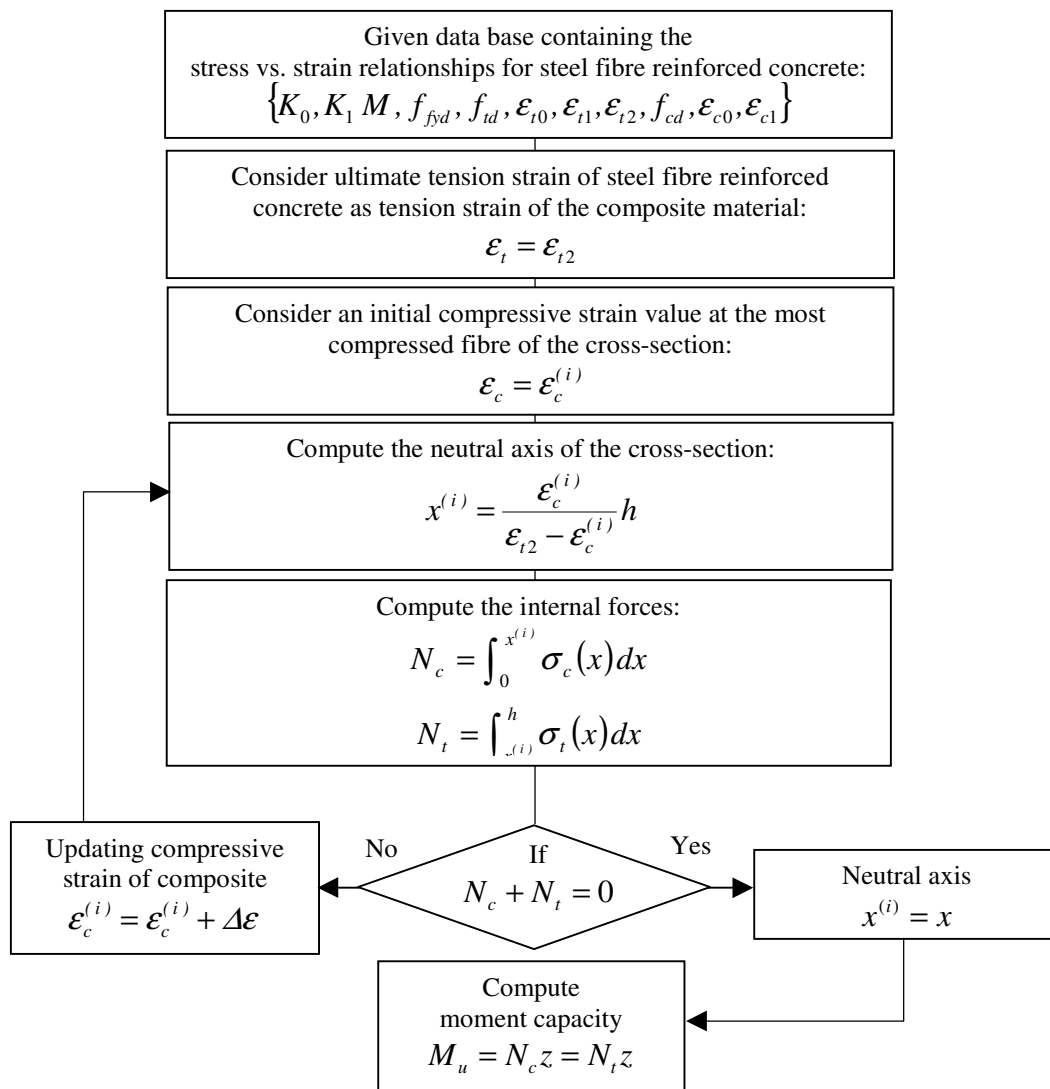
**Figure 4.18:** Determination of moment capacity for steel fibre reinforced concrete

## 4.4 Conclusions

Based on the experimental and theoretical results of bending behaviour of steel fibre reinforced concrete beams the following conclusions can be drawn:

1. **Steel fibre reinforcement** can be effectively used to **increase shear capacity** of reinforced concrete beams especially for beams containing no conventional stirrup reinforcements (RC-A1...A3 and RC-B1...RC-B3).
2. **Failure mode** of beams with no steel fibres and no stirrups was very **brittle**. When **steel fibre reinforcement** was applied, failure became **more ductile**. Failure mode of beams **changed from shear** failure to simultaneous shear and **bending failure** or **clear bending** failure by increasing steel fibre content.
3. **Significant improvement** in **ductility** of reinforced concrete beams was obtained applying steel fibre reinforcement.
4. **Bending capacity** of over reinforced concrete beams were **not significantly** effected by the **steel fibre content**, but produce **tougher behaviour** than in the case of beams made of plain concrete.

5. **Steel fibre** reinforcement can **effectively** be used to **control crack width** and **crack propagation** in reinforced concrete beams. Applying steel fibre reinforcement for reinforced concrete beams **smaller mean crack width** and **grater mean crack spacing** values were obtained related to beams made of plain concrete. However, cracking behaviour was not significantly influenced by the type of steel fibre.
6. Based on the **experimental results** on steel fibre reinforced concrete beams a **modified EC2** calculation was developed for determining **crack width** of reinforced concrete beams applying also **steel fibres**.
7. Based on the **developed mechanical** model for fibre reinforced composite materials in Chapter 3, a simple **design method** was worked out for the analyses of steel fibre reinforced concrete structural elements with or without longitudinal steel bars in **bending**. Model is based on the conventional engineering method used in structural design.



**Figure 4.19:** Stress - strain relationships for steel fibre reinforced concrete

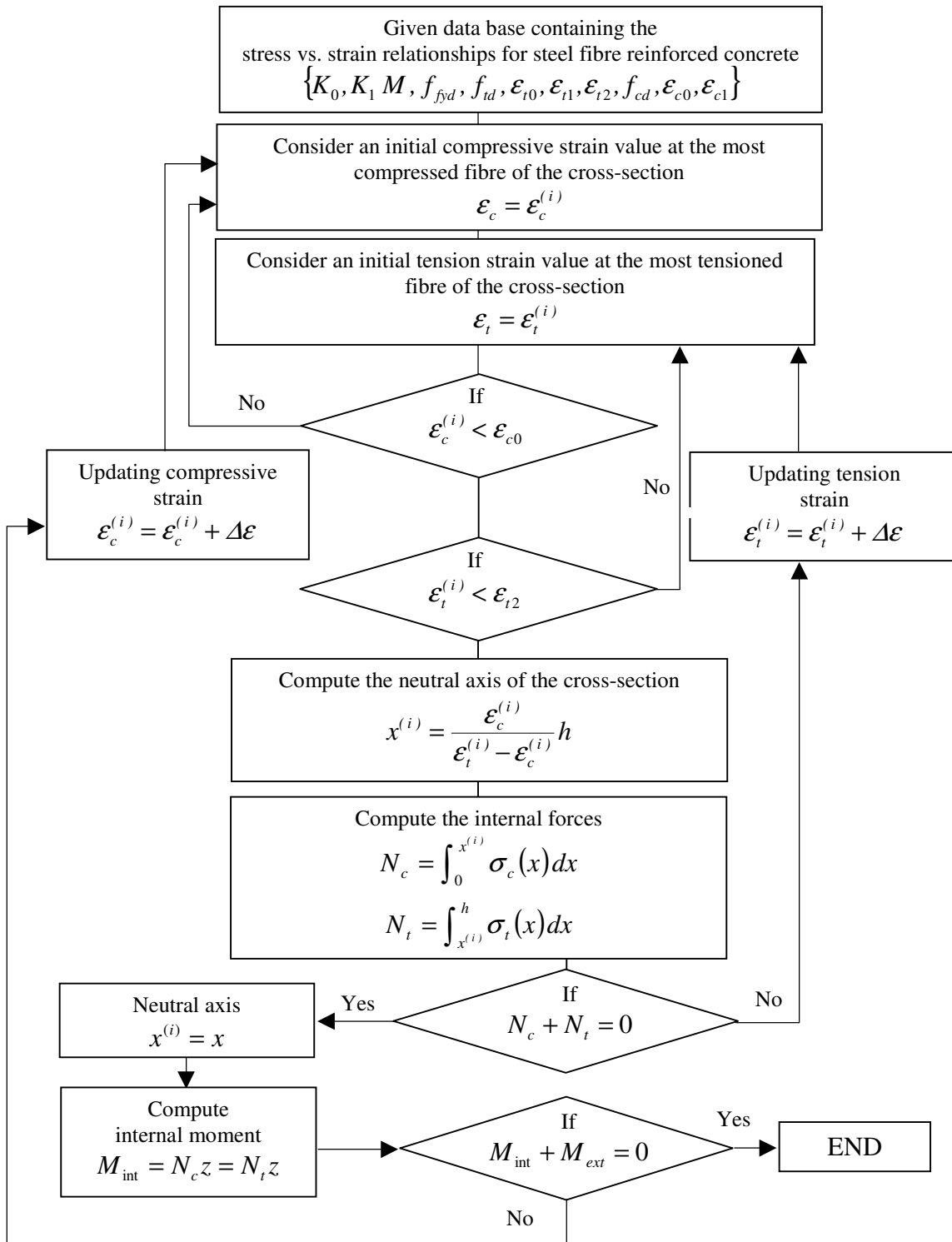


Figure 4.20: Analysis of steel fibre reinforced concrete cross-section in bending

# Chapter 5

## Behaviour of steel fibre reinforced prestressed pretensioned concrete beams

*Similarly to the reinforced concrete beams two series of steel fibre reinforced prestressed pretensioned concrete beams were tested. Experimental parameters were the fibre content (0 V%, 0.5 V%, 1.0 V% hooked-end steel fibre) and the release mode of the prestressing force (gradual and sudden). Experimental constants were the beam geometry and the type of prestressing strand. Beams did not contain any non-prestressed reinforcement.*

*Tests aimed to investigate the effect of steel fibre reinforcement on the transfer length of prestressing strands and the structural behaviour of prestressed concrete. Concrete deformations, released prestressing forces, draw-in of prestressing strands as well as camber of mid-sections were measured during release of prestressing force. Transfer length of prestressing strand was calculated. Finally, bending tests were carried out on the beams determining the failure load and failure mode.*

**Keywords:** *prestressing force, prestressing strand, PC beams, sudden release, gradual release, concrete deformations, end-slip, camber, transfer length*

### 5.1 Experimental programme

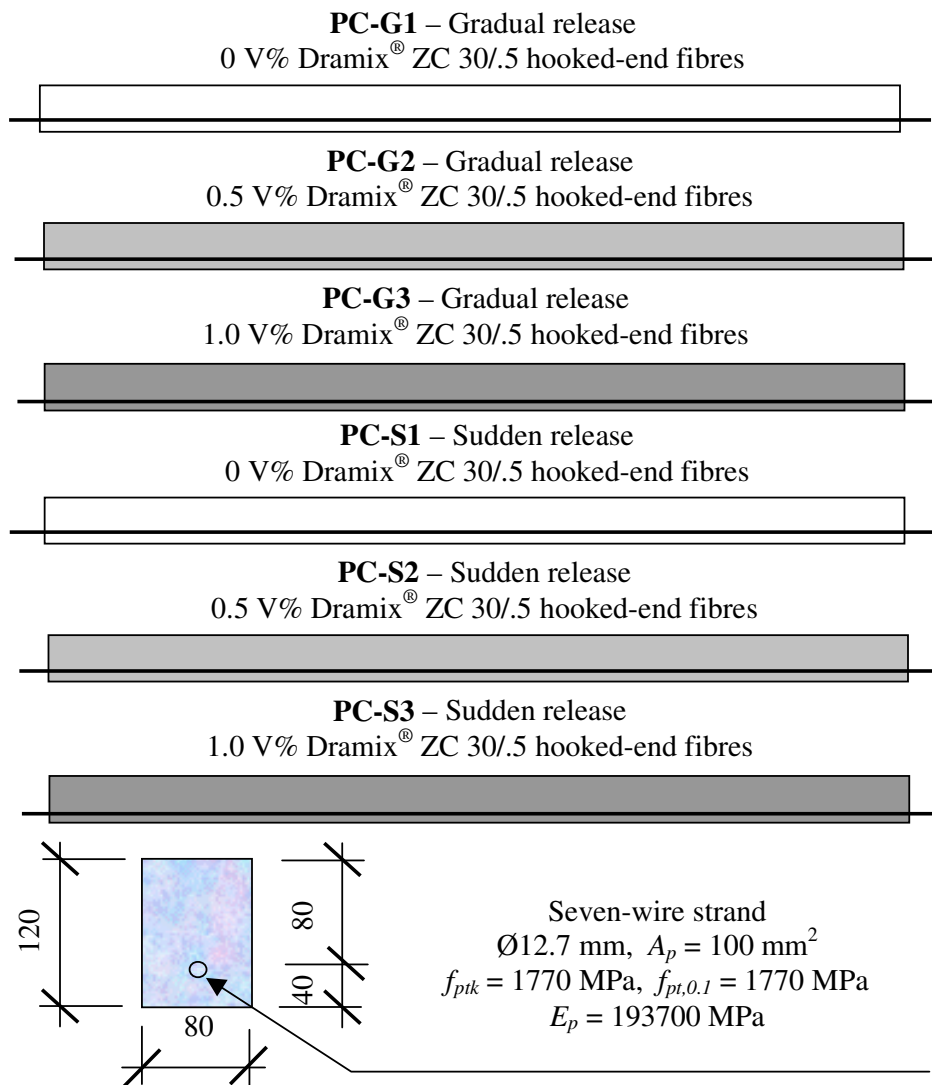
#### 5.1.1 Test specimens and experimental variables

Purpose of the present test series was to study the effect of steel fibres on the structural performances on the prestressed pretensioned concrete beams. Within the experimental program 6 prestressed pretensioned concrete beams were tested applying different fibre contents (0 V%, 0.5 V% and 1.0 V%). Two different mode of release of prestressing force (gradual or sudden release) were applied. Experimental constants were the geometry of the beams and the prestressed reinforcement as well as the type of steel fibre.

Appropriate values of the experimental constants such as the geometry of the beam and the type of prestressing strand were determined according to the following three aspects. *First*, specimens should have geometry as simple as possible, having a

cross-section so that the concrete deformations to be measurable. *Second*, prestressing strand should be placed at the core point of the section to avoid cracking of the section during tension release. *Third*, beams should have a length so that the transfer of the prestressing force can be completely developed within the half of the beam. Hence, all beams were cast with rectangular cross-sections with the geometry of 80×100 mm, prestressed by a seven-wire prestressing strand (characteristic tensile strength: 1770 MPa, nominal yielding strength: 1550 MPa, cross-sectional area: 100 mm<sup>2</sup>) with the diameter of 12.7 mm placed at the core point of the section. Lengths of beams were 2,00 m. Specimens did not contain any other non-prestressed longitudinal reinforcement or stirrup reinforcement except the prestressing strand.

Anchorage properties of reinforcement placed at the end-block region play an important role in the development of prestressing force. End-blocks without transverse reinforcements may crack longitudinally resulting in lower resistance.



**Figure 5.1:** Reinforcing details of prestressed pretensioned concrete beams

**Table 5.1:** *Steel fibre reinforced prestressed pretensioned concrete beams*

Fiber type	Mixture	Release of prestressing force		Compressive strength $f_c$ [MPa]	Splitting strength $f_{sp}$ [MPa]
		Gradual	Sudden		
Dramix <sup>®</sup> ZC 30/.5	REF-3	PC-G1	-	37.58	1.57
	FRC-3 <sup>0.5</sup> ZC 30/.5	PC-G2	-	39.85	2.62
	FRC-3 <sup>1.0</sup> ZC 30/.5	PC-G3	-	38.55	3.63
Dramix <sup>®</sup> ZC 30/.5	REF-4	-	PC-S1	42.70	1.60
	FRC-4 <sup>0.5</sup> ZC 30/.5	-	PC-S2	43.60	2.73
	FRC-4 <sup>1.0</sup> ZC 30/.5	-	PC-S3	41.60	3.70

In order to study the effect of steel fibres on the transfer length of prestressing strands, Dramix<sup>®</sup> ZC 30/.5 hooked-end steel fibres were applied. As in the case of reinforced concrete beams detailed in Chapter 4, three different fibre contents were applied: 0 V%, 0.5 V% and 1.0 V%, respectively.

In practice the release of the prestressing force is generally sudden by cutting the strand. In such a case the transfer length is being developed very quickly without any control possibility during release. However, in case of gradual release of prestressing force concrete deformations, draw-in of strands and the released portion prestressing force are measurable offering possibility to determine the length required to develop the effective prestressing force.

Release of prestressing force was sudden for series PC-S and gradual for series PC-G, respectively (Figure 5.1, Table 5.1).

### 5.1.2 Test set-up and experimental procedure

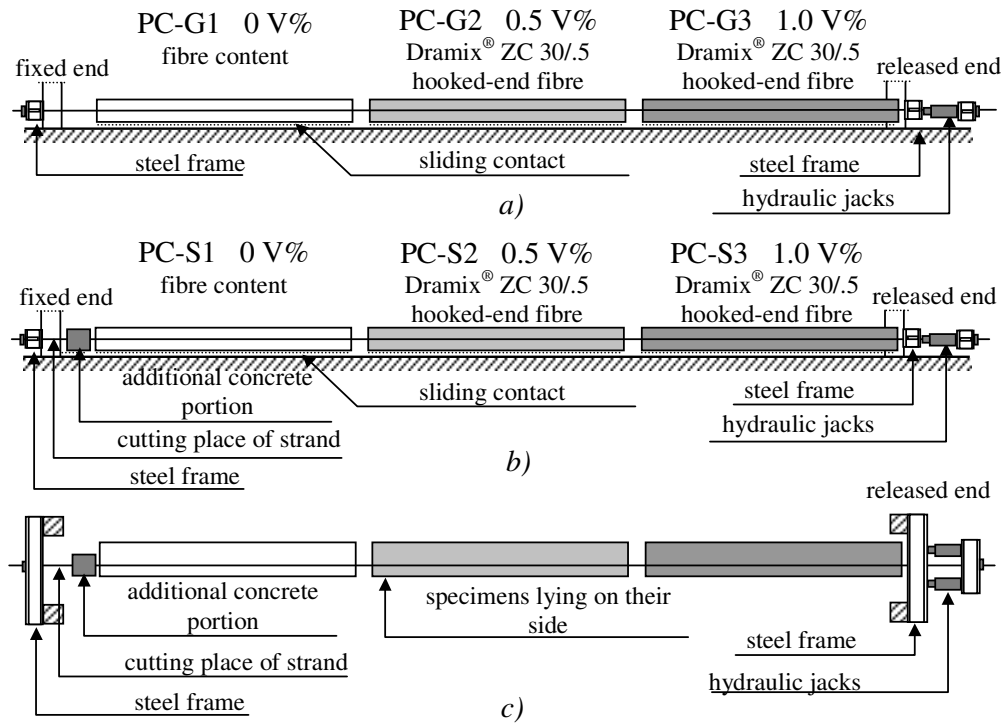
Within one series three specimens were prestressed along one 12.30 m long seven-wire strand (Figure 5.2).

Prestressing force was released by two LZM 40/200 LUKAS type hydraulic jacks with the maximum capacity of 400 kN which were placed at a rigid steel frame shown in Photo 5.1. A steel frame was placed at the fixed end similarly to the released end (Figure 5.2).

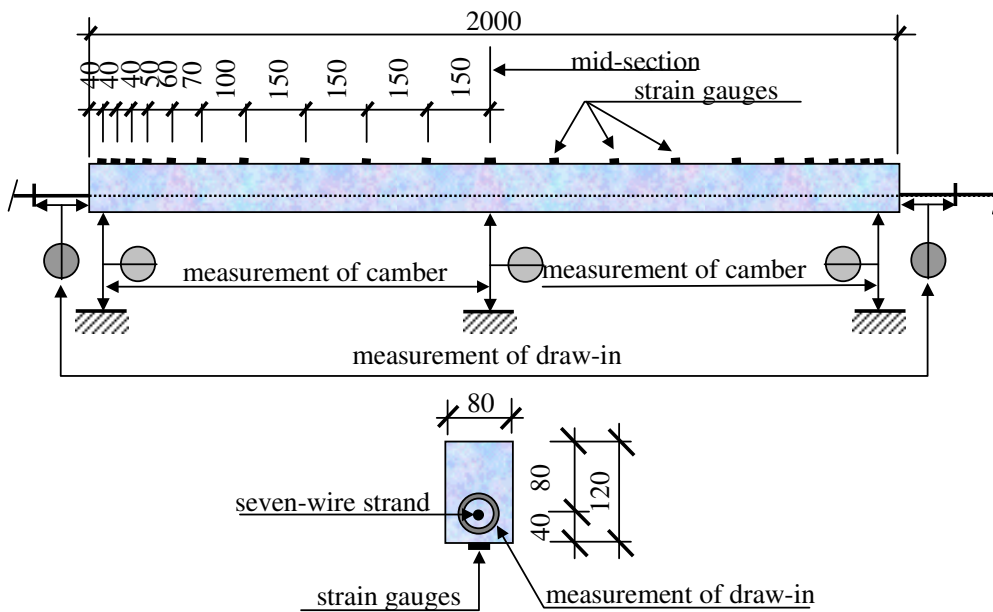
Gradual release of prestressing force for Series PC-G was measured by KYOWA PGKU 500 type stress measuring equipment inserted into the hydraulic system. Sensitivity of the measuring device was 0.1 kN. Force measurements were controlled by the length variation of the tensioned strand.

In case of Series PC-S an additional concrete block was placed between the end of specimens and the steel frame reducing the effect of impact when tension force was suddenly released (Photo 5.2). Sudden release was produced by flame cutting of the seven-wire strand between the rigid steel frame at the fixed end and the additional concrete block as shown in Figure 5.2/b.

Concrete strains were measured with KYOWA type strain gauges of 20 mm length on the most compressed surface of the members (Figure 5.3 and Photo 5.3). Strain gauge arrangement followed the change of the prestressing force. Shorter strain gauge spacing was applied at the end block regions and wider spacing in the middle portions of the specimens

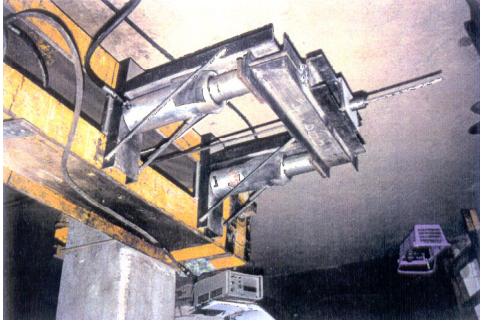


**Figure 5.2:** Arrangement of specimens during tension release  
 a) arrangement for specimens with gradual release  
 b) arrangement for specimens with sudden release (side-view)  
 c) arrangement for specimens with sudden release (top-view)

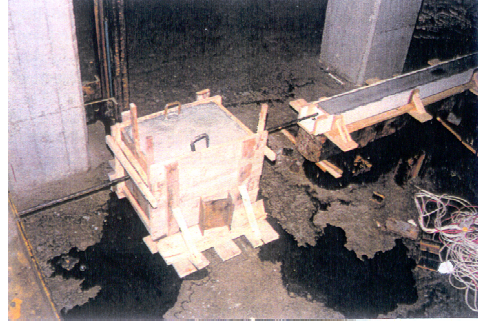


**Figure 5.3:** Measuring of concrete strains, camber of beam and draw-in of strand for PC beams

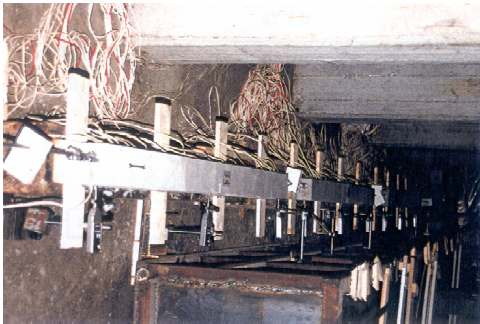




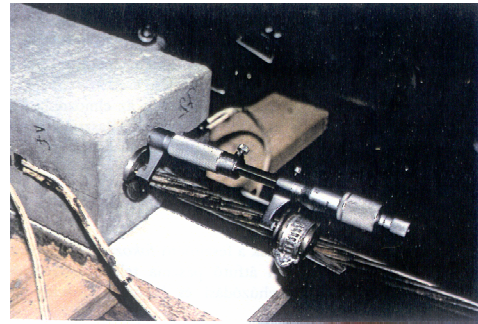
**Photo 5.1:** Hydraulic jack and rigid steel frame support at the released end



**Photo 5.2:** Additional concrete portion reducing the impact forces for PS-C



**Photo 5.3:** Strain gauges on the most compressed surface of PC beams



**Photo 5.4:** Measuring device of strand draw-in

Consequently, 21 strain gauges were placed on each beam. One gauge was placed at the mid-section of the beam and the other 20 gauges were positioned symmetrically on the beam. Strand draw-in,  $s_e$ , with other words the relative displacement between the concrete and strand section was measurable at the butt end of the beam. For determining the draw-in of prestressing strand, a special steel ring measuring devices were fixed to the strand as well as to the butt end of the elements having three imprinted steel balls on each ring in the same position (Figure 5.3). Steel ball distances between the to fixed rings were measured during the tension release with a mechanical measuring device having 0.005 mm sensitivity in each load steps on the both side of the beams as sown in Photo 5.4. Displacement of each member was also measured by MITUTOYO type dial gauges of 0.01 mm sensitivity at the middle section and at both ends (Figure 5.3) to determine camber in each load steps.

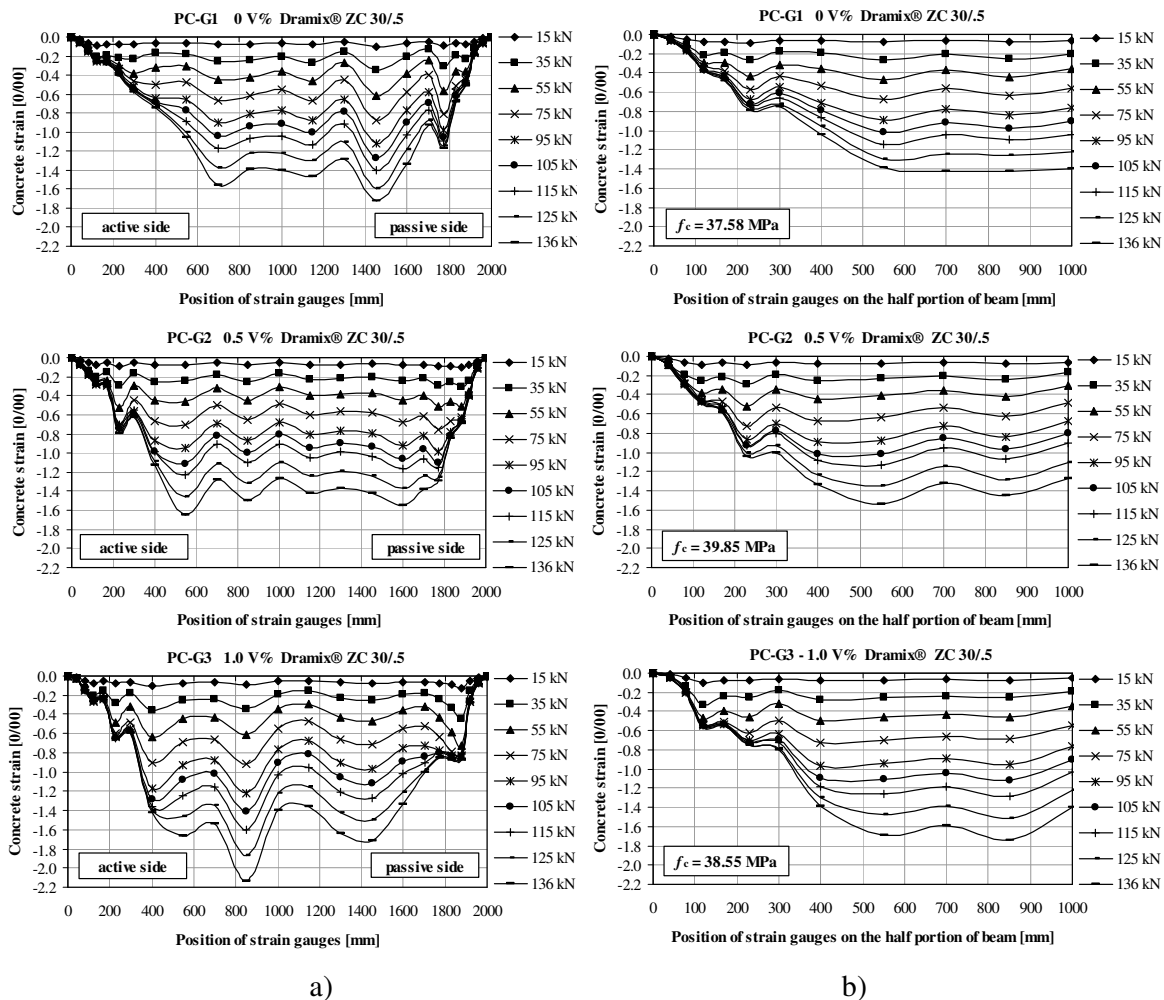
The total applied prestressing force was 136 kN for both Series of beams. When the prestressing force was gradually released (series PC-G), concrete deformations, draw-in of prestressing strand as well as prestressing force were measured at each step of releasing prestressing force and further in time after releasing the total prestressing force as well. Values of released prestressing force were: 15 kN, 35 kN, 55 kN, 75 kN, 95 kN, 105 kN, 115 kN, 125 kN and finally 136 kN in case of gradual release. Deformation measurements continued after total release in 18 h, 25 h, 44 h, 72 h, 116 h, 165 h, 218 h, 381 h, 721 h and 980 h. In case of sudden release of prestressing force the measurements were taken in 1 h, 4 h, 17 h, 43 h, 70 h and 193 h.

## 5.2 Experimental observations and test results

### 5.2.1 Concrete strains during tension release

Concrete strains on the most compressed face of the beam were measured as discussed in Section 5.2. All together 63 strain gauges were used for series PC-G and PC-S, respectively. However, in case of series PC-S, several additional strain gauges were used to study the effect of sudden release of prestressing force on the behaviour of end-block region by acoustic-emission method, which is not discussed here.

Measured concrete compressive strains along the total beam as a function of the released prestressing force are summarised in Figure 5.4/a for series PC-G.

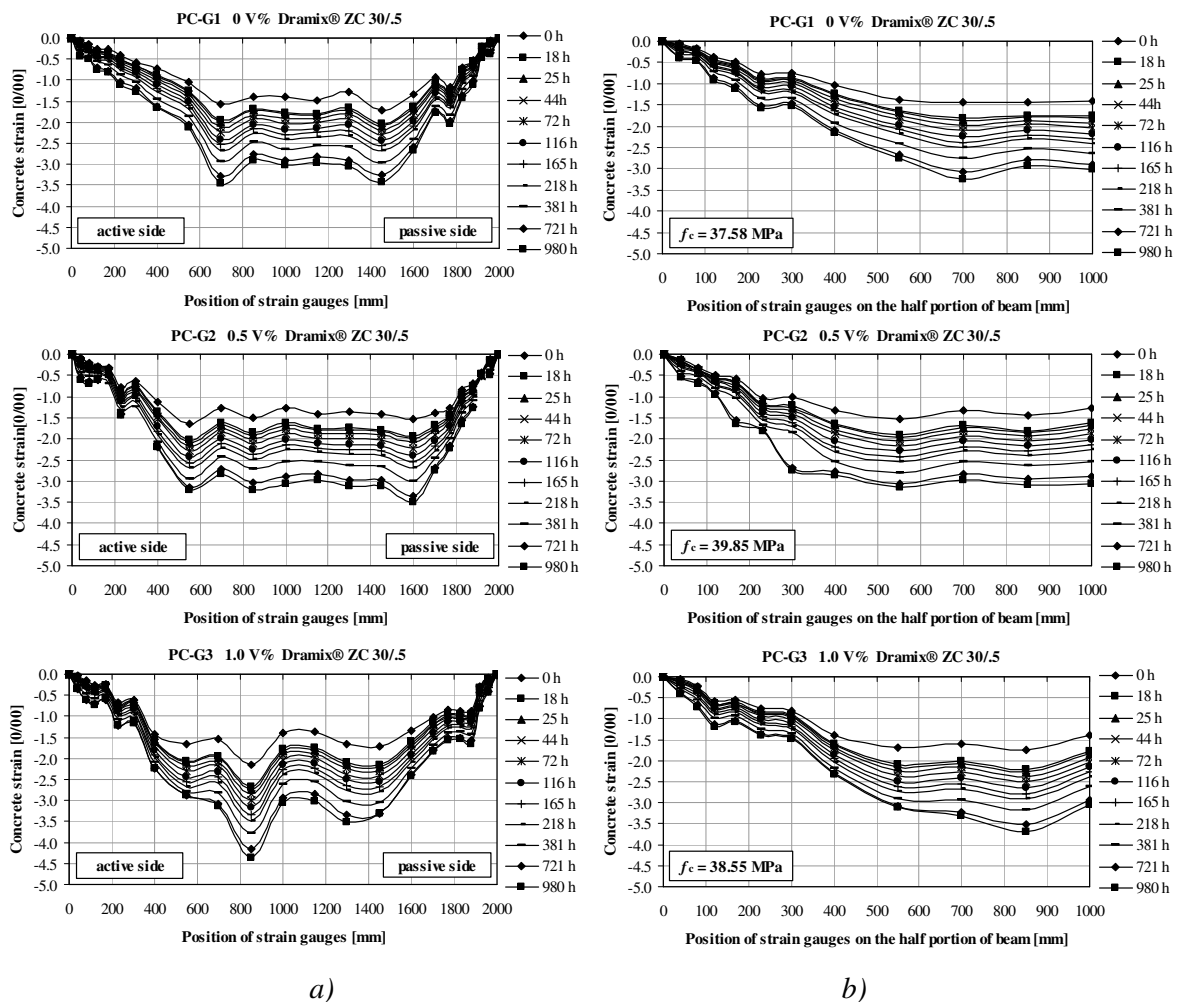


**Figure 5.4:** Measured concrete strain on the most compressed face of beams during gradual release of prestressing force in case of series PC-G

- a) Concrete strain measured at individual measuring points along the total beam  
 b) Calculated mean volumes of concrete strain on the half portion of beam

The three groups of curves represent three prestressed pretensioned concrete beams PC-G1, PC-G2 and PC-G3. Figure 5.4/b represents the mean concrete strains calculated from the measurements of the symmetrically placed strain gauges on the whole beam. The horizontal axes of diagrams shown in Figure 5.4/a represent the position of the individual strain gauges placed on the most compressed face of beam while the vertical axes indicate the measured concrete strains. Concrete strains as a function of time are also summarised in Figure 5.5/a for series PC-G. Mean curves of concrete strains measurements on active and passive sides are presented in Figure 5.5/b.

In case of series PC-S, the concrete strains were measured after the sudden release of prestressing force. Measured and calculated mean concrete strains are presented in Figure 5.6.

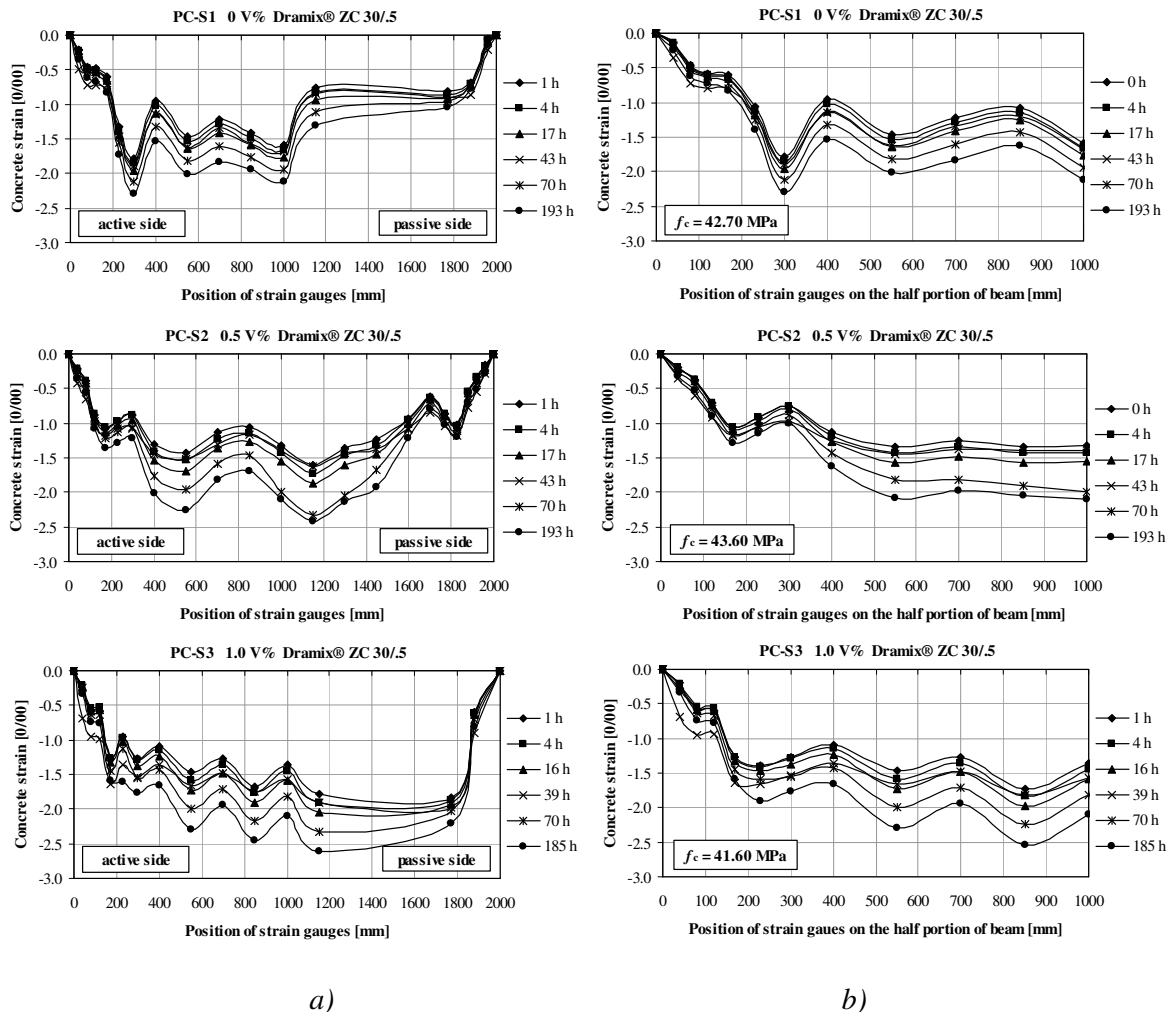


**Figure 5.5:** Measured concrete strains vs. time on the most compressed face of beams after releasing the total prestressing force in case of series PC-G

- a) Concrete strain measured at individual measuring points along the total beam  
 b) Calculated mean values of concrete strain on the half portion of beam

Results indicate lower concrete strains on the active sides of beams, resulting longer development length of prestressing force on the active side. Differences in the concrete strains measured on the active and passive sides were even more significant when the prestressing force was gradually released. However, after releasing the total prestressing force the concrete compressive strains measured in time on the active side corresponded to the strain values measured on the passive side resulting better strain distribution as shown in Figure 5.5. However, sudden release of prestressing force result rather symmetric strain distributions.

Additional concrete portion was placed at the cutting side of strand in order to avoid the impact effect of prestressing force and the effect of friction. Therefore, the response of the released side and of the fixed side was more similar. It was observed on all the three specimens.



**Figure 5.6:** Measured concrete strain on the most compressed face of beams after suddenly release of prestressing force in case of series PC-S

- a) Concrete strain measured at individual measuring points along the total beam  
 b) Calculated mean volumes of concrete strain on the half portion of beam

As diagrams indicate concrete strain measured on the most compressed face of the specimens generally increased applying fibre reinforcement which may be caused by the variation of the porosity of concrete (see Table 2.1).

Comparison of strain measurements indicates that the development of prestressing force needs shorter lengths when steel fibres were applied. Shorter development of the prestressing force can be explained by the effect of steel fibres reducing micro-cracking in the interactional region.

## 5.2.2 Draw-in of prestressing strand

### 5.2.2.1 Released prestressing force versus draw-in for series PC-G

Released prestressing force versus draw-in of prestressing strand relationships for beams series PC-G are presented in Figure 5.7. Dotted lines indicate the measurements on the active and on the passive sides. Mean value of the active and passive side measurements was corrected with the elongation of the strand between the two measuring points as shown in Figure 5.7.

Non-linear relationships for the released prestressing force versus draw-in were obtained from the measured values shown in Figure 5.8. Draw-in versus strand strain relationships were determined as a power function by using the method of minimum squares applied to the measured data. The obtained relationships are the follows for beams containing 0 V%, 0.5 V% and 1.0 V% Dramix® ZC 30/5 hooked-end steel fibre:

$$s_{e,0V\%} = 0.0198 \varepsilon_p^{2.2692} \quad (5.1)$$

$$s_{e,0.5V\%} = 0.0119 \varepsilon_p^{2.4436} \quad (5.2)$$

$$s_{e,1.0V\%} = 0.0087 \varepsilon_p^{2.6750} \quad (5.3)$$

In Eqs. (5.1) to (5.3)  $s_e$  indicates the draw-in [mm] at the butt-end of specimens and  $\varepsilon_p$  indicates the strand strain [%] corresponding to the released prestressing force.

Comparison of the released prestressing force versus draw-in relationships for 0 V%, 0.5 V% and 1.0 V% fibre contents indicates that fibre application produce lesser draw-in of the prestressing strands.

Measured and corrected draw-in values effected by the steel fibre reinforcement are summarised in Table 5.2 for various released prestressing force values. Table 5.2 indicates that the decrease of draw-in of strand within the practical range of 95 to 125 kN prestressing force is between 6 to 22 %. However, draw-ins for 0.5 V% and for 1.0 V% steel fibre contents were not significantly different.

Total release of prestressing force has been taken during 7 h. Draw-in of prestressing strand was registered after release of total prestressing force in further 1000 h. Draw-in was measured on the active and on the passive sides of specimens. Their mean values are summarised in Table 5.3. Time versus measured draw-in relationships are presented in Figure 5.9.

Reliable determination of transfer length of prestressing strand is based on the measured concrete deformations and on the prestressing strand strain versus draw-in relationships. Calculation of transfer length at a given time after releasing the total prestressing force also needs these relationships [Erdély (1996)]. Prestressing strand

strain versus draw-in relationship at a given time is needed taking into consideration the time-dependent phenomena appeared after the total release of prestressing force [Erdély (1996)].

Modified prestressing strand strain versus draw-in relationships were determined multiplying the functions developed in Eqs.(5.1) to (5.3) by the ratio of the measured draw-in at the given time and the corrected value of draw-in determined at 135.8 kN prestressing force. For example in case of beam PC-G3, the mean value of the measured draw-in on the active and on the passive sides at 381 h after releasing the total prestressing force was 1.6025 mm. The corrected draw-in of prestressing strand at 135.8 kN was 1.456 mm. Their ratio was  $1.6025/1.456=1.1006$ . Therefore, the modified non-linear relationship according to Eq. (5.3) measured at 381 hours after the total release of prestressing force is given by the following expression:

$$s_e = 0.0096\varepsilon_p^{2.6750}$$

Based on the method above the modified relationships for each specimen and for each given time were developed and summarised in Tab. 5.4. Table 5.4 includes  $s_e - \varepsilon_p$  and  $\varepsilon_p - s_e$  relationships as well.

**Table 5.2:** Draw-in of prestressing strand for series PC-G measured during gradual release of prestressing force

Released prestressing force [kN]	PC-G1 0 V% Dramix ZC 30/5		PC-G2 0.5 V% Dramix ZC 30/5			PC-G3 1.0 V% Dramix ZC 30/5		
	Mean values [mm]	Corrected means [mm]	Mean values [mm]	Corrected means [mm]	Reduction in draw-in [%]	Mean values [mm]	Corrected means [mm]	Reduction in draw-in [%]
15	0.065	0.000	0.067	0.000	-	0.060	0.000	-
35	0.252	0.071	0.224	0.050	30	0.214	0.037	4-8
55	0.500	0.216	0.421	0.147	32	0.437	0.159	26
75	0.871	0.483	0.727	0.354	27	0.738	0.359	26
95	1.216	0.724	1.034	0.562	22	1.108	0.628	13
105	1.455	0.911	1.291	0.768	16	1.329	0.798	12
115	1.705	1.110	1.483	0.911	18	1.567	0.986	11
125	2.011	1.363	1.802	1.180	13	1.881	1.249	8
135.8	2.256	1.553	1.978	1.302	16	2.142	1.456	6

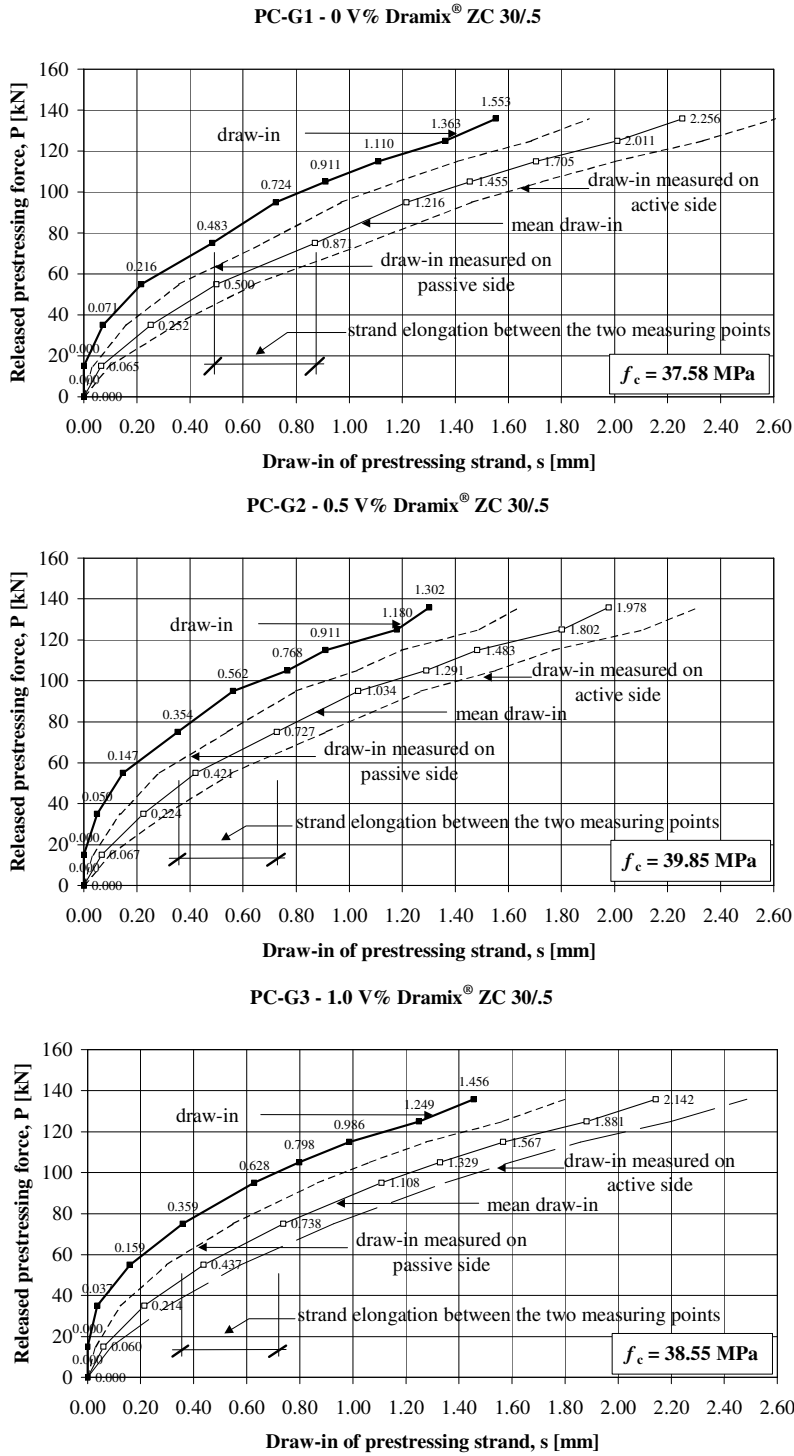


Figure 5.7: Released prestressing force versus draw-in of prestressing strand relationships for beams PC-G1, PC-G2 and PC-G3.

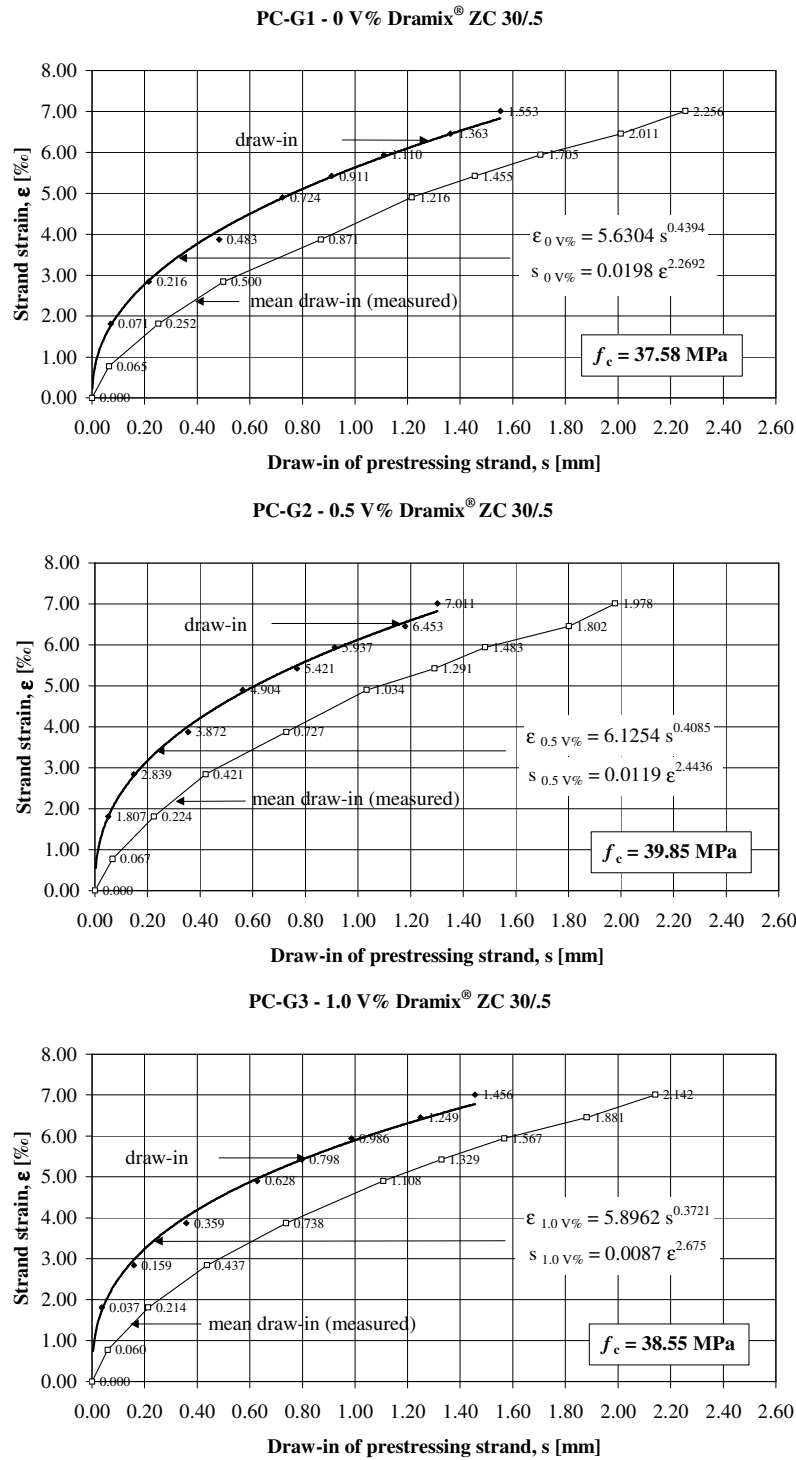
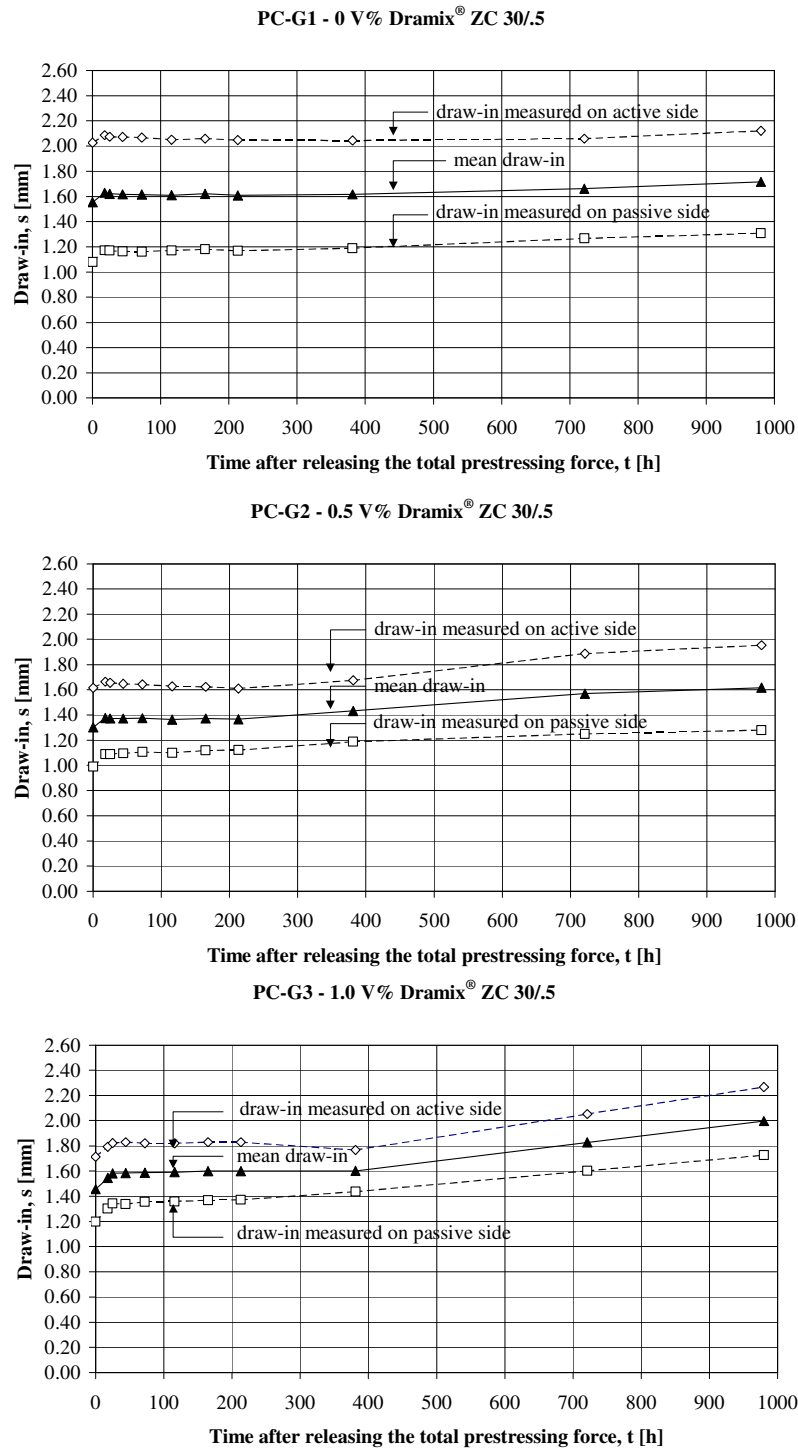


Figure 5.8: Non-linear relationships of released prestressing force and draw-in of prestressing strand for beams PC-G1, PC-G2 and PC-G3.



**Table 5.3:** *Draw-in of prestressing strand measured in time after releasing the total prestressing force for series PC-G*

Time [h]	PC-G1 0 V% Dramix ZC 30/5			PC-G2 0.5 V% Dramix ZC 30/5			PC-G3 1.0 V% Dramix ZC 30/5		
	Active side [mm]	Passive side [mm]	Mean value [mm]	Active side [mm]	Passive side [mm]	Mean value [mm]	Active side [mm]	Passive side [mm]	Mean value [mm]
0	2.0270	1.0800	1.554	1.6140	0.9900	1.3020	1.7140	1.1980	1.4560
18	2.0870	1.1720	1.630	1.6640	1.0890	1.3765	1.7918	1.3017	1.5467
25	2.0730	1.1700	1.622	1.6560	1.0890	1.3725	1.8220	1.3420	1.5820
44	2.0710	1.1640	1.618	1.6460	1.0960	1.3710	1.8300	1.3370	1.5835
72	2.0680	1.1620	1.615	1.6430	1.1050	1.3740	1.8210	1.3540	1.5875
116	2.0510	1.1700	1.611	1.6270	1.0990	1.3630	1.8200	1.3600	1.5900
165	2.0590	1.1810	1.620	1.6230	1.1190	1.3710	1.8290	1.3680	1.5985
213	2.0490	1.1680	1.609	1.6110	1.1200	1.3655	1.8300	1.3710	1.6005
381	2.0450	1.1890	1.617	1.6750	1.1880	1.4315	1.7680	1.4370	1.6025
721	2.0590	1.2660	1.663	1.8870	1.2500	1.5685	2.0518	1.6010	1.8264
980	2.1210	1.3080	1.715	1.9530	1.2790	1.6160	2.2680	1.7260	1.9970



*Figure 5.9: Draw-in of prestressing strand as a function of time after the total release of prestressing force for series PC-G.*

**Table 5.4:** Prestressing strand strain versus draw-in of prestressing strand relationships in time after releasing the total prestressing force for beams PC-G

Time [h]	PC-G1			PC-G2			PC-G3		
	0 V% Dramix ZC 30/5			0.5 V% Dramix ZC 30/5			1.0 V% Dramix ZC 30/5		
0	0.0198 $\epsilon_p^{2.2692}$			0.0119 $\epsilon_p^{2.4436}$			0.0087 $\epsilon_p^{2.6750}$		
18	0.0208 $\epsilon_p^{2.2692}$			0.0126 $\epsilon_p^{2.4436}$			0.0092 $\epsilon_p^{2.6750}$		
25	0.0207 $\epsilon_p^{2.2692}$			0.0125 $\epsilon_p^{2.4436}$			0.0095 $\epsilon_p^{2.6750}$		
44	0.0206 $\epsilon_p^{2.2692}$			0.0125 $\epsilon_p^{2.4436}$			0.0095 $\epsilon_p^{2.6750}$		
72	0.0206 $\epsilon_p^{2.2692}$			0.0126 $\epsilon_p^{2.4436}$			0.0095 $\epsilon_p^{2.6750}$		
116	0.0205 $\epsilon_p^{2.2692}$			0.0125 $\epsilon_p^{2.4436}$			0.0095 $\epsilon_p^{2.6750}$		
165	0.0207 $\epsilon_p^{2.2692}$			0.0125 $\epsilon_p^{2.4436}$			0.0096 $\epsilon_p^{2.6750}$		
213	0.0205 $\epsilon_p^{2.2692}$			0.0125 $\epsilon_p^{2.4436}$			0.0096 $\epsilon_p^{2.6750}$		
381	0.0206 $\epsilon_p^{2.2692}$			0.0131 $\epsilon_p^{2.4436}$			0.0096 $\epsilon_p^{2.6750}$		
721	0.0212 $\epsilon_p^{2.2692}$			0.0143 $\epsilon_p^{2.4436}$			0.0109 $\epsilon_p^{2.6750}$		
980	0.0219 $\epsilon_p^{2.2692}$			0.0148 $\epsilon_p^{2.4436}$			0.0119 $\epsilon_p^{2.6750}$		

### 5.2.2.2 Released prestressing force versus draw-in for series PC-S

Draw-in of prestressing strand was measured in time after the sudden release of prestressing force up to 1600 h. Draw-in was measured both on the active and on the passive side as well. Mean values of the active and passive side draw-in measurements are summarised in Table 5.5. Time versus draw-in relationships are presented in Figure 5.10.

**Table 5.5:** Draw-in of prestressing strand measured after the sudden release of prestressing force for series PC-S

Time [h]	PC-S1			PC-S2			PC-S3		
	0 V% Dramix ZC 30/5			0.5 V% Dramix ZC 30/5			1.0 V% Dramix ZC 30/5		
	Active side [mm]	Passive side [mm]	Mean value [mm]	Active side [mm]	Passive side [mm]	Mean value [mm]	Active Side [mm]	Passive side [mm]	Mean value [mm]
4	-	1.381	-	1.661	1.163	1.412	1.049	1.304	1.176
17	-	1.383	-	1.755	1.206	1.480	1.105	1.343	1.224
21	-	1.442	-	1.746	1.316	1.531	1.123	1.378	1.250
43	-	1.453	-	1.783	1.312	1.547	1.175	1.398	1.286
70	-	1.410	-	1.769	1.277	1.523	1.169	1.399	1.284
91	-	1.459	-	1.797	1.304	1.550	1.249	1.411	1.330
122	-	1.449	-	1.778	1.273	1.525	1.236	1.400	1.318
193	-	1.449	-	1.790	1.259	1.524	1.230	1.391	1.310
356	-	1.492	-	1.822	1.307	1.564	1.261	1.409	1.335
648	-	1.504	-	1.831	1.362	1.596	1.292	1.426	1.359
1564	-	1.595	-	1.859	1.523	1.691	1.411	1.650	1.530

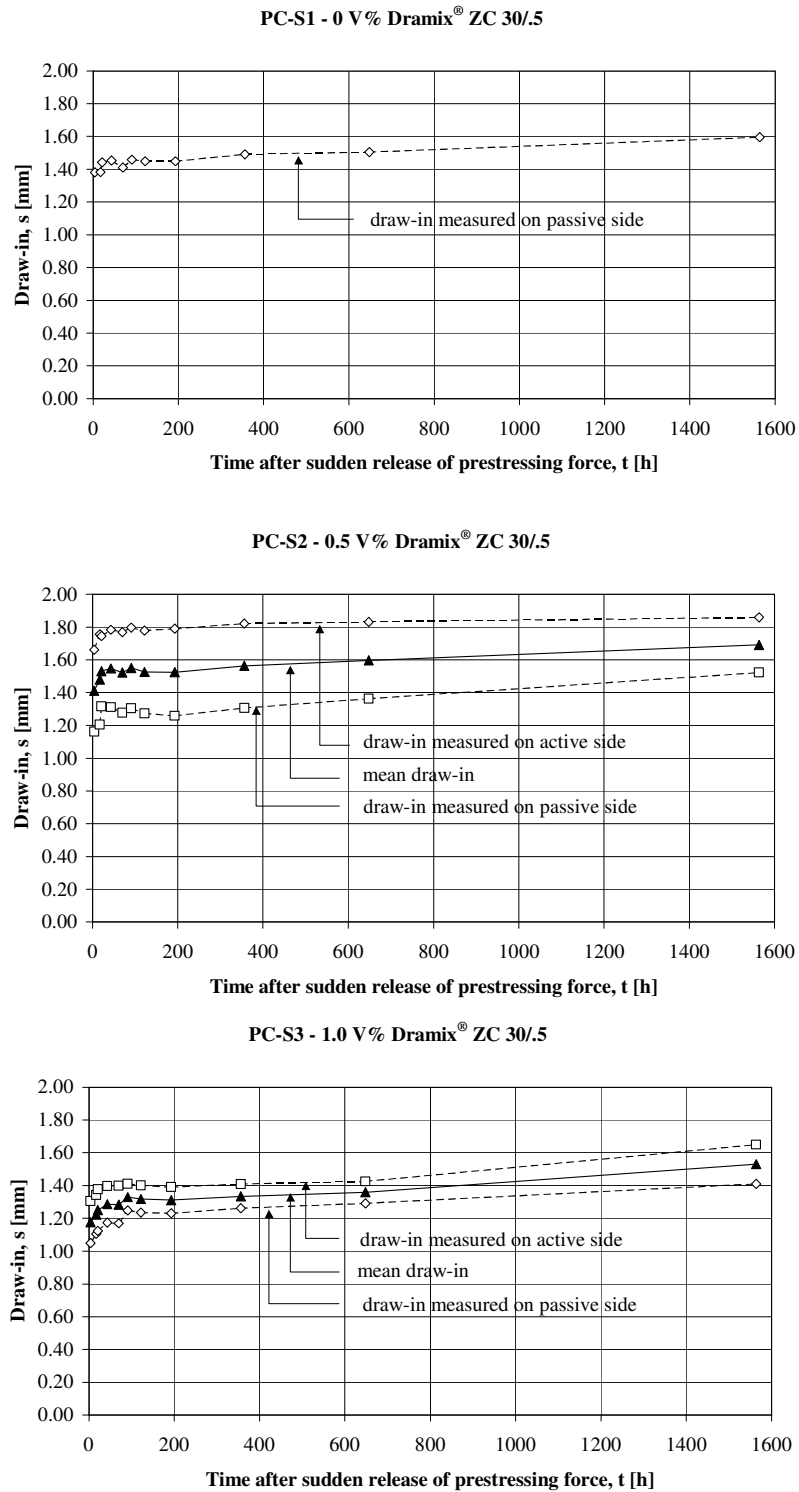


Figure 5.10: Draw-in of prestressing strand as a function of time after the total release of prestressing force for series PC-G.

## 5.2.3 Camber of PC beams

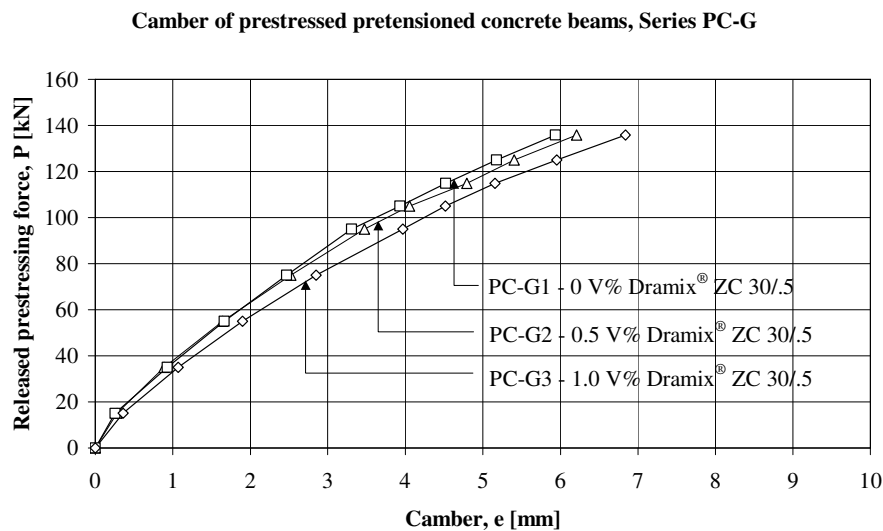
### 5.2.3.1 Camber of series PC-G

Camber of mid-section of prestressed pretensioned concrete beams was calculated according to the measured displacements of specimens as shown in Figure 5.2 for each load step. Determined values are summarised in Table 5.6 and presented in Figure 5.11.

Results indicate that camber of prestressed pretensioned concrete beams made with steel fibres (PC-G2 0.5 V% and PC-G3 1.0 V%) were higher than those for specimens made with no fibres (PC-G1). Increments in camber were 5% (0.5 V%) and 15% (1.0 V%) related to beams having no steel fibres at the total release of prestressing force.

**Table 5.6:** Camber of prestressed pretensioned concrete beams measured under gradual release for series PC-G

Force [kN]	PC-G1		PC-G2		PC-G3	
	0 V% Dramix ZC 30/.5	0.5 V% Dramix ZC 30/.5	0.5 V% Dramix ZC 30/.5	1.0 V% Dramix ZC 30/.5	1.0 V% Dramix ZC 30/.5	1.0 V% Dramix ZC 30/.5
15	0.255		0.285		0.360	
35	0.930		0.890		1.070	
55	1.665		1.645		1.900	
75	2.470		2.525		2.850	
95	3.310		3.470		3.970	
105	3.930		4.055		4.515	
115	4.520		4.795		5.155	
125	5.180		5.405		5.955	
135.8	5.935		6.210		6.840	



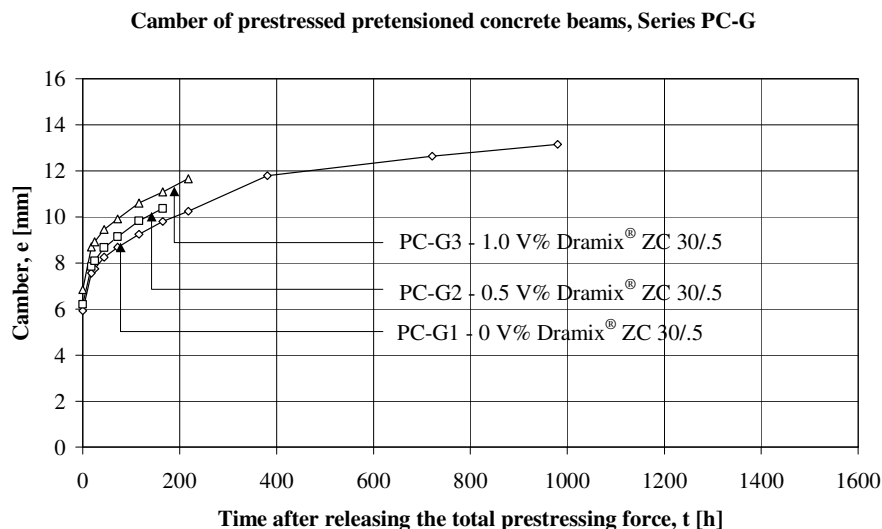
**Figure 5.11:** Camber of prestressed pretensioned concrete beams under gradual release of prestressing force for series PC-G

After releasing the total prestressing force, displacements of specimens were measured in time to further 1000 h. Calculated camber of beams as a function of time after total release are summarised in Table 5.7 and presented in Figure 5.12. In case of beam PC-G2 and in case of PC-G3 displacement was only measurable up to 165 and 218 h.

As result indicates significant increment in camber was detected after releasing the total prestressing force approximately up to 400-600 h in case of PC-G3 containing 1.0 V% fibre content. However, as shown in Figure 5.12 time versus camber relationship suggests an asymptotic behaviour, which asymptote is given at around 14 mm for beams PC-G3.

**Table 5.7:** *Camber of prestressed pretensioned concrete beams measured after releasing the total prestressing force for series PC-G*

Time [h]	PC-G1		PC-G2		PC-G3	
	0 V% Dramix ZC 30/.5		0.5 V% Dramix ZC 30/.5		1.0 V% Dramix ZC 30/.5	
0	5.935		6.210		6.840	
18	7.560		7.850		8.700	
25	7.750		8.100		8.920	
44	8.250		8.670		9.460	
72	8.680		9.140		9.920	
116	9.245		9.830		10.610	
165	9.810		10.370		11.090	
218	10.250		-		11.660	
381	11.790		-		-	
721	12.640		-		-	
980	13.150		-		-	



**Figure 5.12:** *Camber of prestressed pretensioned concrete beams under gradual release of prestressing force for series PC-G*

### 5.2.3.2 Camber of series PC-S

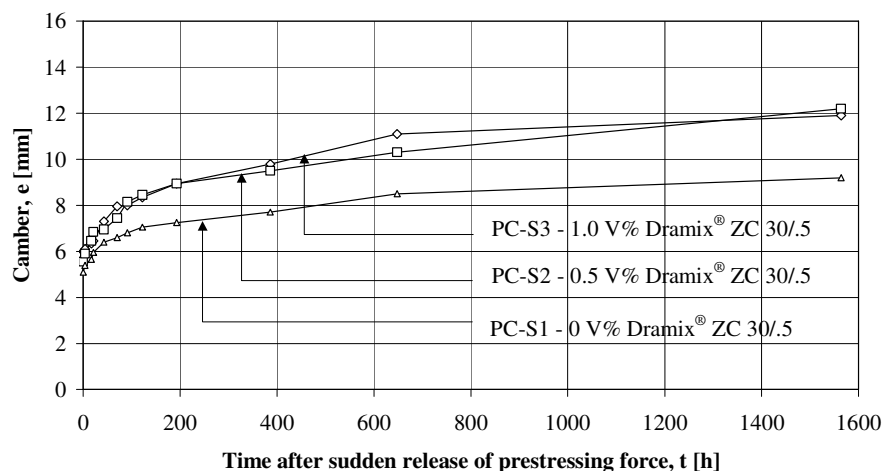
Due to the sudden release placing of the measuring system detecting the displacements of specimens on the beams was not possible. Therefore, theodolit was used to control the displacements of cross-sections. Cambers are summarised in Table 5.8 and presented in Figure 5.13.

Results indicate that lower cambers developed for Series PC-S which may caused by the higher concrete compressive strength. However, similarly to Series PC-G, 1.0 V% fibre content result smaller camber.

**Table 5.8:** Camber of prestressed pretensioned concrete beams measured in time after sudden release of prestressing force for series PC-S

Time [h]	PC-S1	PC-S2	PC-S3
	0 V% Dramix ZC 30/.5	0.5 V% Dramix ZC 30/.5	1.0 V% Dramix ZC 30/.5
0	5.10	5.55	6.00
4	5.40	5.90	6.10
17	5.65	6.45	6.35
21	5.95	6.85	6.45
43	6.40	6.95	7.30
70	6.60	7.45	7.95
91	6.80	8.15	8.00
122	7.05	8.45	8.35
193	7.25	8.95	8.95
386	7.70	9.50	9.80
648	8.50	10.30	11.10
1564	9.20	12.20	11.90

Camber of prestressed pretensioned concrete beams, Series PC-S



**Figure 5.13:** Camber of prestressed pretensioned concrete beams in time after sudden release of prestressing force for series PC-S

## 5.2.4 Determination of transfer length of prestressing strand

### 5.2.4.1 General considerations and governing equations

Transfer length in a prestressed pretensioned concrete member is defined as the length required to develop the effective prestressing force in the tendon by bond. Transfer length is affected by many factors, such as strength of concrete, degree of compaction, transverse reinforcement in the end block, size and type of tendon, type of tendon release, etc. One of the main motivations of the presented research was to study the effect of fibre reinforcement on the transfer length. Transfer length of prestressing tendons is closely related to the draw-in of the tendon as shown in Figure 5.13.

Determination of transfer length of prestressing strand is commonly based only on the measured draw-in values neglecting the concrete deformations. However, according to Figure 5.14 both draw-in and concrete strain values effect the transfer length and the relationships between them can be written in the following term:

$$s_e = \frac{P_0 \ell}{2A_p E_p} - \int_0^{\ell/2} \varepsilon^c d\xi - \int_0^{\ell/2} \varepsilon^p d\xi \quad (5.4)$$

①
④
②
③

where  $s_e$  denotes the draw-in of prestressing strand,  $P_0$  indicates the released prestressing force,  $\ell$  denotes the length of the specimens,  $A_p$  and  $E_p$  represent the area and the Young modulus of the tendon,  $\varepsilon^c$  and  $\varepsilon^p$  are the strains developed in the concrete and strand due to the prestressing, respectively. Terms in Eq. (5.5) are numerated and their physical meaning represented in Figure 5.14. Therefore, the transfer length is determined by the cross-section where  $s_e$  becomes zero.

The applied calculation method for the transfer length of prestressing strand was based on the following assumptions:

- behaviour of prestressing strand is considered to be linear elastic in the whole range of prestressing,
- behaviour of concrete is considered to be linear elastic in the whole range of prestressing,
- classical beam theory is valid (plain sections before loading remain plain after loading) which leads to linear strain distribution over the cross-section,
- relative displacements occur between the concrete and the prestressing strand along the transfer length.

According to the assumptions above, let's consider a portion of prestressed pretensioned concrete specimens before prestressing (i.e.:  $dx_i^c = dx_i^p$ ) and their relative displacements (i.e.:  $\Delta x_{i-1}^p, \Delta x_{i-1}^c, \Delta x_i^p, \Delta x_i^c$ ) after prestressing as shown in Figure 5.15. They represent the relative displacements of the given concrete and prestressing strand sections defined in the sections  $i-1^{\text{th}}$  and section  $i^{\text{th}}$  of specimen.



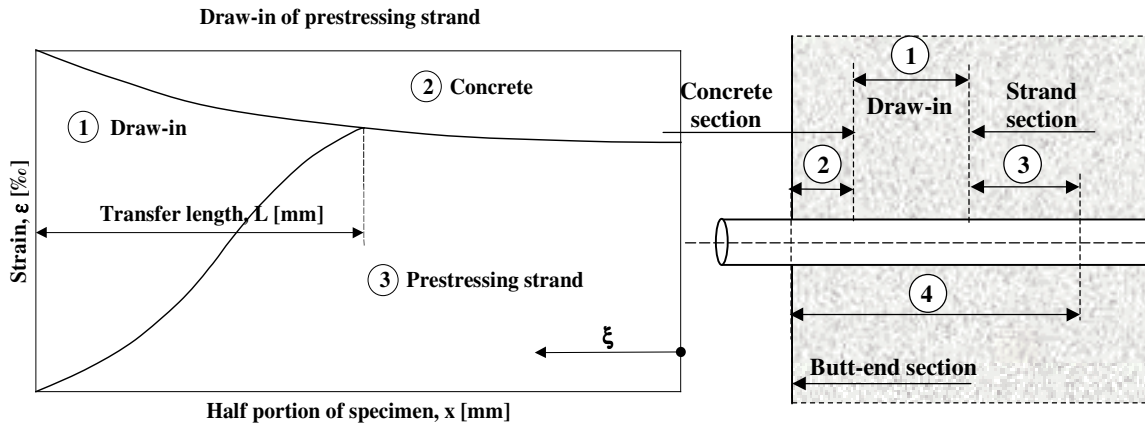


Figure 5.14: Determination of transfer length of prestressing strand using both the measured concrete strains and the draw-in of prestressing strand

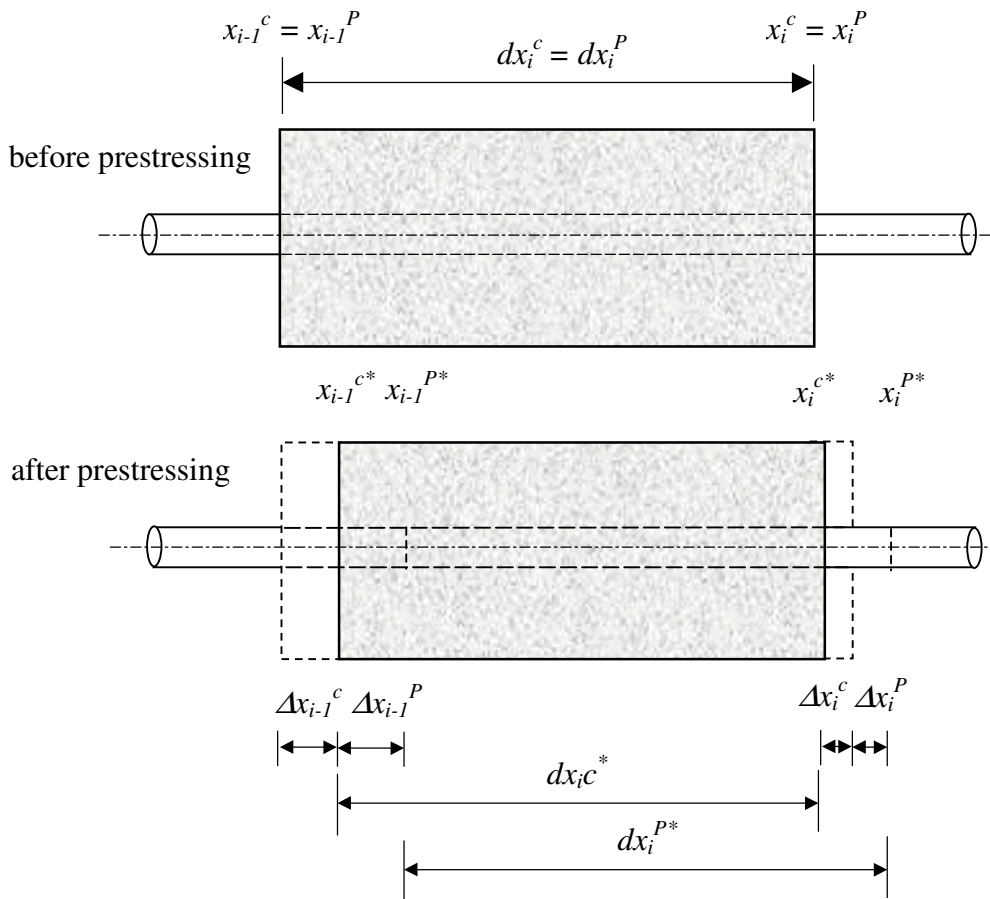


Figure 5.15: Relative displacements over a  $dx$  length of prestressed pretensioned concrete member

The following relationship can be drawn for the concrete and for the prestressing strand portion before the release of prestressing force:

$$dx_i^c = dx_i^P \quad (5.5)$$

After releasing the prestressing force relative displacements occur on both sides of the portions. The deformed length of the prestressing strand can be written as:

$$dx_i^{P*} = dx_i^c - (\Delta x_{i-1}^c + \Delta x_{i-1}^P) + (\Delta x_i^c + \Delta x_i^P) \quad (5.6)$$

where the relative displacements of the concrete portion can be expressed by the use of the measured concrete strains in the sections  $i-1$ <sup>th</sup> (i.e.:  $\varepsilon_{i-1}^c$ ) and  $i$ <sup>th</sup> (i.e.:  $\varepsilon_i^c$ ):

$$\Delta x_i^c - \Delta x_{i-1}^c = \frac{\varepsilon_{i-1}^c + \varepsilon_i^c}{2} dx_i^c / 1000 \quad (5.7)$$

and hence,

$$dx_i^{P*} = dx_i^c - \frac{\varepsilon_{i-1}^c + \varepsilon_i^c}{2} dx_i^c / 1000 - \Delta x_{i-1}^P + \Delta x_i^P \quad (5.8)$$

Operating with the developed non-linear functions for the strand strain versus draw-in relationships, relative displacements of the prestressing strand can be written in the following forms:

$$\Delta x_{i-1}^P = a(\varepsilon_{i-1}^P)^b \quad \text{and} \quad \Delta x_i^P = a(\varepsilon_i^P)^b \quad (5.9)$$

where  $a$  and  $b$  are experimental constants. Substituting Eq.(5.9) into Eq.(5.8):

$$dx_i^{P*} = dx_i^c - \frac{\varepsilon_{i-1}^c + \varepsilon_i^c}{2} dx_i^c / 1000 - a(\varepsilon_{i-1}^P)^b + a(\varepsilon_i^P)^b \quad (5.10)$$

However, deformation of the strand portion caused by the draw-in of strand can be expressed by the use of the developed functions for the strand strain versus draw-in relationships:

$$a(\varepsilon_{i-1}^P)^b - a(\varepsilon_i^P)^b = \frac{\varepsilon_{i-1}^P + \varepsilon_i^P}{2} dx_i^{P*} / 1000 \quad (5.11)$$

Eq. (5.10) and Eq. (5.11) define a non-linear equation system. Unknown parameters are the strain of prestressing strand in the  $i$ <sup>th</sup> section developed by the draw-in (i.e.:  $\varepsilon_i^P$ ) at a given prestressing force and the length of the strand portion defined between the  $i-1$ <sup>th</sup> and  $i$ <sup>th</sup> sections after releasing the given prestressing force (i.e.:  $dx_i^{P*}$ ). Combining Eq. (5.10) and Eq. (5.11) the following function is resulted:

$$A(\varepsilon_i^P)^{b+1} + B_i(\varepsilon_i^P)^b + C_i(\varepsilon_i^P) + D_i = 0 \quad (5.12)$$

where

$$A = \frac{a}{2} \quad (5.13)$$

$$B_i = \frac{a}{2}(\varepsilon_{i-1}^p) + 1000a \quad (5.14)$$

$$C_i = \frac{1}{2} \left( dx_i^c - \frac{\varepsilon_{i-1}^c + \varepsilon_i^c}{2} dx_i^c / 1000 - a(\varepsilon_{i-1}^p)^b \right) \quad (5.15)$$

$$D_i = \frac{1}{2}(\varepsilon_{i-1}^p) \left( dx_i^c - \frac{\varepsilon_{i-1}^c + \varepsilon_i^c}{2} dx_i^c / 1000 - a(\varepsilon_{i-1}^p)^b \right) - 1000a(\varepsilon_{i-1}^p)^b \quad (5.16)$$

Based on the measured concrete strains and the developed strand strain versus draw-in relationships and the derived non-linear relationship in Eq. (5.12) transfer length of prestressing strand can be calculated.

#### 5.2.4.2 Transfer length of prestressing strand for series PC-G

Calculation method of transfer length of strand discussed in the previous section yields to the following non-linear equation systems for specimens PC-G1, PC-G2 and PC-G3, respectively:

$$\begin{aligned} dx_i^{P*} &= dx_i^c - \frac{\varepsilon_{i-1}^c + \varepsilon_i^c}{2} dx_i^c / 1000 - 0.0198(\varepsilon_{i-1}^p)^{2.2692} + 0.0198(\varepsilon_i^p)^{2.2692} \\ 0 &= 19.8(\varepsilon_{i-1}^p)^{2.2692} - 19.8(\varepsilon_i^p)^{2.2692} - \frac{1}{2}(\varepsilon_{i-1}^p) dx_i^{P*} - \frac{1}{2}(\varepsilon_i^p) dx_i^{P*} \end{aligned} \quad (5.17)$$

$$\begin{aligned} dx_i^{P*} &= dx_i^c - \frac{\varepsilon_{i-1}^c + \varepsilon_i^c}{2} dx_i^c / 1000 - 0.0119(\varepsilon_{i-1}^p)^{2.4436} + 0.0119(\varepsilon_i^p)^{2.4436} \\ 0 &= 11.9(\varepsilon_{i-1}^p)^{2.4436} - 11.9(\varepsilon_i^p)^{2.4436} - \frac{1}{2}(\varepsilon_{i-1}^p) dx_i^{P*} - \frac{1}{2}(\varepsilon_i^p) dx_i^{P*} \end{aligned} \quad (5.18)$$

$$\begin{aligned} dx_i^{P*} &= dx_i^c - \frac{\varepsilon_{i-1}^c + \varepsilon_i^c}{2} dx_i^c / 1000 - 0.0087(\varepsilon_{i-1}^p)^{2.6750} + 0.0087(\varepsilon_i^p)^{2.6750} \\ 0 &= 8.7(\varepsilon_{i-1}^p)^{2.6750} - 8.7(\varepsilon_i^p)^{2.6750} - \frac{1}{2}(\varepsilon_{i-1}^p) dx_i^{P*} - \frac{1}{2}(\varepsilon_i^p) dx_i^{P*} \end{aligned} \quad (5.19)$$

By defining the length of the deformed prestressing strand portions and the strand strains caused by the draw-in, transfer length can be expressed.

Results of calculations are graphically summarised in Figures 5.16 to 5.18 for RC-G1, RC-G2 and RC-G3, respectively. Horizontal axis of the diagram indicates the place of the cross sections where concrete deformations were measured and calculated on the half portion of beam, vertical axis denotes the strains (i.e. concrete and strand strains) calculated at the level of the prestressing strand. Transfer length of strand was calculated at each load step which is represented by horizontal dotted lines. Calculated effective prestressing forces based on the deformation of prestressing strand are also given. The vertical dotted lines denote the concrete cross-sections where draw-in does not occur, hence, transfer length is fully developed. Transfer length versus released

prestressing force as well as transfer length versus effective prestressing force relationship are also presented in Figure 5.19 and in Figure 5.20. Transfer length values of specimens at different released prestressing forces are summarised in Table 5.9. Results indicate that the change of the transfer length depends on the applied prestressing force and the fibre content.

These transfer length calculations showed if steel fibres were applied the transfer length was decreased. However, in the practical range of the 95-125 kN prestressing force, the decrease of transfer length in the presented tests was not proportional to the fiber content of the specimens. 0.5 V% fiber content resulted the shortest transfer length.

**Table 5.9:** *Transfer length of prestressed pretensioned concrete beams series PC-G under gradual release*

Force [kN]	PC-G1		PC-G2		PC-G3	
	0 V% Dramix ZC 30/.5	0.5 V% Dramix ZC 30/.5	0.5 V% Dramix ZC 30/.5	1.0 V% Dramix ZC 30/.5	1.0 V% Dramix ZC 30/.5	1.0 V% Dramix ZC 30/.5
15	-	-	-	-	-	-
35	80.000		50.261		45.635	
55	150.926		82.551		86.901	
75	203.885		147.892		145.746	
95	273.240		208.229		215.936	
105	310.528		240.123		250.617	
115	346.107		272.581		299.033	
125	388.285		310.148		335.890	
135.8	420.191		345.974		395.610	

### 5.2.4.3 Proposal

In national codes and recommendations transfer length of prestressing strand are generally defined as a function of the concrete grade, the diameter and type of prestressing strand (Table 5.10).

**Table 5.10:** *Transfer length of  $\varnothing 12.5$  mm 7 wire strand in different national standards*

Standard	Transfer length [ $\varnothing$ ]	Transfer length [mm]	Notation
British Standard		330 mm (+/- 25)	
CEB/FIP	45 $\varnothing$ – 90 $\varnothing$	560 – 1125	
Czech Standard		1900 mm 1700 mm 1500 mm	B400 B500 B600
Polish Standard	50 $\varnothing$ 45 $\varnothing$ 40 $\varnothing$ 35 $\varnothing$	625 mm 560 mm 500 mm 440 mm	B300 B350 B400 B450
Hungarian Standard		810 mm	
DIN	115 $\varnothing$	1440 mm	
Swedish Standard	60 $\varnothing$ 75 $\varnothing$	750 mm 940 mm	Gradual release Sudden release
Russian Standard	75 $\varnothing$	940 mm	

Transfer length in EC2 is:

$$\ell_{bp} = \beta_b \emptyset \quad (5.20)$$

where  $\beta_b$  is experimentally determined for different concrete strengths and nominal diameter of prestressing tendon. According to the experimental results of the present research,  $\beta_b$  parameters were determined taking into account the effect of steel fibre reinforcement (Table 5.11). Based on these values a proposal is presented for design purposes in Table 5.12.

**Table 5.11:** Experimentally obtained  $\beta_b$  for prestressed fibre reinforced concrete beams

Fiber type	Specimens	Compressive strength $f_c$ [MPa]	$\beta_b$ according to EC-2	$\beta_b$ experimentally determined by EC-2	$\beta_b$ modified EC-2
Dramix <sup>®</sup> ZC 30/.5	PC-G1	37.58	63	34	63
	PC-G2	39.85	61	28	52
	PC-G3	38.55	62	32	59

**Table 5.12:** Proposal for the modified  $\beta_b$  parameters taking into account steel fibre reinforcement based on experimental data in Table 5.11 ( $\ell_{bp} = \beta_b \emptyset$ )

Dramix <sup>®</sup> ZC 30/.5 steel fibre content [V%]	$\beta_b$					
	Concrete strength [MPa]					
	25	30	35	40	45	50
No fibres	75	70	65	60	55	50
0.5 V%	65	60	55	50	45	40
1.0 V%	70	65	60	55	50	45

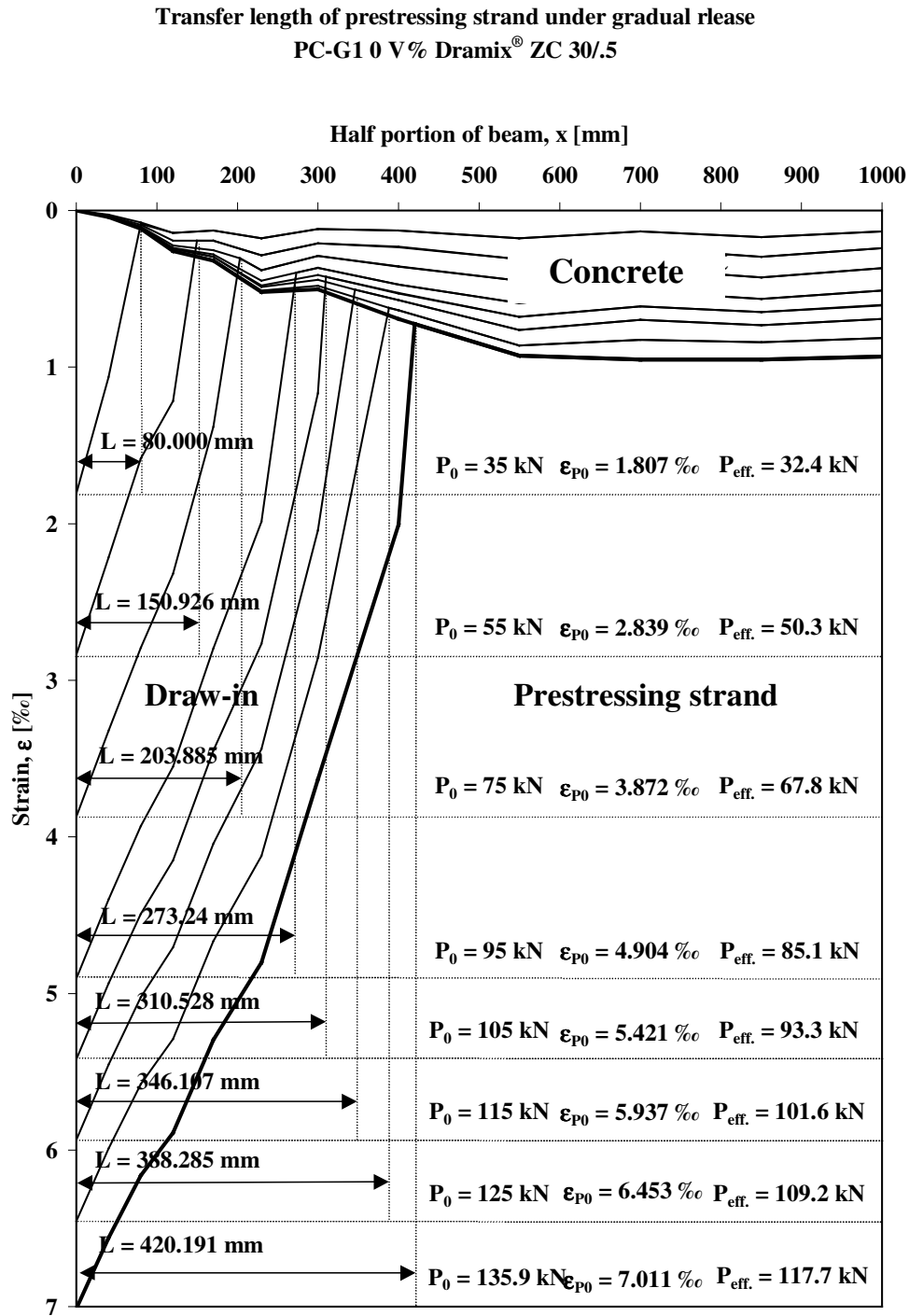
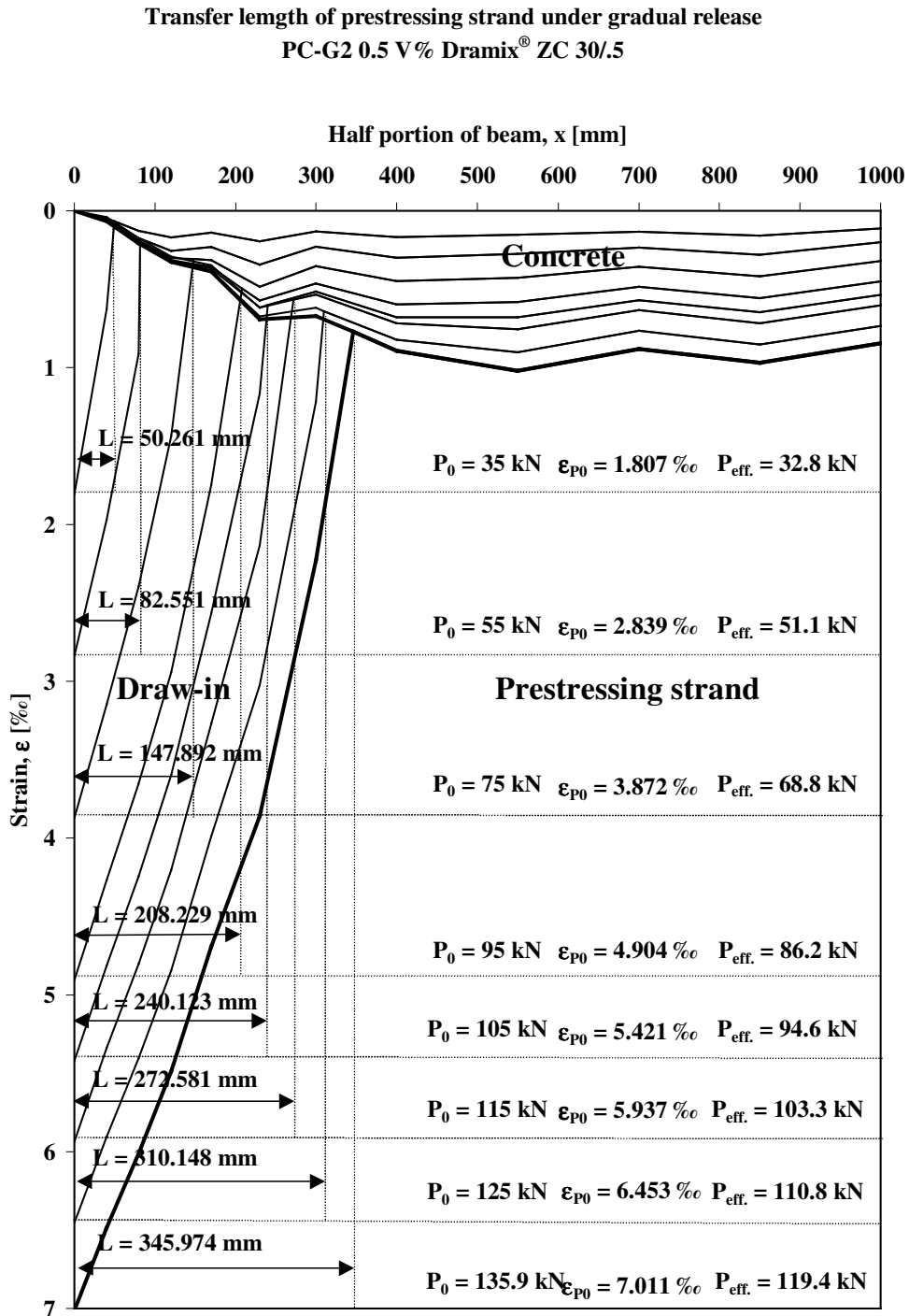


Figure 5.16: Transfer length of prestressing strand under gradual release for beam PC-G1 containing 0 V% Dramix<sup>®</sup> ZC 30/5 hooked-end steel fibres



*Figure 5.17: Transfer length of prestressing strand under gradual release for beam PC-G2 containing 0.5 V% Dramix<sup>®</sup> ZC 30/5 hooked-end steel fibres*

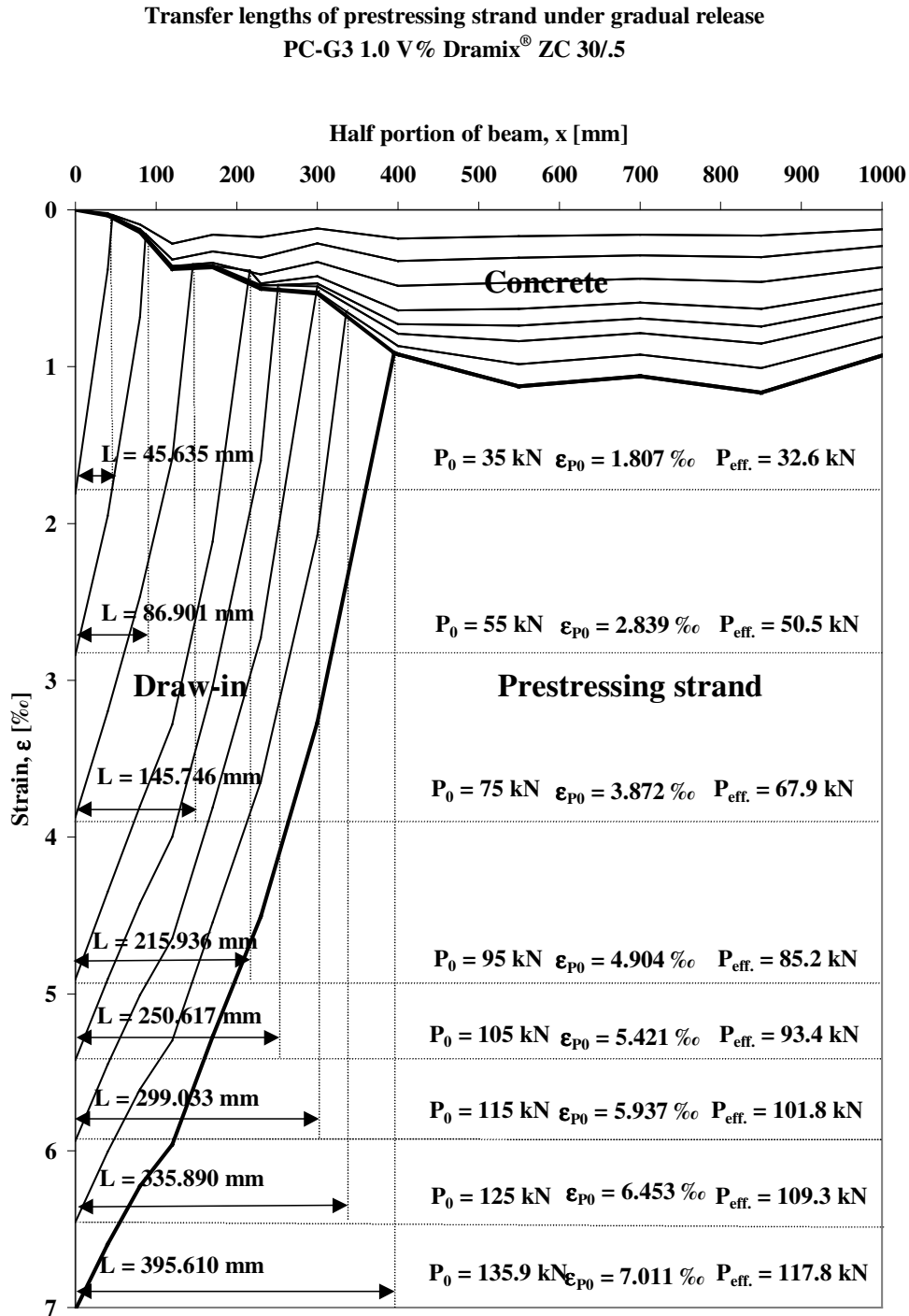
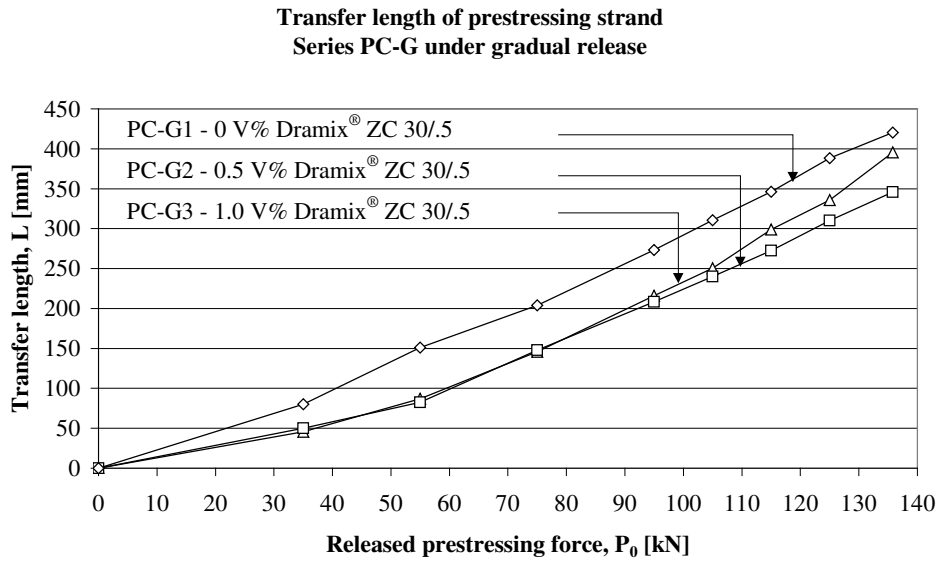
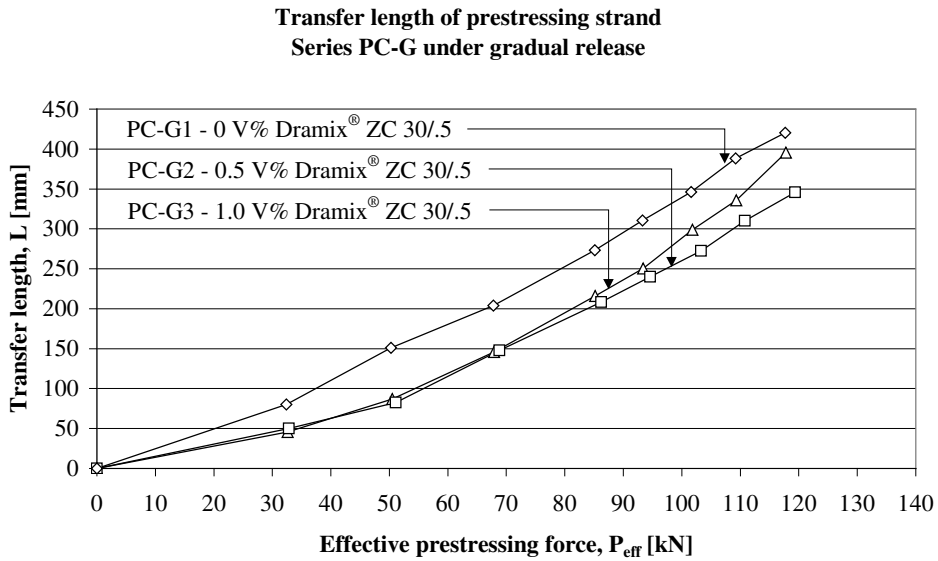


Figure 5.18: Transfer length of prestressing strand under gradual release for beam PC-G3 containing 1.0 V% Dramix<sup>®</sup> ZC 30/5 hooked-end steel fibres





**Figure 5.19:** Transfer length versus released prestressing force relationships Series PC-G under gradual release



**Figure 5.20:** Transfer length versus effective prestressing force relationships Series PC-G under gradual release

## 5.2.5 Bending test

Similarly to beams discussed in Chapter 4 bending tests were carried out on steel fibre reinforced prestressed pretensioned concrete beams after release of prestressing force. All beams were tested in four-point bending. Span was 1800 mm, shear-span was 600 mm. Span to depth ratio ( $a/d$ ) was 5, since geometry of the beams and the prestressed reinforcement was constant in case of all beams,.

Force was applied by two LUKAS type hydraulic jacks with the capacity of 100 kN each. Hydraulic jacks worked in one hydraulic circle, therefore jack forces were the same during loading. Tests were performed in force control. Force increments were 1.0 kN according to the calculated failure loads of the tested beams. Mid-span deflections of beams were monitored by an LVDT type W20. Force (one jack force) – mid-span deflections were registered graphically. Concrete strains over the mid-section were also measured by strain gauges.

### 5.2.5.1 Failure loads and failure modes

Failure loads and failure modes of steel fibre reinforced prestressed pretensioned concrete beams are summarised in Figure 5.21 for Series PC-G and for Series PC-S. The beams of Series PC-G and Series PC-S are numerated according to the fibre content. Their parameters are also presented for each beam. Shear failure, splitting failure and bending failure of beams are indicated by continuous line, dotted line and shaded area, respectively. Failure loads and failure modes of steel fibre reinforced prestressed pretensioned concrete beams and their compressive strengths at 28 days are summarised in Table 5.13.

Increasing failure load was observed by increasing steel fibre content for series PC-G even if the concrete compressive strengths were not proportional to the fibre contents. However, increment in failure load was not proportional to the fibre content for beams PC-S due to the significant impact load, which caused splitting cracks in the end block region of beams and the lower compressive strength applying 1.0V% fibre content.

**Table 5.13:** Failure loads and failure modes of steel fibre reinforced prestressed pretensioned concrete beams

Fiber type	Mixture	Release of prestressing force		Compressive strength $f_c$ [MPa]	Failure load $F_u$ [kN]	Age at testing [day]	Failure Mode
		Gradual	Sudden				
Dramix® ZC 30/5	REF-3	PC-G1	-	37.58	8.20	128	S
	FRC-3 <sup>0.5</sup> <sub>ZC 30/5</sub>	PC-G2	-	39.85	8.85	128	S+B
	FRC-3 <sup>1.0</sup> <sub>ZC 30/5</sub>	PC-G3	-	38.55	9.45	128	B
Dramix® ZC 30/5	REF-4	-	PC-S1	42.70	12.70	98	B+SP
	FRC-4 <sup>0.5</sup> <sub>ZC 30/5</sub>	-	PC-S2	43.60	12.60	98	B+S+SP
	FRC-4 <sup>1.0</sup> <sub>ZC 30/5</sub>	-	PC-S3	41.60	12.00	98	B+S+SP

S: shear failure

B: bending failure

SP: failure caused by the splitting of concrete cover

Notation	Fibre reinforcement	Failure load	Stirrup reinforcement	Failure mode
PC-G1	No fibre	$F_u = 8.20$ kN	No stirrups	Shear
PC-G2	0.5 V%	$F_u = 8.85$ kN	No stirrups	Shear Bending
PC-G3	1.0 V%	$F_u = 9.45$ kN	No stirrups	Bending
PC-S1	No fibre	$F_u = 12.70$ kN	No stirrups	Bending Splitting
PC-S2	0.5 V%	$F_u = 12.60$ kN	No stirrups	Bending Shear Splitting
PC-S3	1.0 V%	$F_u = 12.00$ kN	No stirrups	Bending Shear Splitting

**Figure 5.21:** Failure modes and failure loads of steel fibre reinforced prestressed pretensioned concrete beams

Failure modes of beams with no steel fibres were very brittle and sudden for both series of beams as common for prestressed members. When steel fibre reinforcement was applied failure became more ductile. Failure developed on the side of tendon release for beams PC-G and on the side of cutting of tendons for beams denoted PC-S. However, failure mode of beams changed from shear failure (PC-G1) to simultaneous shear and bending failure (PC-G2) by increasing the steel fibre content. Finally, clear bending failure was observed applying 1.0 V% steel fibres (PC-G3).

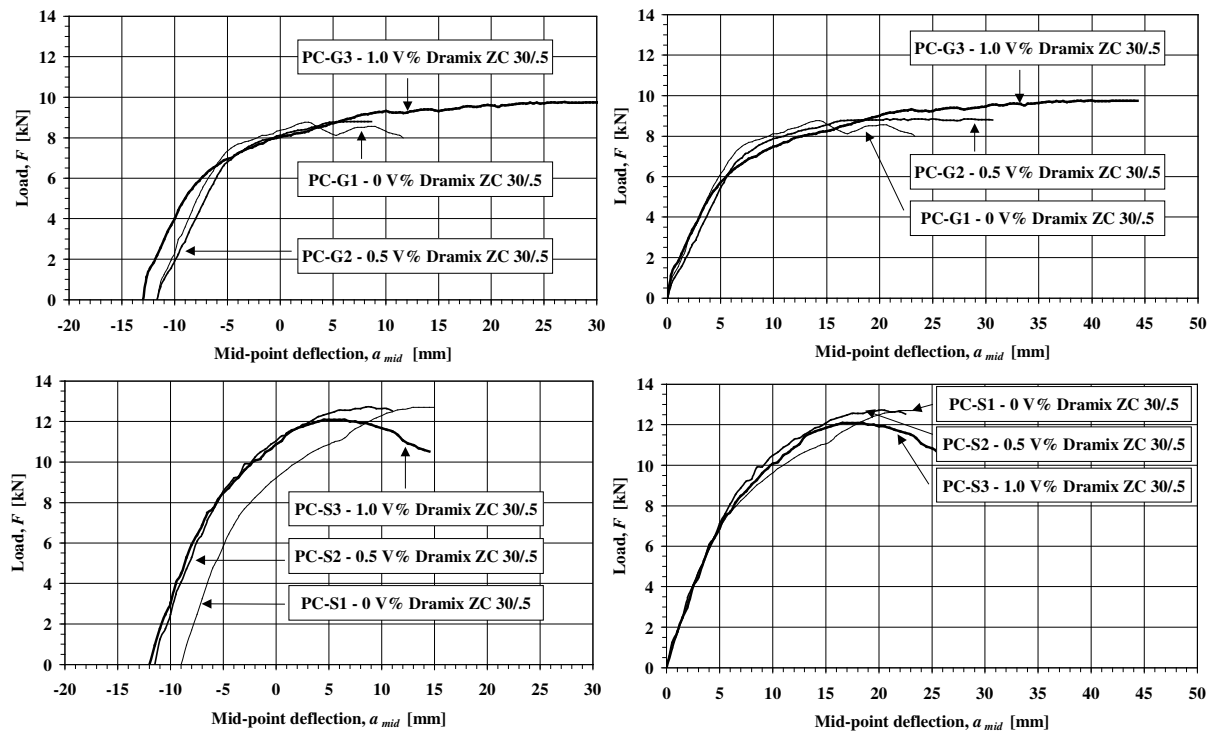
Due to the sudden release of prestressing force splitting cracks were observed at the end block region of beams in bending for beams PC-S. Directions of these cracks were more or less parallel to the prestressing strand and formed at the depth of the prestressing strand. By increasing load, opening of splitting cracks resulted splitting failure combined with bending and/or shear failure.

### 5.2.5.2 Load vs. deflection relationships

Load vs. mid-point deflection relationships are summarised in Figure 5.22. Characteristic points of the curves (mid-point deflections at failure load and ultimate mid-point deflections) are summarised in Table 5.11. Relationships presented in the first column take into consideration the camber of steel fibre reinforced prestressed pretensioned concrete beams measured at the total release of prestressing force (135.8 kN) by negative deflection values. In order to compare the stiffness of beams, second column in Figure 5.21 represents the load vs. deflection relationships neglecting the effect of camber.

Results indicate that stiffness of beams were not considerably effected by the steel fibre content. However, significant improvement in ultimate mid-point deflection was observed by increasing fibre content for beams denoted by PC-G. In case of beams PC-S, no considerable difference in the ultimate mid-point deflection was observed.

Generally, due to the impact effect of prestressing force combined splitting and shear failure was obtained for Series PC-S, and hence, as diagram also indicates rigid failure was achieved.



**Figure 5.22:** Load vs. mid-point deflection relationships for steel fibre reinforced prestressed pretensioned concrete beams

**Table 5.14:** Mid-point deflection at failure load and ultimate mid-point deflection of steel fibre reinforced prestressed pretensioned concrete beams

Fiber type	Mixture	Release of prestressing force		Failure load $F_u$ [kN]	$a_{mid,f}$ at failure [mm]	$a_{mid,t}$ ultimate [mm]	$\frac{a_{mid,f}}{a_{mid,t}}$	Failure mode
		Gradual	Sudden					
Dramix® ZC 30/5	REF-3	PC-G1		8.20	14.32	23.31	0.61	S
	FRC-3 <sup>0.5</sup> <sub>ZC 30/5</sub>	PC-G2		8.85	28.30	30.64	0.92	S+B
	FRC-3 <sup>1.0</sup> <sub>ZC 30/5</sub>	PC-G3		9.45	44.29	44.29	1.00	B
Dramix® ZC 30/5	REF-4	-	PC-S1	12.70	22.00	24.00	0.92	B+SP
	FRC-4 <sup>0.5</sup> <sub>ZC 30/5</sub>	-	PC-S2	12.60	20.00	22.50	0.89	B+S+SP
	FRC-4 <sup>1.0</sup> <sub>ZC 30/5</sub>	-	PC-S3	12.00	18.50	26.50	0.70	B+S+SP

S: shear failure

B: bending failure

SP: failure caused by the splitting of concrete cover

### 5.3 Conclusions

Based on the experimental and theoretical results of bending behaviour of prestressed pretensioned steel fibre reinforced concrete beams the following conclusions can be drawn:

1. **Strain measurements indicate** that the **development of prestressing force** needs **shorter lengths** when steel fibres are applied.
2. **Concrete strain** measured on the most compressed face of the specimens generally **increased applying fibre reinforcement** which might be caused by the variation of the porosity of concrete.
3. Released **prestressing force versus draw-in** relationships for 0 V%, 0.5 V% and 1.0 V% **fibre contents indicate** that fibre application produce **lower draw-in** of the prestressing strands.
4. **Cambers** of prestressed pretensioned concrete beams made with **steel fibres were higher** than those for specimens made with no fibres.
5. Transfer length calculations showed if **steel fibres** were applied the **transfer length** was **decreased**. However, in the practical range of the 95 to 125 kN prestressing force the **decrease** of transfer length in the presented tests was **not proportional** to the **fiber content** of the specimens. 0.5 V% fiber content resulted the shortest transfer length.
6. **Increasing failure** load was observed by increasing **steel fibre** content. However, increment in failure load was not proportional to the fibre content for beams PC-S due to the **significant impact load**.
7. **Failure modes** of beams with no steel fibres were very **brittle**. When **steel fibre reinforcement** was applied failure became **more ductile**. Failure mode of beams **changed from shear** failure (PC-G1) to simultaneous shear and **bending failure** (PC-G2) by increasing steel fibre content. Further, **clear bending** failure was observed applying 1.0 V% steel fibres (PC-G3).

# Chapter 6

## Behaviour of steel fibre reinforced concrete deep beams in shear

*16 steel fibre reinforced concrete deep beams were tested in shear. Experimental parameters were the applied fibre content (75 kg/m<sup>3</sup>, 150 kg/m<sup>3</sup>), the concrete mix proportions (FRC-1 and FRC-2), the geometry of the specimens (Db-a and DB-b) and the characteristic fibre orientation. Experimental constants were the type of steel fibres (Dramix<sup>®</sup> ZP 305). Conventional reinforcements (longitudinal or transversal steel bar) were not applied.*

*Purposes of the tests were to study the effect of fibre content and fibre orientation on the shear properties of steel fibre reinforced concrete deep beams.*

**Keywords:** deep beam, fibre orientation, shear test, shear strength, size effect

### 6.1 Experimental programme

#### 6.1.1 Test specimens and experimental variables

Experimental programme involved of 16 steel fibre reinforced concrete deep beams applying different steel fibre contents, characteristic fibre directions, concrete mix proportions and specimen geometries.

Two types of deep beam specimens were cast as discussed in Chapter 2 and shown in Figure 6.1. Deep beams denoted by DB-a and Db-b had a geometry of 500×170×100 mm and 820×340×80 mm, respectively. Specimens denoted by Db-a and Db-b were sawn out of concrete slab elements with a geometry of 800×500×100 mm (cast in formwork denoted by A), and 820×630×80 mm (cast in formworks noted by B), respectively.

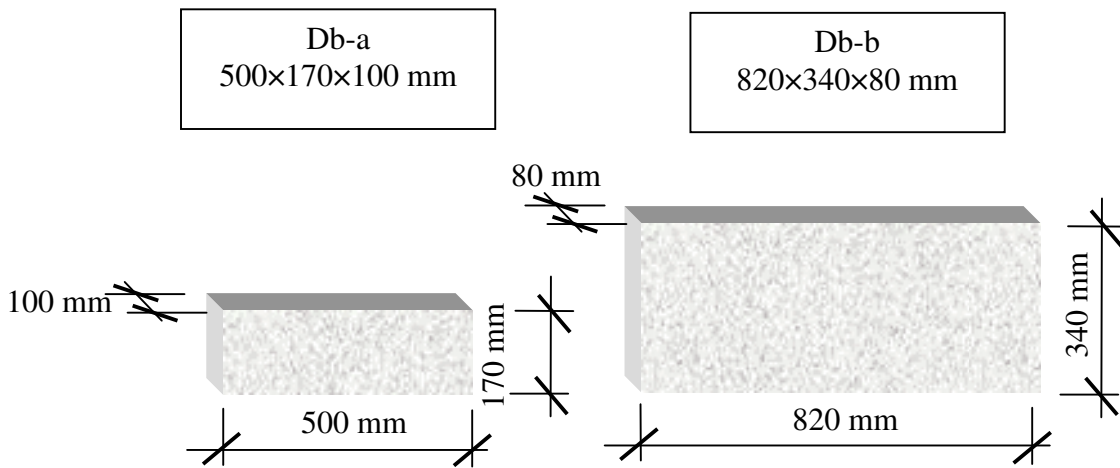
Two relatively high fibre dosages 75 kg/m<sup>3</sup> (~1.0 V%) and 150 kg/m<sup>3</sup> (~2.0 V%) were applied. Steel fibre reinforcements were the product of BEKAERT, Dramix<sup>®</sup> ZP 305 hooked-end steel fibres. Conventional longitudinal or transversal (stirrups) reinforcements were not applied.

Two characteristic fibre directions were introduced in the material during casting as discussed in Chapter 2. They were perpendicular to each other and noted by roman numbers I and II, respectively.

Deep beam specimens made of concrete types FRC-1 (FRC-1<sup>75</sup><sub>ZP 305</sub> and FRC-1<sup>150</sup><sub>ZP 305</sub>) and FRC-2 (FRC-2<sup>75</sup><sub>ZP 305</sub> and FRC-2<sup>150</sup><sub>ZP 305</sub>).

Specimens were cast and sawn out of slabs in the Laboratory of Department of Reinforced Concrete Structures and Department of Construction Materials and Engineering Geology, University of Technology Budapest.

Experimental parameters are summarised in Table 6.1.



**Figure 6.1:** Geometry of steel fibre reinforced concrete deep beam specimens

**Table 6.1:** Experimental parameters of steel fibre reinforced concrete deep beams

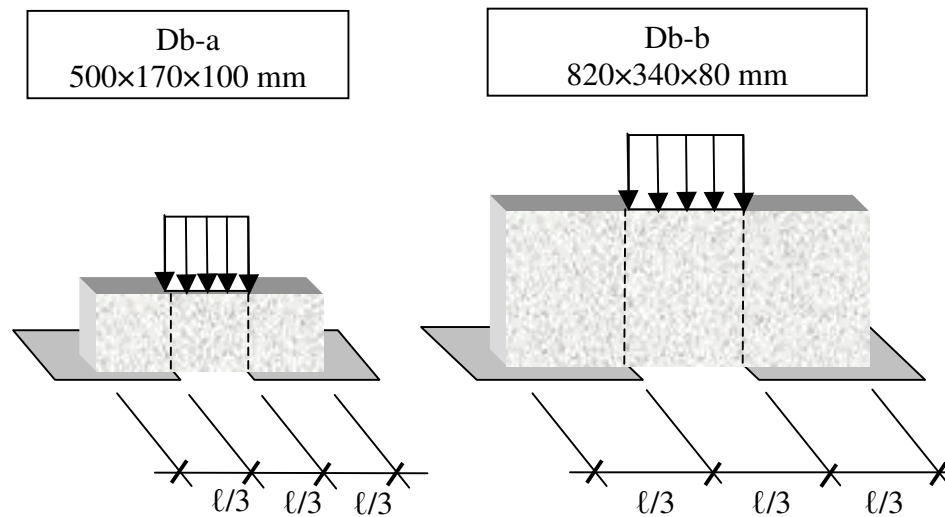
No.	Notation of deep beam	Concrete mix	Fibre content [kg/m <sup>3</sup> ]	Characteristic fibre direction	Date of casting	Date of testing	Age at testing [day]
1	DB-a1	FRC-1	75	I	05.11.99.	30.11.01.	755
2	DB-a2			II	05.11.99.	30.11.01.	755
3	DB-a3		150	I	08.12.99.	30.11.01.	715
4	DB-a4			II	08.12.99.	30.11.01.	715
5	DB-a5	FRC-2	75	I	05.11.99.	30.11.01.	755
6	DB-a6			II	05.11.99.	30.11.01.	755
7	DB-a7		150	I	08.12.99.	30.11.01.	715
8	DB-a8			II	08.12.99.	30.11.01.	715
9	DB-b1	FRC-1	75	I	05.11.99.	21.11.01.	746
10	DB-b2			II	05.11.99.	20.11.01.	745
11	DB-b3		150	I	08.12.99.	19.11.01.	702
12	DB-b4			II	08.12.99.	20.11.01.	703
13	DB-b5	FRC-2	75	I	05.11.99.	20.11.01.	745
14	DB-b6			II	05.11.99.	21.11.01.	746
15	DB-b7		150	I	08.12.99.	19.11.01.	702
16	DB-b8			II	08.12.99.	20.11.01.	703

### 6.1.2 Experimental set-up and test procedure

Shear tests were performed on all deep beam specimens. Schematic test arrangements can be seen in Figure 6.2. Test set-up and test arrangement for deep beams noted by Db-a can be seen in Photo 6.1.

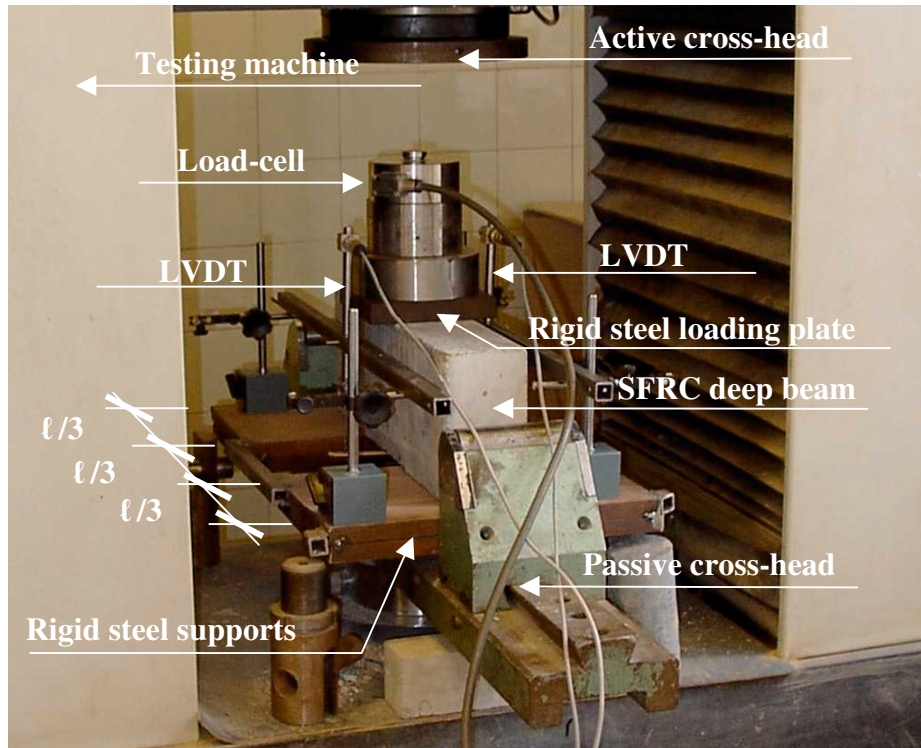
Shear tests on deep beams denoted by Db-a were carried-out by a displacement controlled Instron type servo-hydraulic testing machine with the capacity of 500 kN. Displacements were measured by two LVDTs as shown in Photo 6.1. Deep beams denoted by Db-a were placed on rigid steel plate supports positioned on the passive cross head of testing machine (Photo 6.1). Supporting steel plates were connected to each other. Load was determined according to the measuring of the load-cell placed between the specimens and the active cross head of testing machine. Speed of cross-head was 0.2 mm/min. Tests were performed in the laboratory of the Department of Construction Materials and Engineering Geology.

Tests on specimens Db-b were performed on a force controlled testing machine with the capacity of 6000 kN. Force was gradually released. Load steps were 10 kN according to the calculated failure load. Specimens were placed on a rigid steel plates as in the case of specimens Db-a. Tests were performed in the laboratory of the Department of Reinforced Concrete Structures.



**Figure 6.2:** Schematic arrangements for shear tests of steel fibre reinforced concrete deep beams





**Photo 6.1:** Test set-up and test arrangement for shear test of steel fibre reinforced concrete deep beams DB-a

## 6.2 Experimental results

Experimental results of shear tests for steel fibre reinforced concrete deep beams are summarised in Table 6.2. Failure loads, ultimate shear forces, shear strengths and failure lines as well as the characteristic fibre directions summarised on Photo 6.2 for specimens Db-a and on Photo 6.3 for specimens Db-b, respectively.

Shear strength of deep beams (denoted by  $\tau_u$  in Photo 6.2) were calculated from the ultimate shear force,  $V_u$  and the cross-section area,  $A$ . Calculated shear strengths are numerically summarised in Table 6.2 for each specimen and in Figure 6.3 for Db-a and in Figure 6.4 for Db-b. Effect of concrete mix and steel fibre content on the mean values of shear strengths are summarised in Figure 6.5.

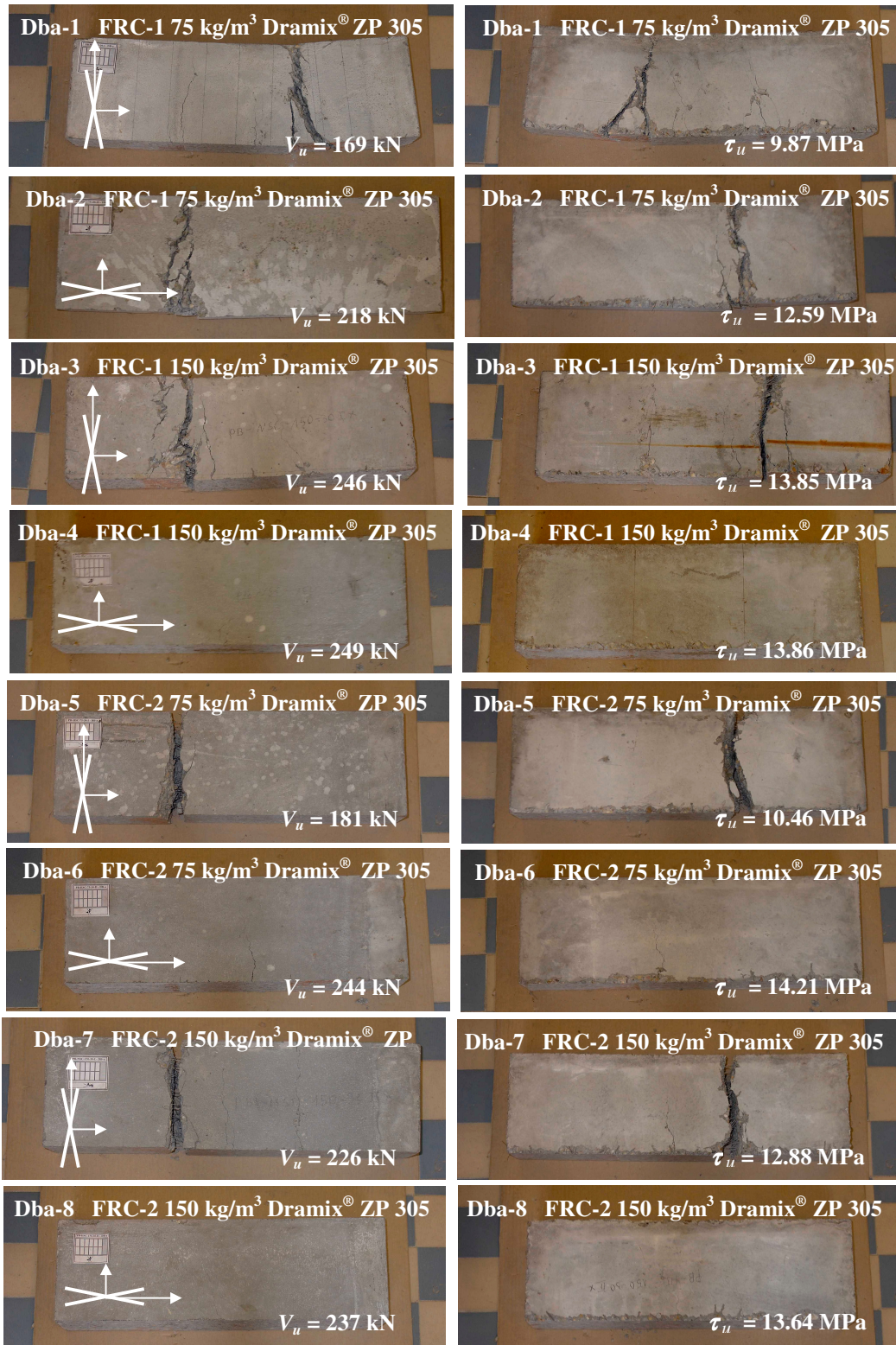
Test results indicate that steel fibre reinforcement can be effectively used to increase shear strength of concrete (Table 6.2, Figures 6.3 to 6.5). Higher shear strengths were obtained applying  $150 \text{ kg/m}^3$  Dramix<sup>®</sup> ZP 305 hooked-end steel fibres related to shear strength of specimens containing  $75 \text{ kg/m}^3$  steel fibres. Higher shear strengths were obtained in the case of concrete mix FRC-2 than in the case of FRC-1 for specimens Db-a. However, for both types of specimens, the increment in shear strength was higher for mix FRC-1.

Significant size effect was observed on shear strength. Higher shear strength was obtained for specimens DB-a than specimens Db-b.

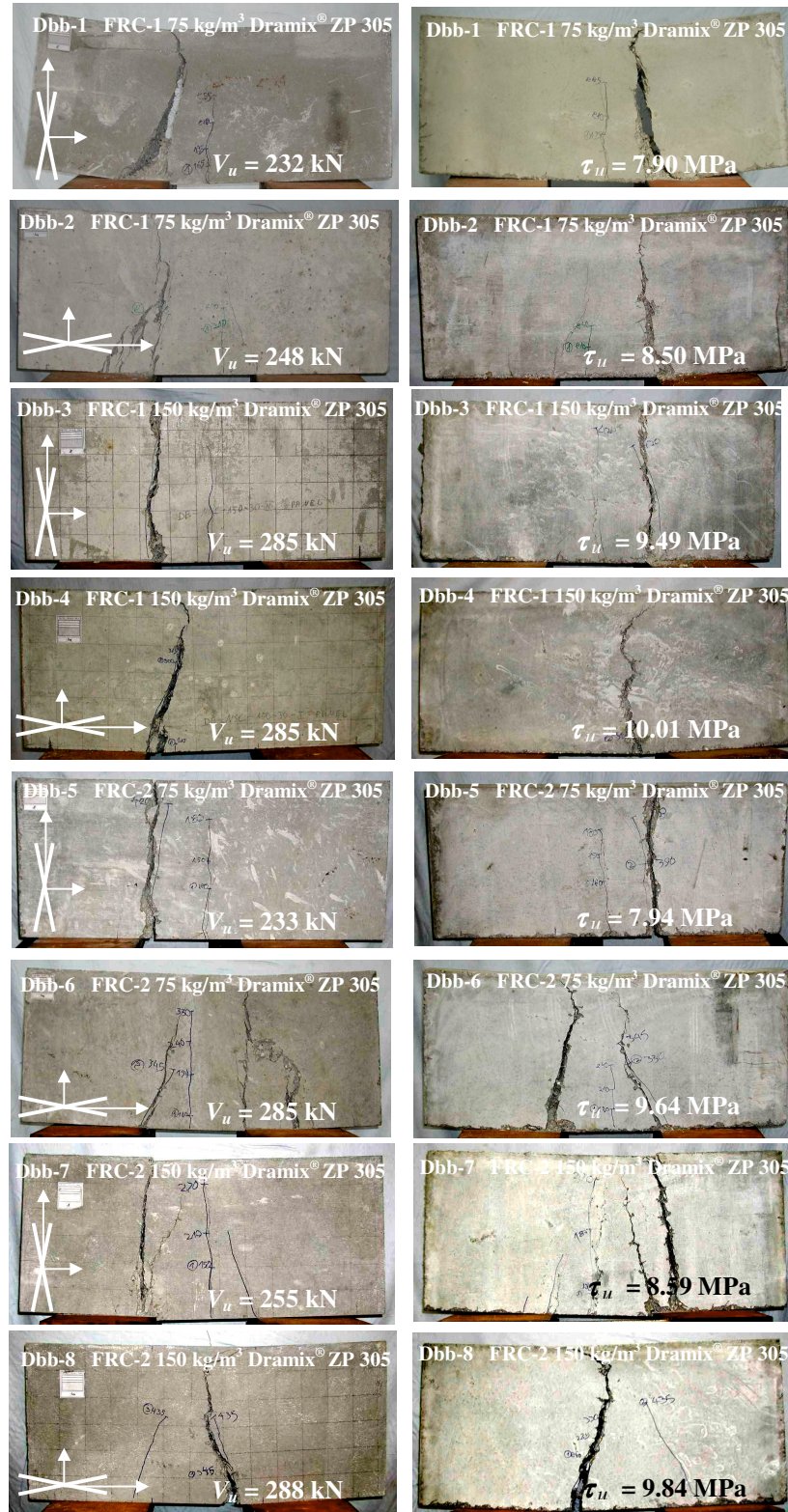
Considerable effect of the characteristic fibre direction was obtained for both types of specimens. Higher shear strengths were achieved when the characteristic fibre direction was perpendicular to the shear force (notation: II) related to the other case when the characteristic fibre direction was parallel to shear force (notation I.).

**Table 6.2:** Results of shear test for steel fibre reinforced concrete deep beams

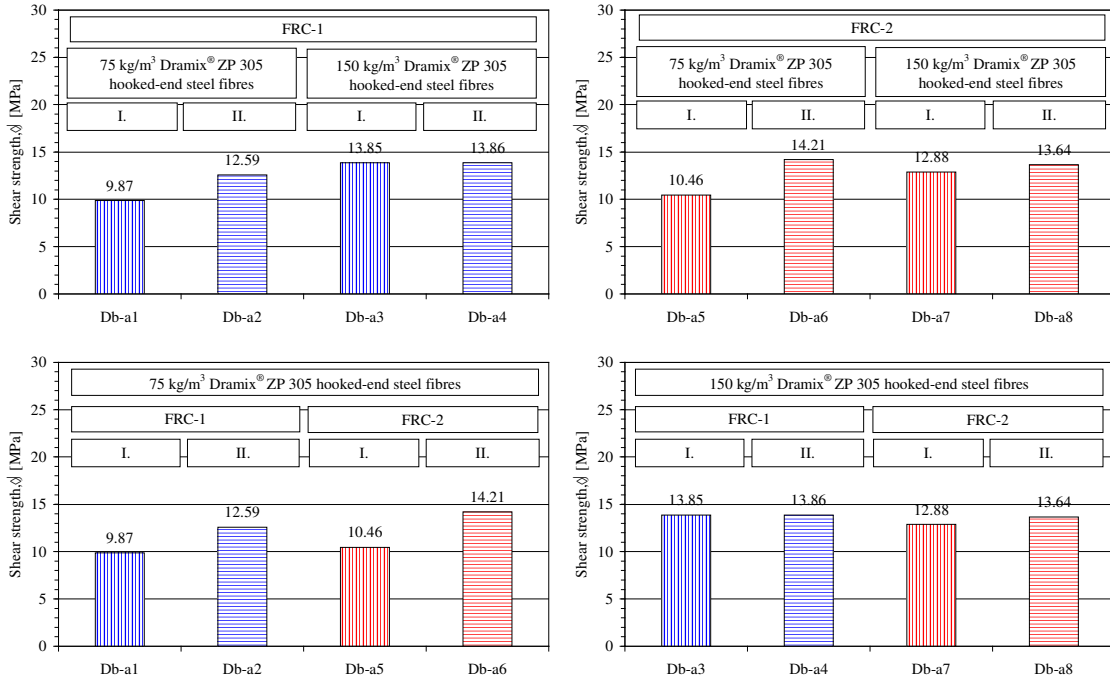
Notation of deep beam	Concrete composition	Concrete strength at 28 days	Failure load $F_u$ [kN]	Ultimate shear force $V_u$ [kN]	Shear strength $\tau_u$ [Mpa]	Mean shear strength
1	DB-a1 FRC-1 <sup>75</sup> <sub>ZP 305 - I</sub>	39.10	338	169	9.87	11.23
2	DB-a2 FRC-1 <sup>75</sup> <sub>ZP 305 - II</sub>		436	218	12.59	
3	DB-a3 FRC-1 <sup>150</sup> <sub>ZP 305 - I</sub>	33.48	492	246	13.85	13.86
4	DB-a4 FRC-1 <sup>150</sup> <sub>ZP 305 - II</sub>		498	249	13.86	
5	DB-a5 FRC-2 <sup>75</sup> <sub>ZP 305 - I</sub>	44.04	362	181	10.46	12.34
6	DB-a6 FRC-2 <sup>75</sup> <sub>ZP 305 - II</sub>		488	244	14.21	
7	DB-a7 FRC-2 <sup>150</sup> <sub>ZP 305 - I</sub>	36.80	452	226	12.88	13.27
8	DB-a8 FRC-2 <sup>150</sup> <sub>ZP 305 - II</sub>		474	237	13.64	
9	DB-b1 FRC-1 <sup>75</sup> <sub>ZP 305 - I</sub>	39.10	464	232	7.90	8.20
10	DB-b2 FRC-1 <sup>75</sup> <sub>ZP 305 - II</sub>		496	248	8.50	
11	DB-b3 FRC-1 <sup>150</sup> <sub>ZP 305 - I</sub>	33.48	570	285	9.49	9.75
12	DB-b4 FRC-1 <sup>150</sup> <sub>ZP 305 - II</sub>		570	285	10.01	
13	DB-b5 FRC-2 <sup>75</sup> <sub>ZP 305 - I</sub>	44.04	466	233	7.94	8.79
14	DB-b6 FRC-2 <sup>75</sup> <sub>ZP 305 - II</sub>		570	285	9.64	
15	DB-b7 FRC-2 <sup>150</sup> <sub>ZP 305 - I</sub>	36.80	510	255	8.59	9.22
16	DB-b8 FRC-2 <sup>150</sup> <sub>ZP 305 - II</sub>		576	288	9.84	



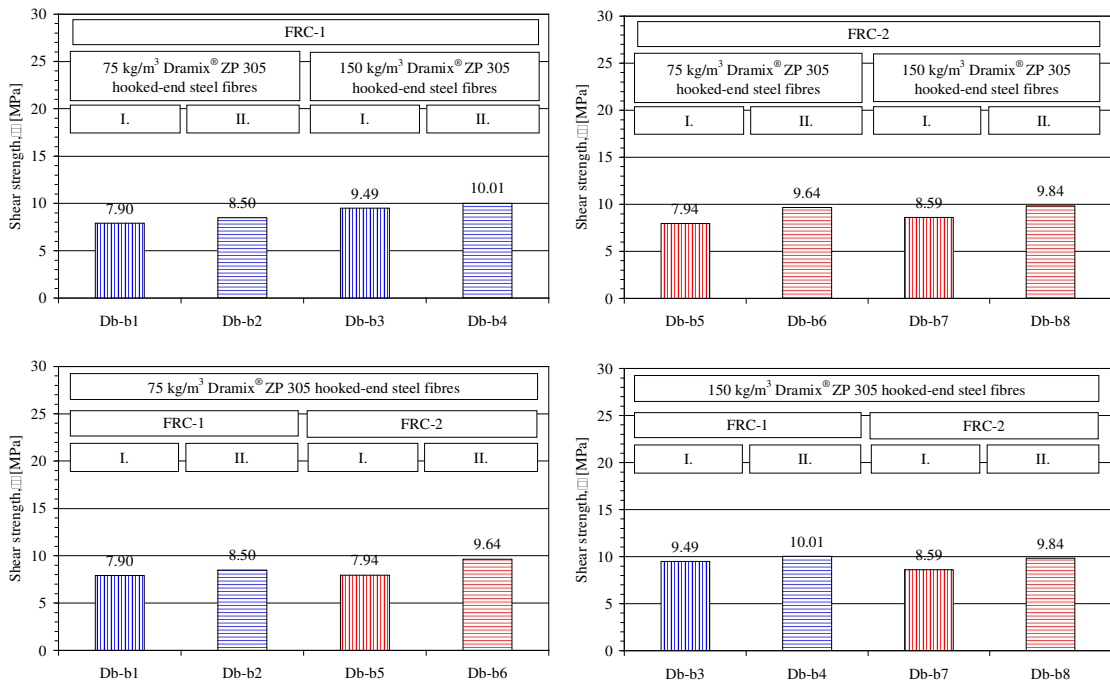
**Photo 6.2:** Experimental results of shear tests for steel fibre reinforced concrete deep beams denoted by Db-a. First and second columns represent the two sides of specimens, respectively. Ultimate shear loads, shear strengths and characteristic fibre directions are indicated on the photos.



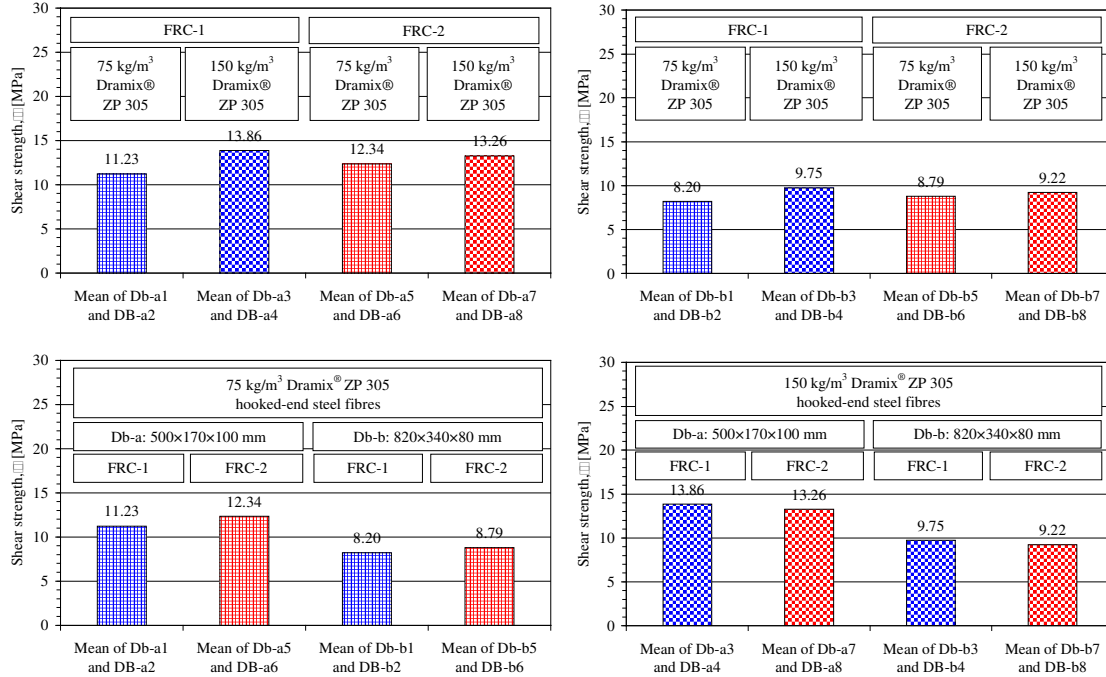
**Photo 6.3:** Experimental results of shear tests for steel fibre reinforced concrete deep beams denoted by Db-b. First and second columns represent the two sides of specimens, respectively. Ultimate shear loads, shear strengths and characteristic fibre directions are indicated on the photos.



**Figure 6.3:** Shear strength ( $V_u / A$ ) of steel fibre reinforced concrete deep beams noted by Db-a. Vertical and horizontal strips in the diagrams indicate parallel and perpendicular characteristic fibre direction to the shear force, respectively. Blue and red colours indicate concrete mixes FRC-1 and FRC-2, respectively.



**Figure 6.4:** Shear strength ( $V_u / A$ ) of steel fibre reinforced concrete deep beams noted by Db-b. Vertical and horizontal strips in the diagrams indicate parallel and perpendicular characteristic fibre direction to the shear force, respectively. Blue and red colours indicate concrete mixes FRC-1 and FRC-2, respectively.



**Figure 6.5:** Variation of shear strength effect by the concrete composition and Dramix® ZP 305 hooked-end steel fibre content

### 6.3 Conclusions

Based on the experimental results on shear tests of steel fibre reinforced concrete deep beams the following main conclusions can be drawn:

1. Shear capacity of deep beams were experimentally studied by applying only high steel fibre contents ( $75 \text{ kg/m}^3$  and  $150 \text{ kg/m}^3$ ). The observed increment in shear strengths ( $V_u/bd$ ) was 5% and 36% by increasing the steel fibre content from  $75 \text{ kg/m}^3$  (~1.0 V%) to  $150 \text{ kg/m}^3$  (~2.0 V%).
2. Variation of **shear strength** was proportional to the variation of **compressive strength**. Higher increment in shear strength was obtained when the compressive strength was higher.
3. **Shear strength** was influenced by the **characteristic fibre direction** applying relatively high steel fibre contents ( $75 \text{ kg/m}^3$  and  $150 \text{ kg/m}^3$ ). Higher shear strengths were observed when the characteristic fibre direction was perpendicular to the shear force related to the other cases when the characteristic fibre direction was parallel to the shear force.
4. **Size effect** was observed on shear strength of deep beams. Higher shear strength was obtained in the case of specimens Db-a ( $500 \times 170 \times 100 \text{ mm}$ ) than in the case of specimens Db-b ( $820 \times 340 \times 80 \text{ mm}$ ).

# Chapter 7

## Behaviour of steel fibre reinforced concrete slabs in bending

*Chapter 7 deals with an experimental study on the structural behaviour of steel fibre reinforced concrete slabs. Experimental parameters were the concrete mix proportions (FRC-1 and FRC-2), the fibre contents (75 kg/m<sup>3</sup> and 150 kg/m<sup>3</sup> steel fibres) and the privilege fibre directions. Experimental constants were the geometry of slabs (600×600×50 mm), the type of steel fibres (Dramix<sup>®</sup> ZP 305 hooked-end steel fibre) and the developed test method.*

*Purpose of the test was to study the structural performances of concrete slabs affected by steel fibre content and characteristic fibre direction.*

*Crack patterns at failure, failure loads, as well as load - deflection relationships were registered.*

**Keywords:** *concrete slab, steel fibre reinforced concrete, bending behaviour, failure load, crack pattern, load-deflection relationship*

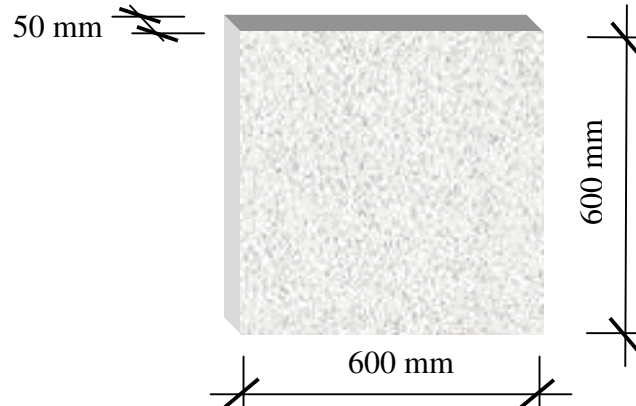
### 7.1 Experimental programme

#### 7.1.1 Test specimens and experimental variables

Experimental program involved of 4 steel fibre reinforced concrete slabs applying different steel fibre contents and concrete mix proportions.

Geometry of slabs were 600×600×50 mm. Dimensions of slabs were defined so that rational slab behaviour could be performed ( $\ell_x/d = \ell_y/d = 600/50 = 12$ ). Slabs were cast in formwork noted by C as discussed in Chapter 2.

Steel fibre reinforcement was the product of BEKAERT, Dramix<sup>®</sup> ZP 305 hooked-end steel fibre. Purpose of the experiment was to study the structural performance of concrete slabs effect by steel fibres and their orientation. For this reason, two relatively high dosages of fibres 75 kg/m<sup>3</sup> and 150 kg/m<sup>3</sup> were applied which were ~1.0 V% and ~2.0 V% fibre contents, respectively.



**Figure 7.1:** Geometry of steel fibre reinforced concrete slabs

**Table 7.1:** Experimental parameters of steel fibre reinforced concrete slab tests

No.	Notation of slab	Concrete type	Fibre type	Fibre content [kg/m <sup>3</sup> ]	Date of casting	Date of testing	Age of slab at testing [day]
1	S-1	FRC-1		75	05.11.99	06.02.02	821
2	S-2	FRC-1	Dramix®	150	08.12.99	08.02.02	790
3	S-3	FRC-2	ZP 305	75	05.11.99	07.02.02	822
4	S-4	FRC-2		150	08.12.99	08.02.02	790

Since the configuration of slabs was quadratic only one characteristic fibre orientation was introduced.

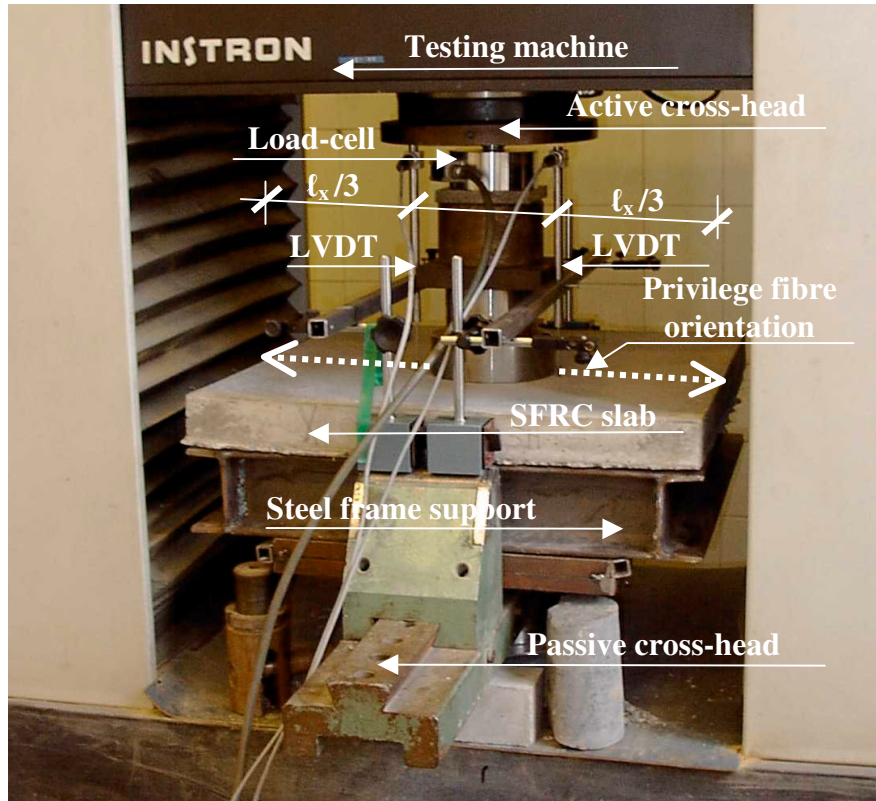
Slabs made of concrete mixes FRC-1 (FRC-1<sup>75</sup><sub>ZP 305</sub> and FRC-1<sup>150</sup><sub>ZP 305</sub>) and FRC-2 (FRC-2<sup>75</sup><sub>ZP 305</sub> and FRC-2<sup>150</sup><sub>ZP 305</sub>). Specimens manufactured in the Laboratory of Department of Reinforced Concrete Structures, and Department of Construction Materials and Engineering Geology, Budapest University of Technology and Economics.

Experimental parameters containing date of casting and date of testing are summarised in Table. 7.1.

### 7.1.2 Test set-up and experimental procedure

New experimental set-up was developed testing steel fibre reinforced concrete slabs. The most simple test arrangement and test method was performed. Two-way slabs were simply supported on a rigid steel frames produced by a steel girder I120 (MSZ 500, A37) lying on the passive cross-head of testing machine. Slabs were loaded in their central points. Tests were carried-out in displacement control by LVDTs placed on the passive cross-head the Instron type servo-hydraulic testing machine with the capacity of 500 kN. Displacements of steel fibre reinforced concrete slabs were directly measured by LVDTs placed in the third points of one of the span. Slabs were placed on the steel frame support so that the





**Photo 7.1:** Test set-up and test arrangement for bending test of steel fibre reinforced concrete slabs

characteristic fibre orientation should always be in one direction as shown in Photo 7.1. Load was determined according to the measuring of the load-cell placed between the central point of slabs and the active cross-head of Instron. Rate of cross-head displacement was 0.2 mm/min. Avoiding the damage of test set-up maximum measured deflection in the third point of the span was 8 mm ( $l/75$ ). Tests were performed in the Laboratory of Department of Construction Materials and Engineering Geology.

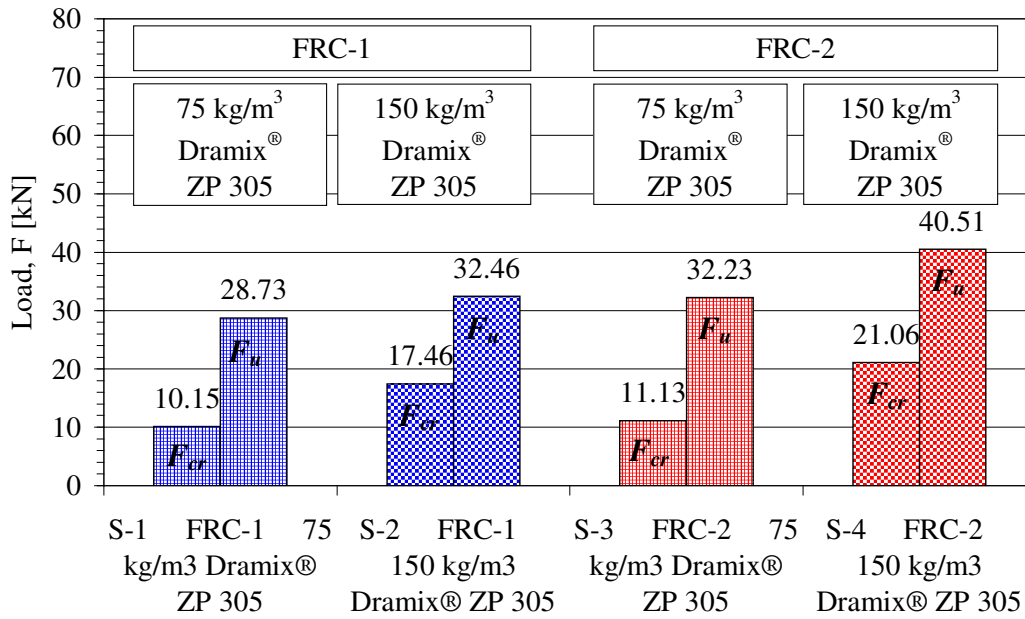
## 7.2 Experimental results and observations

### 7.2.1 Failure loads

Cracking loads ( $F_{cr}$ ) and failure loads ( $F_u$ ) as well as increments of cracking loads and failure loads of steel fibre reinforced concrete slabs are summarised in Table 7.2 and represented in Figure 7.2. Increments are explained as a function of fibre content (150 kg/m<sup>3</sup> vs. 75 kg/m<sup>3</sup>) and as a function of concrete mix (FRC-2 vs. FRC-1). In the first case cracking load of slab S-2 (FRC-1, 150 kg/m<sup>3</sup>) and S-4 (FRC-2, 150 kg/m<sup>3</sup>) are related to the cracking load of slab S-1 (FRC-1, 75 kg/m<sup>3</sup>) and S-3 (FRC-2, 75 kg/m<sup>3</sup>), respectively. In the last two columns failure load of S-3 (FRC-2, 75 kg/m<sup>3</sup>) and S-4 (FRC-2, 150 kg/m<sup>3</sup>) are related to the failure load of slab S-1 (FRC-1, 75 kg/m<sup>3</sup>) and S-2 (FRC-1, 150 kg/m<sup>3</sup>), respectively.

**Table 7.2:** Cracking loads and failure loads of steel fibre reinforced concrete slabs

No.	Notation of slabs	Concrete mix	$F_{cr}$ [kN]	$F_u$ [kN]	Increment in cracking load 150 kg/m <sup>3</sup> vs. 75 kg/m <sup>3</sup>	Increment in cracking load FRC-2 vs. FRC-1	Increment in failure load 75 kg/m <sup>3</sup> vs. 150 kg/m <sup>3</sup>	Increment in failure load FRC-1 vs. FRC-2
1	S-1	FRC-1 <sup>75</sup> <sub>ZP 305</sub>	10.15	28.73	ref.	ref.	ref.	ref.
2	S-2	FRC-1 <sup>150</sup> <sub>ZP 305</sub>	17.46	32.46	+ 72 %	ref.	+ 13 %	ref.
3	S-3	FRC-2 <sup>75</sup> <sub>ZP 305</sub>	11.13	32.23	ref.	+ 10 %	ref.	+ 12 %
4	S-4	FRC-2 <sup>150</sup> <sub>ZP 305</sub>	21.06	40.51	+ 89 %	+ 21 %	+ 25 %	+ 25 %

**Figure 7.2:** Cracking load and failure load of steel fibre reinforced concrete slabs made of concrete mix FRC-1 and FRC-2 applying 75 kg/m<sup>3</sup> and 150 kg/m<sup>3</sup> ZP 305 Dramix<sup>®</sup> hooked-end steel fibres

Results indicate that significant increment in cracking load was obtained by applying 150 kg/m<sup>3</sup> Dramix<sup>®</sup> ZP 305 hooked-end steel fibres related to slabs containing 75 kg/m<sup>3</sup> Dramix<sup>®</sup> ZP 305 hooked-end steel fibres. However, cracking loads of slabs were not significantly effected by the concrete mix proportions.

When the fibre content was 75 kg/m<sup>3</sup>, 10.15 kN ( for S-1) and 11.13 kN (for S-3) cracking load was obtained for slabs made of concrete type FRC-1 and FRC-2, respectively. Otherwise, 17.46 kN (for S-2, made of FRC-1) and 21.06 kN (for S-4, made of FRC-2) was the cracking load for slabs applying 150 kg/m<sup>3</sup> steel fibres. Consequently, more or less the same increment in cracking load was obtained in the case of mix FRC-1 (72 %) and in the case of mix FRC-2 (89 %). In contrary to the significant increment in cracking load by the increase of fibre content, cracking load was not considerably effected by the change of concrete mix from FRC-1 to FRC-2. Increment in cracking load was 10 % ( for S-3, made of FRC-2), and 21 % (for S-4, made of FRC-2) when 75 kg/m<sup>3</sup> and 150 kg/m<sup>3</sup> steel fibres were applied, related to slab S-1 (FRC-1) and S-2 (FRC-1), respectively.

Failure load increased by applying  $150 \text{ kg/m}^3$  steel fibres related to slab containing  $75 \text{ kg/m}^3$  steel fibres. By the use of  $150 \text{ kg/m}^3$  steel fibres 13 % (for S-2, made of FRC-1,  $F_u = 32.46 \text{ kN}$ ) and 25 % (for S-4, made of FRC-2,  $F_u = 40.51 \text{ kN}$ ) increment in failure load was achieved related to slabs S-1 (FRC-1,  $F_u = 28.73 \text{ kN}$ ) and S-3 (FRC-2,  $F_u = 32.23 \text{ kN}$ ), containing  $75 \text{ kg/m}^3$  steel fibres, respectively. By the change of concrete type from FRC-1 to FRC-2, 12 % (for S-3, made of FRC-2,  $75 \text{ kg/m}^3$ ) and 25 % (for S-4, made of FRC-2,  $150 \text{ kg/m}^3$ ) increment was obtained related to slabs S-1 (made of FRC-1,  $75 \text{ kg/m}^3$ ) and S-2 (made of FRC-1,  $150 \text{ kg/m}^3$ ), respectively.

## 7.2.2 Load vs. deflection relationships

Similarly to Table 7.2 and Figure 7.2, the corresponding deflections measured at cracking loads and failure loads, as well as their increments as a function of the fibre content and the concrete compositions are summarised in Table 7.3 and Figure 7.3. Load vs. deflection relationships and the schematic arrangement of measuring system for steel fibre reinforced concrete slab tests are presented in Figure 7.4.

As results indicate, deflections corresponding to the cracking loads as well as to the failure loads of steel fibre reinforced slabs increased applying  $150 \text{ kg/m}^3$  Dramix<sup>®</sup> ZP 305 hooked-end steel fibres related to slabs containing  $75 \text{ kg/m}^3$  Dramix<sup>®</sup> ZP 305 hooked-end steel fibres.

However, deflection measured at cracking loads were not significantly effect by the type of concrete. 0.82 mm (for S-1, made of FRC-1) and 1.10 mm (for S-3, made of FRC-2) deflections were obtained for slabs containing  $75 \text{ kg/m}^3$  steel fibre content. Otherwise, 1.48 mm (for S-2, made of FRC-1) and 1.83 mm (for S-4, made of FRC-2) deflections were measured on slabs applying  $150 \text{ kg/m}^3$  steel fibres. Hence, more or less the same increment in deflection was obtained by the increase of fibre content in the case of both concrete mix FRC-1 (80 %) and FRC-2 (66 %).

In contrast to the notable increment in deflection measured at cracking by the increase of fibre content, the variation of concrete type from FRC-1 to FRC-2 did not significantly effect the deflection applying the same fibre content. When  $75 \text{ kg/m}^3$  fibres were applied 34 % (S-3, FRC-2), when  $150 \text{ kg/m}^3$  fibres were used 24 % (S-4, FRC-2) increments in deflections were obtained related to slab S-1 (made of FRC-1) and S-2 (made of FRC-1), respectively.

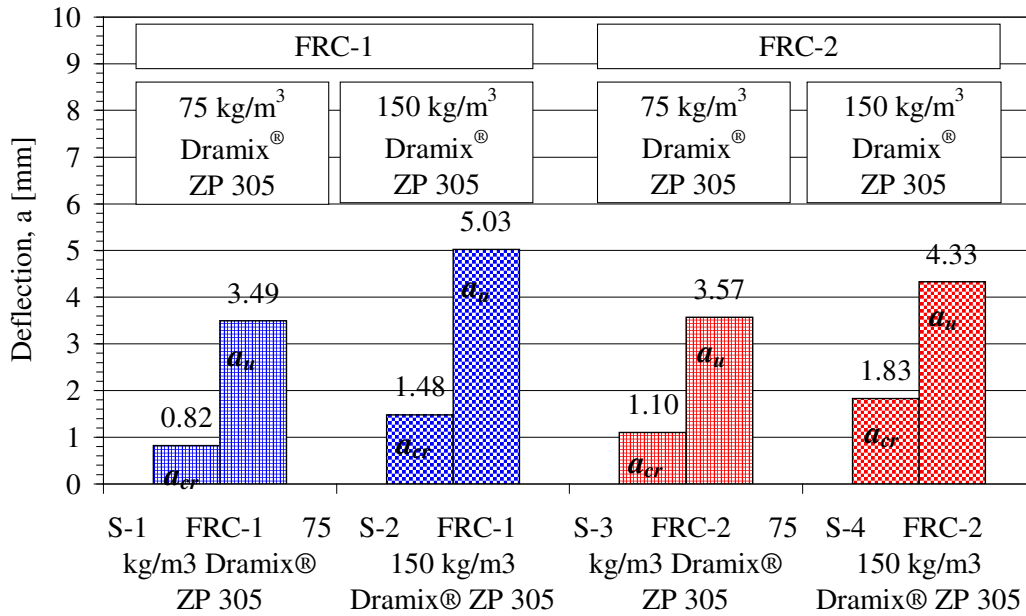
Deflection at failure loads also increased applying  $150 \text{ kg/m}^3$  steel fibres related to slabs containing  $75 \text{ kg/m}^3$  steel fibres. By the use of  $150 \text{ kg/m}^3$  fibre content 44 % (for S-2, made of FRC-1,  $a_{Fu} = 5.03 \text{ mm}$ ) and 21 % (for S-4, made of FRC-2,  $a_{Fu} = 4.33 \text{ mm}$ ) increment in deflection at failure load was measured, related to slabs S-1 (made of FRC-1,  $a_{Fu} = 3.49 \text{ mm}$ ) and S-3 (made of FRC-2,  $a_{Fu} = 3.57 \text{ mm}$ ), containing  $75 \text{ kg/m}^3$  steel fibres, respectively.

2 % (for S-3, made of FRC-2,  $75 \text{ kg/m}^3$ ) and 21 % (for S-4, made of FRC-2,  $150 \text{ kg/m}^3$ ) increments were obtained related to slabs S-1 (made of FRC-1,  $75 \text{ kg/m}^3$ ) and S-2 (made of FRC-1,  $150 \text{ kg/m}^3$ ) by the variation of concrete mix from FRC-1 to FRC-2, respectively.

Figure 7.3 indicates, that  $150 \text{ kg/m}^3$  Dramix<sup>®</sup> ZP 305 hooked-end steel fibres provides more smooth load vs. deflection relationships than  $75 \text{ kg/m}^3$  Dramix<sup>®</sup> ZP 305 hooked-end steel fibres. Due to the relatively high fibre dosage, significant strain-hardening behaviour was obtained after cracking. However, better elastic-plastic behaviour was obtained by the use of concrete mix FRC-2.

**Table 7.3:** Measured deflections at cracking load and at failure load of steel fibre reinforced concrete slabs

Notation of slab	Concrete type	$a_{Fcr}$ [mm]	$a_{Fu}$ [mm]	Increment in deflection at cracking 150 kg/m <sup>3</sup> vs 75 kg/m <sup>3</sup>	Increment in deflection at cracking FRC-2 vs. FRC-1	Increment in deflection at failure load 150 kg/m <sup>3</sup> vs 75 kg/m <sup>3</sup>	Increment in deflection at failure load FRC-2 vs. FRC-1
1	S-1 FRC-1 <sup>75</sup> <sub>ZP 305</sub>	0.82	3.49	ref.	ref.	ref.	ref.
2	S-2 FRC-1 <sup>150</sup> <sub>ZP 305</sub>	1.48	5.03	+ 80 %	ref.	+ 44 %	ref.
3	S-3 FRC-2 <sup>75</sup> <sub>ZP 305</sub>	1.10	3.57	ref.	+ 34 %	ref.	+ 2 %
4	S-4 FRC-2 <sup>150</sup> <sub>ZP 305</sub>	1.83	4.33	+ 66 %	+ 24 %	+ 21 %	+ 21 %

**Figure 7.3:** Measured deflections at cracking load and at failure load of steel fibre reinforced concrete slabs made of concrete mix FRC-1 and FRC-2 applying 75 kg/m<sup>3</sup> and 150 kg/m<sup>3</sup> Dramix® ZP 305 hooked-end steel fibres

### 7.2.3 Crack development and failure line

After bending tests of steel fibre reinforced concrete slabs, crack pattern was analysed as a function of steel fibre content and characteristic fibre direction.

Failure lines of slabs can be seen in Photo 7.2. Photos were made after bending tests representing deformations at different failure load levels. Failure loads as well as the schematic representation of the characteristic fibre directions are also presented on the Photo 7.2. Photos indicate that directions of crack propagations were more or less parallel with the characteristic fibre direction. However, crack propagation was effected by the used concrete mix and applied fibre content as well. In the case of concrete mix FRC-2 (for S-3 and S-4) smaller amount of cracks were developed on the surface of slabs, than in the case of concrete mix FRC-1 (for S-1 and S-2), considering the same fibre content. In case of both concrete mixes, 75 kg/m<sup>3</sup> fibre content resulted more cracks than 150 kg/m<sup>3</sup> fibre content.

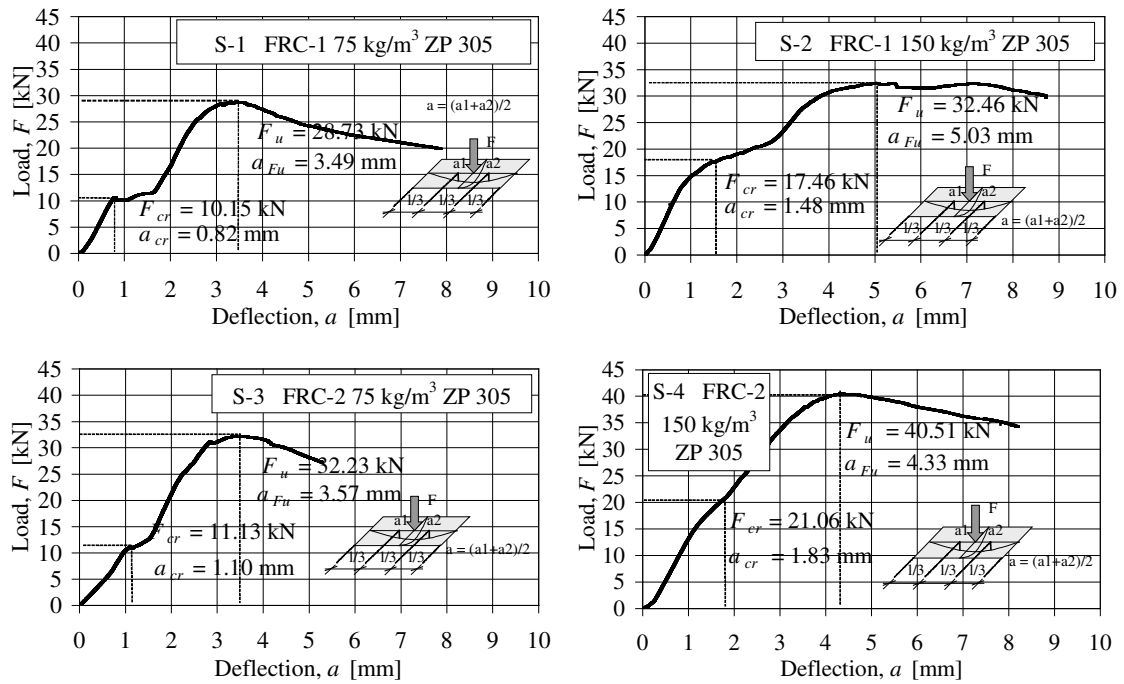


Figure 7.4: Load vs. deflection relationships for steel fibre reinforced concrete slabs

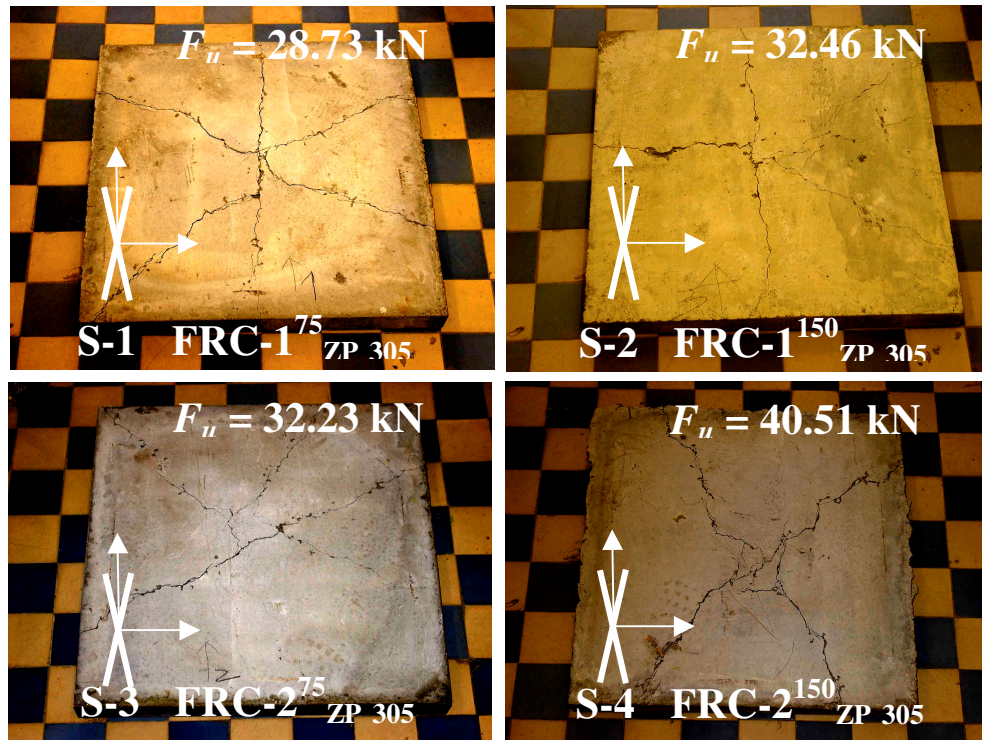
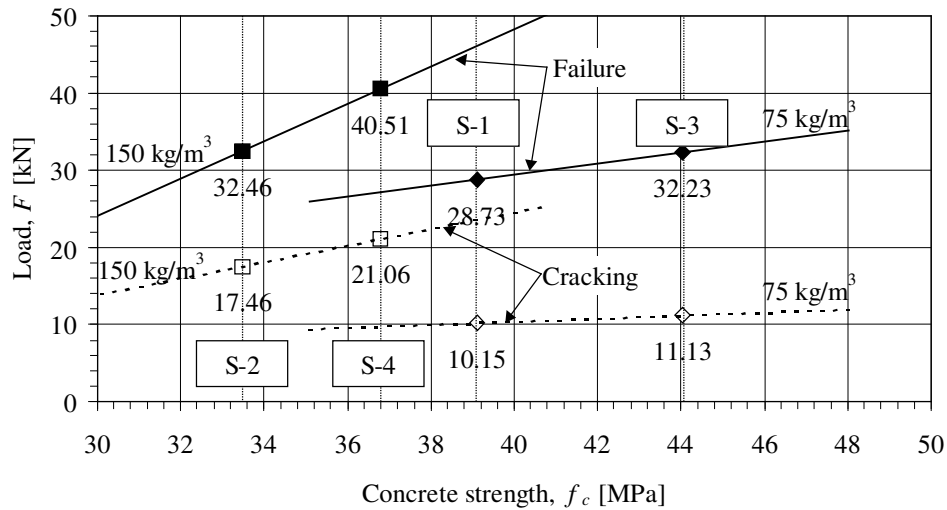


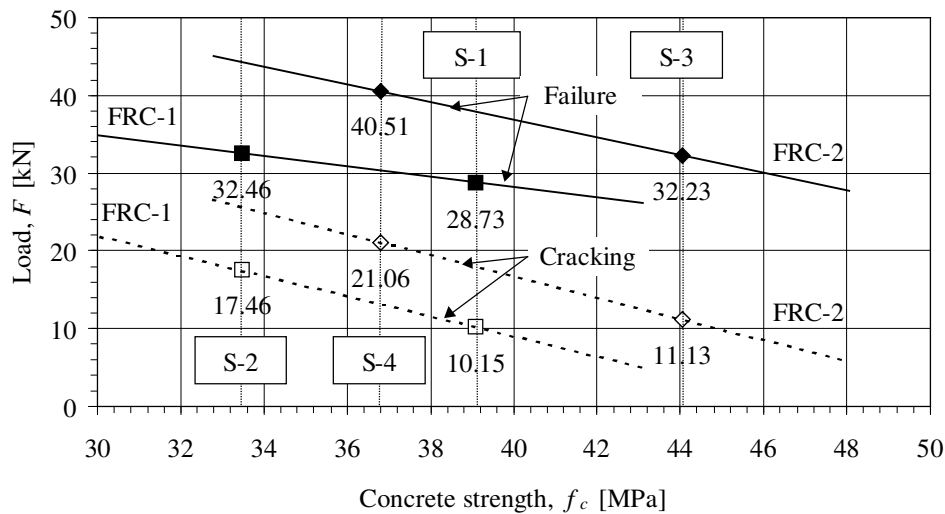
Photo 7.2: Crack patterns and failure loads of steel fibre reinforced concrete slabs. Characteristic fibre directions are indicated on the photos.

### 7.2.4 Effect of compressive strength

Cracking load as well as failure load of steel fibre reinforced concrete slabs as a function of concrete strength measured on 240×100×100 prisms are summarised in Figure 7.5 - 7.6. Effect of concrete mix (FRC-1 and FRC-2) and Dramix® ZP 305 hooked-end steel fibre contents (75 kg/m<sup>3</sup> and 150 kg/m<sup>3</sup>) are illustrated in Figure 7.5 and Figure 7.6. Dotted and continuous lines indicate cracking loads and failure loads, respectively. Vertical dotted lines sign the steel-fibre reinforced concrete slabs, S-1, S-2, S-3 and S-4.



**Figure 7.5:** Cracking load as well as failure load of steel fibre reinforced concrete slabs as a function of the concrete strength and Dramix® ZP 305 hooked-end steel fibre content. Dotted lines and continuous lines indicate the cracking load and failure load, respectively.



**Figure 7.6:** Cracking load as well as failure load of steel fibre reinforced concrete slabs as a function of the concrete strength and the concrete compositions (FRC-1 and FRC-2). Dotted lines and continuous lines indicate the cracking load and failure load, respectively.

Diagrams indicate that structural performance of steel-fibre reinforced concrete slabs are strongly depend on the steel fibre content and on the concrete mix as well. However, tendencies in cracking loads and in failure loads are different.

Considering the same steel fibre content Figure 7.5 indicates that cracking load as well as failure load increased by the change of concrete mix from FRC-1 (for S-1 and S-2) to FRC-2 (for S-3 and S-4).

By 9.90% increment in compressive strength in case of slab S-2 (made of FRC-1, 150 kg/m<sup>3</sup> steel fibres) 21% and 25% increment in cracking load and in failure was obtained related to slab S-4 (made of FRC-2, 150 kg/m<sup>3</sup> steel fibres).

Otherwise for S-3 (made of FRC-2, 75 kg/m<sup>3</sup>), 12.6% increment in concrete strength yield to 10% and 12% increment in cracking load and in failure load related to slab S-1 (made of FRC-1, 75 kg/m<sup>3</sup>), respectively.

However, for both concrete mix lower cracking load and failure load was obtained by the use of 75 kg/m<sup>3</sup> fibre content related to mixes containing 150 kg/m<sup>3</sup> steel fibres, even if the concrete strength increased.

Main reason of the observed phenomena and tendencies shown in Figure 7.5 and in Figure 7.6 may lie in the higher porosity of concrete mix containing 150 kg/m<sup>3</sup> steel fibres. However, despite of the lower concrete strength of mixtures made with 150 kg/m<sup>3</sup> steel fibres, both cracking load and failure load of slabs increased, related to the mixtures containing 75 kg/m<sup>3</sup> steel fibres.

### 7.3 Conclusions

Based on the experimental results on bending tests of steel fibre reinforced concrete slabs the following main conclusions can be drawn:

1. **New test method** as well as **test set-up** were developed for bending test of simply supported steel fibre reinforced concrete slabs.
2. **Cracking load** of steel-fibre reinforced concrete slabs are strongly **effect** by the applied **steel fibre** content and the **concrete mix**.
3. **Failure load** of steel-fibre reinforced concrete slabs are also strongly **effect** by the applied **fibre content** and the used **concrete mix**.
4. **Deflection** measured at **cracking load** of steel-fibre reinforced concrete slabs is effect by the applied **steel fibre** content and the used concrete mix.
5. **Deflection** measured at **failure load** of steel-fibre reinforced concrete slabs are effect by the applied **steel fibre** content and the used concrete mix.
6. **Significant post cracking behaviour** was observed after cracking of steel fibre reinforced concrete slabs which was proportional to the applied **steel fibre** content.
7. **Crack propagation** and **crack distribution** of slabs were effect by the characteristic fibre direction. Direction of the main crack propagation was more or less parallel to the **characteristic fibre direction**.
8. **Steel fibre reinforcement** can effectively be used to reduce **crack width**, to control crack propagation and crack distribution of steel fibre reinforced concrete slabs. Smaller amount of cracks were developed applying higher steel fibre content.

---

# References

## Publications

**Abrishami, H.H., Mitchell, D. (1996)** "Analysis of Bond Stress Distribution in Pullout Specimens", *Journal of Structural Engineering*, Vol. 122, No. 3, March, 1996, pp. 255-261.

**Acharya, D.N., Kemp, K.O. (1965)** "Significance of Dowel Forces on the Shear Failure of Rectangular Reinforced Concrete beams Without Web Reinforcement", *Journal of the American Concrete Institute*, Proceedings Vol. 62, No. 10, October, 1965, pp. 1265-1279.

**ACI (1987)** "Fiber Reinforced Concrete Properties and Applications", *ACI SP-105*, Detroit, Michigan, 1987.

**ACI Committee 544 (1984)** "Guide for Specifying Mixing, Placing, and Finishing Steel Fiber Reinforced Concrete", *ACI SP-81*, 1984, pp. 441-447.

**ACI Committee 544 (1986)** "State-of-the-Art Report on Fiber Reinforced Concrete", *ACI Committee Report*, 1986.

**ACI Committee 544 (1988)** "Design Considerations for Steel Fiber Reinforced Concrete", *ACI Committee Report, ACI Structural Journal*, September-October, 1988, pp. 563-580.

**ACI Committee 211 (1989)** "Standard Practice for Selecting Proportions for Normal, Heavyweight, and Mass Concrete", *ACI 211.1-89*, American Concrete Institute, Detroit, Michigan 1989, 38 p.

**ACI Committee 215 (1990)** "Considerations for Design of Concrete Structures Subjected to Fatigue Loading", *ACI Manual of Concrete Practice*, 1990, Part I, pp. 215-1 to 215-25.

**Agarwal, B., and Broutman, L. (1980)** "Analysis and Performance of Fiber Composites", *John Wiley & Sons*, New York, 1980, pp. 78-81.

**Anderson, N.S., Ramirez, J.A. (1989)** "Detailing of Stirrup Reinforcement", *ACI Structural Journal*, Vol. 86, No. 5, September-October, 1989., pp. 507-515.

**Armelin, H.S., Bantia, N. (1998)** "Steel Fiber Rebound in Shotcrete", *Concrete International*, September, 1998 pp. 74-79.



- 
- ASCE-ACI Committee 445 on Shear and Torsion (1998)** "Recent Approaches to Shear Design of Structural Concrete", *Journal of Structural Engineering*, Vol. 124, No. 12, December, 1998, pp. 1375-1417.
- Balaguru, P. (1994)** "Contribution of Fibers to Crack Reduction of Cement Composites During the Initial and Final Setting Period", *ACI Materials Journal*, Vol. 91, No. 3, May-June, 1994, pp. 280-288.
- Balaguru, P, and Ezeldin, A.S. (1987)** "Behavior of Partially Prestressed Beams Made with High Strength Fiber Reinforced Concrete", *ACI SP-105: Fiber Reinforced Concrete Properties and Applications*, American Concrete Institute, Detroit, Michigan, 1987, pp. 517-563.
- Balaguru, P., Narahari, R., Patel, M. (1992)** "Flexural Toughness of Steel Fiber Reinforced Concrete", *ACI Material Journal*, Vol. 86, No. 6, November-December, 1992, pp. 541-546.
- Balaguru, P., and Ramkrishnan. V. (1986)** "Freeze-Thaw Durability of Fiber Reinforced Concrete", *ACI Journal*, Vol.83, 1986, pp. 374-382.
- Balaguru, P., and Ramkrishnan. V. (1988)** "Properties of Fiber Reinforced Concrete: Workability, Behavior under Long-Term Loading, and Air-Void Characteristics", *ACI Materials Journal*, Vol. 85, May-June 1988, pp.189-196.
- Balaguru, P.N., and Shah, S.P. (1992)** "Fiber-Reinforced Cement Composites" *McGraw-Hill Inc.* 1992.
- Balázs, L. Gy., Erdélyi, L., Kovács, I. (1997)** "Fiber Reinforced Prestressed Concrete", *Proceedings of the FIP Symposium 1997, Johannesburg*, Vol. 1, pp. 223-232.
- Balázs, L., Gy., Kovács, I. (1997)** "Increase in shear strength of beam by applying fiber reinforcement", *Proceedings in honour of Prof. Mehlhorn's 65<sup>th</sup> birthday*, Sept. 1997, pp.10-17.
- Balázs, L., Gy., Kovács I. (1999)** "Flexural behavior of RC and PC beams with steel fibers", *Proceedings of the 3<sup>th</sup> RILEM/ACI Workshop on High Performance Fiber Reinforced Cement Composites*, Mainz, May 17-19. 1999, pp. 499-509.
- Balázs, L., Gy., Kovács I. (1999)** "Concrete members with Traditional Reinforcement and Fibers", *Proceedings of the fib Symposium, Prague*, Oct. 13-15. 1999., pp.
- Banthia, N., Trottier, J. F. (1995)** "Test Methods for Flexural Toughness Characterization of Fiber Reinforced Concrete: Some Concerns and a Proposition", *ACI Material Journal*, Vol. 92, No. 1, January-February 1995, pp. 48-57.
- Batson et al. (1972)** "Flexural Fatigue Strength of Steel Fiber Reinforced Concrete Beams", *ACI Journal*, Vol. 69, No.11, 1972, pp. 673-677.
- Bekaert (1994)** "DRAMIX: Stahlfasern - die neuzeitliche Betonbewehrung" *Bekaert*, Belgien
- Brock, J. (1964)** "The Riddle of Shear Failure and Its Solution", *ACI Journal*, Proceedings Vol. 61, No. 12, December, 1964, pp. 1587-1636.
- Bolander, J. E., Saito, S. (1992)** "Discrete Modeling of Short-Fiber Reinforcement in Cementitious Composites", *Advance Cement Based Materials* / July, 1992, pp.76-86.
-

- Chern, J.C., and Young, C.H. (1989)** "Compressive Creep and Shrinkage of Steel Fiber Reinforced Concrete", *The International Journal of Cement Composites and Lightweight Concrete*, Vol. 11, No.4, 1989, pp. 205-214.
- Chern, J.C., Yang, H.J., and Chen, H.-W. (1992)** "Behavior of Steel Fiber Reinforced Concrete in Multiaxial Loading", *ACI Materials Journal*, Vol. 89, No. 1, January-February, 1992, pp. 32-41.
- Craig, R. (1987)** "Flexural Behavior and Design of Reinforced Fiber Concrete Members", *ACI SP-105: Fiber Reinforced Concrete Properties and Applications*, American Concrete Institute, Detroit, Michigan, 1987, pp. 517-563.
- Craig, R.J., Parr, J.A., Germain, E., Mosquera, V., Kamilaes, S. (1986)** "Fiber Reinforced Beams in Torsion", *ACI Journal* / November-December, 1986, pp. 934-942.
- DIN (1991)** "DIN Merkblatt – Grundlagen zur Bemessung von Industriefusböden aus Stahlfaserbeton"
- Di Prisco, M., Caruso, M.L., Piatti, S., (1994)** "On Fiber Role in Dowel Action", *Studia E Ricerche*, Vol. 15, Politecnico di Milano, Italia, 1994
- Dombi J. (1993)** "Applying steel fibre reinforcement in Siome type concrete tubes", (in Hungarian) *Közlekedésépítés- és Mélyépítéstudományi Szemle*, XLIII. Évfolyam, 8. Szám, 1993, pp. 306-313.
- Dubey, A., Banthis, N. (1998)** "Influence of High-Reactivity Metakaolin and Silica Fume on the Flexural Toughness of High-Performance Steel Fiber-Reinforced concrete", *ACI Material Journal*, Vol. 95, No. 3, May-June, 1998, pp. 284-292.
- Dulácska, E. (1994)** "Design problems of steel fibre reinforced concrete structures", (in Hungarian), *Közlekedésépítés és Mélyépítéstudományi Szemle*, XLIV. Évfolyam, 7. Szám, 1994, pp. 263-274.
- Dulácska, E. (1996)** "Experimental study on the behaviour of steel fibre reinforced concrete beams", (in Hungarian) *Közúti Közlekedés- és Mélyépítéstudományi Szemle*, XLVI. Évfolyam, 10. Szám, 1996, pp. 402-407.
- El-Niema, E. I. (1991)** "Reinforced Concrete Beams with Steel Fibers under Shear", *ACI Structural Journal*, Vol. 88, No. 2, March-April, 1991, pp. 178-183.
- Erdélyi A., (1993)** "The toughness of Steel Fiber Reinforced Concrete", *Periodica Politechnica*, 1993, Vol. 37, No. 4, pp. 329-344.
- Erdélyi, L. (1996)** "Transmission Length Determination Based on Measured Draw-In and Concrete Strain", *Periodica Polytechnica*, 1996.
- Erdélyi, L., Kovács, I., Balázs, L., Gy. (1999)** "Determination of transmission length in steel fibre reinforced concrete beams", (in Hungarian) *Proceedings of the 1<sup>st</sup> International Conference on Steel Fibre Reinforced Concrete – from the research to the practice*, Budapest, 1999, március 4-5., pp. 151-171.
- Falkner, H., and Teutsch, M. (1993)** "Dauerhafte Bauwerke aus Faserbeton" *Braunschweiger Bauseminar 11-12. Nov. 1993*, Heft 105, Braunschweig 202 p.
- Falkner, H., Kubat, B, and Drosen, S. (1994)** "Durchstanzversuche an Platten aus Stahlfaserbeton", *Bautechnik*, Vol. 71, 1994, Helf 8., pp 460-467.

- Fattuhi, N.I. (1987)** "SFRC Corbel Tests", *ACI Structural Journal* / March-April, 1987, pp. 119-123.
- FIP (1982)** "Prestressing Steel: 7. Test for the determination of tendon transmission length under static conditions", *Report*, FIP, 1982
- Gokoz, U.N., and Naaman, A.E. (1981)** "Effect of Strain-Rate on the Behaviour of Fibers in Mortar", *International Journal of Cement Composites*, Vol.3, No.3, Aug. 1981, pp. 187-202.
- Goldfein, S. (1965)** "Fibrous Reinforcement for Portland Cement", *Modern Plastics*, Vol.42, No.8, 1965, pp. 156-160.
- Gopalaratnam, V.S., and Abu-Mathkour, H.J. (1987)** "Investigation of the Pull-Out Characteristics of Steel Fibers from Mortar Matrices", *Proceedings, International Symposium on Fiber Reinforced Concrete, Madras*, Dec. 1987, pp. 2.201-2.211.
- Gopalartnam, V.S. (1991)** "Fracture Toughness of Fiber Reinforced Concrete", *ACI Materials Journal*, Vol.88., No.4, 1991, pp.339-353.
- Gopalaratnam, V.S., and Shah, S.P. (1986)** "Properties of Steel Fiber Reinforced Concrete Subjected to Impact Loading", *ACI Journal*, Vol.83, No.1, 1986, pp. 117-126.
- Gray, R.J., and Johnston, C.D. (1978)** "Measurement of Fiber-Matrix Interfacial Bond Strength in Steel Fiber-Reinforced Cementitious Composites", *Proceedings of the RILEM Symposium: Testing and Test Methods of Fiber Cement Composites*, Construction Press, Lancaster, 1978, pp. 317-328.
- Groth, P., Noghabai, K. (1996)** "Fracture Mechanics Properties of Steel Fibre Reinforce High-Performance Concrete", *Proceedings of the 4<sup>th</sup> International Symposium on Utilization of High-Strength/High-Performance Concrete, Paris*, 1996, pp. 747-756.
- Hannant D.J. (1975)** "Additional Data on Fiber Corrosion in Cracked Beams and Theoretical Treatment of the Effect of Fiber Corrosion on Beam Load Capacity", *RILEM Symposium on Fiber Reinforced Cement and Concrete*, Vol. II, 1975, pp. 533-538.
- Hannant, D.J. (1978)** "Fiber Cements and Fiber Concretes, Wiley, Chicester, 1978, 219 p.
- Hannant D.J. (1989)** "Ten Year Flexural Durability Tests on Cement Sheets Reinforced with Fibrillated Polypropylene Networks", *Fiber Reinforced Cements and Concretes-Recent Developments*, Elsevier, 1989, pp. 572-563.
- Hanecka, S., Krizma, M., Ravinger, J., Shawkat, S. (1994)** "Contribution to Limit State of the Second Group of Beam Subjected to Moving Load"
- Hashin, Z. (1983)** "Analysis of composite materials", *Journal of applied Mechanics*, Vol. 50, September, 1983, pp. 481-505.
- Houde, J., Prezeau, A., and Roux, R. (1987)** "Creep of Concrete Containing Fibers and Silica Fume", *ACI SP-105: Fiber Reinforced Concrete Properties and Applications*, American Concrete Institute, Detroit, Michigan, 1987, pp. 101-118.

- Hsu, T.T.C. (1998)** "Stresses and Crack Angles in Concrete Membrane Elements", *Journal of Structural Engineering*, Vol. 124, No. 12, December, 1998, pp. 1476-1484.
- Hsu, T.T.C., Mau, S.T., Chen, B. (1987)** "Theory of Shear Transfer Strength of Reinforced Concrete", *ACI Structural Journal*, March-April, 1987, pp. 149-160.
- Imam, M., Vandewalle, L. (1996)** "How Efficient are Steel Fibres in High Strength Concrete Beams?", Proceedings of the 4<sup>th</sup> International Symposium on Utilization of High-Strength/ High-Performance Concrete, Paris, 1996, pp. 1067-1076.
- JSCE (The Japan Society of Civil Engineers) (1984)** "Method of Tests for Steel Fiber Reinforced Concrete", *Concrete Library of JSCE, Part III-2*, 1984.
- Kani, G.N.J. (1964)** „The Riddle of Shear Failure and Its Solution“, *Journal of the American Concrete Institute*, Proceedings, Vol. 61, No. 4, April, 1964, pp. 441-467.
- Kausay, T., (1994)** "Acélhuzal-szálerősítésű betonok tulajdonságai és teherbírása", *BETON, II. évfolyam*, 6. Szám, 1994, pp. 5-11.
- Khajuria, A, Bohra, K., and Balaguru, P. (1991)** "Long-Term Durability of Synthetic Fibers in Concrete", *ACI SP-126: Durability of Concrete*, American Concrete Institute, Detroit, Michigan, 1987, pp. 851-868.
- Kiss, R., (1996)** "Experimental study on the shear capacity of beams reinforced by hungarian made steel and polypropylene fibres", (in Hungarian), *BME Vasbetonszerkezetek Tanszéke*, Budapest, 1996.
- Kormeling, H.A., Reinhardt, H.W., and Shah, S.P. (1980)** "Static and Fatigue Properties of Concrete Beams Reinforced with Continuous Bars and with Fibers", *ACI Journal* / January- February, 1980., pp.36-42.
- Kotsovos, M.D. (1983)** "Mechanisms of 'Shear' Failure", *Magazine of Concrete Research*, Vol. 35, No. 123, June, 1983., pp. 99-106.
- Kovács, I. (1996)** "Beton szívósságának növelése acélszálakkal", Diplomamunka, *BME Vasbetonszerkezetek Tanszéke*
- Kovács, I. (1997)** "Shear capacity of steel fiber reinforced concrete beams", *Proceedings of the 1th International Conference of Ph.D. Students, Miskolc*, Hungary, August 1997.
- Kovács I., Erdélyi, L., Balázs, L., Gy. (1997)** "Acélszálerősítésű vasbetongerendák törési viselkedése", *BME Vasbetonszerkezetek Tanszékének Tudományos Közleményei*, 1997., Budapest, pp.119-130.
- Kovács I. (1998)** "Szálerősítésű betonok modellezése egytengelyű húzásban" *BME Vasbetonszerkezetek Tanszékének Tudományos Közleményei*, 1998., Budapest, pp. 97-111.
- Kovács, I. (1998)** "Modeling of Plastic Matrix-Fiber Interaction in Fiber Reinforced Concrete", *Proceedings of the 2<sup>nd</sup> International Ph.D. Symposium in Civil Engineering*, Budapest, Hungary, 29-28 August 1998., pp.15-22.
- Kovács, I., Erdélyi, L., Balázs, L., Gy. (1999)** "Vasbeton gerendák törési viselkedése acélszálerősítés és hagyományos vasalás egyidejű alkalmazása esetén", *Szálerősítésű betonok – a kutatástól az alkalmazásig – Konferenciakiadvány*, Budapest, 1999., március 4-5., pp. 139-151.

- Kovács, I. (1999)** "Szálerősítésű betonok modellezése egytenglyű feszültségállapotban", *Szálerősítésű betonok – a kutatástól az alkalmazásig – Konferenciakiadvány*, Budapest, 1999. március 4-5., pp. 171-194.
- Kovács I., (1999)** "Design Method for Steel Fiber Reinforced Concrete Based on an Engineering Model", *Proceedings of the 2nd International Conference of Ph.D. Students*, Miskolc, Hungary, August 20-22. 1999.
- Krstulovic-Opara, N., Malak, S. (1997)** "Tensile Behavior of Slurry Infiltrated Mat Concrete (SIMCON)", *ACI Material Journal*, Vol. 94, No. 1, January-February, 1997., pp. 39-46.
- Krstulovic-Opara, N., Malak, S. (1997)** "Micromechanical Tensile Behavior of Slurry Infiltrated Continuous-Fiber-Mat Reinforced Concrete (SIMCON)", *ACI Material Journal*, Vol. 94, No. 5, September-October, 1997., pp. 373-387.
- Krstulovic-Opara, N., Dogan, E., Uang, C.M., Haghayeghi, A.R. (1997)** "Flexural Behavior of Composite R.C.-Slurry Infiltrated Mat Concrete (SIMCON) Members", *ACI Structural Journal*, Vol. 94, No. 5, September-October, 1997., pp. 502-512.
- Krstulovic-Opara, N., Al-Shannag, M.J. (1999)** "Slurry Infiltrated Mat Concrete (SIMCON)-Based Shear Retrofit of Reinforced Concrete Members", *ACI Structural Journal*, Vol. 96, No. 1, January-February, 1999., pp. 105-114.
- Kulla, J., (1996)** "Dimensional Analysis of Bond Modulus in Fiber Pullout", *Journal of Structural Engineering*, Vol. 122, No. 7, July, 1996., pp. 783-787.
- Li, V.C., Ward, R., Hamza, A.M. (1992)** "Steel and Synthetic Fibers as Shear Reinforcement", *ACI Material Journal*, Vol. 89, No. 5, September-October, 1992., pp. 499-507.
- Lim, T.Y., Paramasivam, P., Lee, S.L. (1987)** "Analytical Model for Tensile Behavior of Steel-Fiber Concrete", *ACI Materials Journal* / July-August, 1987., pp.286-298.
- Lim, T.Y., Paramasivam, P., Lee, S.L. (1987)** "Shear and Moment Capacity of Reinforced Steel-Fibre-concrete Beams", *Magazine of concrete Research*, Vol. 39, No. 140, September, 1987., pp. 148-160.
- Litvin, A. (1985)** "Report to Wire Reinforcement Institute on Properties of Concrete Containing Polypropylene Fibers", *CTL, Portland Cement Association*, Skokie, Illinois, 1985.
- Maage, Magne (1978)**. "Fibre Bond and Friction in Cement and Concrete", *Proceedings of the RILEM Symposium: Testing and Test Methods of Fiber Cement Composites*, Construction Press, Lancaster, 1978., pp. 329-336.
- Mangat, P.S., and Azari, M.M. (1986)**. "Compression Creep Behavior of Steel Fiber Reinforced Cement Composites", *Materials and Structures*, RILEM, Vol.19, 1986., pp. 361-370.
- Mangat, P.S., Molloy, B.T., and Gurusamy, K. (1989)** "Marine Durability of Steel Fiber Reinforced Concrete of High Water/Cement Ratio", *Fiber Reinforced Cements and Concretes-Recent Developments*, Elsevier, 1989., pp.553-562.

- Mansur, M.A., and Ong, K.C.G. (1991)** "Behavior of Reinforced Fiber Concrete Deep Beams in Shear", *ACI Structural Journal*, Vol. 88, No. 1, January-February, 1991., pp. 98-105.
- Mansur, M.A., Ong, K.C.G., and Paramasivam, P. (1986)** "Shear Strength of Fibrous Concrete Beams Without Stirrups", *Journal of Structural Engineering*, Vol. 112, No. 9, September, 1986., pp. 2066-2079.
- Marti, P. (1986)** "Staggered Shear Design of simply Supported Concrete Beams", *ACI Journal*, January-February, 1986., pp. 36-42.
- Mau, S.T., Hsu, T.T.C. (1987)** "Shear Strength Prediction for Deep Beams with Web Reinforcement", *ACI Structural Journal*, November-December, 1987., pp. 513-522.
- Mobasher, B., Stang, H., and Shah, S.P. (1990)** "Microcracking in Fiber Reinforced Concrete", *Cement and Concrete Research*, Vol.20, 1978., pp.665-676.
- Morse, D.C., and Williamson, G.R. (1977)** "Corrosion Behavior of Steel Fibrous Concrete", *NTIS*, Springfield, Virginia, May 1977., 36 pp.
- Naaman, A.E. (1992)** "SIFCON: Tailored Properties for Structural Performance" *Proceedings of the RILEM/ACI Workshop on High Performance Fiber Re-inforced Cement Composites, Mainz 1991* (ed. Reinhardt and Naaman), E & FN Spon London, 1992., pp. 18-38.
- Naaman, A.E. (1998)** "The Simplest Ideas are often the Best", *Concrete International Cement, Ceramic & Polymeric Composites*, July, 1998., pp. 57-62.
- Naaman, A.E., Gopalaratnam, V.S. (1983)** "Impact Properties of Steel Fiber Reinforced Concrete in Bending", *International Journal of Cement Composites and Lightweight Concrete*, Vol.5, No.4, 1983., pp. 225-233.
- Naaman, A.E., Najm, H. (1991)** "Bond-Slip Mechanism of Steel Fibers in Concrete", *ACI Materials Journal* / March-April 1991., pp. 135-145.
- Naaman, A.E., Otter, D., and Najm, H. (1991)** "Elastic modulus of SIFCON in Tension and Compression", *ACI Materials Journal*/Nov-Dec. 1991., pp.603-612.
- Naaman, A.E., Reinhardt, H-W. (1998)** "High Performance Fiber Reinforced Cement Composites 2", *Proceedings of the 2<sup>nd</sup>. Int. RILEM Workshop, Ann Arbor, USA, June 11-14., 1995.*, EFN Spon, Suffolk, 1995.
- Naaman, A.E., and Shah, S.P. (1976)** "Pull-Out Mechanism in Steel Fibre Reinforced Concrete", *Proceedings*, ASCE, Vol.102, ST8, Aug. 1976, pp. 1537-1558.
- Narayanan, R., Kareem-Palanjian, A.S. (1986)** "Torsion, Bending, and Shear in Prestressed Concrete Beams Containing Steel Fibers", *ACI Journal* / May-June, 1986., pp. 423-431.
- Narayanan, R. and Darwish, I.Y.S. (1987)** "Use of Steel Fibers as Shear Reinforcement", *ACI Structural Journal*/May-June, 1987., pp. 216-227.
- Narayan Swamy, R., Jones, R., Chiam, T.P. (1993)** "Influence of Steel Fibers on the Shear Resistance of Lightweight Concrete I-Beams", *ACI Structural Journal*, Vol. 90, No. 1, January-February, 1993., pp. 103-114.

- Nürnbergzrová, T., Babál, B., Komlós, B., Janotka, I. (1994)** "Strain Properties of Fibre-Reinforced Concretes", *Proceedings of the 1th Slovakian Conference on Concrete Structures*, 1994., pp. 36-45.
- Pinchin, D.J., and Tabor, D. (1978)** "Interfacial Contact Pressure and Frictional Stress Transfer in Steel Fiber Cement", *Proceedings of the RILEM Symposium: Testing and Test Methods of Fiber Cement Composites*, Construction Press, Lancaster, 1978., pp. 337-344.
- Ramakrishnan, V., and Josifek, C. (1987)** "Performance Characteristics and Flexural Fatigue Strength of Concrete Steel Fiber Composites", *Proceeding of the International Symposium on Fiber Reinforced Concrete*, Oxford and IBH Publishing Co. Pvt. Ltd., New Delhi, India, 1987., pp.273-284.
- Ramakrishnan, V., Oberling, G., and Tatnall, P. (1987)** "Flexural Fatigue Strength of Steel Fiber Reinforced Concrete", *ACI SP-105: Fiber Reinforced Concrete Properties and Applications*, American Concrete Institute, Detroit, Michigan, 1987., pp. 225-245.
- Ramirez, J.A., Breen, J.E. (1991)** "Evaluation of a Modified Truss-Model Approach for Beams in Shear", *ACI Structural Journal*, Vol. 88, No. 5, September-October, 1991., pp. 562-571.
- Reineck, K.H. (1991)** "Ultimate Shear Force of Structural Concrete Members without Transverse Reinforcement Derived from a Mechanical Model", *ACI Structural Journal*, Vol. 88, No. 5, September-October, 1991., pp. 592-602.
- Reineck, K.H. (1993)** "Modelling Structural Concrete with Strut-and-Tie Models Shear in B-Regions", *Studi e Ricerche*, Vol. 14, Politecnico di Milano, Italia, 1993., pp. 165-196.
- Reinhardt, H.W. (1992)** "Introductory Note: Fibers and Cement, a Useful Cooperation" *Proceedings of the RILEM/ACI Workshop on High Performance Fiber Reinforced Cement Composites*, Mainz 1991 (ed. Reinhardt and Naaman), E & FN Spon London, 1992., pp. 84-99.
- Reinhardt, H.W, and Naaman, A.E. (1992)** "High Performance Fiber Reinforced Cement Composites", *Proceedings of the 1<sup>st</sup> Int. RILEM/ACI Workshop*, Mainz, June 23-26, 1991., Chapman & Hall, London
- Reinhardt, H. W. and Naaman, A. E. (1999)** "High Performance Fiber Reinforced Cement Composites", *Proceedings of the 3th. Int. RILEM/ACI Workshop*, Mainz, Germany, May 17-19, 1999.
- RILEM (1978)** "Testing and Test Methods of Fiber Cement Composites", *Proceedings of the RILEM Symposium 1978.*, Construction Press, Lancaster
- RILEM (1999)** "Test and Design Methods for Steel fibre reinforced concrete (TC TDF-162, *Technical Report*, for the RILEM Technical Committee, TC-TDF 162,1999
- Romualdi, J. P., Batson, G. B. (1963)** "Tensile Strength of Concrete Affected by Uniformly Distributed Beams with Closely Spaced Reinforcement", *ACI Journal*, Vol.60, No.6., June 1963., pp. 775-790.
- Romualdi, J. P., Batson, G. B. (1964)** "Tensile Strength of Concrete Affected by Uniformly Distributed and Closely Spaced Short Lengths of Wire Reinforcement",

---

*Journal of the American Concrete Institute*, Proceedings Vol. 61, No. 6, June, 1964., pp. 657-670.

**Samer Ezeldin, A., Shiah, T.W. (1995)** "Analytical Immediate and Long-Term Deflections of Fiber-Reinforced Concrete Beams", *Journal of Structural Engineering*, Vol. 121, No. 4, April, 1995., pp. 727-738.

**Sanat, K., Niyogi, G.I., Dwarakanathan (1985)** "Fiber Reinforcement Beams under Moment and Shear", *Journal of Structural Engineering*, Vol. 111, No. 3, March, 1985, pp. 516-527.

**Schellekens, J.C.J., De Borst, R. (1990)** "The Use of the Hoffman Yield Criterion in Finite Element Analysis of Anisotropic Composites", *Computers & Structures*, Vol. 37, No. 6, 1990., pp. 1087-1096.

**Schnütgen, B. (1989)** "Rohre aus Stahlfaserbeton", *Beton- und Stahlbetonbau* 84 (1989), H. 4, pp.97-101.

**Shah, S.P. (1990)** "Fiber Reinforced Concrete", *Concrete International*, Vol.12, No.3, 1990, pp. 81-82.

**Sharma, A.K. (1986)** "Shear Strength of Steel Fiber Reinforced Concrete Beams", *ACI Journal* / July-August, 1986., pp.624-628.

**Siao, W.E. (1994)** "Shear Strength of Short Reinforced Concrete Walls, Corbels, and Deep Beams", *ACI Structural Journal*, Vol. 91, No. 2, March-April, 1994., pp. 123-131.

**Sorushian, P, and Marikunte, S. (1992)** "High Performance Cellulose Fiber Reinforced Cement" *Proceedings of the RILEM/ACI Workshop on High Performance Fiber Reinforced Cement Composites, Mainz 1991* (ed. Reinhardt and Naaman), E & FN Spon London, 1992., pp. 84-99.

**Spadea, G., Bencardio, F. (1997)** "Behavior of Fiber-Reinforced Concrete Beams under Cyclic Loading", *Journal of Structural Engineering*, Vol. 123, No. 5, May, 1997., pp. 660-668.

**Stang, H., Mobasher, B., and Shah, S.P. (1990)** "Quantitative Damage Characterization in Polypropylene Fiber Reinforced Concrete", *Cement and Concrete Research*, Vol.20, 1990., pp. 540-558.

**Stang, H. (1998)** "Application of the Stress-Crack Width Relationship in the Design of FRC-Structures", *Technical Report*, for the RILEM Technical Committee, TC-TDF 162, Test and Design Methods for Steel Fibre Reinforced Concrete, 1998.

**Stang, H. , Rossi, P., (1999)** "Design of fiber Reinforced concrete" *RILEM TC 162-TDF Test and Design Methods for Steel fiber Reinforced Concrete Recommendations for Design of Fibre Reinforced concrete*, 1999

**Stroeven, P. (1995)** "Steel Fibre Reinforcement at Boundaries in Concrete Elements", *New Development in Concrete Science and Technology DeCSAT'95*, Printing House Nanjing Univ. of Chemical Technology, pp.658-663.

**Swamy, R.N., Jones, R., Chiam, A.T.P. (1993)** "Influence of Steel Fibers on the Shear Resistance of Lightweight Concrete I-Beams", *ACI Structural Journal* / January-February, 1993., pp.103-114.



- Tan, K.H., Murugappan, K., Paramasivam, P. (1993)** "Shear Behavior of Steel Fiber Reinforced Concrete Beams", *ACI Structural Journal*, Vol. 89, No. 6, January-February, 1993., pp.3-11.
- Theodorakopoulos, D.D., Swamy, R.N. (1999)** "Steel Fibers to Resist Punching Shear and an Engineering Model to Enhance Durable Service Life", *Proceedings of the 3th RILEM Workshop on High Performance Fiber Reinforced Cement Composites, Mainz 1999* (ed. Reinhardt and Naaman), RILEM Publications S.A.R.L., 1999., pp.575-585.
- Torrenti, J.M., Djebri, B. (1992)** "Comportement des Bétons de Fibres sous Sollicitations Biaxiales", *Annales de L'Institut Technique du Batiment et des Travaux Publics* No. 503-Mai, 1992., Série: Béton 289, pp. 106-111.
- Torrenti, J.M., Djebri, B. (1995)** "Behaviour of Steel-Fibre Reinforced Concretes Under Biaxial Compression Loads", *Cement & Concrete Composites* / 17., 1995., pp. 261-266.
- Ulfkjaer, J.P., Krenk, S., rinckner, R. (1995)** "Analytical Model for Fictitious Crack Propagation in concrete Beams", *Journal of Engineering Mechanics*, Vol. 121, No. 1, January, 1995., pp. 7-15.
- Valle, M., Buyukozturk, O. (1992)** "Behavior of Fiber Reinforced High Strength Concrete Under Direct Shear", *Studi E Ricerche*, Vol. 13, Politecnico di Milano, Italia, 1992., pp. 161-193.
- WAJA (1995)** "Hullámosított acélszálak gyártása", *Tanulmány*, WAJA Klub Miskolc, 1995., November
- Wafa, F.F., Hasnat, A., Tarabolsi, O.F. (1992)** "Presstressed Fiber Reinforcement Concrete Beams Subjected to Torsion", *ACI Structural Journal*, Vol. 89, no. 3, May-June, 1992., pp.272-283.
- Ward, R.J., Li, V.C. (1990)** "Dependence of Flexural Behavior of Fiber Reinforced Mortar on Material Fracture Resistance and Beam Size", *ACI Materials Journal*, Vol. 87, No. 6, November-December, 1990., pp. 627-637.
- Weber, J.W. (1979)** "Empirischen Formeln zur Beschreibung der Festigkeitsentwicklung und der Entwicklung des E-Moduls von Beton", *Beton+Vertigteil-Technik*, 12/1979., pp. 753-756.
- Wu, G.Y., Shivaroj, S.K., Ramakrishnan, V. (1989)** "Flexural Fatigue Strength, Endurance Limit, and Impact Strength of Fiber Reinforced Refractory Concretes", *Fiber Reinforced Cements and Concretes: Recent Developments*, Elsevier, New York, 1989., pp. 261-273.
- Zararis, P.D. (1996)** "Concrete shear Failure in Reinforced-Concrete elements", *Journal of Structural Engineering*, Vol. 122, No. 9, September 1996., pp. 1006-1015.
- Zielinski, Z.A., Rigotti, M. (1995)** "Tests on Shear Capacity of Reinforced Concrete", *Journal of Structural Engineering*, Vol. 121, No. 11, November, 1995., pp. 1660-1666.

## **Standard Specifications for fibre reinforced concrete**

- AFNOR P 18-409 (1993)** "Béton avec fibres métalliques. Essai de flexion."
- ASTM C 1018-89 (1990)** "Standard Test Method for Flexural Toughness and First-Crack Strength of Fiber-Reinforced Concrete"
- ASTM A 820-90** "Standard Specification for Steel Fibers for fiber Reinforced Concrete"
- ASTM C 995-91** "Standard Test Method for Time of Flow of Fiber Reinforced Concrete through Inverted Slump Cone"
- ASTM C 1018-89** "Standard Test Method for Flexural Toughness and First-Crack Strength of Fiber Reinforced Concrete (Using Beam with Third-Point Loading)"
- DBV-Merkblatt (1991)** "Grundlagen zur Bemessung von Industriefussböden aus Stahlfaserbeton"
- DBV-Merkblatt (1992)** "Technologie des Stahlfaserbetons- und Stahlfaserpritzbeton"
- DBV-Merkblatt (1992)** "Bemessungsgrundlagen für Stahlfaserbeton im Tunnelbau"
- DBV-Merkblatt Anhang A (1992)** ". Empfehlungen für Einzelprüfungen"
- DBV-Merkblatt Anhang B (1992)** ". Empfehlungen für Einstufungs-, Eignungs- und Güteprüfungen"
- Vorläufige Richtlinien (1995)** "Vorläufige Richtlinien für die Prüfung und Güteüberwachung von Erzeugnissen aus Faserbeton"
- JSCE-SF1 (1984)** "Method of making steel fiber reinforced concrete in the laboratory"
- JSCE-SF2 (1984)** "Method of making specimens for strength and toughness tests of steel fiber reinforced concrete"
- JSCE-SF3 (1984)** "Method of making specimens for strength and toughness tests of shotcreted steel fiber reinforced concrete"
- JSCE-SF4 (1984)** "Method of tests for flexural strength and flexural toughness of steel fiber reinforced concrete"
- JSCE-SF5 (1984)** "Method of tests for compressive strength and compressive toughness of steel fiber reinforced concrete"
- JSCE-SF6 (1984)** "Method of tests for shear strength of steel fiber reinforced concrete"
- JSCE-SF7 (1984)** "Method of tests for fiber content of steel fiber reinforced concrete"
- UNE 83-500-89 Parte 1** "Hormigones con fibras de acero y/o polipropileno. Classification y definiciones"
- UNE 83-500-89 Parte 2** "Hormigones con fibras de acero y/o polipropileno. Classification y definiciones"
- UNE 83-501-86** "Hormigones con fibras de acero y/o polipropileno. Toma de muestras de hormigon fresco."

---

**UNE 83-502-88** “Hormigones con fibras de acero y/o polipropileno. Fabricación en laboratorio.”

**UNE 83-503-88** “Hormigones con fibras de acero y/o polipropileno. Medida de docilidad por medio del cono invertido.”

**UNE 83-504-90** “Hormigones con fibras de acero y/o polipropileno. Fabricación probetas para los ensayos de laboratorio.”

**UNE 83-505-86** “Hormigones con fibras de acero y/o polipropileno. Extracción y conservación de probetas testigo.”

**UNE 83-506-86** “Hormigones con fibras de acero y/o polipropileno. Refrentado de probetas con mortero de azufre.”

**UNE 83-507-86** “Hormigones con fibras de acero y/o polipropileno. Rotura por compresión.”

**UNE 83-508-90** “Hormigones con fibras de acero y/o polipropileno. Determinación del índice de tenacidad a compresión.”

**UNE 83-509-88** “Hormigones con fibras de acero y/o polipropileno. Rotura por flexotracción.”

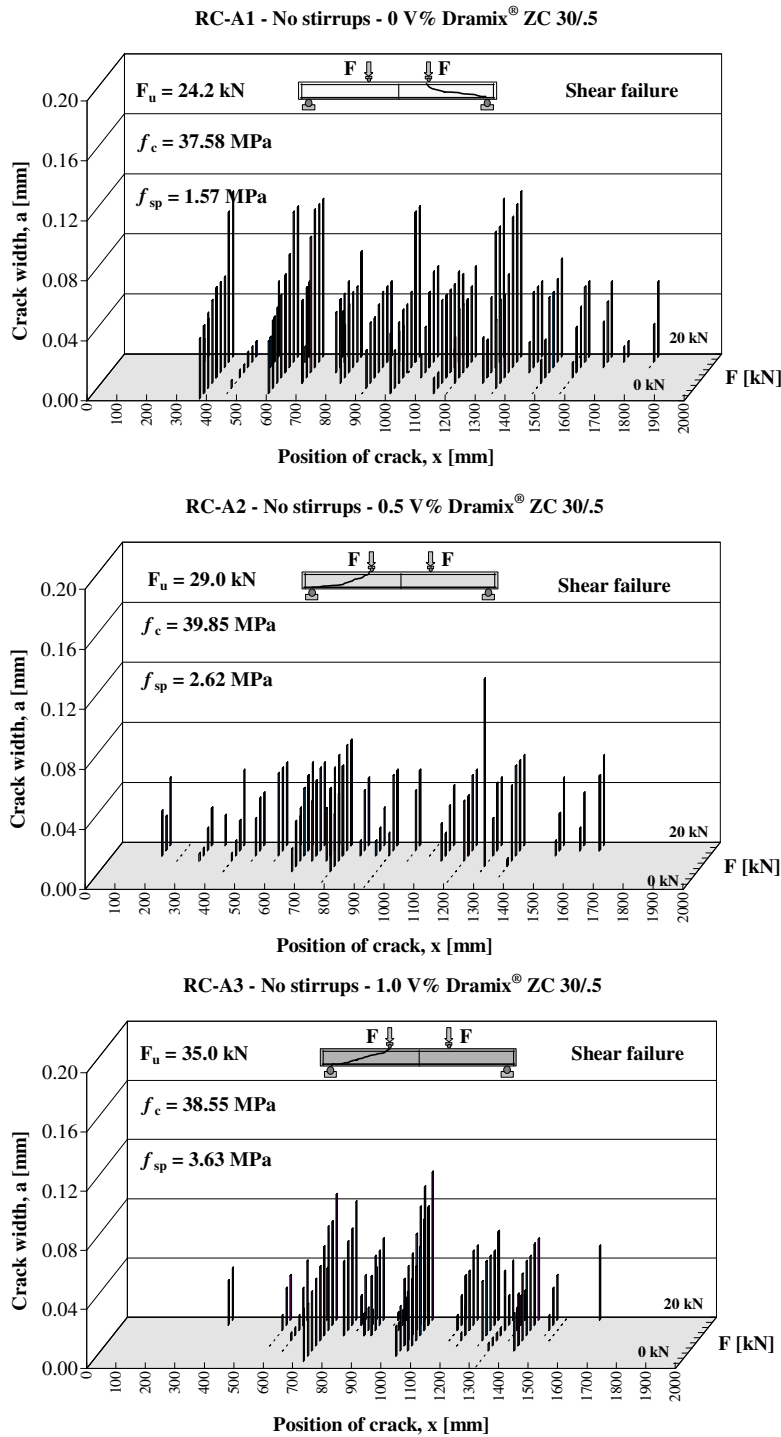
**UNE 83-510-89** “Hormigones con fibras de acero y/o polipropileno. Determinación del índice de tenacidad de resistencia a primera fisura.”

**UNE 83-511-89** “Hormigones con fibras de acero y/o polipropileno. Determinación del resistencia a cortante.

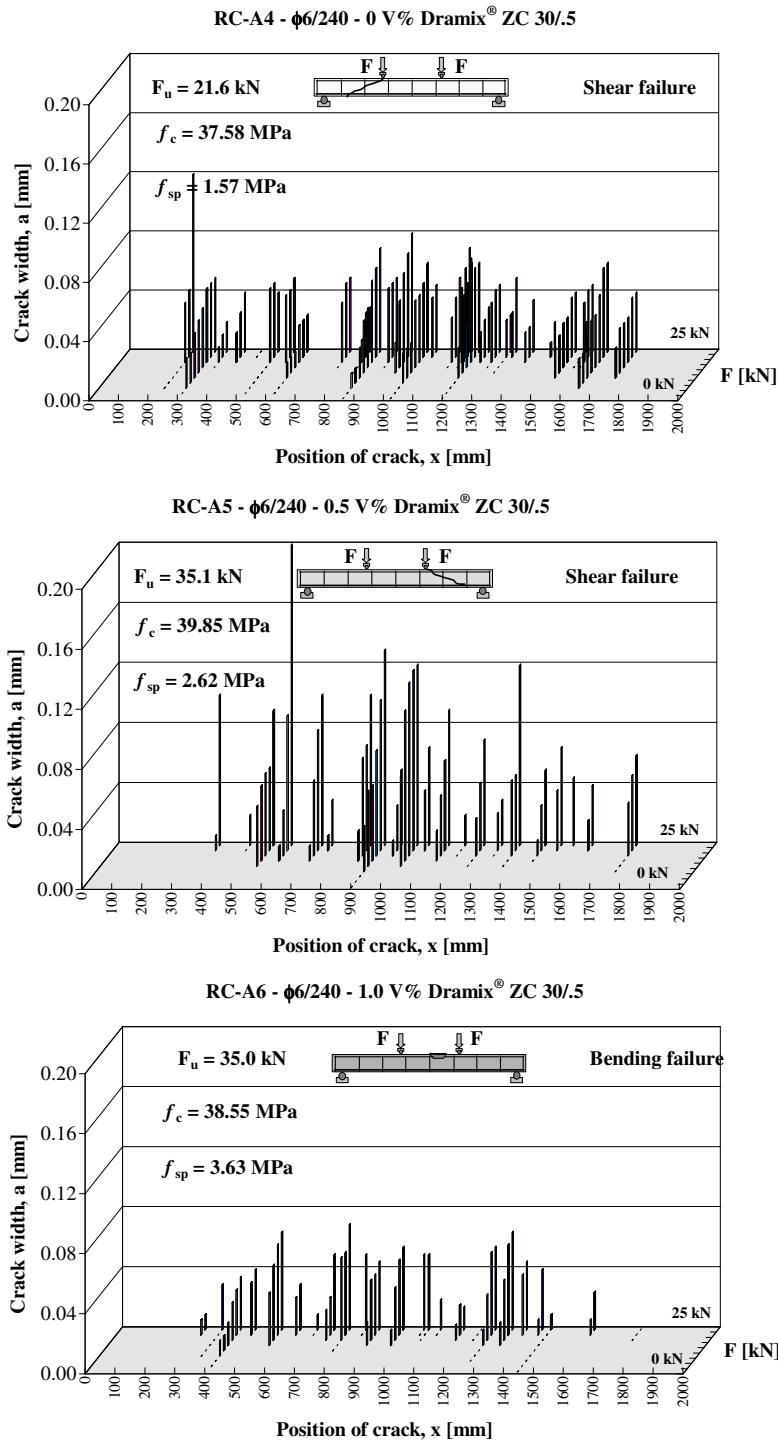
**UNE 83-512-89** “Hormigones con fibras de acero y/o polipropileno. Determinación del contenido de fibras de acero.”

**UNE 83-514-90** “Hormigones con fibras de acero y/o polipropileno. Determinación de la resistencia al impacto.”

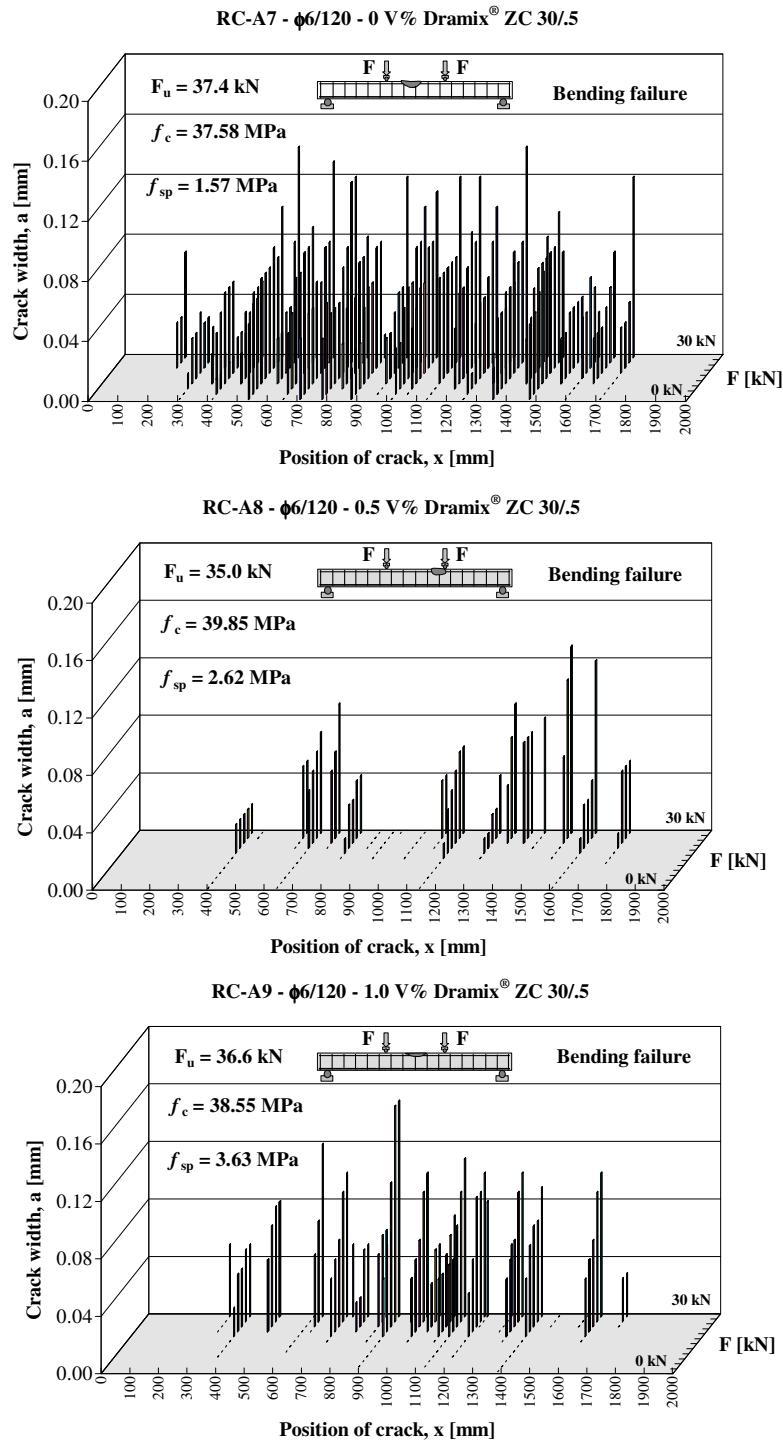
# Appendix



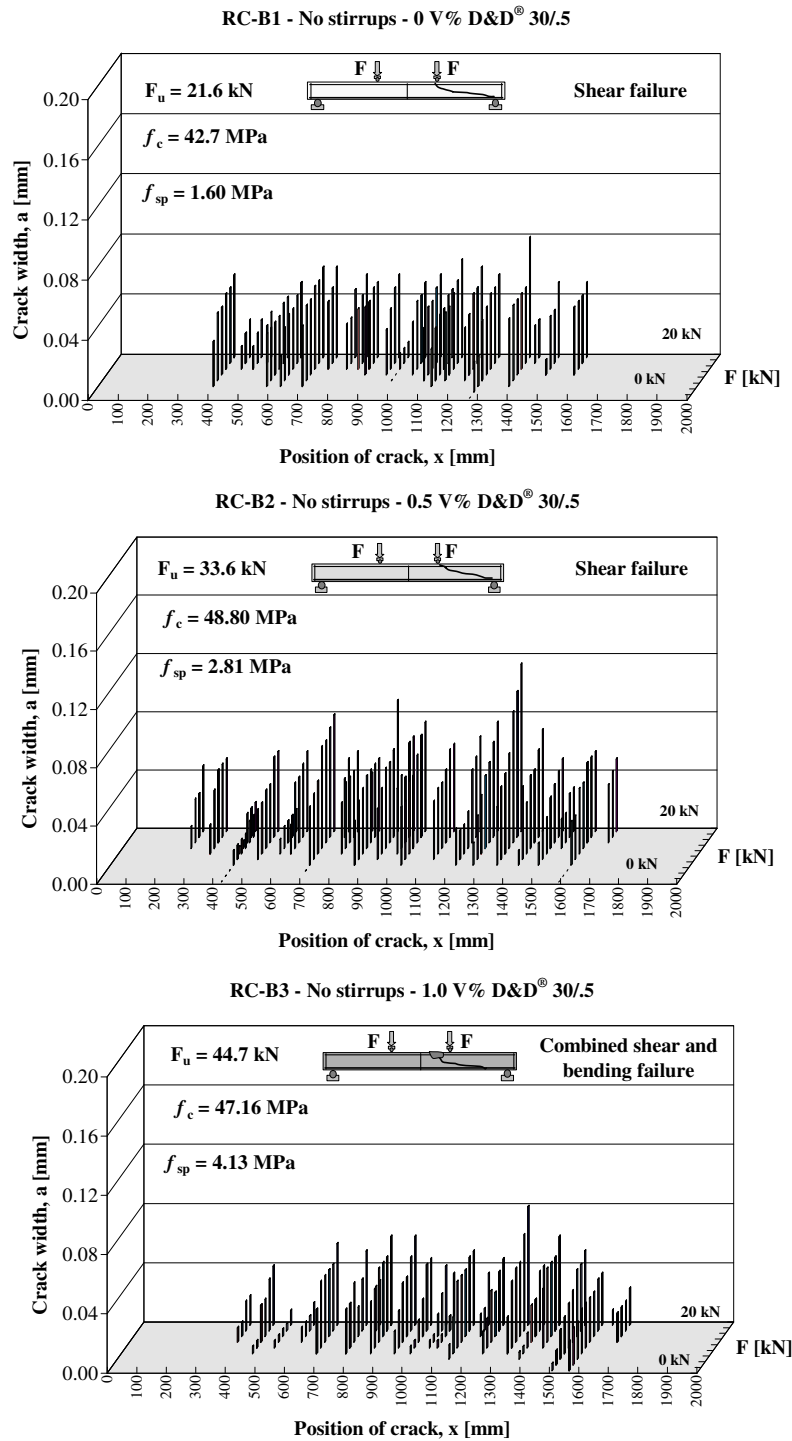
**Figure A1:** 3D representation of load ( $F$ ) versus crack width ( $a$ ) relationships of beams RC-A1...RC-A3 measured at each load steps at the high of the tensioned steel bars. The horizontal axis of the diagram indicates the position of the cracks along the beam.



**Figure A2:** 3D representation of load ( $F$ ) versus crack width ( $a$ ) relationships of beams RC-A4...RC-A6 measured at each load steps at the high of the tensioned steel bars. The horizontal axis of the diagram indicates the position of the cracks along the beam.

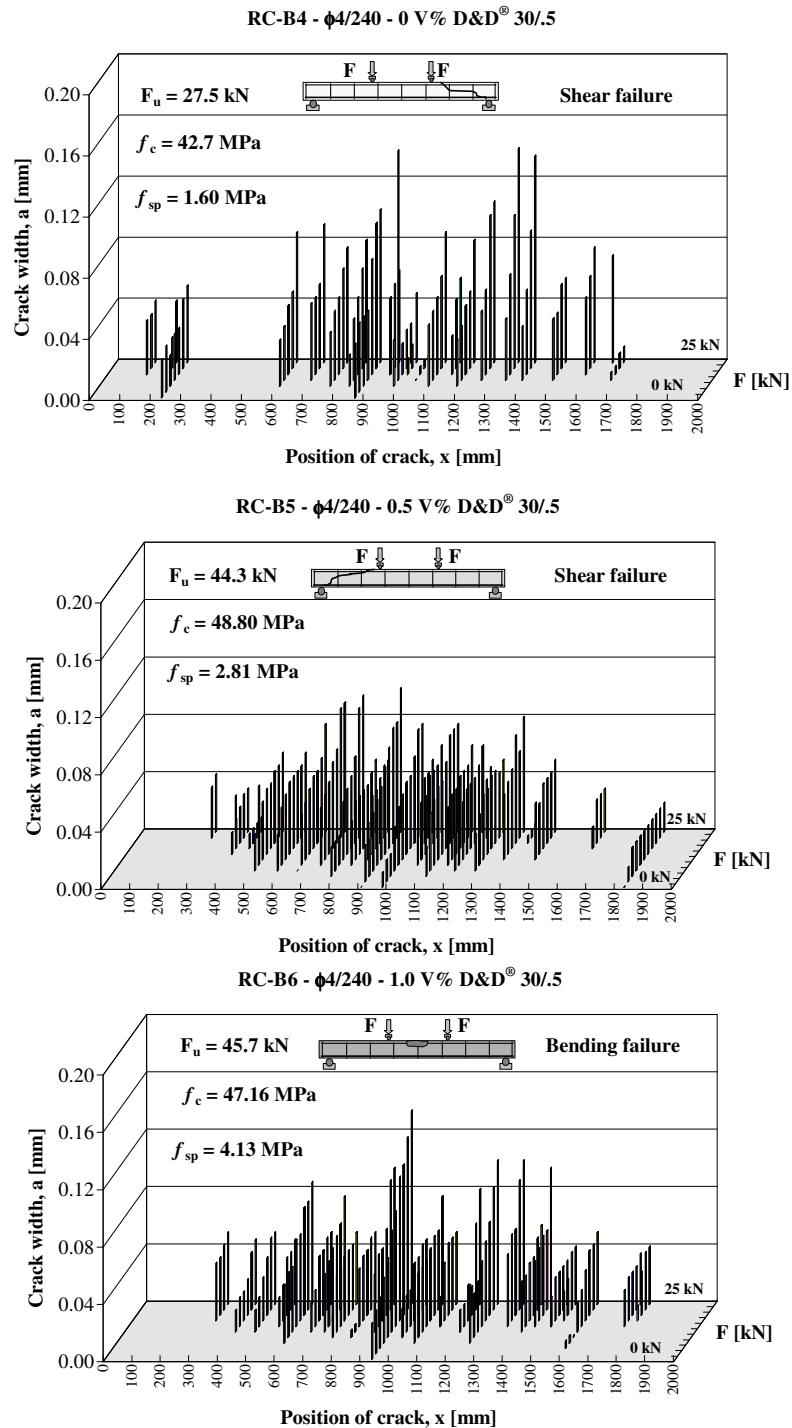


**Figure A3:** 3D representation of load ( $F$ ) versus crack width ( $a$ ) relationships of beams RC-A7...RC-A9 measured at each load steps at the high of the tensioned steel bars. The horizontal axis of the diagram indicates the position of the cracks along the beam.

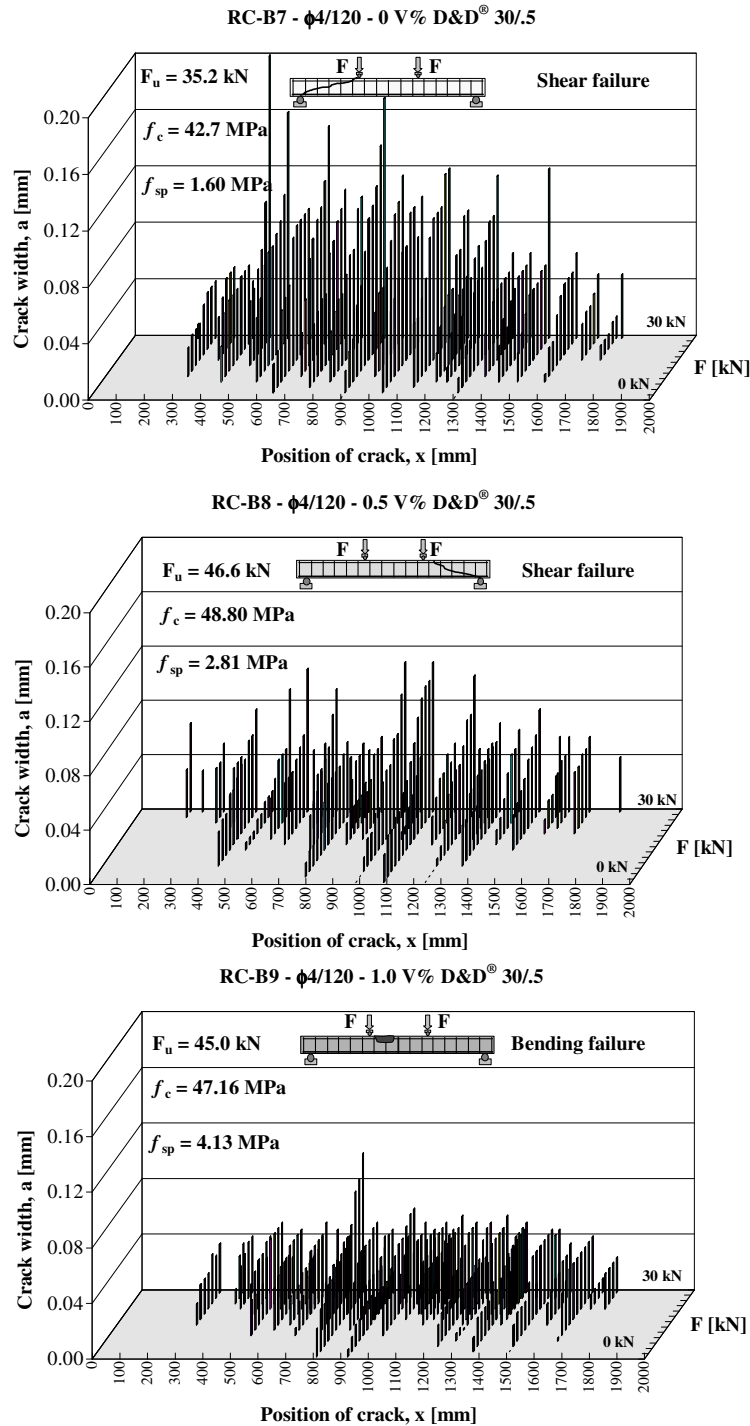


**Figure A4:** 3D representation of load ( $F$ ) versus crack width ( $a$ ) relationships of beams RC-B1...RC-B3 measured at each load steps at the high of the tensioned steel bars. The horizontal axis of the diagram indicates the position of the cracks along the beam.

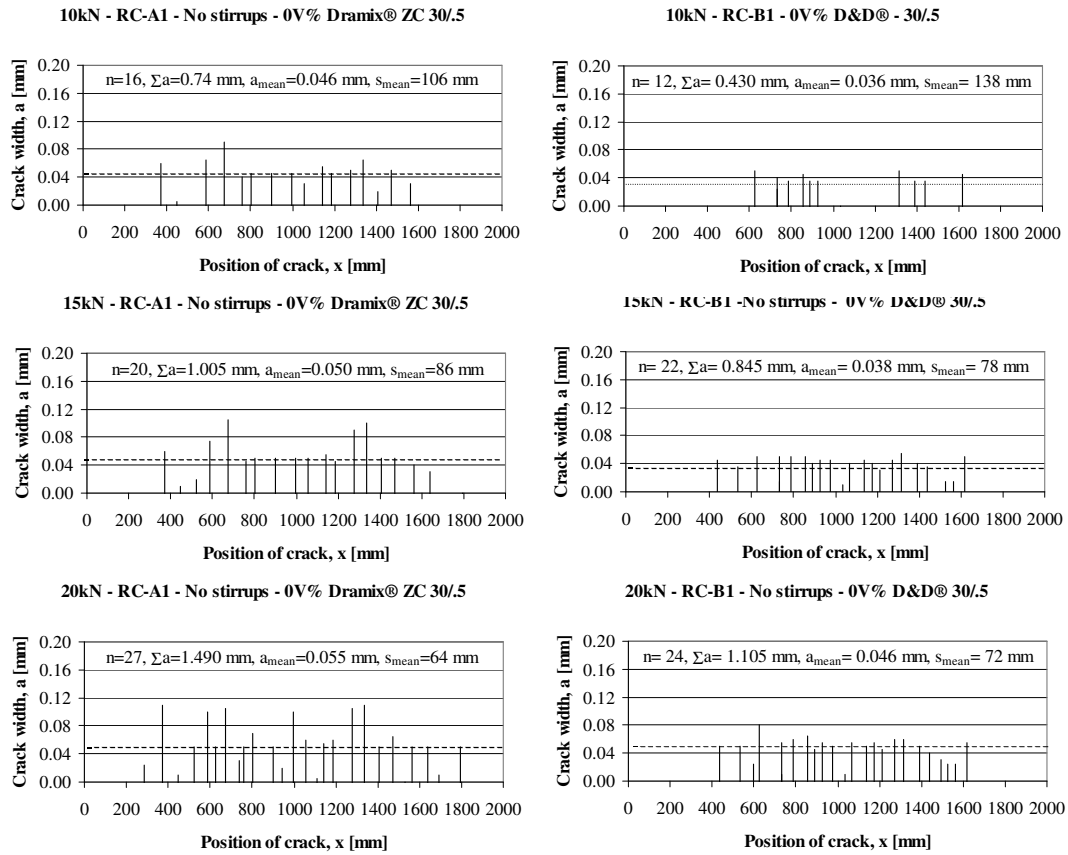




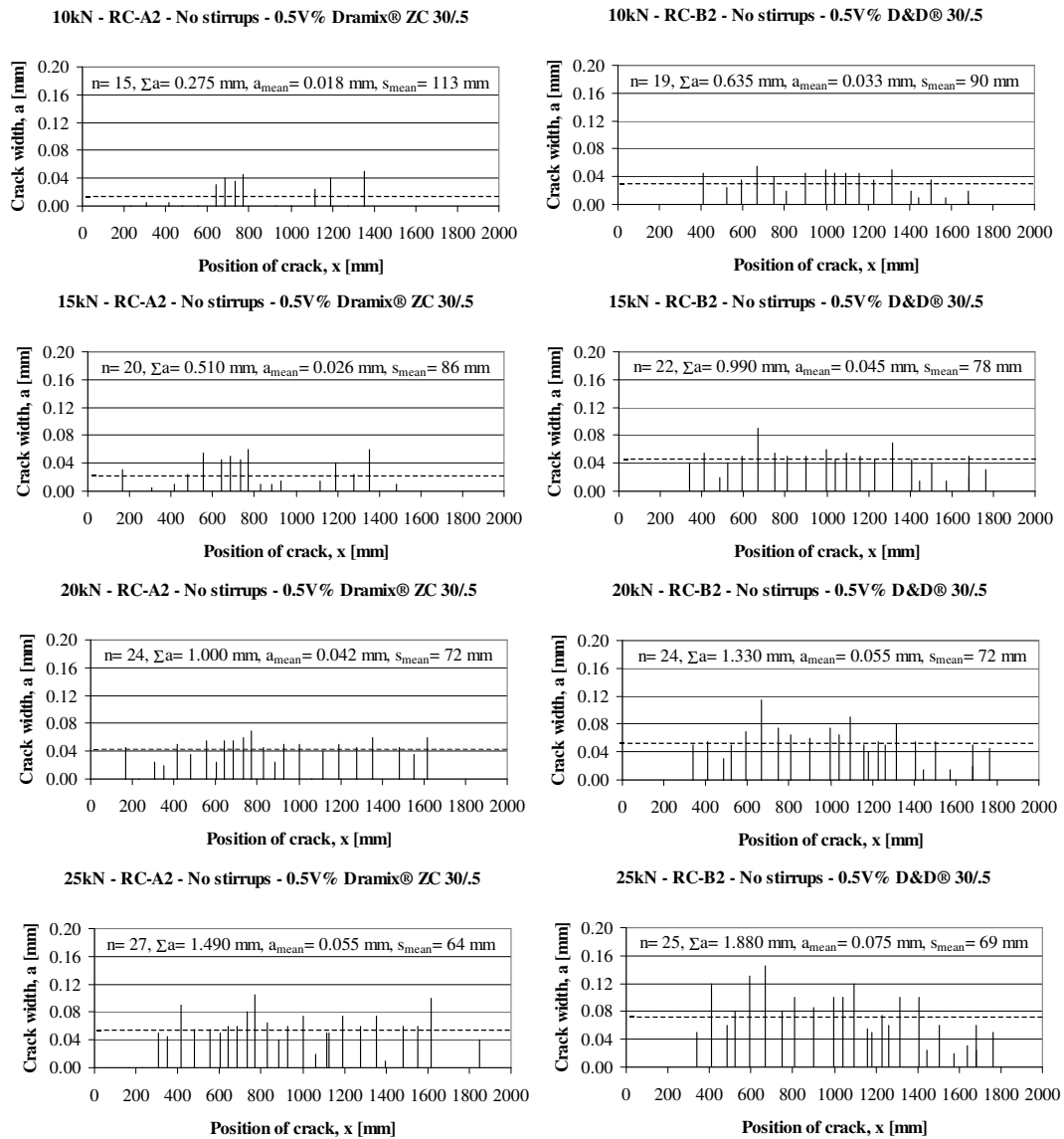
**Figure A5:** 3D representation of load ( $F$ ) versus crack width ( $a$ ) relationships of beams RC-B4...RC-B6 measured at each load steps at the high of the tensioned steel bars. The horizontal axis of the diagram indicates the position of the cracks along the beam.



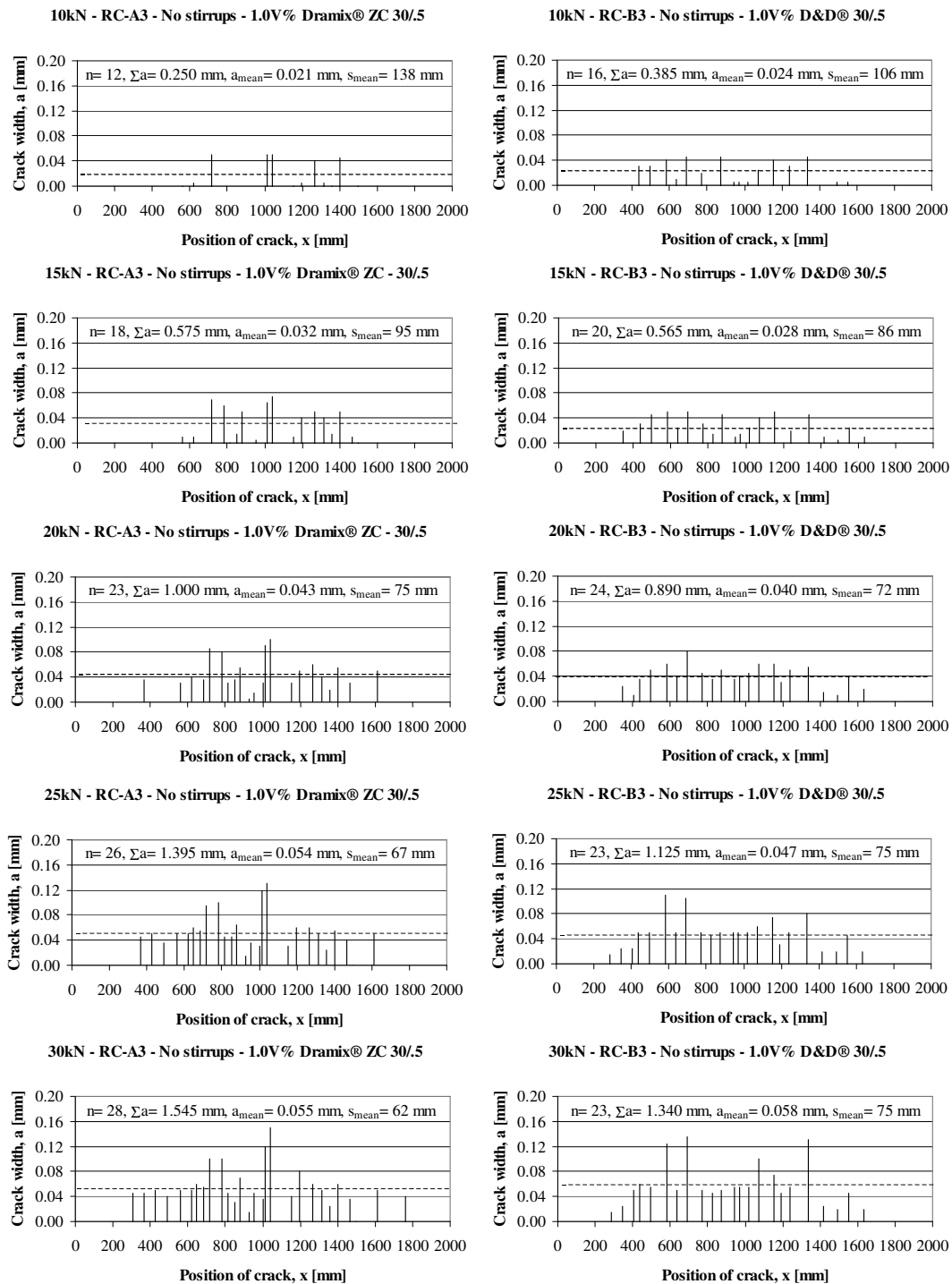
**Figure A6:** 3D representation of load ( $F$ ) versus crack width ( $a$ ) relationships of beams RC-B7...RC-B9 measured at each load steps at the high of the tensioned steel bars. The horizontal axis of the diagram indicates the position of the cracks along the beam.



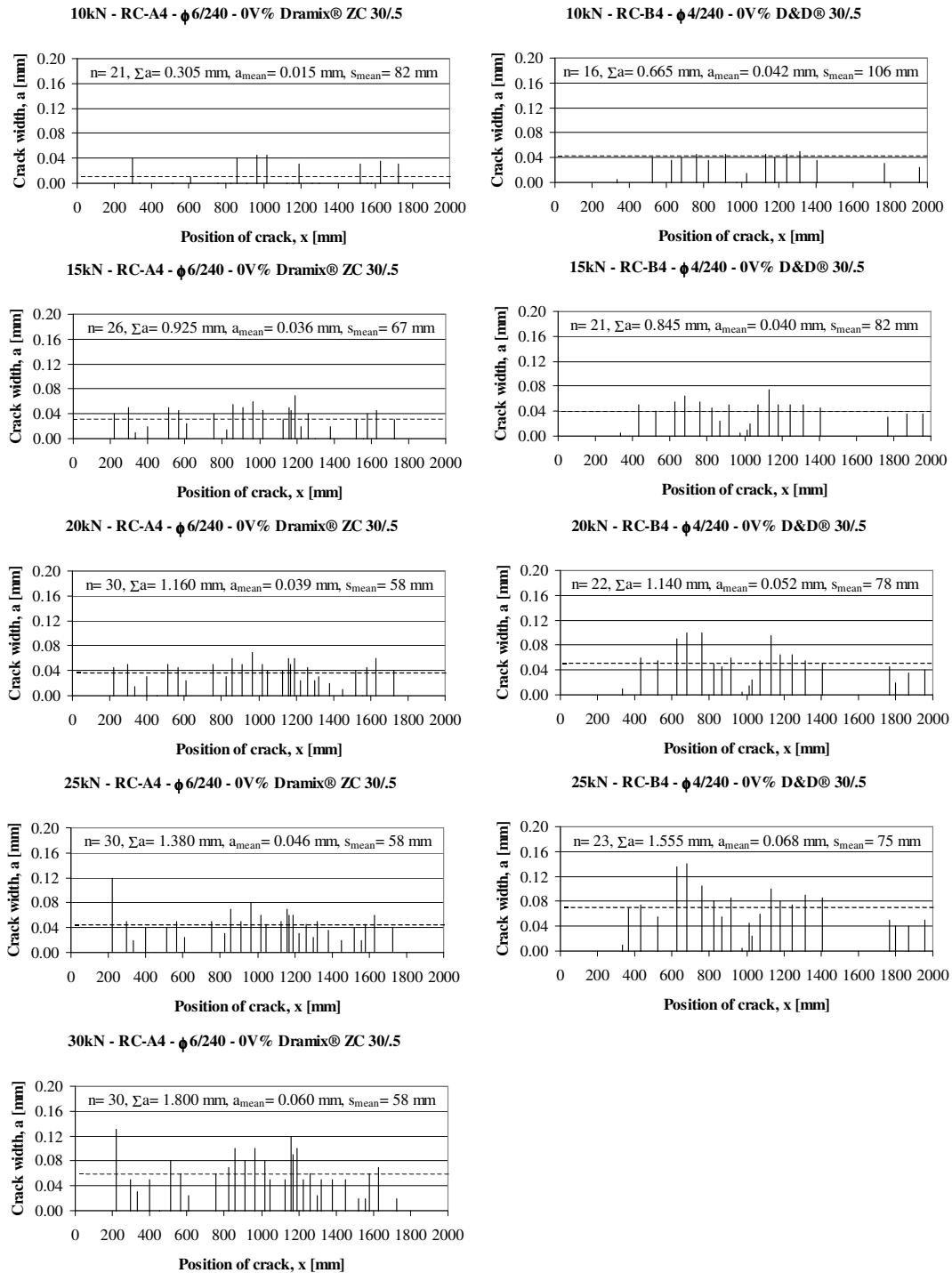
**Figure A7:** Crack distributions of beam RC-A1 having 0V% Dramix® ZC 30/5 hooked-end steel fibres and of beam RC-B1 having 0V% D&D® 30/5 crimped steel fibres at different load levels. The horizontal dotted line indicates the mean crack width at the given load step.



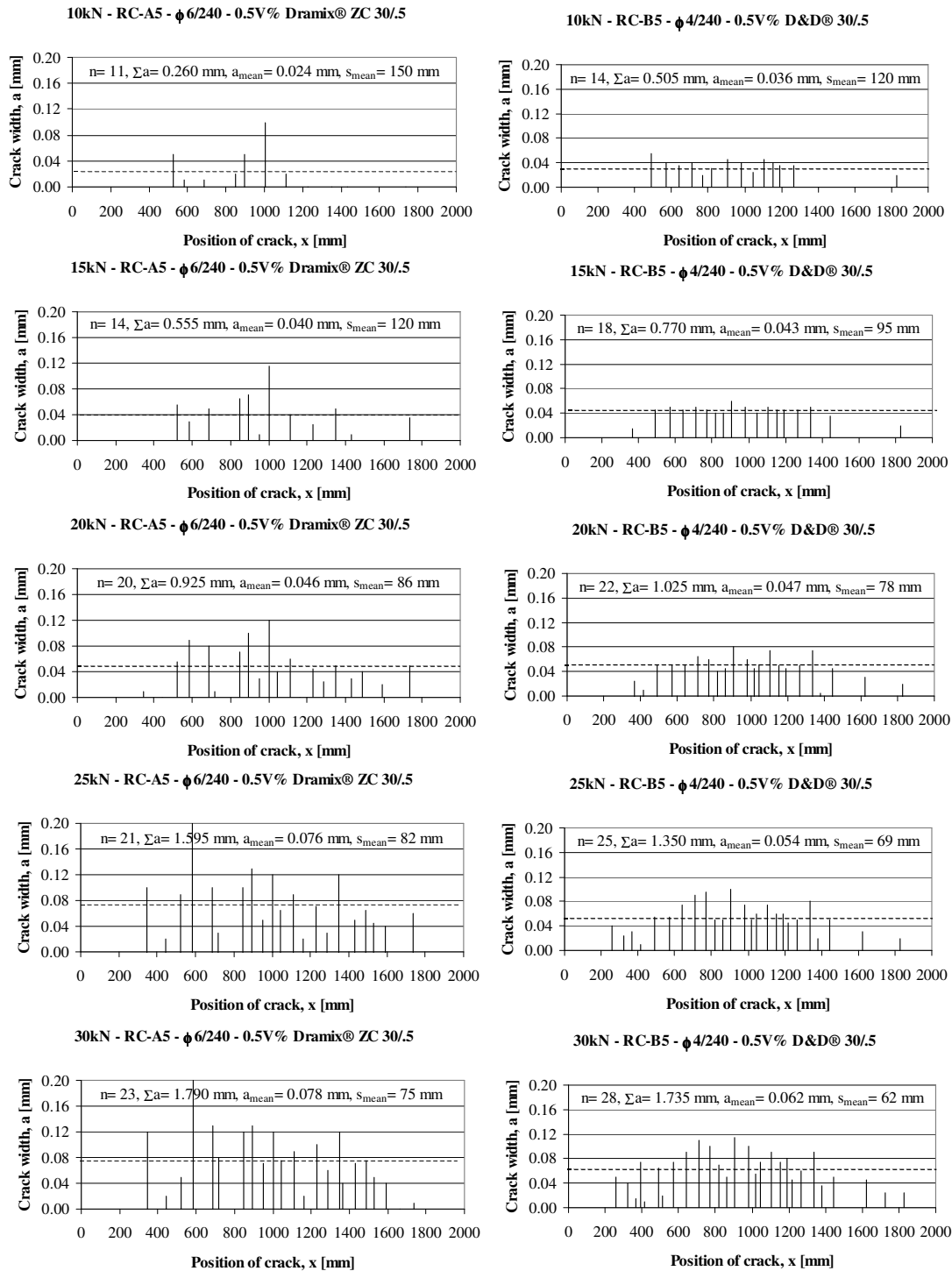
**Figure A8:** Crack distributions of beam RC-A2 having 0.5V% DRAMIX® ZC 30/5 hooked-end steel fibres and of beam RC-B2 having 0.5V% D&D® 30/5 crimped steel fibres at different load levels. The horizontal axis of the diagrams indicates the position of the cracks. The horizontal dotted line indicates the mean crack width at the given load step.



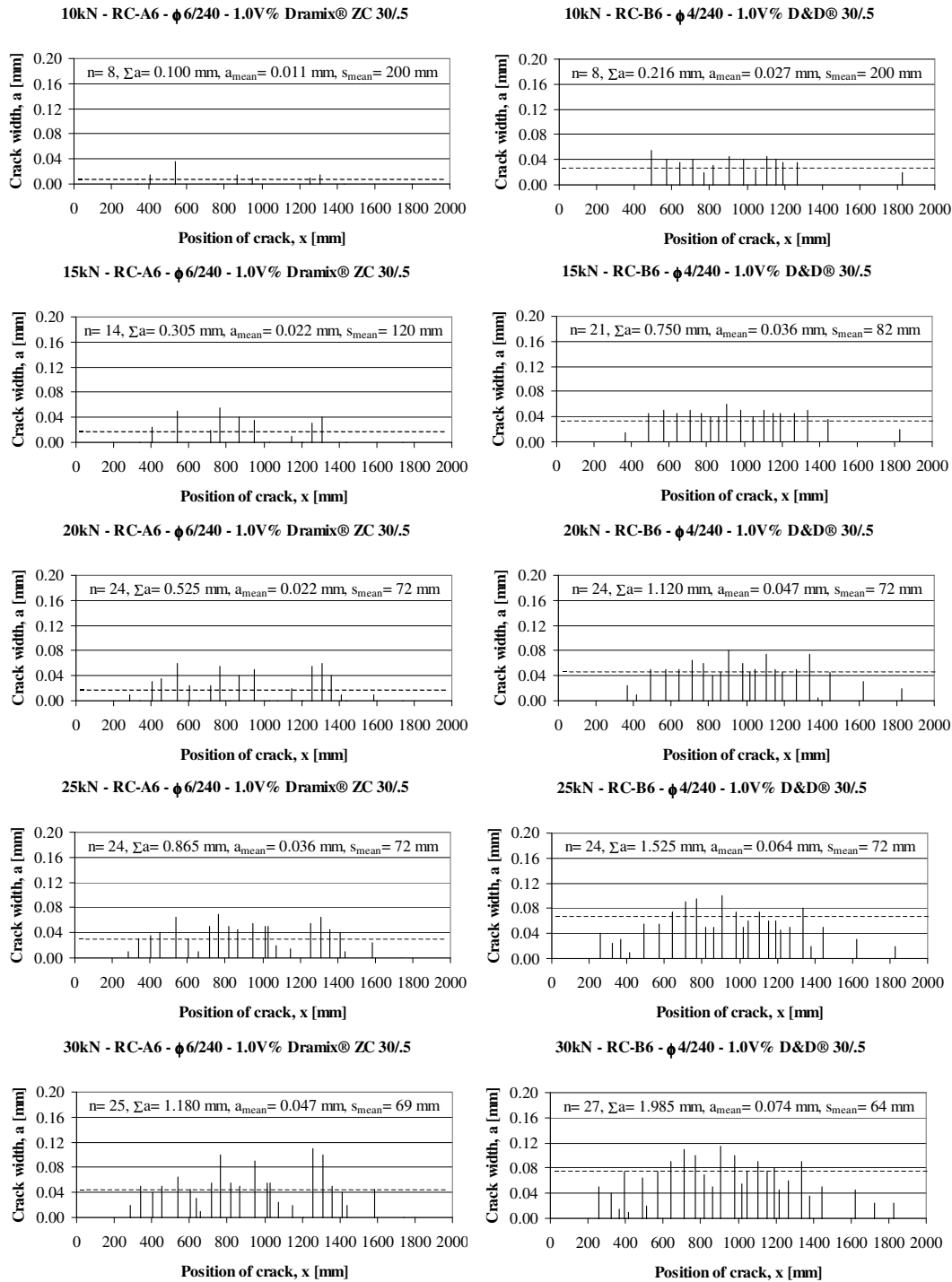
**Figure A9:** Crack distributions of beam RC-A3 having 1.0 V% Dramix® ZC 30/5 hooked-end steel fibres and of beam RC-B3 having 1.0 V% D&D® 30/5 crimped steel fibres at different load levels. The horizontal axis of the diagrams indicates the position of the cracks. The horizontal dotted line indicates the mean crack width at the given load step.



**Figure A10:** Crack distributions of beam RC-A4 having  $\phi 6/240$  stirrup reinforcement and 0 V% Dramix® ZC 30/5 hooked-end steel fibres and of beam RC-B4 having  $\phi 4/240$  stirrup reinforcement and 0 V% D&D® 30/5 crimped steel fibres at different load levels. The horizontal axis of the diagrams indicates the position of the cracks. The horizontal dotted line indicates the mean crack width at the given load step.

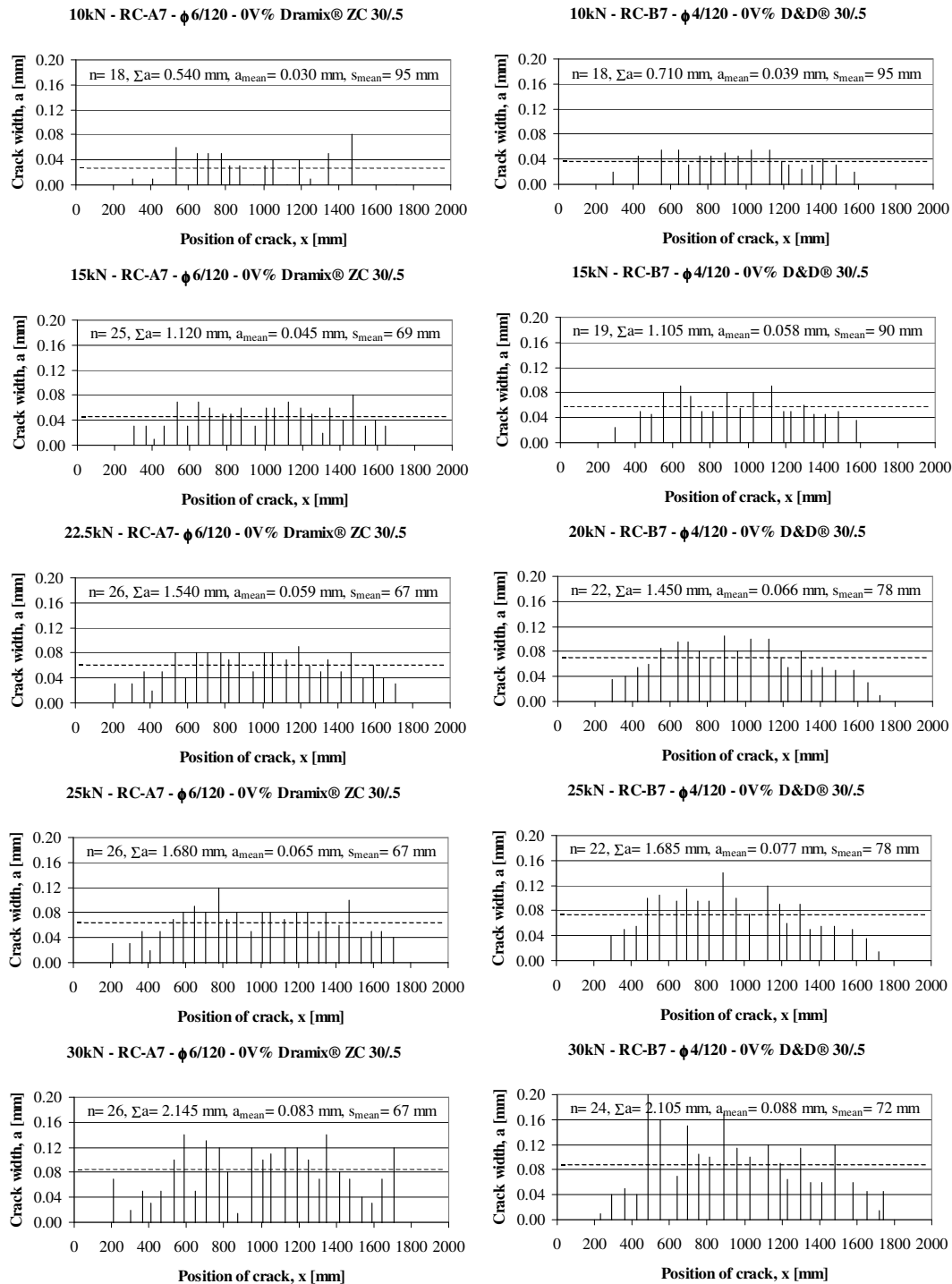


**Figure A11:** Crack distributions of beam RC-A5 having  $\phi 6/240$  stirrup reinforcement and 0.5 V% Dramix® ZC 30/5 hooked-end steel fibres and of beam RC-B5 having  $\phi 4/240$  stirrup reinforcement and 0.5 V% D&D® 30/5 crimped steel fibres at different load levels. The horizontal axis of the diagrams indicates the position of the cracks. The horizontal dotted line indicates the mean crack width at the given load step.

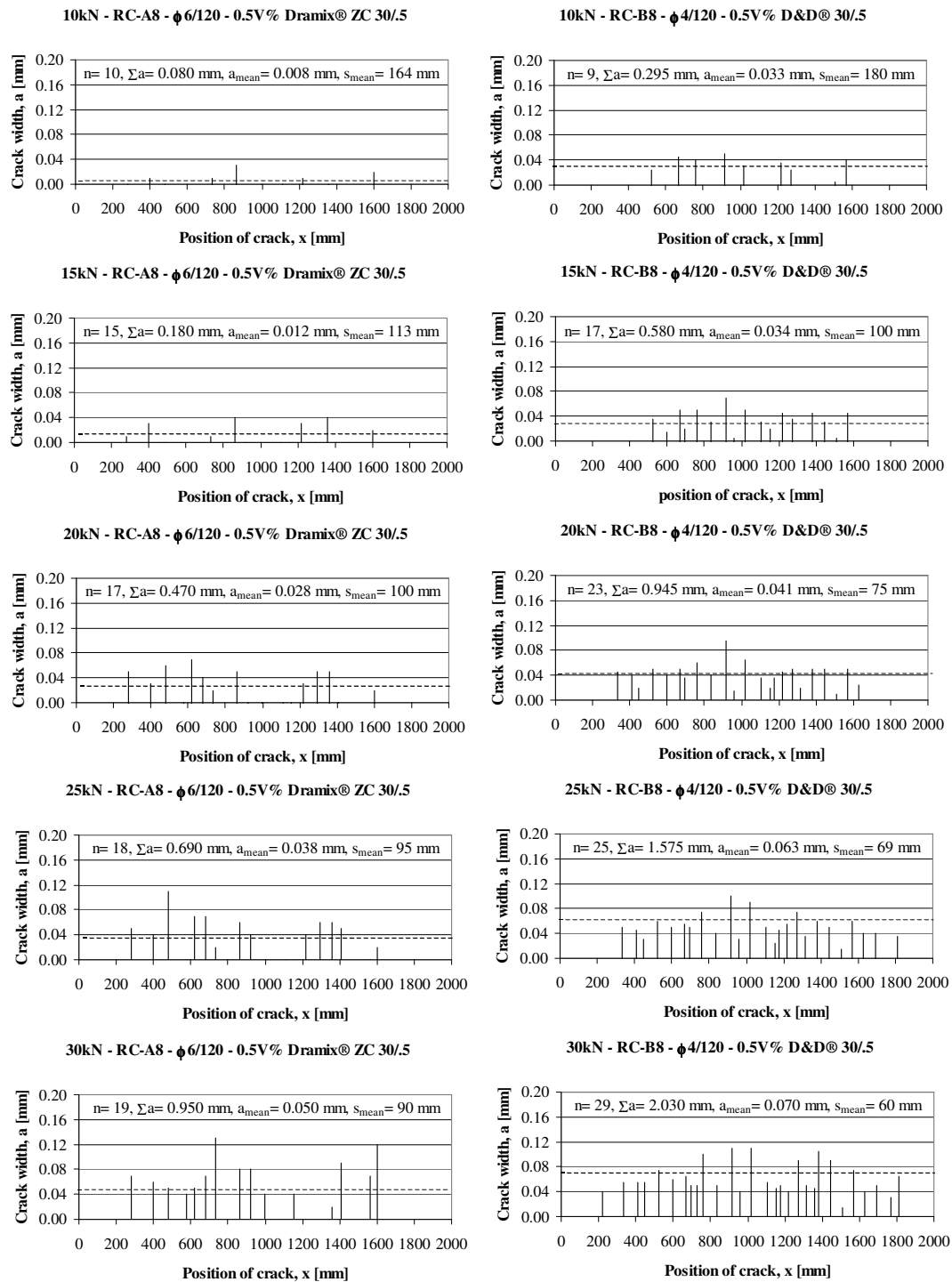


**Figure A12:** Crack distributions of beam RC-A6 having  $\phi$ 6/240 stirrup reinforcement and 1.0 V% Dramix® ZC 30/5 hooked-end steel fibres and of beam RC-B6 having  $\phi$ 4/240 stirrup reinforcement and 1.0 V% D&D® 30/5 crimped steel fibres at different load levels. The horizontal axis of the diagrams indicates the position of the cracks. The horizontal dotted line indicates the mean crack width at the given load step.

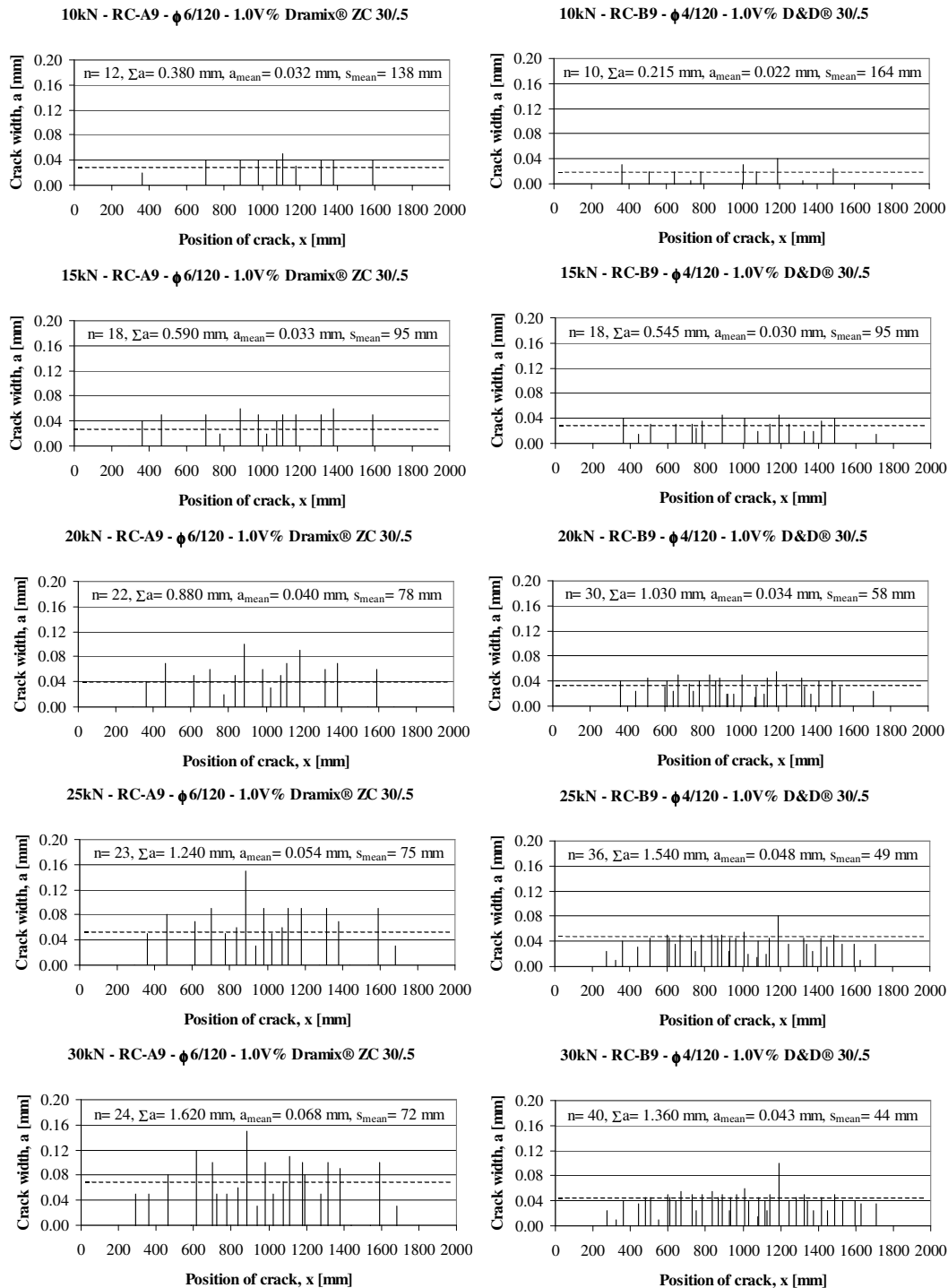




**Figure A13:** Crack distributions of beam RC-A7 having  $\emptyset 6/120$  stirrup reinforcement and 0 V% Dramix<sup>®</sup> ZC 30/5 hooked-end steel fibres and of beam RC-B7 having  $\emptyset 4/120$  stirrup reinforcement and 0 V% D&D<sup>®</sup> 30/5 crimped steel fibres at different load levels. The horizontal axis of the diagrams indicates the position of the cracks. The horizontal dotted line indicates the mean crack width at the given load step.



**Figure A14:** Crack distributions of beam RC-A8 having  $\phi$ 6/120 stirrup reinforcement and 0.5 V% Dramix® ZC 30/5 hooked-end steel fibres and of beam RC-B8 having  $\phi$ 4/120 stirrup reinforcement and 0.5 V% D&D® 30/5 crimped steel fibres at different load levels. The horizontal axis of the diagrams indicates the position of the cracks. The horizontal dotted line indicates the mean crack width at the given load step.



**Figure A15:** Crack distributions of beam RC-A9 having  $\phi$ 6/120 stirrup reinforcement and 1.0 V% Dramix® ZC 30/5 hooked-end steel fibres and of beam RC-B9 having  $\phi$ 4/120 stirrup reinforcement and 1.0 V% D&D® 30/5 crimped steel fibres at different load levels. The horizontal axis of the diagrams indicates the position of the cracks. The horizontal dotted line indicates the mean crack width at the given load step.

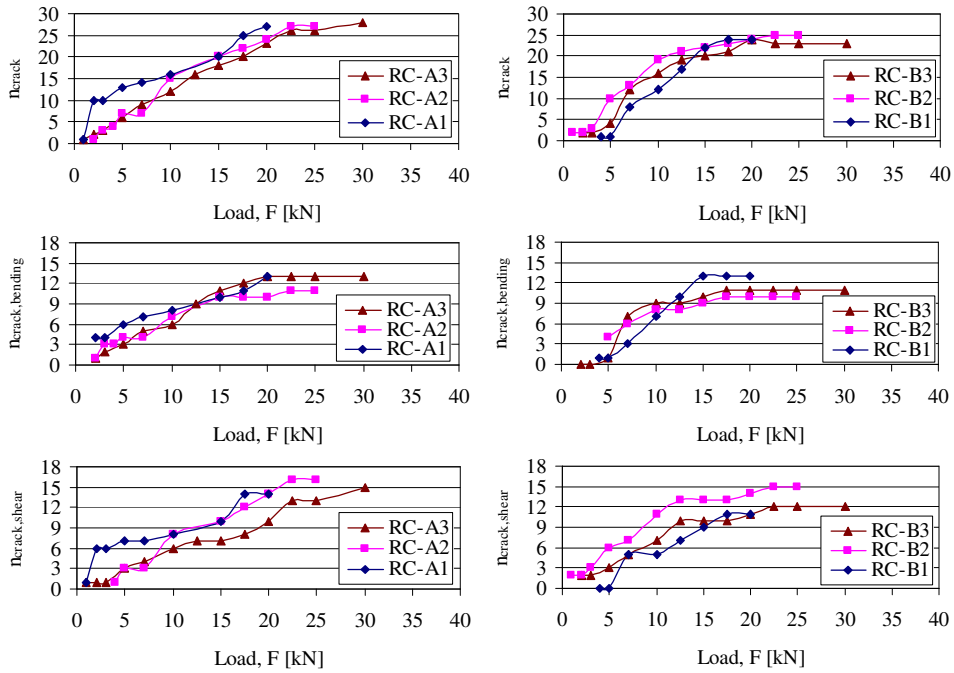


Figure A16: load vs. crack number relationships for RCA1...A3 and RC-B1...B3

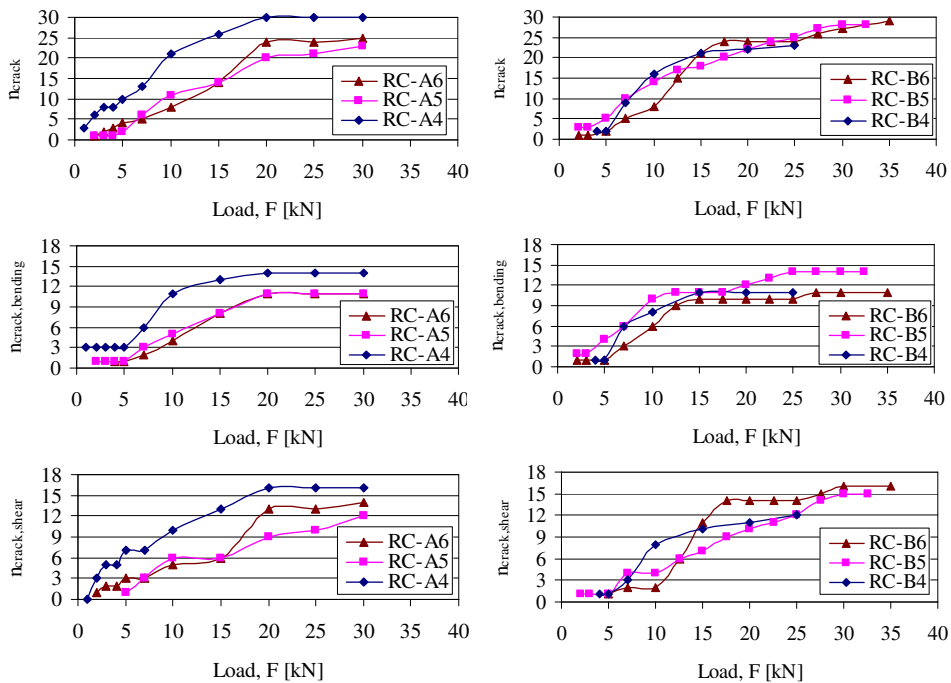


Figure A17: Load vs. crack number relationships for RCA4...A6 and RC-B4...B36

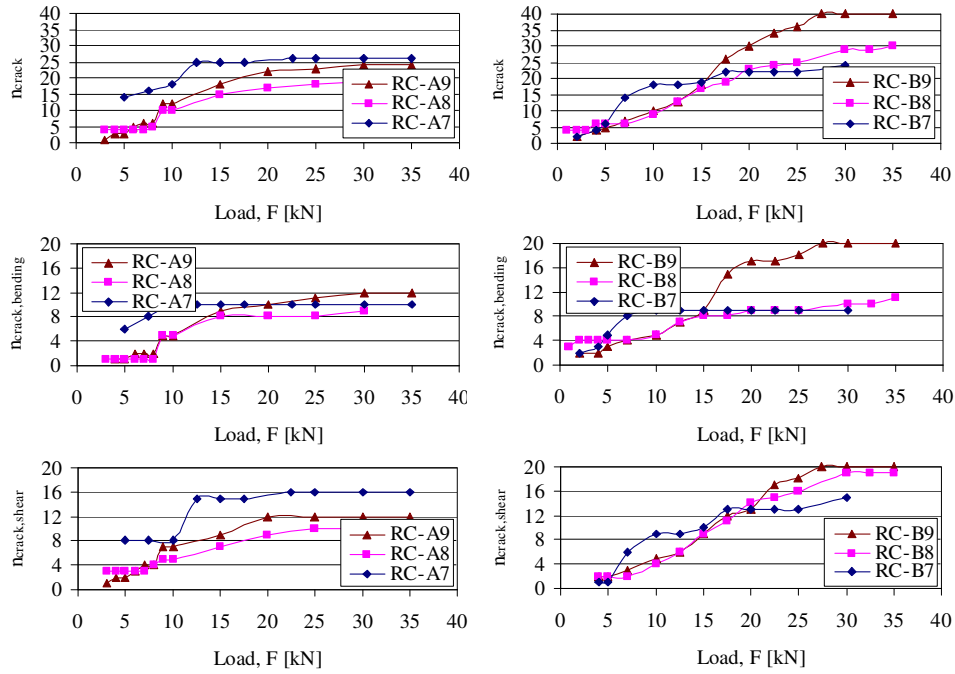


Figure A18: Load vs. crack number relationships for RC-A7...A9 and RC-B7...B9

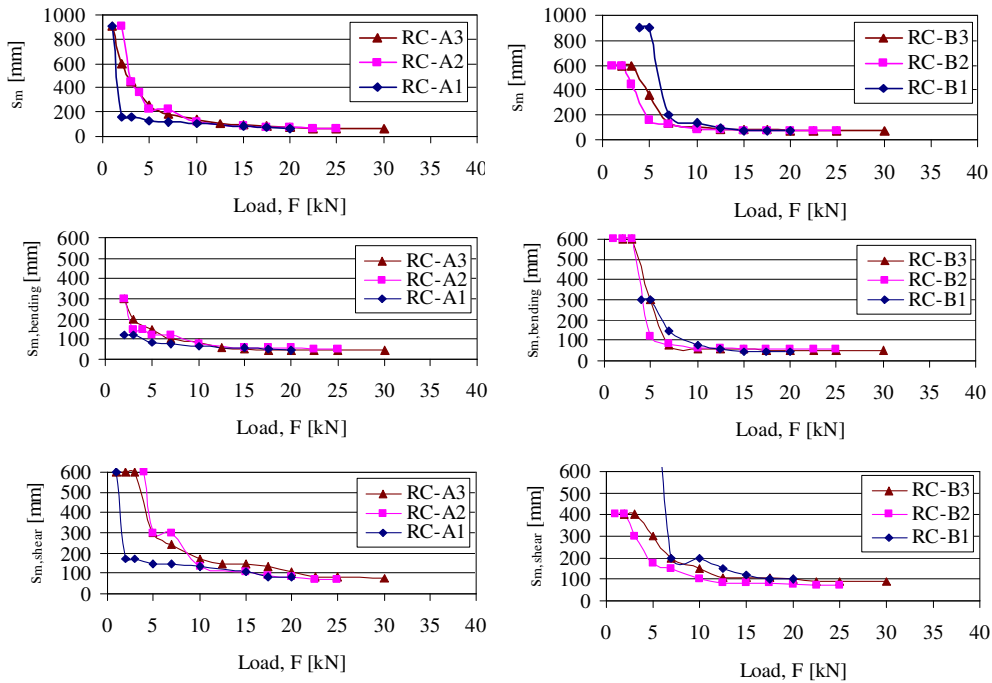


Figure A19: Load vs. crack spacing relationships for RC-A1...A3 and RC-B1...B3

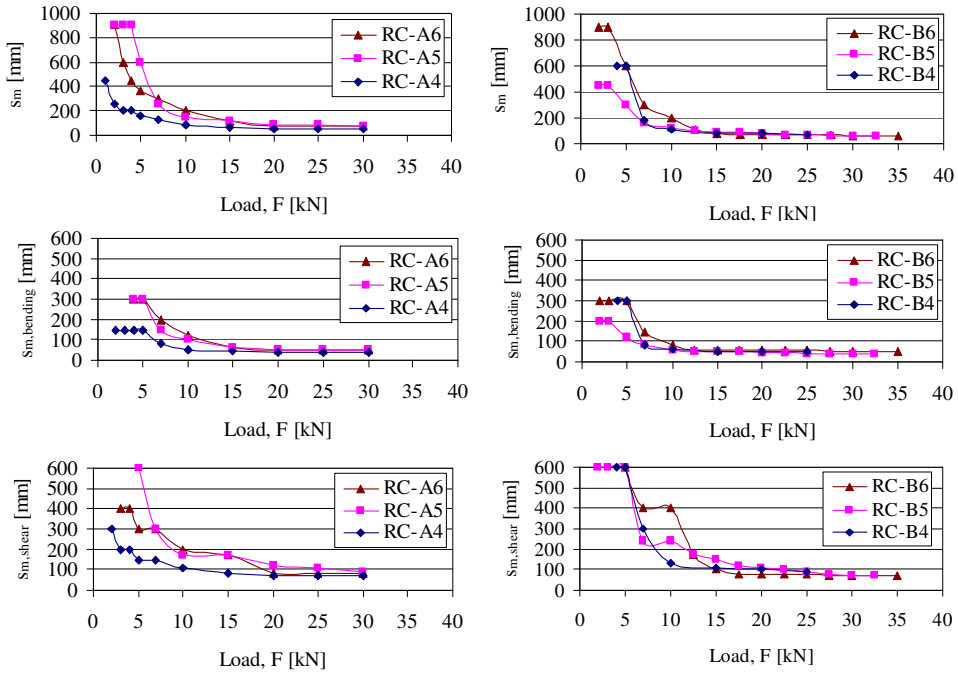


Figure A20: Load vs. crack spacing relationships for RC-A4...A6 and RC-B4...B6

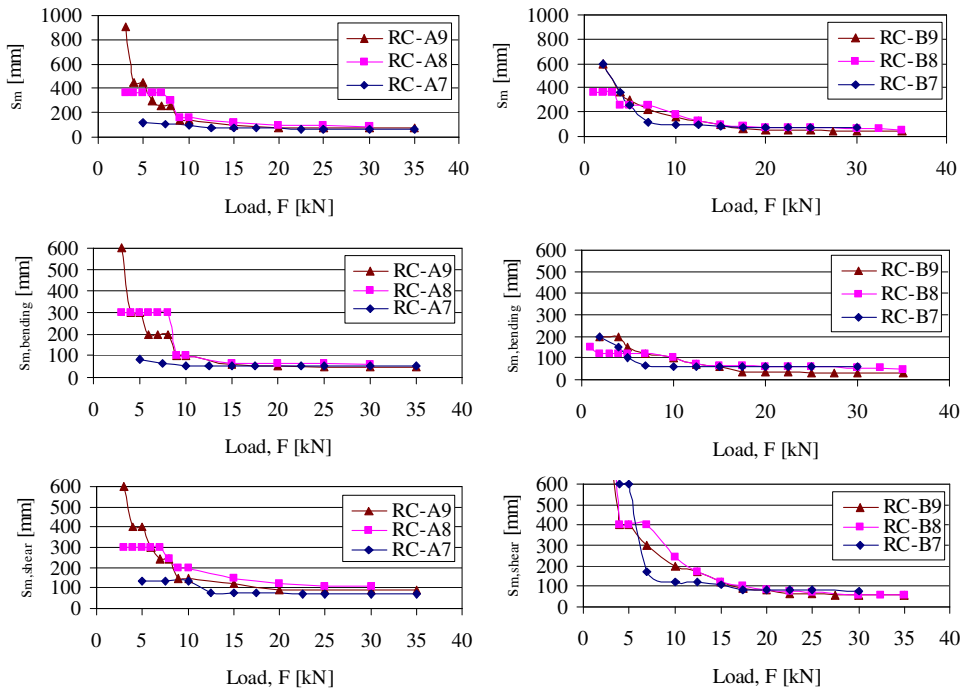
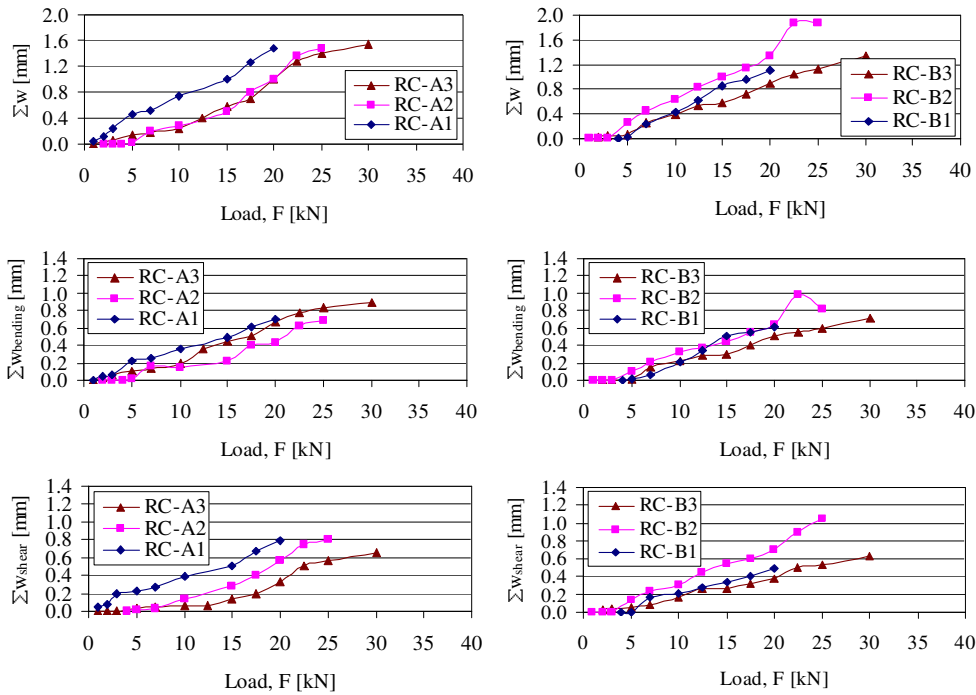
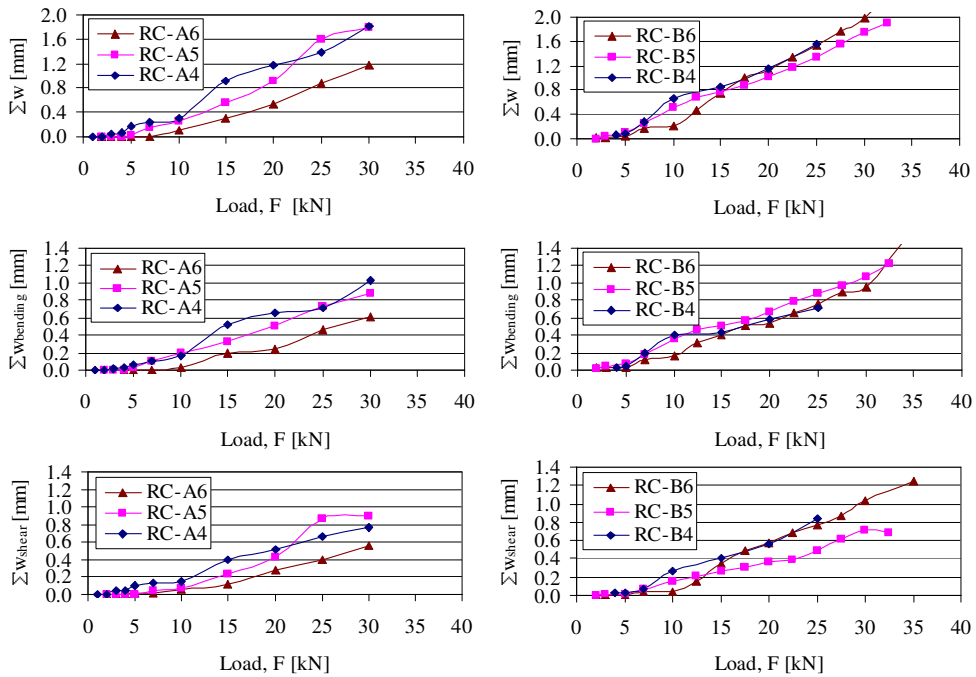


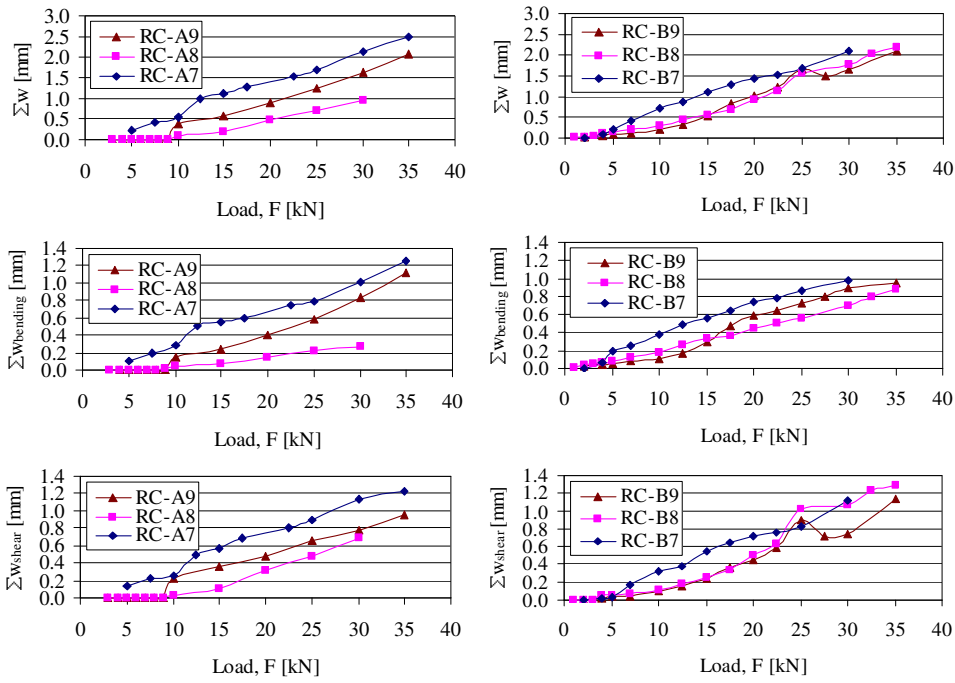
Figure A21: Load vs. crack spacing relationships for RC-A7...A9 and RC-B7...B9



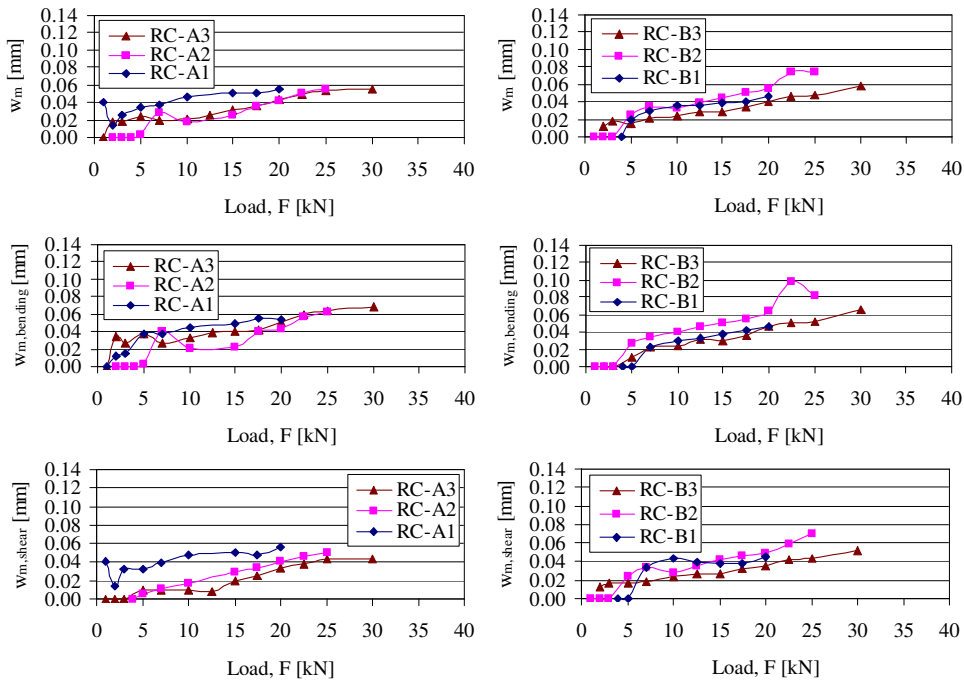
**Figure A22:** Load vs. sum of crack width relationships for RC-A1...A3 and RC-B1...B3



**Figure A23:** Load vs. sum of crack width relationships for RC-A4...A6 and RC-B4...B6

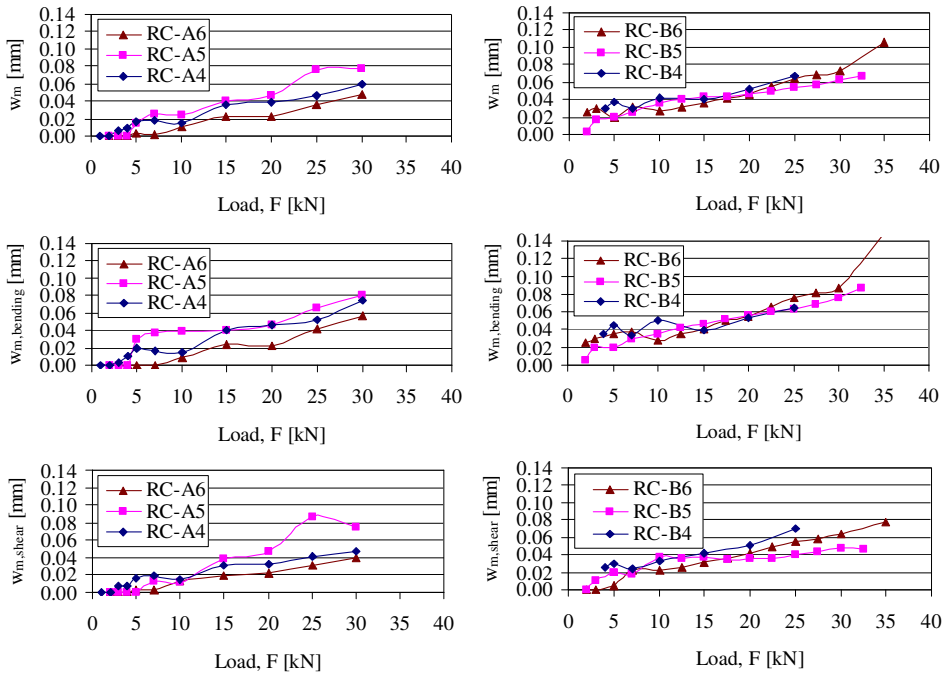


**Figure A24:** Load vs. sum of crack width relationships for RC-A7...A9 and RC-B7...B9

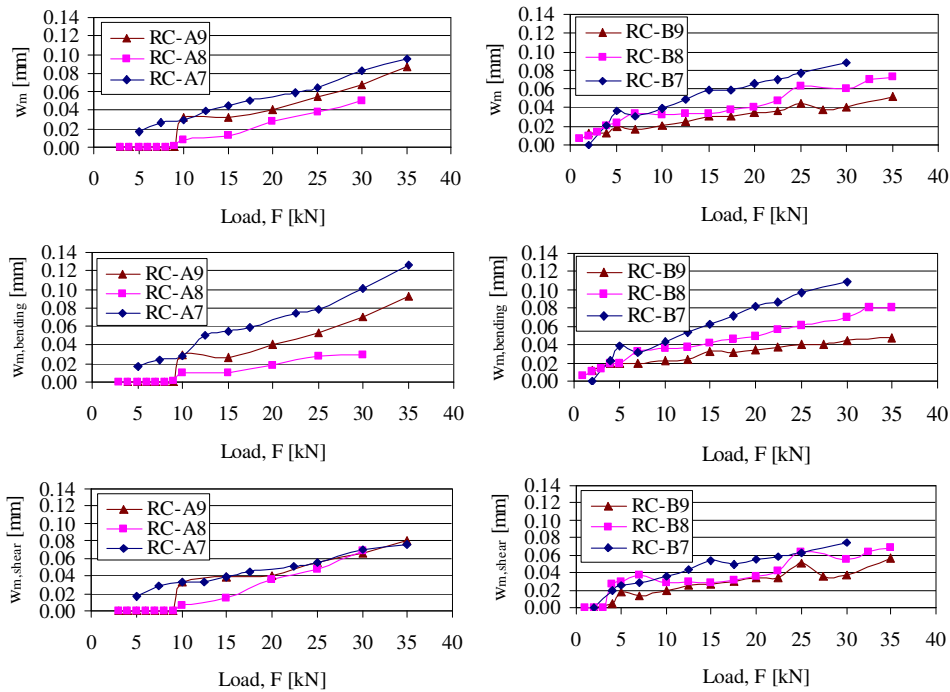


**Figure A25:** Load vs. mean crack width relationships for RC-A1...A3 and RC-B1...B3

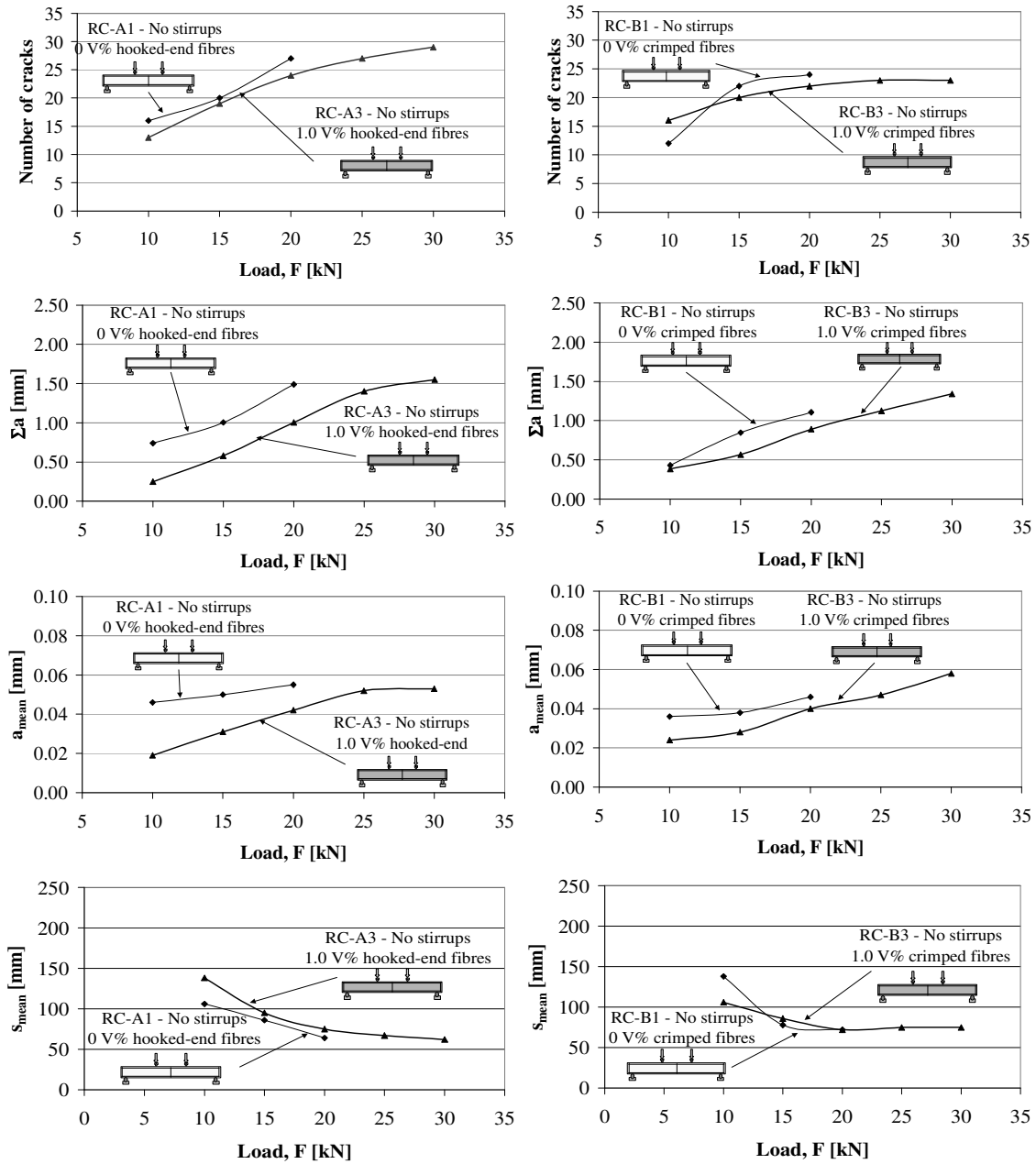




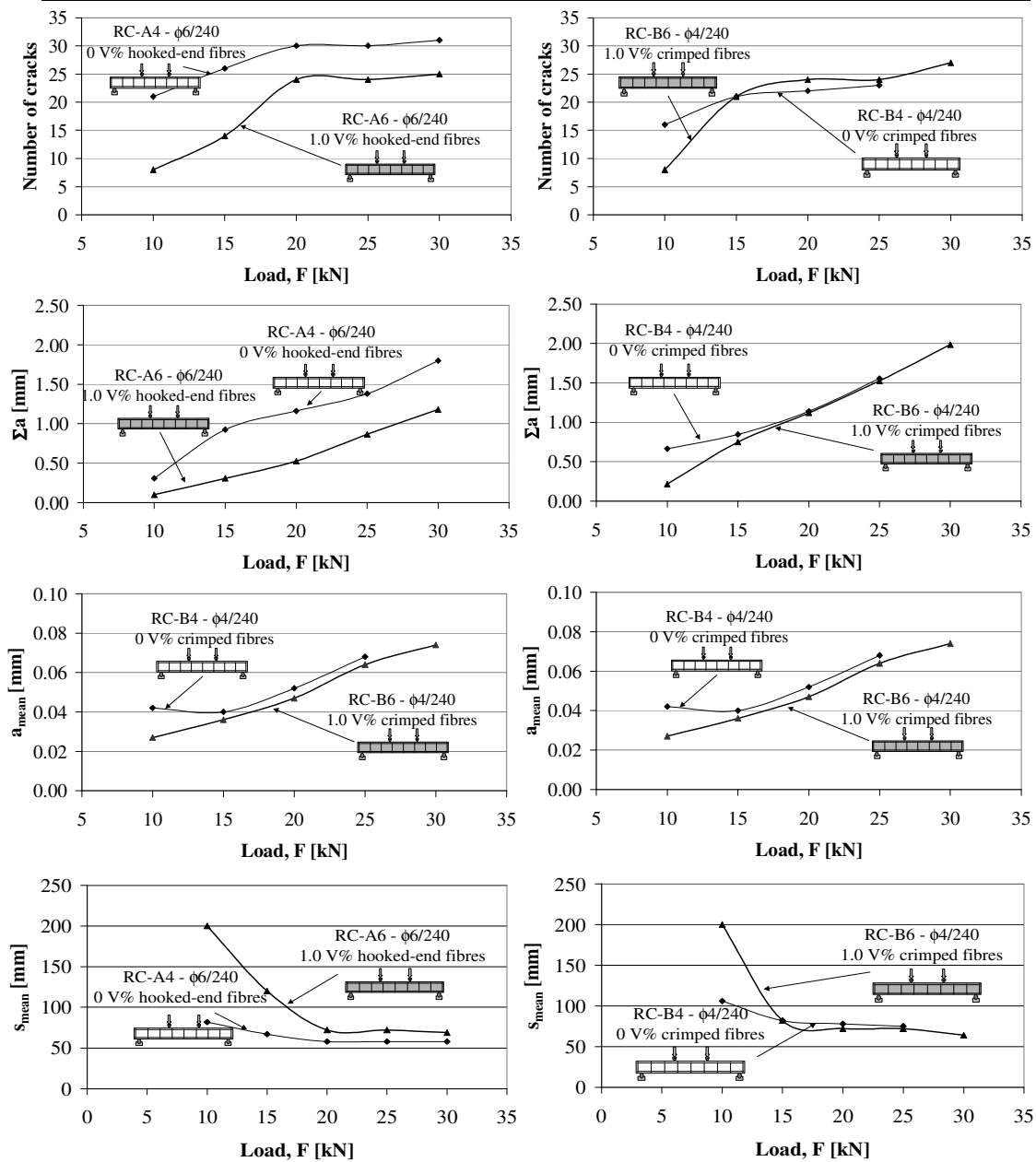
**Figure A26:** Load vs. mean crack width relationships for RC-A4...A6 and RC-B4...B6



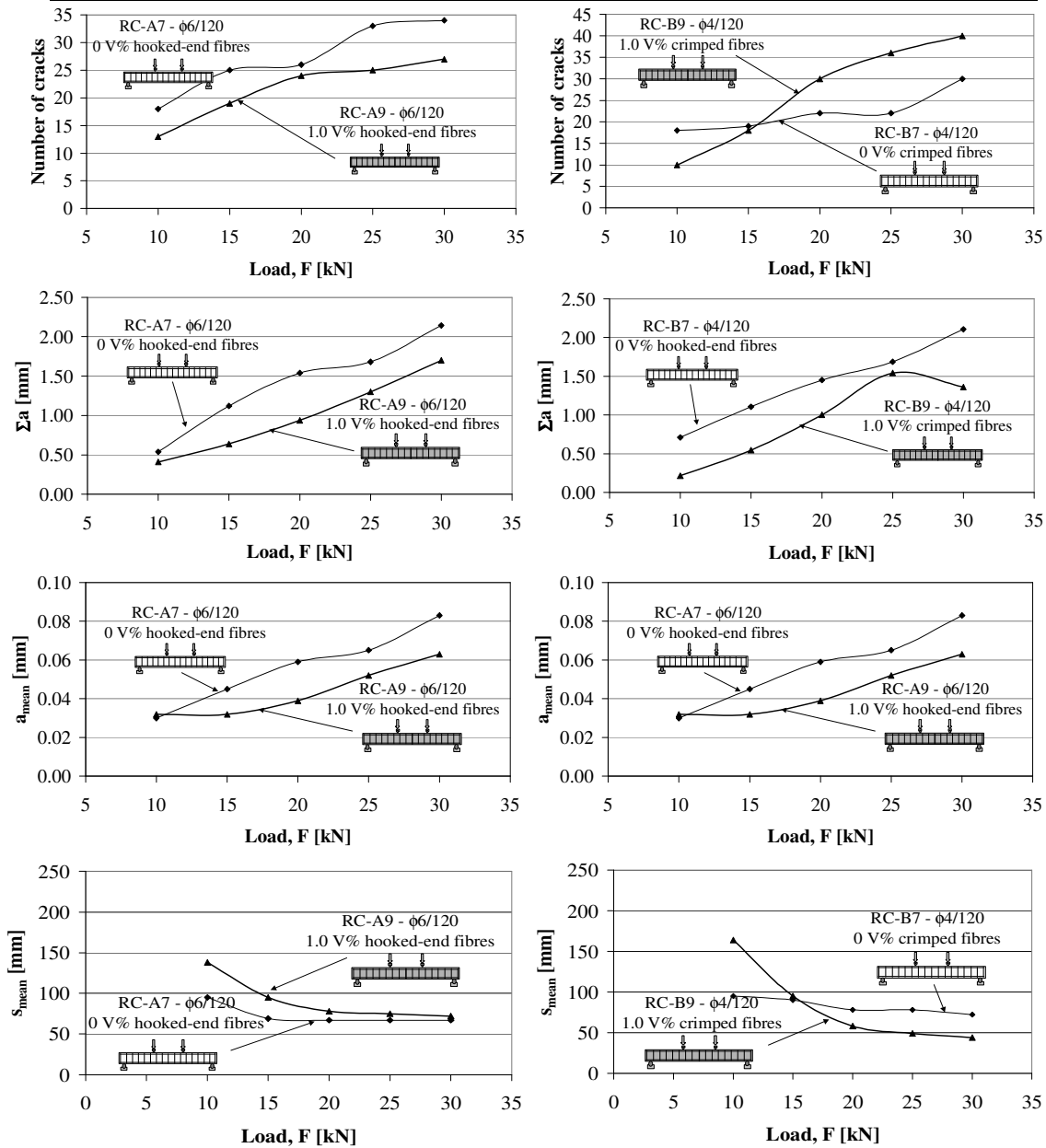
**Figure A27:** Load vs. mean crack width relationships for RC-A7...A9 and RC-B7...B9



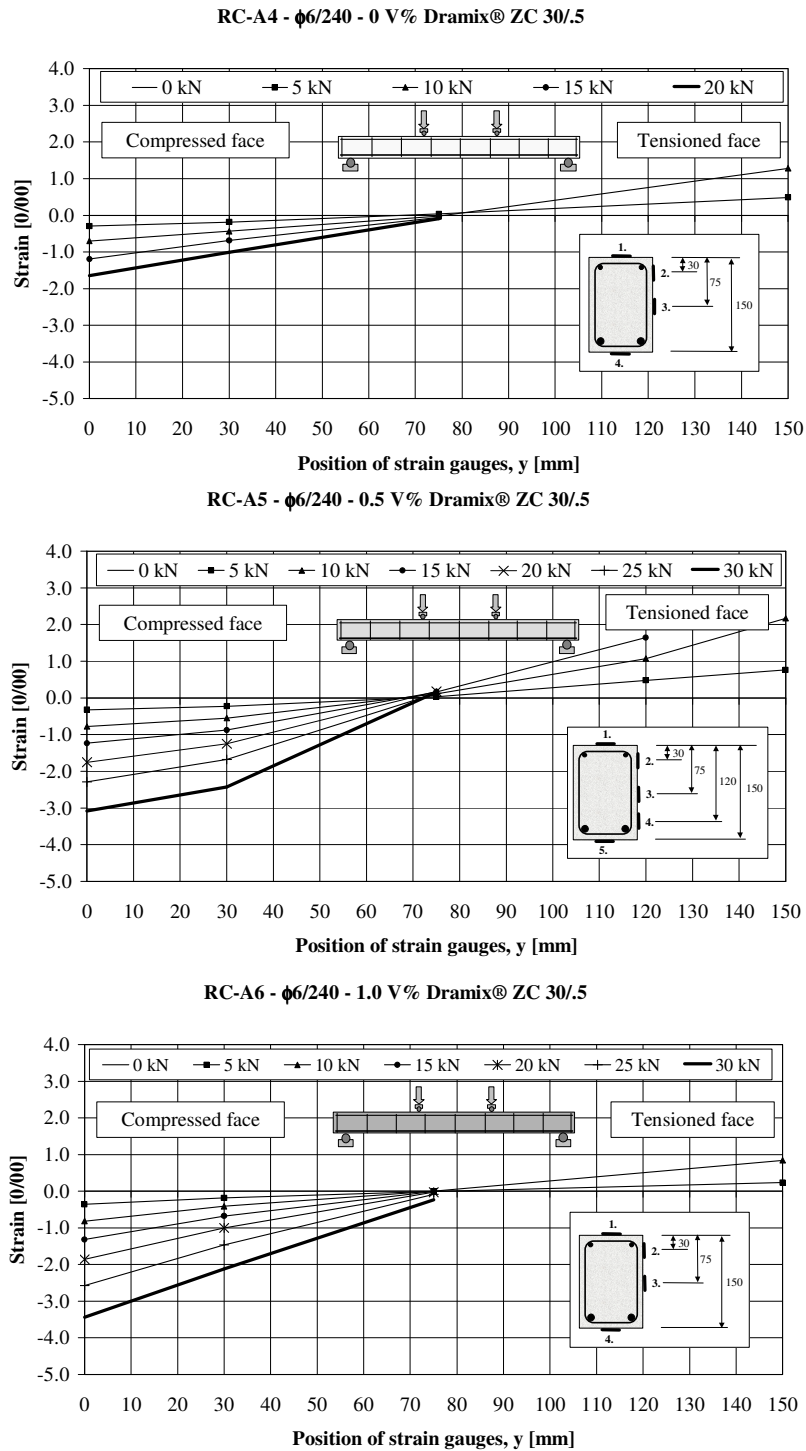
**Figure A28:** Load versus number of cracks relationship ( $F - \Sigma n$ ), Load versus sum of crack widths relationship ( $F - \Sigma a$ ), Load versus mean crack width relationship ( $F - a_{mean}$ ), Load versus mean crack spacing relationship ( $F - s_{mean}$ ) for beams RC-A1 and RC-A3 (Series A) represented in the first column and for beams RC-B1 and RC-B3 (Series B) represented in the second column).



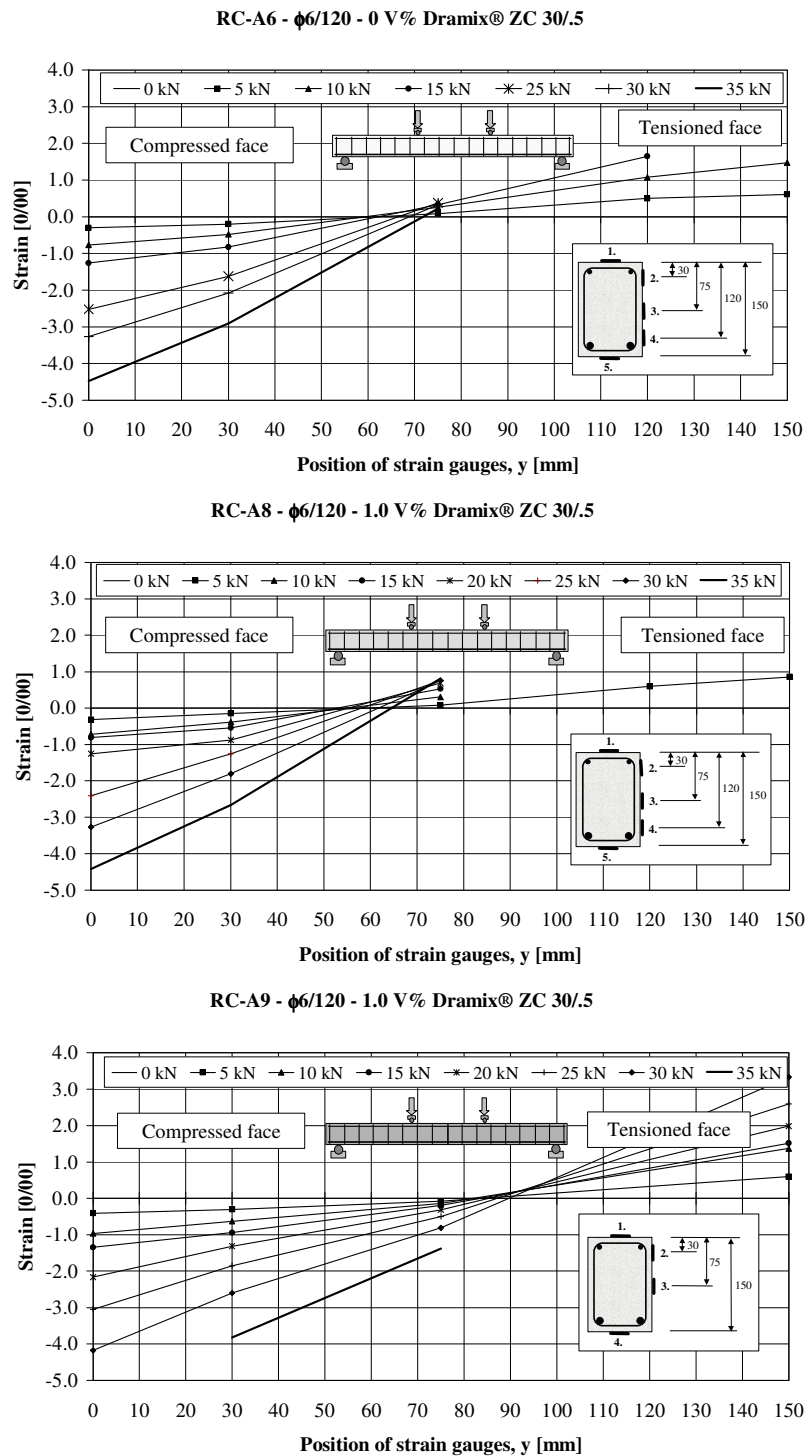
**Figure A29:** Load versus number of cracks relationship ( $F - \Sigma n$ ),  
 Load versus sum of crack widths relationship ( $F - \Sigma a$ ),  
 Load versus mean crack width relationship ( $F - a_{mean}$ ),  
 Load versus mean crack spacing relationship ( $F - s_{mean}$ )  
 for beams RC-A4 and RC-A6 (Series A) represented in the first column  
 and for beams RC-B4 and RC-B6 (Series B) represented in the second  
 column).



**Figure A30:** Load versus number of cracks relationship ( $F - \Sigma n$ ), Load versus sum of crack widths relationship ( $F - \Sigma a$ ), Load versus mean crack width relationship ( $F - a_{mean}$ ), Load versus mean crack spacing relationship ( $F - s_{mean}$ ) for beams RC-A7 and RC-A9 (Series A) represented in the first column and for beams RC-B7 and RC-B9 (Series B) represented in the second column).



**Figure A31:** Strain distribution in the mid-section of beams RC-A4...RC-A6 in loading. Horizontal axis of the diagram indicates the position of the strain gauges, vertical axis of the diagram indicate the measured concrete strain.



**Figure A32:** Strain distribution in the mid-section of the beams RC-A7...RC-A9 in loading. Horizontal axis of the diagram indicates the position of the strain gauges, vertical axis of the diagram indicates the measured concrete strain.

**Table A1: Measured crack widths for beams RC-A1**

Measured crack width along the beam containing 0V% DRAMIX® ZC 30/5 hooked-end steel fibres

Load F [kN]	Type of crack (B: bending crack; S: shear crack)																											
	S	B	B	S	S	S	S	S	S	B	B	B	S	B	B	S	S	S	S	B	B	S	S	B	S	S	B	B
Cracks																												
Position of the appeared crack along the beam x[mm]																												
	1	2	3	4	5	6	7	8	9	10	11	12	13	14	15	16	17	18	19	20	21	22	23	24	25	26	27	
1.0	0.040																											
2.0	0.045	0.040	0.010	0.000	0.000	0.000	0.000	0.035	0.000	0.000																		
3.0	0.050	0.025	0.010	0.045	0.000	0.000	0.000	0.050	0.045	0.025	0.000																	
5.0	0.055	0.040	0.055	0.055	0.015	0.000	0.000	0.050	0.040	0.030	0.030	0.055	0.030															
7.0	0.060	0.045	0.055	0.055	0.025	0.010	0.005	0.055	0.040	0.045	0.025	0.060	0.035	0.015														
10.0	0.060	0.045	0.055	0.065	0.050	0.030	0.005	0.065	0.045	0.045	0.050	0.090	0.045	0.030	0.040	0.020												
15.0	0.060	0.050	0.055	0.100	0.050	0.040	0.010	0.075	0.050	0.045	0.090	0.105	0.050	0.050	0.045	0.050	0.000	0.020	0.030	0.030								
17.5	0.100	0.100	0.060	0.105	0.055	0.050	0.010	0.100	0.050	0.050	0.090	0.105	0.050	0.060	0.045	0.050	0.025	0.030	0.040	0.040	0.015	0.010	0.020	0.000	0.010			
20.0	0.110	0.100	0.055	0.110	0.065	0.050	0.010	0.100	0.050	0.060	0.105	0.105	0.070	0.060	0.050	0.050	0.050	0.050	0.050	0.050	0.025	0.050	0.020	0.000	0.010	0.030	0.005	

**Table A2: Measured crack widths for beams RC-A2**

Measured crack width along the beam containing 0.5V% DRAMIX® ZC 30/5 hooked-end steel fibres

Load F [kN]	Type of crack (B: bending crack; S: shear crack)																											
	B	B	B	S	S	S	B	B	S	B	S	S	S	B	B	B	S	S	S	S	S	S	S	B	S	S		
Cracks																												
Position of the appeared crack along the beam x[mm]																												
	1	2	3	4	5	6	7	8	9	10	11	12	13	14	15	16	17	18	19	20	21	22	23	24	25	26	27	
2.0	0.000																											
3.0	0.000	0.000	0.000																									
4.0	0.000	0.000	0.000	0.000																								
5.0	0.000	0.010	0.000	0.000	0.015	0.000	0.000																					
7.0	0.000	0.035	0.000	0.005	0.030	0.000	0.125																					
10.0	0.000	0.045	0.040	0.050	0.030	0.005	0.000	0.000	0.000	0.025	0.000	0.005	0.000	0.040	0.035													
15.0	0.015	0.060	0.040	0.060	0.045	0.010	0.025	0.000	0.055	0.015	0.000	0.005	0.025	0.050	0.045	0.010	0.010	0.000	0.030	0.010								
17.5	0.050	0.070	0.050	0.060	0.050	0.020	0.045	0.040	0.055	0.030	0.000	0.015	0.035	0.055	0.055	0.040	0.015	0.000	0.023	0.025	0.050	0.015						
20.0	0.050	0.070	0.050	0.060	0.055	0.050	0.045	0.050	0.055	0.040	0.000	0.025	0.035	0.055	0.060	0.045	0.025	0.000	0.045	0.045	0.060	0.035	0.020	0.025				
22.5	0.055	0.100	0.060	0.060	0.060	0.090	0.060	0.075	0.055	0.040	0.000	0.035	0.050	0.060	0.080	0.065	0.035	0.020	0.045	0.055	0.060	0.050	0.025	0.045	0.035	0.010	0.045	
25.0	0.060	0.105	0.075	0.075	0.060	0.090	0.060	0.075	0.055	0.050	0.000	0.050	0.055	0.060	0.080	0.065	0.040	0.020	0.000	0.060	0.100	0.060	0.045	0.050	0.050	0.010	0.040	

**Table A3: Measured crack widths for beams RC-A3**

Measured crack width along the beam containing 1V% DRAMIX® ZC 30/5 hooked-end steel fibres

Load F [kN]	Type of crack (B: bending crack; S: shear crack)																											
	S	B	B	B	S	S	B	S	B	B	S	S	B	B	S	B	B	S	S	S	B	S	S	S	S	S	S	
Cracks																												
Position of the appeared crack along the beam x[mm]																												
	1	2	3	4	5	6	7	8	9	10	11	12	13	14	15	16	17	18	19	20	21	22	23	24	25	26	27	28
1.0	0.000																											
2.0	0.000	0.035																										
3.0	0.000	0.035	0.020																									
5.0	0.005	0.040	0.030	0.040	0.000	0.025																						
7.0	0.005	0.045	0.045	0.045	0.000	0.035	0.000	0.000	0.000																			
10.0	0.005	0.050	0.050	0.050	0.005	0.045	0.040	0.000	0.005	0.000	0.000	0.000																
12.5	0.005	0.060	0.055	0.060	0.005	0.050	0.050	0.000	0.020	0.000	0.000	0.000	0.050	0.015	0.040	0.000												
15.0	0.040	0.070	0.065	0.075	0.010	0.050	0.050	0.010	0.040	0.010	0.015	0.000	0.060	0.015	0.050	0.010	0.000	0.005										
17.5	0.020	0.070	0.080	0.080	0.025	0.055	0.050	0.025	0.050	0.020	0.020	0.000	0.065	0.010	0.050	0.025	0.020	0.010	0.000	0.030								
20.0	0.040	0.085	0.090	0.100	0.040	0.055	0.060	0.030	0.050	0.030	0.020	0.000	0.080	0.035	0.055	0.030	0.030	0.015	0.005	0.035	0.050	0.035	0.030					
22.5	0.040	0.095	0.100	0.130	0.045	0.055	0.060	0.045	0.060	0.030	0.020	0.000	0.080	0.035	0.065	0.040	0.045	0.035	0.015	0.035	0.050	0.040	0.030	0.050	0.020	0.060		
25.0	0.050	0.095	0.120	0.130	0.050	0.055	0.060	0.050	0.060	0.030	0.025	0.000	0.100	0.045	0.065	0.040	0.045	0.035	0.015	0.045	0.050	0.055	0.030	0.050	0.035	0.060		
30.0	0.050	0.100	0.120	0.150	0.050	0.060	0.060	0.050	0.080	0.040	0.025	0.000	0.100	0.030	0.070	0.035	0.045	0.045	0.015	0.045	0.050	0.055	0.035	0.050	0.040	0.060	0.045	0.040

**Table A4: Measured crack widths for beams RC-A4**

Measured crack width along the beam containing  $\phi 6/240 - 0V\%$  DRAMIX® ZC 30/5 hooked-end steel fibres

Load F [kN]	Type of crack (B: bending crack; S: shear crack)																													
	B	B	B	S	S	S	S	S	S	S	S	B	B	B	S	S	B	B	B	B	S	S	S	B	B	S	S	B	S	S
Cracks																														
Position of the appeared crack along the beam x[mm]																														
	1	2	3	4	5	6	7	8	9	10	11	12	13	14	15	16	17	18	19	20	21	22	23	24	25	26	27	28	29	30
857	1018	1193	296	511	610	1630	222	1521	1727	823	965	1300	336	755	1161	913	1128	1263	1578	1557	397	565	1168	1226	1378	452	1048	1451	1320	
1	0.000	0.000	0.000																											
2	0.000	0.000	0.000	0.000	0.000	0.000																								
3	0.010	0.000	0.000	0.020	0.000	0.000	0.020	0.000																						
4	0.010	0.020	0.000	0.020	0.000	0.000	0.020	0.000																						
5	0.020	0.020	0.020	0.030	0.000	0.010	0.030	0.000	0.020	0.020																				
7	0.035	0.020	0.025	0.035	0.000	0.010	0.035	0.000	0.025	0.030	0.000	0.020	0.000																	
10	0.040	0.045	0.030	0.040	0.000	0.010	0.035	0.000	0.030	0.030	0.000	0.045	0.000	0.000	0.000	0.000	0.000	0.000	0.000	0.000	0.000	0.000	0.000	0.000	0.000	0.000	0.000	0.000	0.000	
15	0.055	0.045	0.070	0.050	0.050	0.025	0.045	0.040	0.030	0.030	0.015	0.060	0.000	0.010	0.040	0.050	0.050	0.030	0.040	0.040	0.000	0.020	0.045	0.045	0.020	0.020	0.000	0.040	0.010	0.030
20	0.060	0.050	0.060	0.050	0.050	0.025	0.060	0.045	0.040	0.040	0.030	0.070	0.025	0.015	0.050	0.060	0.050	0.040	0.045	0.045	0.000	0.030	0.045	0.050	0.025	0.020	0.000	0.040	0.010	0.030
25	0.070	0.060	0.060	0.050	0.040	0.025	0.060	0.120	0.040	0.040	0.030	0.080	0.025	0.020	0.050	0.070	0.050	0.050	0.045	0.045	0.020	0.040	0.050	0.060	0.030	0.035	0.000	0.045	0.020	0.050
30	0.100	0.080	0.100	0.050	0.080	0.025	0.070	0.130	0.020	0.020	0.070	0.100	0.025	0.030	0.060	0.120	0.080	0.050	0.060	0.060	0.020	0.050	0.060	0.090	0.050	0.050	0.000	0.050	0.050	0.050

**Table A5: Measured crack widths for beams RC-A5**

Measured crack width along the beam containing  $\phi 6/240 - 0.5V\%$  DRAMIX® ZC 30/5 hooked-end steel fibres

Load F [kN]	Type of crack (B: bending crack; S: shear crack)																													
	B	S	B	B	S	S	S	S	B	S	B	S	B	B	B	S	B	B	S	S	S	S	S	S						
Cracks																														
Position of the appeared crack along the beam x[mm]																														
	1	2	3	4	5	6	7	8	9	10	11	12	13	14	15	17	18	19	20	21	23	24	25							
896	1738	1005	1229	1348	524	584	849	686	1111	1434	951	1165	1288	344	720	445	1044	1487	1591	1528	1364	1664								
2.0	0.000																													
3.0	0.000																													
4.0	0.000																													
5.0	0.030	0.000																												
7.0	0.050	0.000	0.060	0.000	0.000	0.040																								
10.0	0.050	0.000	0.100	0.000	0.000	0.050	0.010	0.020	0.010	0.020	0.000																			
15.0	0.070	0.035	0.115	0.025	0.050	0.055	0.030	0.065	0.050	0.040	0.010	0.010	0.000	0.000																
20.0	0.100	0.050	0.120	0.045	0.050	0.055	0.090	0.070	0.080	0.060	0.030	0.030	0.000	0.025	0.010	0.010	0.000	0.040	0.040	0.020										
25.0	0.130	0.060	0.120	0.070	0.120	0.090	0.200	0.100	0.100	0.090	0.050	0.050	0.020	0.030	0.100	0.030	0.020	0.065	0.065	0.040	0.045									
30.0	0.130	0.010	0.120	0.100	0.120	0.050	0.200	0.120	0.130	0.090	0.070	0.070	0.020	0.060	0.120	0.080	0.020	0.075	0.075	0.040	0.050	0.040	0.000							

**Table A6: Measured crack widths for beams RC-A6**

Measured crack width along the beam containing  $\phi 6/240 - 1V\%$  DRAMIX® ZC 30/5 hooked-end steel fibres

Load F [kN]	Type of crack (B: bending crack; S: shear crack)																								
	S	S	B	S	B	S	B	S	B	B	B	S	S	S	S	S	S	B	B	B	S	S	S	S	
Cracks																									
Position of the appeared crack along the beam x[mm]																									
	1	2	3	4	5	6	7	8	9	10	11	12	13	14	15	16	17	18	19	20	21	22	23	24	25
1441	402	1255	341	767	540	866	1312	947	716	1032	1150	1208	1741	284	452	602	660	822	1016	1072	1360	1412	1587	637	
2	0.000																								
3	0.000	0.000																							
4	0.000	0.000	0.000																						
5	0.000	0.010	0.000	0.000																					
7	0.000	0.010	0.000	0.000	0.000																				
10	0.000	0.015	0.010	0.000	0.000	0.035	0.015	0.015	0.010																
15	0.000	0.025	0.030	0.000	0.055	0.050	0.040	0.040	0.035	0.020	0.000	0.010	0.000	0.000											
20	0.000	0.030	0.055	0.000	0.055	0.060	0.040	0.060	0.050	0.025	0.000	0.020	0.000	0.000	0.010	0.035	0.025	0.000	0.000	0.000	0.000	0.040	0.010	0.010	
25	0.010	0.035	0.055	0.030	0.070	0.065	0.045	0.065	0.055	0.050	0.050	0.015	0.000	0.000	0.010	0.040	0.030	0.010	0.050	0.050	0.020	0.045	0.040	0.025	
30	0.020	0.040	0.110	0.050	0.100	0.065	0.050	0.100	0.090	0.055	0.055	0.020	0.000	0.000	0.020	0.050	0.045	0.010	0.055	0.055	0.025	0.050	0.040	0.045	0.030



**Table A7: Measured crack widths for beams RC-A7**

Measured crack width along the beam containing  $\phi 6/120 - 0V\%$  DRAMIX® ZC 30/5 hooked-end steel fibres

Load F [kN]	Type of crack (B: bending crack; S: shear crack)																									
	Cracks																									
	Position of the appeared crack along the beam x[mm]																									
	1	2	3	4	5	6	7	8	9	10	11	12	13	14	15	16	17	18	19	20	21	22	23	24	25	26
	300	410	532	648	704	778	876	1010	1128	1250	1350	1472	1592	1708	950	1050	818	1194	368	465	587	1308	1420	1536	1644	208
5.0	0.000	0.000	0.050	0.000	0.040	0.040	0.020	0.000	0.000	0.000	0.030	0.050	0.000	0.000												
7.5	0.000	0.010	0.060	0.040	0.050	0.060	0.030	0.030	0.000	0.020	0.050	0.070	0.000	0.000	0.000	0.000										
10.0	0.010	0.010	0.060	0.050	0.050	0.050	0.030	0.030	0.000	0.010	0.050	0.080	0.000	0.000	0.000	0.040	0.030	0.040								
12.5	0.030	0.020	0.070	0.070	0.050	0.050	0.050	0.050	0.070	0.040	0.050	0.080	0.000	0.000	0.030	0.050	0.050	0.060	0.020	0.020	0.030	0.010	0.030	0.030	0.030	
15.0	0.030	0.010	0.070	0.070	0.060	0.050	0.060	0.060	0.070	0.050	0.060	0.080	0.040	0.000	0.030	0.060	0.050	0.060	0.030	0.030	0.030	0.020	0.040	0.030	0.030	
17.5	0.040	0.010	0.070	0.080	0.060	0.070	0.060	0.060	0.070	0.050	0.060	0.080	0.040	0.030	0.040	0.060	0.050	0.070	0.040	0.040	0.040	0.040	0.040	0.040	0.040	0.030
22.5	0.030	0.020	0.080	0.080	0.080	0.080	0.080	0.080	0.070	0.060	0.070	0.080	0.060	0.030	0.050	0.080	0.070	0.090	0.050	0.050	0.040	0.050	0.050	0.040	0.040	0.030
25.0	0.030	0.020	0.070	0.090	0.080	0.120	0.080	0.080	0.070	0.080	0.080	0.100	0.050	0.040	0.050	0.080	0.070	0.080	0.050	0.050	0.080	0.050	0.060	0.040	0.050	0.030
30.0	0.020	0.030	0.100	0.050	0.130	0.120	0.015	0.100	0.120	0.100	0.140	0.070	0.030	0.120	0.120	0.110	0.080	0.120	0.050	0.050	0.140	0.070	0.080	0.040	0.070	0.070
35.0	0.010	0.000	0.130	0.050	0.150	0.160	0.015	0.120	0.130	0.090	0.140	0.090	0.030	0.200	0.170	0.130	0.120	0.170	0.030	0.030	0.170	0.070	0.100	0.020	0.080	0.070

**Table A8: Measured crack widths for beams RC-A8**

Measured crack width along the beam containing  $\phi 6/120 - 0.5V\%$  DRAMIX® ZC 30/5 hooked-end steel fibres

Load F [kN]	Type of crack (B: bending crack; S: shear crack)																		
	Cracks																		
	Position of the appeared crack along the beam x[mm]																		
	1	2	3	4	5	6	7	8	9	10	11	12	13	14	15	16	17	18	19
	860	397	1601	1360	278	482	732	997	1108	1220	576	921	1155	1295	1408	621	678	1565	1080
3	0.000	0.000	0.000	0.000															
4	0.000	0.000	0.000	0.000															
5	0.000	0.000	0.000	0.000															
6	0.000	0.000	0.000	0.000															
7	0.000	0.000	0.000	0.000															
8	0.000	0.000	0.000	0.000	0.000														
9	0.010	0.000	0.000	0.000	0.000	0.000	0.000	0.000	0.000	0.000	0.000	0.000	0.000	0.000	0.000				
10	0.030	0.010	0.020	0.000	0.000	0.000	0.010	0.000	0.000	0.010	0.000	0.000	0.000	0.000	0.000	0.000			
15	0.040	0.030	0.020	0.040	0.010	0.000	0.010	0.000	0.000	0.000	0.030	0.000	0.000	0.000	0.000	0.000	0.000		
20	0.050	0.030	0.020	0.050	0.050	0.060	0.020	0.000	0.000	0.030	0.000	0.000	0.000	0.050	0.000	0.070	0.040		
25	0.060	0.040	0.020	0.060	0.050	0.110	0.020	0.000	0.000	0.040	0.000	0.040	0.000	0.060	0.050	0.070	0.070	0.000	
30	0.060	0.120	0.020	0.070	0.050	0.130	0.040	0.000	0.000	0.040	0.080	0.040	0.000	0.090	0.050	0.070	0.090	0.000	0.000

**Table A9: Measured crack widths for beams RC-AI**

Measured crack width along the beam containing  $\phi 6/120 - 1V\%$  DRAMIX® ZC 30/5 hooked-end steel fibres

Load F [kN]	Type of crack (B: bending crack; S: shear crack)																							
	Cracks																							
	Position of the appeared crack along the beam x[mm]																							
	1	2	3	4	5	6	7	8	9	10	11	12	13	14	15	16	17	18	19	20	21	22	23	24
	1382	882	1113	360	1182	585	838	700	982	1076	1314	1590	465	615	774	1024	1276	290	1442	1192	1540	1680	940	721
3	0.000																							
4	0.000	0.000	0.000																					
5	0.000	0.000	0.000																					
6	0.000	0.000	0.000	0.000	0.000																			
7	0.000	0.000	0.000	0.000	0.000	0.000	0.000	0.000	0.000	0.000	0.000	0.000	0.000	0.000	0.000									
8	0.000	0.000	0.000	0.000	0.000	0.000	0.000	0.000	0.000	0.000	0.000	0.000	0.000	0.000	0.000									
9	0.000	0.000	0.000	0.000	0.000	0.000	0.000	0.000	0.000	0.000	0.000	0.000	0.000	0.000	0.000	0.000								
10	0.040	0.040	0.050	0.020	0.030	0.000	0.000	0.040	0.040	0.040	0.040	0.040	0.040	0.040	0.040									
15	0.060	0.060	0.050	0.040	0.050	0.000	0.000	0.050	0.050	0.040	0.050	0.050	0.050	0.050	0.000	0.020	0.020	0.000	0.000					
20	0.070	0.100	0.070	0.040	0.090	0.000	0.050	0.060	0.060	0.050	0.060	0.060	0.070	0.050	0.020	0.030	0.000	0.000	0.000	0.000	0.000	0.000	0.000	0.000
25	0.070	0.150	0.090	0.050	0.090	0.000	0.060	0.090	0.090	0.060	0.090	0.090	0.080	0.070	0.050	0.050	0.000	0.000	0.000	0.000	0.000	0.000	0.030	0.030
30	0.090	0.150	0.110	0.050	0.100	0.000	0.060	0.100	0.100	0.070	0.100	0.100	0.080	0.120	0.050	0.050	0.050	0.050	0.000	0.080	0.000	0.030	0.030	0.050
35	0.090	0.210	0.170	0.040	0.100	0.000	0.070	0.110	0.110	0.110	0.110	0.110	0.130	0.160	0.050	0.100	0.050	0.050	0.000	0.130	0.000	0.040	0.060	0.070

**Table A10: Measured crack widths for beams RC-B1**

*Measured crack width along the beam containing 0V% D&D® - 30/.5 crimped fibres*

Load	Type of crack (B: bending crack; S: shear crack)																							
F [kN]	B	S	B	S	S	S	S	B	B	B	B	B	S	S	B	B	B	B	B	S	S	S	S	
	Cracks																							
	1	2	3	4	5	6	7	8	9	10	11	12	13	14	15	16	17	18	19	20	21	22	23	24
	Position of the appeared crack along the beam x[mm]																							
	731	628	887	1318	1391	1615	1437	731	789	926	1034	855	438	532	977	1065	1136	1173	1211	1273	1524	1563	597	1492
4	0.000																							
5	0.020																							
7	0.020	0.045	0.025	0.040	0.020	0.030	0.035	0.020																
10	0.040	0.050	0.035	0.050	0.035	0.045	0.035	0.025	0.035	0.035	0.000	0.045												
13	0.045	0.050	0.040	0.050	0.040	0.045	0.035	0.020	0.040	0.045	0.000	0.045	0.045	0.010	0.035	0.030	0.045							
15	0.050	0.050	0.040	0.055	0.040	0.050	0.035	0.015	0.050	0.045	0.010	0.050	0.045	0.035	0.045	0.040	0.045	0.040	0.030	0.045	0.015	0.015		
18	0.050	0.050	0.045	0.055	0.045	0.050	0.040	0.015	0.050	0.050	0.010	0.055	0.045	0.035	0.045	0.050	0.050	0.045	0.030	0.050	0.020	0.020	0.025	0.025
20	0.055	0.080	0.045	0.060	0.050	0.055	0.040	0.010	0.060	0.055	0.010	0.065	0.050	0.050	0.050	0.055	0.050	0.055	0.045	0.060	0.025	0.025	0.025	0.030

**Table A11: Measured crack widths for beams RC-B2**

*Measured crack width along the beam containing 0.5V% D&D® - 30/.5 crimped fibres*

Load	Type of crack (B: bending crack; S: shear crack)																								
F [kN]	S	S	S	S	S	S	B	B	B	B	S	B	B	S	B	S	S	S	S	B	B	S	S		
	Cracks																								
	1	2	3	4	5	6	7	8	9	10	11	12	13	14	15	16	17	18	19	20	21	22	23	24	25
	Position of the appeared crack along the beam x[mm]																								
	411	1576	1313	524	593	667	809	749	998	1158	1506	1093	899	1231	1406	1039	1443	1683	1684	486	1764	338	1262	1182	1638
1	0.000	0.000																							
2	0.000	0.000																							
3	0.000	0.000	0.000																						
5	0.030	0.010	0.040	0.015	0.010	0.040	0.025	0.015	0.040	0.030															
7	0.030	0.010	0.045	0.020	0.050	0.050	0.020	0.030	0.040	0.040	0.030	0.035	0.045	0.045	0.035	0.020	0.045	0.010	0.005	0.020					
10	0.045	0.010	0.050	0.025	0.035	0.055	0.020	0.040	0.050	0.045	0.035	0.045	0.045	0.045	0.035	0.020	0.045	0.010	0.005	0.020					
13	0.045	0.010	0.070	0.035	0.050	0.065	0.025	0.050	0.050	0.050	0.040	0.055	0.045	0.045	0.045	0.050	0.015	0.005	0.040	0.020	0.015				
15	0.055	0.015	0.070	0.040	0.050	0.090	0.050	0.055	0.060	0.050	0.040	0.055	0.050	0.045	0.045	0.045	0.015	0.020	0.050	0.020	0.030	0.040			
18	0.055	0.015	0.075	0.045	0.060	0.100	0.055	0.065	0.070	0.050	0.055	0.060	0.060	0.045	0.050	0.065	0.015	0.020	0.050	0.030	0.030	0.045	0.040		
20	0.055	0.015	0.080	0.050	0.070	0.115	0.065	0.075	0.075	0.050	0.055	0.090	0.060	0.055	0.055	0.065	0.015	0.020	0.050	0.030	0.045	0.050	0.050	0.040	
23	0.070	0.020	0.100	0.050	0.100	0.140	0.350	0.075	0.100	0.050	0.060	0.085	0.060	0.060	0.060	0.090	0.025	0.025	0.055	0.055	0.050	0.050	0.060	0.050	0.030
25	0.120	0.020	0.100	0.080	0.130	0.145	0.100	0.080	0.100	0.055	0.060	0.120	0.085	0.075	0.100	0.100	0.025	0.025	0.060	0.060	0.050	0.050	0.060	0.050	0.030

**Table A12: Measured crack widths for beams RC-B3**

*Measured crack width along the beam containing 1V% D&D® - 30/.5 crimped fibres*

Load	Type of crack (B: bending crack; S: shear crack)																							
F [kN]	S	S	S	B	S	B	B	B	B	B	B	S	B	S	S	B	S	S	S	B	B	S	S	
	Cracks																							
	1	2	3	4	5	6	7	8	9	10	11	12	13	14	15	16	17	18	19	20	21	22	23	
	Position of the appeared crack along the beam x[mm]																							
	438	496	636	874	689	1019	1337	773	1073	1154	1238	1554	968	1494	583	941	344	1416	1633	823	1192	402	286	
2	0.020	0.005																						
3	0.025	0.010																						
5	0.025	0.020	0.005	0.010																				
7	0.030	0.025	0.005	0.025	0.025	0.005	0.030	0.015	0.015	0.035	0.030	0.005												
10	0.030	0.030	0.010	0.045	0.045	0.005	0.045	0.020	0.025	0.040	0.030	0.005	0.005	0.005	0.040	0.005								
13	0.030	0.035	0.025	0.045	0.050	0.015	0.045	0.035	0.040	0.050	0.040	0.025	0.005	0.005	0.050	0.005	0.020	0.010	0.010					
15	0.030	0.045	0.025	0.045	0.050	0.025	0.045	0.030	0.040	0.050	0.020	0.025	0.015	0.005	0.050	0.010	0.020	0.010	0.010	0.015				
18	0.035	0.045	0.040	0.050	0.065	0.045	0.045	0.040	0.050	0.050	0.035	0.035	0.025	0.005	0.050	0.010	0.020	0.010	0.020	0.015	0.030			
20	0.035	0.050	0.040	0.050	0.080	0.045	0.055	0.045	0.060	0.060	0.050	0.040	0.040	0.010	0.060	0.035	0.025	0.015	0.020	0.035	0.030	0.010		
23	0.050	0.050	0.050	0.050	0.100	0.045	0.075	0.050	0.060	0.060	0.050	0.045	0.050	0.010	0.100	0.040	0.025	0.020	0.020	0.040	0.030	0.025	0.005	
25	0.050	0.050	0.050	0.050	0.105	0.050	0.080	0.050	0.060	0.075	0.050	0.045	0.050	0.020	0.110	0.050	0.025	0.020	0.020	0.045	0.030	0.025	0.015	
30	0.060	0.055	0.050	0.050	0.135	0.055	0.130	0.050	0.100	0.075	0.055	0.045	0.055	0.020	0.125	0.055	0.025	0.025	0.020	0.045	0.045	0.050	0.015	

**Table A13: Measured crack widths for beams RC-B4**

Measured crack width along the beam  $\phi 4/240$  containing 0V% D&D<sup>®</sup> - 30/5 crimped fibres

Load F [kN]	Type of crack (B: bending crack; S: shear crack)																							
	B	S	B	B	B	S	S	S	B	B	S	S	S	S	B	B	S	S	B	B	B	S	S	S
Cracks																								
Position of the appeared crack along the beam x[mm]																								
	1	2	3	4	5	6	7	8	9	10	11	12	13	14	15	16	17	18	19	20	21	22	23	
	1132	1767	824	1032	1178	1407	1956	918	1247	523	624	678	332	758	974	1318	429	869	1014	1071	1872	1803	368	
4	0.035	0.025																						
5	0.045	0.030																						
7	0.045	0.020	0.030	0.030	0.020	0.030	0.020	0.040	0.035															
10	0.045	0.030	0.035	0.150	0.040	0.035	0.025	0.045	0.045	0.040	0.035	0.040	0.005	0.045	0.000	0.050								
15	0.075	0.030	0.045	0.020	0.050	0.045	0.035	0.050	0.050	0.040	0.055	0.065	0.005	0.055	0.005	0.050	0.050	0.025	0.010	0.050	0.035			
20	0.095	0.045	0.050	0.025	0.065	0.050	0.040	0.060	0.065	0.055	0.090	0.100	0.010	0.100	0.005	0.055	0.060	0.045	0.015	0.055	0.035	0.020		
25	0.100	0.050	0.080	0.025	0.080	0.085	0.050	0.085	0.075	0.055	0.135	0.140	0.010	0.105	0.005	0.090	0.075	0.055	0.045	0.060	0.040	0.040	0.070	

**Table A14: Measured crack widths for beams RC-B5**

Measured crack width along the beam  $\phi 4/240$  containing 0.5V% D&D<sup>®</sup> - 30/5 crimped fibres

Load F [kN]	Type of crack (B: bending crack; S: shear crack)																												
	B	S	B	B	B	S	S	S	B	B	B	B	B	S	S	S	S	S	B	S	S	B	S	S	S	S			
Cracks																													
Position of the appeared crack along the beam x[mm]																													
	1	2	3	4	5	6	7	8	9	10	11	12	13	14	15	16	17	18	19	20	21	22	23	24	25	26	27	28	
	981	1829	906	1106	773	491	571	641	1265	1193	709	817	1048	1155	861	1337	1447	369	416	1621	1017	1379	257	1221	326	1724	392	514	
2.0	0.010	0.000	0.000																										
3.0	0.015	0.010	0.025																										
5.0	0.015	0.020	0.025	0.020	0.020																								
7.0	0.030	0.020	0.040	0.040	0.020	0.025	0.025	0.000	0.025	0.025																			
10.0	0.040	0.020	0.045	0.045	0.020	0.055	0.040	0.035	0.035	0.035	0.040	0.030	0.025	0.040															
12.5	0.045	0.020	0.050	0.050	0.040	0.040	0.045	0.040	0.045	0.040	0.045	0.040	0.040	0.045	0.025	0.045	0.025												
15.0	0.050	0.020	0.060	0.050	0.045	0.045	0.050	0.045	0.045	0.045	0.050	0.040	0.040	0.045	0.040	0.050	0.035	0.015											
17.5	0.050	0.020	0.070	0.060	0.050	0.045	0.050	0.050	0.050	0.045	0.060	0.040	0.050	0.050	0.040	0.055	0.045	0.020	0.010	0.015									
20.0	0.060	0.020	0.080	0.075	0.060	0.050	0.050	0.050	0.050	0.045	0.065	0.040	0.050	0.050	0.045	0.075	0.045	0.025	0.010	0.030	0.045	0.005							
22.5	0.075	0.020	0.080	0.075	0.090	0.050	0.050	0.055	0.045	0.050	0.090	0.045	0.050	0.050	0.050	0.060	0.045	0.030	0.010	0.030	0.045	0.005	0.035	0.040					
25.0	0.075	0.020	0.100	0.075	0.095	0.055	0.055	0.075	0.050	0.060	0.090	0.050	0.060	0.060	0.050	0.080	0.050	0.030	0.010	0.030	0.050	0.020	0.040	0.045	0.025	0.050			
27.5	0.090	0.020	0.100	0.085	0.095	0.060	0.055	0.080	0.060	0.060	0.105	0.055	0.065	0.065	0.050	0.090	0.050	0.015	0.010	0.045	0.055	0.030	0.050	0.045	0.035	0.025	0.050		
30.0	0.100	0.025	0.115	0.090	0.100	0.065	0.075	0.090	0.060	0.080	0.110	0.070	0.075	0.075	0.050	0.090	0.050	0.015	0.010	0.045	0.055	0.035	0.050	0.045	0.040	0.025	0.075	0.020	
32.5	0.130	0.020	0.120	0.090	0.100	0.065	0.050	0.090	0.080	0.090	0.130	0.085	0.085	0.085	0.090	0.100	0.080	0.020	0.010	0.050	0.060	0.050	0.065	0.050	0.030	0.025	0.013	0.020	

**Table A15: Measured crack widths for beams RC-B6**

Measured crack width along the beam  $\phi 4/240$  containing 1V% D&D<sup>®</sup> - 30/5 crimped fibres

Load F [kN]	Type of crack (B: bending crack; S: shear crack)																												
	h	ny	ny	h	h	h	h	h	h	ny	ny	ny	h	h	ny	ny	h	ny	ny	ny	ny	ny	ny	ny	ny	h	ny	ny	
Cracks																													
Position of the appeared crack along the beam x[mm]																													
	1	2	3	4	5	6	7	8	9	10	11	12	13	14	15	16	17	18	19	20	21	22	23	24	25	26	27		
	936	1588	587	1044	1238	743	988	808	1176	389	457	654	701	876	1392	527	1093	1329	1425	1482	1739	1512	1771	292	796	1693	238		
2.0	0.025																												
3.0	0.030																												
5.0	0.035	0.005																											
7.0	0.045	0.005	0.040	0.030	0.040																								
10.0	0.055	0.001	0.045	0.045	0.030	0.015	0.020	0.005																					
12.5	0.070	0.020	0.045	0.045	0.035	0.040	0.025	0.005	0.015	0.015	0.015	0.020	0.040	0.040	0.035														
15.0	0.080	0.025	0.060	0.045	0.045	0.040	0.025	0.040	0.015	0.020	0.020	0.025	0.045	0.050	0.035	0.020	0.020	0.050	0.045	0.020	0.025								
17.5	0.100	0.035	0.060	0.050	0.055	0.045	0.040	0.045	0.025	0.020	0.030	0.045	0.050	0.050	0.040	0.025	0.040	0.060	0.050	0.030	0.030	0.020	0.010	0.040					
20.0	0.105	0.045	0.075	0.055	0.065	0.045	0.040	0.045	0.020	0.025	0.040	0.045	0.055	0.060	0.040	0.040	0.050	0.060	0.055	0.030	0.030	0.025	0.030	0.040					
22.5	0.120	0.045	0.075	0.055	0.085	0.045	0.045	0.050	0.060	0.040	0.050	0.050	0.060	0.090	0.050	0.040	0.050	0.090	0.055	0.030	0.030	0.040	0.040	0.045					
25.0	0.135	0.050	0.085	0.075	0.100	0.050	0.045	0.050	0.080	0.045	0.050	0.050	0.075	0.095	0.055	0.045	0.050	0.100	0.095	0.030	0.035	0.040	0.040	0.050					
27.5	0.150	0.055	0.095	0.100	0.100	0.050	0.045	0.050	0.090	0.050	0.050	0.055	0.100	0.095	0.065	0.050	0.060	0.100	0.095	0.030	0.035	0.050	0.050	0.050	0.050	0.045			
30.0	0.150	0.070	0.100	0.105	0.135	0.050	0.050	0.050	0.095	0.050	0.050	0.080	0.100	0.105	0.065	0.065	0.060	0.140	0.105	0.030	0.035	0.050	0.050	0.050	0.045	0.050			
35.0	0.170	0.070	0.110	0.150	0.150	0.050	0.550	0.050	0.115	0.100	0.050	0.100	0.125	0.135	0.150	0.070	0.060	0.120	0.150	0.030	0.035	0.050	0.050	0.050	0.070	0.035	0.070		

**Table A16: Measured crack widths for beams RC-B7**

Measured crack width along the beam  $\phi 4/120$  containing 0V% D&D® - 30/5 crimped fibres

Load F [kN]	Type of crack (B: bending crack; S: shear crack)																							
	B	B	S	B	B	B	S	B	S	S	S	B	B	S	S	S	S	S	S	S	S	S	S	
Cracks																								
Position of the appeared crack along the beam x[mm]																								
	1	2	3	4	5	6	7	8	9	10	11	12	13	14	15	16	17	18	19	20	21	22	23	24
	891	1298	639	1029	755	1126	552	1231	426	1579	1482	814	1193	1415	960	1353	697	293	486	360	1656	1722	1742	232
2.0	0.000	0.000																						
4.0	0.015	0.010	0.020	0.040																				
5.0	0.025	0.050	0.025	0.035	0.035	0.045																		
7.0	0.030	0.025	0.050	0.050	0.040	0.045	0.045	0.010	0.025	0.005	0.020	0.035	0.020	0.025										
10.0	0.050	0.025	0.055	0.055	0.045	0.055	0.055	0.030	0.045	0.020	0.030	0.045	0.035	0.040	0.045	0.030	0.030	0.020						
12.5	0.060	0.055	0.060	0.065	0.050	0.065	0.075	0.040	0.050	0.020	0.040	0.050	0.045	0.030	0.055	0.035	0.050	0.025						
15.0	0.080	0.060	0.090	0.080	0.050	0.090	0.080	0.050	0.050	0.035	0.050	0.050	0.045	0.055	0.045	0.075	0.025	0.045						
17.5	0.100	0.065	0.095	0.080	0.075	0.100	0.080	0.050	0.050	0.045	0.050	0.060	0.050	0.050	0.065	0.050	0.085	0.025	0.050	0.030	0.025	0.010		
20.0	0.105	0.080	0.095	0.100	0.080	0.100	0.085	0.055	0.055	0.050	0.050	0.070	0.070	0.055	0.080	0.050	0.095	0.035	0.060	0.040	0.030	0.010		
22.5	0.115	0.090	0.095	0.100	0.090	0.100	0.090	0.050	0.055	0.050	0.055	0.070	0.070	0.055	0.095	0.050	0.100	0.040	0.070	0.050	0.030	0.010		
25.0	0.140	0.090	0.095	0.075	0.095	0.120	0.105	0.060	0.055	0.050	0.055	0.095	0.090	0.055	0.100	0.050	0.115	0.040	0.100	0.050	0.035	0.015		
30.0	0.170	0.115	0.070	0.100	0.105	0.120	0.160	0.065	0.040	0.060	0.120	0.100	0.090	0.060	0.115	0.060	0.150	0.040	0.200	0.050	0.045	0.015	0.045	0.010

**Table A17: Measured crack widths for beams RC-B8**

Measured crack width along the beam  $\phi 4/120$  containing 0.5V% D&D® - 30/5 crimped fibres

Load F [kN]	Type of crack (B: bending crack; S: shear crack)																													
	B	B	B	B	S	S	S	B	S	S	B	B	S	S	B	S	S	S	B	S	S	S	S	S	S	B	S	S	B	
Cracks																														
Position of the appeared crack along the beam x[mm]																														
	1	2	3	4	5	6	7	8	9	10	11	12	13	14	15	16	17	18	19	20	21	22	23	24	25	26	27	28	29	30
	916	762	1019	1220	667	1571	521	1274	1511	597	835	1152	1381	697	962	1106	1446	335	446	412	1174	1316	1626	1691	1814	222	729	1358	1769	822
1.0	0.020	0.000	0.000																											
2.0	0.030	0.000	0.000	0.010																										
3.0	0.030	0.000	0.010	0.015																										
4.0	0.035	0.005	0.020	0.015	0.030	0.025																								
5.0	0.035	0.010	0.020	0.015	0.030	0.030																								
7.0	0.045	0.025	0.030	0.030	0.045	0.030																								
10.0	0.050	0.040	0.030	0.035	0.045	0.040	0.025	0.025	0.005																					
12.5	0.060	0.045	0.045	0.045	0.050	0.040	0.030	0.030	0.005	0.010	0.020	0.015	0.045																	
15.0	0.070	0.050	0.050	0.045	0.050	0.045	0.035	0.035	0.005	0.015	0.030	0.020	0.045	0.020	0.005	0.030	0.030													
17.5	0.085	0.050	0.050	0.045	0.050	0.050	0.040	0.045	0.010	0.025	0.040	0.020	0.045	0.020	0.005	0.030	0.040	0.045	0.010											
20.0	0.095	0.060	0.065	0.045	0.050	0.050	0.050	0.050	0.010	0.040	0.040	0.020	0.050	0.035	0.015	0.035	0.050	0.045	0.020	0.040	0.035	0.020	0.025							
22.5	0.100	0.075	0.065	0.050	0.055	0.060	0.055	0.055	0.015	0.050	0.050	0.020	0.055	0.045	0.020	0.050	0.050	0.050	0.020	0.045	0.045	0.035	0.040	0.040						
25.0	0.100	0.075	0.090	0.055	0.055	0.060	0.060	0.075	0.015	0.050	0.040	0.025	0.060	0.050	0.030	0.050	0.050	0.050	0.030	0.045	0.045	0.035	0.040	0.040	0.350					
30.0	0.110	0.100	0.110	0.040	0.065	0.075	0.075	0.090	0.015	0.060	0.050	0.045	0.105	0.050	0.040	0.055	0.090	0.055	0.055	0.050	0.040	0.050	0.065	0.040	0.050	0.045	0.030			
32.5	0.120	0.100	0.140	0.040	0.075	0.050	0.105	0.100	0.005	0.090	0.055	0.050	0.115	0.070	0.050	0.090	0.100	0.070	0.040	0.065	0.050	0.050	0.030	0.090	0.100	0.040	0.055	0.045	0.040	
35.0	0.100	0.115	0.150	0.030	0.100	0.090	0.105	0.100	0.005	0.065	0.095	0.060	0.150	0.095	0.060	0.090	0.090	0.100	0.025	0.090	0.060	0.050	0.020	0.050	0.100	0.030	0.055	0.040	0.030	0.030

Table A18: Measured crack widths for beams RC-B9

Measured crack width along the beam containing 17%<math>D_{min}</math> - 50.5 crimped fibres		
Load	Type of crack (if bending crack, S = shear crack)	Crack
P (kN)		1 2 3 4 5 6 7 8 9 10 11 12 13 14 15 16 17 18 19 20 21 22 23 24 25 26 27 28 29 30 31 32 33 34 35 36 37 38 39 40
11.50		
13.00		
14.50		
16.00		
17.50		
19.00		
20.50		
22.00		
23.50		
25.00		
26.50		
28.00		
29.50		
31.00		
32.50		
34.00		
35.50		
37.00		
38.50		
40.00		
41.50		
43.00		
44.50		
46.00		
47.50		
49.00		
50.50		
52.00		
53.50		
55.00		
56.50		
58.00		
59.50		
61.00		
62.50		
64.00		
65.50		
67.00		
68.50		
70.00		
71.50		
73.00		
74.50		
76.00		
77.50		
79.00		
80.50		
82.00		
83.50		
85.00		
86.50		
88.00		
89.50		
91.00		
92.50		
94.00		
95.50		
97.00		
98.50		
100.00		

# Subject Index

- A**
- Acrylic fibre 16
  - Aggregates 36
  - A-glass fibre 16
  - Air content 36
  - Anisotropic features 33
  - Anchorage properties of fibre 32
  - Aramid fibre 16
  - Axially prestressed member 18
- B**
- Balling effect 32
  - Bamboo fibre 16
  - Behaviour in compression 19, 44, 46, 54
  - Behaviour in tension 22, 24, 53
  - Bending 15, 65, 66, 122, 160
  - Bending failure 105, 106, 160
  - Bond 22, 23, 150
  - Brittleness 22
- C**
- Camber 134, 147, 148, 149
  - Characteristic fibre orientation 40
  - Cellulose fibre 16
  - Cement based material 16, 33
  - Cracking behaviour 23, 115
  - Crack width 115, 116, 118, 119
  - Crack development 115, 116
  - Crack pattern 116, 117
  - Crack spacing 115, 116, 118
  - Crimped fibre 15, 37, 38
  - Cross-section of fibre 15
  - Coconut fibre 16
  - Collocated fibre 15
  - Compression 15, 18
  - Compressive strength 20, 21, 44, 46, 49
  - Compressive toughness 18
  - Conclusions 34, 68, 127, 163
  - Concrete 15
  - Concrete mixes 35
  - Concrete mixers 37
  - Concrete strain 136, 137, 138
  - Construction material 15
- D**
- Debonding of fibre 23
  - Deformed fibres 15
  - Deep beam 18, 31
  - Ductility 16
  - Dry mixing 36
  - Draw-in 134, 135, 139, 140, 142, 144
- E**
- E-glass fibre 16
  - Elephant grass fibre 16
  - Energy absorption 16, 27, 115
  - Experimental programme 101, 131
- F**
- Failure mode 104, 106, 107, 108  
110, 160, 161
  - Failure load 104, 106, 107, 108  
110, 160, 161
  - Fibre aspect ratio 15, 16, 19, 32
  - Fibre applications 16, 17, 30, 31
  - Fibre length 15, 16
  - Fibre diameter 15, 16
  - Fibre orientation 18, 26, 32, 35
  - Fibre reinforced concrete 15
  - Fibre reinforced corbels 32
  - Fibre reinforced slab 18
  - Fibre reinforced wall 32

Flexural toughness	15, 26, 29, 63, 65		
	66		
Four point bending	102, 106, 107		
Force-flow	73		
Formworks	38		
<b>G</b>			
Glass fibre	15, 16		
Gradual release	133, 134, 136, 137		
<b>H</b>			
High steel fibre content	23		
High strength concrete	15		
High performance concrete	15		
Hooked-end fibre	15, 37, 38		
<b>I</b>			
Impact resistance	33		
Industrial floor	33		
<b>K</b>			
Krizotil fibre	16		
Krocidolit fibre	16		
<b>L</b>			
Literature review	20, 21, 24, 26, 52, 53		
	62, 63		
Load – deflection relationship	27, 66		
	110, 114, 162		
Localised fibre yielding	23		
Low steel fibre content	23		
<b>M</b>			
Material compositions	35		
Material properties	15		
Mean crack width	116, 118, 119		
Mean crack spacing	116, 118, 120		
Mechanical model	72, 76		
Mechanical device	72, 76		
Medium steel fibre content	23		
Mixing process	18		
Mixing sequence	36		
Modelling	71, 122, 126, 127, 128		
	129, 151		
Modulus of elasticity	16, 18		
Mortal	16		
Multiple cracking	25		
<b>N</b>			
Natural fibre	15		
NEG AR glass fibre	16		
Number of crack	116		
Nylon	16		
<b>P</b>			
Partially prestressed member	18		
Paddled fibre	15		
Plain concrete	18		
Polyester fibre	16		
Polyethylene fibre	16		
Polypropylene fibre	15		
Porosity	18, 36		
Post-peak behaviour	18		
Prestressed pretensioned concrete			
beams	131, 133, 134		
Prestressing force	133, 134, 139, 142		
Prestressing tendon	133, 134		
Punching shear strength	18		
Pull-out of fibre	23		
<b>R</b>			
Reinforcing bar	102, 107, 108		
Reinforcing detail	101, 103, 107, 108		
<b>S</b>			
SIFCON	33		
Sisal fibre	16		
Shear behaviour	102, 105, 106, 107		
Shear failure	104, 105, 106, 107		
Shear reinforcement ratios	109, 110		
	112		
Shear span to depth ratio	31		
Shear strength	18, 105		
Steel fibre	15		
Steel fibre reinforced concrete	15, 101		
Steel fibre reinforced concrete beam			
	101, 106, 107		
Stirrup reinforcement	102, 105, 106, 107		
Straight fibre	15		
Stress – strain relationship	23, 28, 47		
	51, 74, 122, 124, 125		
Splitting strength	15, 18, 24, 26, 53, 57		
Stainless fibre	16		
Sudden release	133, 134, 138, 145		

Superplasticizer 36

**T**

Tension 15

Tensile strength 22, 24, 26

Test specimens 35, 38, 39, 42, 43  
101, 131, 132

Toughness indexes 15, 26, 29, 66

Transfer length of tendon 31, 150  
153, 154, 155, 156, 157, 158

Transfer mechanism of fibres 23

**U**

Undulated fibre 15

**W**

Water to cement ratio 36, 50, 61

Workability of concrete 35

Wood fibre 16